

# Hot QCD White Paper

M. Arslanok<sup>1</sup>, S. A. Bass<sup>2</sup>, A. A. Baty<sup>3</sup>, I. Bautista<sup>4</sup>, C. Beattie<sup>1</sup>, F. Becattini<sup>5</sup>, R. Bellwied<sup>6</sup>, Y. Berdnikov<sup>7</sup>, A. Berdnikov<sup>7</sup>, J. Bielcik<sup>8</sup>, J. T. Blair<sup>9</sup>, F. Bock<sup>10</sup>, B. Boimska<sup>11</sup>, H. Bossi<sup>1</sup>, H. Caines<sup>1</sup>, Y. Chen<sup>§12</sup>, Y.-T. Chien<sup>§13</sup>, M. Chiu<sup>14</sup>, M. E. Connors<sup>\*§13</sup>, M. Csanád<sup>15</sup>, C.L. da Silva<sup>§16</sup>, A. P. Dash<sup>17</sup>, G. David<sup>18,14</sup>, K. Dehmelt<sup>18</sup>, V. Dexheimer<sup>§19</sup>, X. Dong<sup>§20</sup>, A. Drees<sup>18</sup>, L. Du<sup>21</sup>, J. M. Durham<sup>§16</sup>, R.J. Ehlers<sup>20,22</sup>, H. Elfner<sup>23,24,25</sup>, O. Evdokimov<sup>26</sup>, M. Finger<sup>27</sup>, M. Finger Jr.<sup>27</sup>, J. Frantz<sup>28</sup>, A. D. Frawley<sup>29</sup>, C. Gale<sup>21</sup>, F. Geurts<sup>3</sup>, V. Gonzalez<sup>30</sup>, N. Grau<sup>31</sup>, S. V. Greene<sup>32</sup>, S. K. Grossberndt<sup>33</sup>, T. Hachiya<sup>34</sup>, X. He<sup>13</sup>, U. Heinz<sup>35</sup>, B. Hong<sup>36</sup>, T. J. Humanic<sup>35</sup>, D. Ivanishchev<sup>37</sup>, B. V. Jacak<sup>22,20</sup>, J. Jahan<sup>6</sup>, S. Jeon<sup>21</sup>, H.R. Jheng<sup>12</sup>, J. Jia<sup>§18</sup>, E. G. Judd<sup>22</sup>, J. I. Kapusta<sup>38</sup>, I. Karpenko<sup>8</sup>, V. Khachatryan<sup>39</sup>, D.E. Kharzeev<sup>18,14</sup>, M. Kim<sup>22</sup>, B. Kimelman<sup>32</sup>, J.L. Klay<sup>40</sup>, S. R. Klein<sup>20</sup>, A. G. Knospe<sup>41</sup>, V. Koch<sup>20</sup>, D. Kotov<sup>7,37</sup>, G. K. Krintiras<sup>42</sup>, R. Kunnawalkam Elayavalli<sup>§32</sup>, C. M. Kuo<sup>43</sup>, J. G. Lajoie<sup>44</sup>, Y.-J. Lee<sup>§12</sup>, W. Li<sup>3</sup>, J. Liao<sup>§39</sup>, I. Likmeta<sup>6</sup>, S. H. Lim<sup>45</sup>, M. X. Liu<sup>16</sup>, C. Loizides<sup>10</sup>, R. Longo<sup>46</sup>, X. Luo<sup>47</sup>, M. Luzum<sup>48</sup>, R. Ma<sup>§14</sup>, A. Majumder<sup>§30</sup>, S. Mak<sup>2</sup>, C. Markert<sup>9</sup>, Y. Mehtar-Tani<sup>§14</sup>, A. C. Mignerey<sup>49</sup>, N. Minafra<sup>42</sup>, D. P. Morrison<sup>14</sup>, B. Mueller<sup>2</sup>, J.L. Nagle<sup>50</sup>, A. Narde<sup>46</sup>, C. E. Nattrass<sup>51</sup>, T. Niida<sup>§52</sup>, J. Noronha<sup>§46</sup>, J. Noronha-Hostler<sup>§46</sup>, R. Nouicer<sup>14</sup>, N. Novitzky<sup>§10</sup>, E. O'Brien<sup>14</sup>, G. Odyniec<sup>20</sup>, V. A. Okorokov<sup>53</sup>, J. D. Osborn<sup>14</sup>, J.-F. Paquet<sup>\*§32</sup>, S. Park<sup>54</sup>, P. Parotto<sup>55</sup>, D.V. Perepelitsa<sup>§50</sup>, P. Petreczky<sup>§14</sup>, C. Pinkenburg<sup>14</sup>, M. Praszalowicz<sup>56</sup>, C. Pruneau<sup>30</sup>, J. Putschke<sup>30</sup>, N.V. Ramasubramanian<sup>57,18</sup>, R. Rapp<sup>58</sup>, C. Ratti<sup>§6</sup>, K.F. Read<sup>10,51</sup>, P. Rebello Teles<sup>59</sup>, R. Reed<sup>41</sup>, T. Rinn<sup>14</sup>, G. Roland<sup>12</sup>, M. Rosati<sup>44</sup>, C. Royon<sup>42</sup>, L. Ruan<sup>14</sup>, T. Sakaguchi<sup>14</sup>, S. Salur<sup>60</sup>, M. Sarsour<sup>13</sup>, A. S. Menon<sup>6</sup>, B. Schenke<sup>14</sup>, N. V. Schmidt<sup>10</sup>, A. Schmier<sup>51</sup>, T. Schäfer<sup>61</sup>, J. Seger<sup>62</sup>, R. Seto<sup>63</sup>, Oveis Sheibani<sup>6</sup>, C. Shen<sup>§30</sup>, Z. Shi<sup>16</sup>, E. Shulga<sup>18</sup>, A. M. Sickles<sup>46</sup>, M. Singh<sup>38</sup>, B.K.Singh<sup>64</sup>, N. Smirnov<sup>1</sup>, K.L. Smith<sup>16</sup>, H. Song<sup>65</sup>, I. Soudi<sup>30</sup>, A. G. Stahl Leitner<sup>66</sup>, P. Steinberg<sup>14</sup>, M. Stephanov<sup>26</sup>, M. Strickland<sup>§19</sup>, M. Sumbera<sup>67,8</sup>, D. Sunar Cerci<sup>68</sup>, Y. Tachibana<sup>§69</sup>, A.H. Tang<sup>14</sup>, D. Tapia Takaki<sup>42</sup>, D. Teaney<sup>§18</sup>, D. Thomas<sup>70</sup>, A.R. Timmins<sup>§6</sup>, P. Tribedy<sup>§14</sup>, Z. Tu<sup>§14</sup>, S. Tuo<sup>§32</sup>, O. V. Rueda<sup>6</sup>, J. Velkovska<sup>§32</sup>, R. Venugopalan<sup>14</sup>, F. Videbæk<sup>14</sup>, S. A. Voloshin<sup>30</sup>, V. Vovchenko<sup>6</sup>, G. Vujanovic<sup>§71</sup>, X. Wang<sup>46</sup>, F. Wang<sup>72</sup>, X.-N. Wang<sup>§20</sup>, S. Weyhmler<sup>1</sup>, W. Xie<sup>72</sup>, N. Xu<sup>20</sup>, Y. Yang<sup>73</sup>, X. Yao<sup>§74</sup>, Z. Ye<sup>3</sup>, H.-U. Yee<sup>26</sup>, and W.A. Zajc<sup>75</sup>

<sup>1</sup>Yale University, New Haven, Connecticut, USA

<sup>2</sup>Duke University, Durham, North Carolina, USA

<sup>3</sup>Rice University, Houston, Texas, USA

<sup>4</sup>Benemérita Universidad Autónoma de Puebla, Puebla, Mexico

<sup>5</sup>University of Florence, Firenze, Italy

<sup>6</sup>University of Houston, Houston, Texas, USA

<sup>7</sup>Peter the Great St.Petersburg Polytechnic University, St.Petersburg, Russia

<sup>8</sup>Czech Technical University in Prague, Prague, Czech Republic

<sup>9</sup>University of Texas at Austin, Austin, Texas, USA

<sup>10</sup>Oak Ridge National Laboratory, Oak Ridge, Tennessee, USA

<sup>11</sup>National Centre for Nuclear Research, Warsaw, Poland

<sup>12</sup>Massachusetts Institute of Technology, Cambridge, Massachusetts, USA

<sup>13</sup>Georgia State University, Atlanta, Georgia, USA

<sup>14</sup>Brookhaven National Laboratory, Upton, New York, USA

<sup>15</sup>Eötvös Loránd University, Budapest, Hungary

<sup>16</sup>Los Alamos National Laboratory, Los Alamos, New Mexico, USA

<sup>17</sup>University of California Los Angeles, Los Angeles, California, USA

<sup>18</sup>Stony Brook University, Stony Brook, New York, USA

<sup>19</sup>Kent State University, Kent, Ohio, USA

<sup>20</sup>Lawrence Berkeley National Laboratory, Berkeley, California, USA

<sup>21</sup>McGill University, Montreal, Québec, Canada

<sup>22</sup>University of California Berkeley, Berkeley, California, USA

<sup>23</sup>GSI Helmholtzzentrum für Schwerionenforschung, Darmstadt, Germany

<sup>24</sup>Institute for Theoretical Physics, Goethe University, Frankfurt am Main, Germany

<sup>25</sup>Frankfurt Institute for Advanced Studies, Frankfurt am Main, Germany

- <sup>26</sup> *University of Illinois Chicago, Chicago, Illinois, USA*  
<sup>27</sup> *Charles University, Prague, Czech Republic*  
<sup>28</sup> *Ohio University, Athens, Ohio, USA*  
<sup>29</sup> *Florida State University, Tallahassee, Florida, USA*  
<sup>30</sup> *Wayne State University, Detroit, Michigan, USA*  
<sup>31</sup> *Augustana University, Sioux Falls, South Dakota, USA*  
<sup>32</sup> *Vanderbilt University, Nashville, Tennessee, USA*  
<sup>33</sup> *City University of New York, New York, New York, USA*  
<sup>34</sup> *Nara Women's University, Nara, Japan*  
<sup>35</sup> *The Ohio State University, Columbus, Ohio, USA*  
<sup>36</sup> *Korea University, Seoul, Republic of Korea*  
<sup>37</sup> *NRC Kurchatov Institute – PNPI, Gatchina, Russia*  
<sup>38</sup> *University of Minnesota, Minneapolis, Minnesota, USA*  
<sup>39</sup> *Indiana University, Bloomington, Indiana, USA*  
<sup>40</sup> *California Polytechnic State University, San Luis Obispo, California, USA*  
<sup>41</sup> *Lehigh University, Bethlehem, Pennsylvania, USA*  
<sup>42</sup> *University of Kansas, Lawrence, Kansas, USA*  
<sup>43</sup> *National Central University, Taoyuan City, Taiwan*  
<sup>44</sup> *Iowa State University, Ames, Iowa, USA*  
<sup>45</sup> *Pusan National University, Busan, Republic of Korea*  
<sup>46</sup> *University of Illinois Urbana-Champaign, Urbana, Illinois, USA*  
<sup>47</sup> *Central China Normal University, Wuhan, China*  
<sup>48</sup> *University of São Paulo, São Paulo, Brazil*  
<sup>49</sup> *University of Maryland, College Park, Maryland, USA*  
<sup>50</sup> *University of Colorado Boulder, Boulder, Colorado, USA*  
<sup>51</sup> *University of Tennessee, Knoxville, Tennessee, USA*  
<sup>52</sup> *University of Tsukuba, Tsukuba, Japan*  
<sup>53</sup> *National Research Nuclear University MEPhI, Moscow, Russia*  
<sup>54</sup> *Mississippi State University, Starkville, Mississippi, USA*  
<sup>55</sup> *Pennsylvania State University, University Park, Pennsylvania, USA*  
<sup>56</sup> *Jagiellonian University, Krakow, Poland*  
<sup>57</sup> *CEA, Paris-Saclay, Île-de-France, France*  
<sup>58</sup> *Texas A&M University, College Station, Texas, USA*  
<sup>59</sup> *Centro Brasileiro de Pesquisas Físicas, Rio de Janeiro, Brazil*  
<sup>60</sup> *Rutgers University, Piscataway, New Jersey, USA*  
<sup>61</sup> *North Carolina State University, Raleigh, North Carolina, USA*  
<sup>62</sup> *Creighton University, Omaha, Nebraska, USA*  
<sup>63</sup> *University of California Riverside, Riverside, California, USA*  
<sup>64</sup> *Banaras Hindu University, Varanasi, India*  
<sup>65</sup> *Peking University, Beijing, China*  
<sup>66</sup> *CERN, European Organization for Nuclear Research, Geneva, Switzerland*  
<sup>67</sup> *Nuclear physics institute CAS, Řež, Czech Republic*  
<sup>68</sup> *Adiyaman University, Adiyaman, Turkey*  
<sup>69</sup> *Akita International University, Akita-city, Japan*  
<sup>70</sup> *The University of Texas at Austin, Austin, Texas, USA*  
<sup>71</sup> *University of Regina, Regina, Saskatchewan, Canada*  
<sup>72</sup> *Purdue University, West Lafayette, Indiana, USA*  
<sup>73</sup> *National Cheng Kung University, Tainan, Taiwan*  
<sup>74</sup> *University of Washington, Seattle, Washington, USA*  
<sup>75</sup> *Columbia University, New York, New York, USA*

---

§ Writing committee

\* Writing committee co-chairs: mconnors@gsu.edu, jean-francois.paquet@vanderbilt.edu

**Abstract**

Hot QCD physics studies the nuclear strong force under extreme temperature and densities. Experimentally these conditions are achieved via high-energy collisions of heavy ions at the Relativistic Heavy Ion Collider (RHIC) and the Large Hadron Collider (LHC). In the past decade, a unique and substantial suite of data was collected at RHIC and the LHC, probing hydrodynamics at the nucleon scale, the temperature dependence of the transport properties of quark-gluon plasma, the phase diagram of nuclear matter, the interaction of quarks and gluons at different scales and much more. This document, as part of the 2023 nuclear science long range planning process, was written to review the progress in hot QCD since the 2015 Long Range Plan for Nuclear Science, as well as highlight the realization of previous recommendations, and present opportunities for the next decade, building on the accomplishments and investments made in theoretical developments and the construction of new detectors. Furthermore, this document provides additional context to support the recommendations voted on at the Joint Hot and Cold QCD Town Hall Meeting, which are reported in a separate document.

# Contents

|       |  |    |
|-------|--|----|
| 1     | Executive Summary . . . . .  | 6  |
| 2     | Introduction . . . . .   | 8  |
| 3     | Progress since the last Long Range Plan . . . . .  | 11 |
| 3.1   | Macroscopic: collectivity, flow and thermal properties . . . . .   | 11 |
| 3.1.1 | The hydrodynamic limit of QCD: collectivity, flow and transport coefficients of quark-gluon plasma . . . . . | 11 |
| 3.1.2 | Mapping the QCD phase diagram . . . . .  | 18 |
| 3.1.3 | Thermal photons/dileptons . . . . .  | 23 |
| 3.1.4 | Initial condition . . . . .  | 27 |
| 3.1.5 | Chirality and vorticity in QCD . . . . .   | 32 |
| 3.2   | Mesoscopic: emergence of the quark-gluon plasma and approach to equilibrium . . . . .                        | 37 |
| 3.2.1 | Small Collision Systems . . . . .  | 37 |
| 3.2.2 | Small systems & small size limit of the QGP . . . . .  | 37 |
| 3.2.3 | Onset of hydrodynamics . . . . .   | 40 |
| 3.2.4 | Medium response of partonic excitations . . . . .  | 44 |
| 3.2.5 | Jet Modification in Small Systems . . . . .  | 46 |
| 3.3   | Microscopic I: Jets and leading hadrons . . . . .  | 48 |
| 3.3.1 | Simultaneous results from end-to-end simulator frameworks . . . . .  | 49 |
| 3.3.2 | Jet quenching theory . . . . .   | 52 |
| 3.3.3 | Phenomenology of Hard Heavy Flavors . . . . .  | 58 |
| 3.3.4 | Jets, leading hadrons and coincidence measurements . . . . .   | 60 |
| 3.3.5 | Jet substructure . . . . .   | 62 |
| 3.3.6 | Heavy-flavor tagged jets . . . . .   | 67 |
| 3.3.7 | Bayesian methods for hard probes . . . . .   | 69 |
| 3.4   | Microscopic II: Quarkonia, open heavy flavor, electromagnetics and bound states . . . . .                    | 71 |
| 3.4.1 | Theory: heavy flavor . . . . .   | 71 |
| 3.4.2 | Experiment: quarkonia . . . . .  | 75 |
| 3.4.3 | Experiment: open heavy flavor . . . . .  | 78 |
| 3.4.4 | Exotic hadronic bound states . . . . .   | 82 |
| 3.4.5 | Electroweak processes . . . . .  | 83 |
| 3.4.6 | Ultra-peripheral Collisions . . . . .  | 87 |
| 3.5   | Interdisciplinary . . . . .  | 95 |
|       | Nuclear structure . . . . .  | 95 |
|       | Quantum electrodynamics and physics beyond the standard model . . . . .                                      | 95 |
|       | Phase diagram and relativistic fluid dynamics in astrophysics . . . . .                                      | 95 |
|       | Machine learning . . . . .   | 95 |
| 4     | Hot QCD facilities . . . . .   | 96 |
| 4.1   | RHIC . . . . .   | 96 |
| 4.2   | LHC . . . . .  | 98 |

|       |  |     |
|-------|--|-----|
| 5     | Future Prospects . . . . .   | 100 |
| 5.1   | Macroscopic: collectivity, flow and thermal properties . . . . .                           | 100 |
| 5.1.1 | Open Questions and Future opportunities related to collectivity . . . . .                  | 100 |
| 5.1.2 | Narrowing the QCD critical point search . . . . .  | 102 |
| 5.1.3 | Future opportunities to study thermal properties of the QGP . . . . .                      | 103 |
| 5.1.4 | Future opportunities for studying the initial conditions . . . . .                         | 104 |
| 5.1.5 | Future opportunities to study chirality and vorticity in heavy-ion collisions . . . . .    | 105 |
| 5.2   | Mesoscopic: emergence of the quark-gluon plasma and approach to equilibrium . . . . .      | 107 |
| 5.2.1 | Future Experimental Exploration of Collectivity in Small Systems . . . . .                 | 107 |
| 5.2.2 | The next steps for understanding small systems . . . . .                                   | 108 |
| 5.2.3 | Prospective studies of medium response to partonic excitation . . . . .                    | 109 |
| 5.2.4 | Further investigations of jet quenching in small systems . . . . .                         | 110 |
| 5.3   | Microscopic: Hard Probes . . . . .   | 110 |
| 5.3.1 | Prospective jet measurements and theoretical advances . . . . .                            | 110 |
| 5.3.2 | Prospective heavy-flavor and quarkonia measurements and theoretical advances . . . . .     | 112 |
| 5.3.3 | Prospective measurements and theoretical advances related to initial state nPDFs . . . . . | 117 |
| 6     | Summary . . . . .  | 122 |

## 1 Executive Summary

Collisions of large nuclei at the Relativistic Heavy Ion Collider (RHIC) and the Large Hadron Collider (LHC) create a plasma of quarks and gluons with the properties of the early Universe, including an extraordinarily high temperature and near symmetry between matter and antimatter. This “hot” regime of Quantum Chromodynamics (QCD) lies at the intersection of nuclear physics with many-body quantum field theory, relativistic fluid dynamics, and condensed matter, probing the dynamical properties of quarks and gluons — the fundamental degrees of freedom of nuclear matter — at extreme densities and temperature. The newly built and mission-critical sPHENIX detector, and complementary STAR upgrades at RHIC, together with increased luminosity at the LHC and upgraded detectors at ALICE, ATLAS, CMS and LHCb, will enable a multimessenger era for hot QCD based on the combined constraining power of low-energy hadrons, jets, thermal electromagnetic radiation, heavy quarks, and exotic bound states. Successful theory collaborations [1–3] have paved the way for significant developments and breakthroughs in the next decade; state-of-the-art numerical simulations, assisted by machine learning techniques, will provide quantified uncertainties on the viscosities, jet transport coefficients, and other properties of the plasma, including detailed information on these quantities’ dependence on the plasma’s temperature. Meanwhile, experimental measurements exploring the formation of quark-gluon plasma at the proton scale will provide an unparalleled opportunity to understand the regime of applicability of relativistic fluid dynamics, which will transform our understanding of this topic. The phase diagram of nuclear matter will be redrawn by the analysis results of the completed RHIC systematic scan of collision energies, which probes the high baryon density regime of hot QCD, in synergy with astrophysical constraints from electromagnetic and gravitational observations of neutron stars and their mergers.

The purpose of this document is to serve as input to the U.S. Long Range Plan for Nuclear Physics by providing additional context and support for the goals of the hot QCD community described in the white paper from the Joint Hot/Cold QCD Town Hall meeting. The recommendations and initiatives established by the QCD community during the Town Hall Meeting at MIT in September 2022 are described in a separate white paper. The present document focuses on hot QCD physics by highlighting the scientific progress since the 2015 Long Range Plan, describing the recent successes and plans for the experimental facilities, and future prospects for addressing remaining open questions. Following the immensely successful implementation of the previous Long Range Plan recommendations, we recommended the following, based on the requirements to advance the understanding of hot QCD physics in the next decade and beyond.

### **Capitalizing on past investments at RHIC, the LHC, and theory**

Building upon previous investments, we recommend support for full operation of the RHIC facilities, maintaining U.S. leadership within the LHC heavy-ion program, and a healthy base theory program, as well as for the scientists involved in all these efforts.

- Our understanding of QCD was transformed by the discoveries at RHIC in previous decades. To successfully complete the previously established RHIC scientific mission, it is crucial to support the RHIC running necessary for the sPHENIX program [4] as well as the resources to fully analyze the data collected from all RHIC experiments, including the highly successful Beam Energy Scan-II. The planned RHIC running will also enable STAR to extend measurements in the rapidity with its new forward upgrades [5]. As RHIC is a unique and versatile facility capable of addressing several open questions, we note the additional opportunities described in the sPHENIX and STAR Beam Use Proposals if an opportunity for additional RHIC running occurs [4,5].
- The LHC, the world’s premier facility at the energy frontier, enables detailed studies of QCD at the highest temperatures through its ultrarelativistic heavy-ion program. It is essential for the U.S. to maintain its established leadership within the heavy-ion LHC program through data analysis as

well as important detector upgrades across ALICE, ATLAS, CMS and LHCb, including the proposed ALICE 3 detector [6].

- Advancements of QCD and interpretation of measurements rely on a strong theory community pushing to advance the field, working in close collaboration with the experimental community. Collaborations such as BEST and JETSCAPE, focused on collectively addressing specific outstanding challenges, have proven extremely successful. Robust support for the base theory program, including opportunities for theorists to learn and exchange ideas, are also crucial for advancing our understanding of QCD and developing the direction of future experimental pursuits.

### **Increasing U.S. participation in the LHC Heavy-Ion Program**

As RHIC is transformed into the Electron-Ion Collider (EIC), the LHC heavy-ion program will become the world's leading hot QCD facility. To maintain U.S. leadership in experimental hot QCD physics, supporting increased participation in the LHC programs is crucial, including detector upgrades required to capitalize on the planned luminosity increase. This luminosity will enable more precise measurements of rare probes and more differential measurements, strengthening our understanding of the underlying physics as the field evolves from discoveries to precision science.

Supporting targeted detector R&D and U.S.-led upgrades at the LHC experiments will enable opportunities for new and unique measurements, train the next generation of nuclear physicists and enhance the synergy between collider programs at LHC and the future EIC.

### **Increasing resources for high-performance computing and the development of machine-learning applications and open-source software**

With the increased luminosity and massive amount of data to be collected, high-performance computing is essential for the acquisition, storage, and timely analysis of experimental data. Likewise, the growth of theoretical physics depends on the use of cutting-edge computing facilities and algorithms. Machine learning techniques are now being applied to address theoretical, numerical, and experimental challenges and require increasing investment in cutting-edge computing resources, including hardware, and in the development of a high-quality software base accessible to the community. Past successes, including the dramatic advances made in finite temperature lattice QCD calculations, would not have been possible without access to leading class computing resources, USQCD computing facilities as well as the SciDAC program. Therefore access to these state-of-the-art computing resources will be vital for continued success and additional breakthroughs [7].

### **Exploring the high baryon density frontier**

Intermediate-energy nuclear collisions at RHIC and in international facilities provide a unique opportunity to search for the QCD critical point and for evidence of a first-order phase transition at high baryon density. The field is in an unequaled position to contribute to the study of neutron stars and their mergers, combining collider constraints on the nuclear equation of state with the invaluable information now provided by gravitational wave measurements. Following the highly successful BES-II at RHIC, U.S. leadership in mapping the QCD phase diagram should continue through funding theoretical developments [8,9] and collaborations such as BEST [1], as well as exploring opportunities for participation at international experimental facilities [10].

### **Enhanced investment in the growth and development of a diverse, equitable workforce**

With the suite of opportunities in the field of hot QCD in the coming decades, a robust workforce is vital for continued success. Pursuing the above recommendations successfully will critically depend on increased attention to workforce development. Therefore, it is crucial to have an enforced community code of conduct, as well as programs to support underrepresented minority scientists and to increase diversity at every level, including faculty and leadership positions to ensure a thriving and productive community.

## 2 Introduction

Ultra-relativistic heavy ion collisions seek to understand the most extreme form of nuclear matter, the quark-gluon plasma, which formed the early universe in the first few microseconds after the Big Bang and which may be formed in the extraordinary pressures present in the merger of neutron stars. The strength of interactions of quarks and gluons allows the plasma to maintain cohesion even under its explosive relativistic expansion. This quark-gluon collectivity leads to a clear correlation between the initial geometry of colliding nuclei and the momentum anisotropy of the final particles.

Evidence for collectivity in the collision of smaller systems was confirmed by a series of experiments at RHIC with proton-gold, deuteron-gold, and  $^3\text{He}$ -gold collisions, which showed a distinct correlation between small nuclei's variable geometry and the final hadron's anisotropy measure  $v_n$  (Section 3.2.2). This observation of fluid behavior in ever-smaller collision systems provided a renewed impetus to understand the limits of applicability of relativistic fluid dynamics, and how the system can approach local equilibrium shortly after the impact of the nuclei. Insights from weakly-coupled finite-temperature field theory, holography, and kinetic theory are being combined to better understand the approach to equilibrium of strong-coupled quark-gluon plasma (Section 3.2).

The limits of the formation of quark-gluon plasma have also been probed in two extensive Beam Energy Scan experiments at RHIC. The larger net-baryon density found at lower collision energies gives access to a wider region of the phase diagram of nuclear matter, enabling the search for a critical point (Section 3.1.2). The search for a clear experimental signal of a critical point has advanced side-by-side with crucial new lattice calculations of the equation of state at finite baryon chemical potential; the latter has not found signs of a critical point at  $\mu_B/T \lesssim 2-3$ , driving the search for a critical point in the lower range of collision energies. The increasing complexity of modeling nuclear collisions at intermediate energies has been met with considerable theoretical progress, with new models of the initial condition, generalized hydrodynamic simulations with conserved charges, and more; these advances benefited considerably from the effort of the dedicated BEST topical collaboration (Section 3.1.1). Connections with the astrophysics community have been strengthened by a joint interest in constraining the phase diagram of nuclear matter in a broad range of conditions, including those found in neutron stars and in neutron-star mergers, which can now be studied by a combination of electromagnetic signals and gravitational waves.

The diverse set of measurements provided by soft hadrons, jets, soft and hard electromagnetic probes, and heavy flavors also make possible multimessenger studies in heavy-ion collisions. Aided by machine learning, multiple systematic comparisons of heavy-ion simulations with large sets of measurements have now been performed. This has provided increasingly methodical constraints on the properties of strongly-coupled quark-gluon plasma, in particular, its shear and bulk viscosity (Section 3.1.1) and the interaction rate of energetic light and heavy partons with the plasma (Section 3.3). A combination of new lattice calculations and experimental measurements, along with theoretical advances, have advanced our understanding of the formation of open heavy hadrons and quarkonium, and the insight they can provide about the properties of quark-gluon plasma (Sections 3.4.1-3.4.3).

The large experimental effort to study the modification of jets in heavy-ion collisions can now benefit from the large increase in statistical precision due to increased luminosity and the upgraded detectors which enable refined measurements of correlations between electroweak bosons and jets (Section 3.3.4), and increasingly fine-grained understanding of the internal structure of jets (Section 3.3.5). Open software modeling environments such as the JETSCAPE framework can now provide a systematic comparison of jet calculations with this ensemble of new measurements. Modeling advances now make it possible to study both the interaction of hard partons with the quark-gluon plasma and the resulting wake left in the plasma by the parton (Section 3.2.4). This ability to study the plasma's response to these perturbations provides an important connection to the plasma's approach to equilibrium early in the collision (Section 3.2.3).



The isobar program at RHIC made possible a careful search for signals of the chiral magnetic effect in nuclear collisions (Section 3.1.5). The observed sensitivity of the results to small differences in the nuclear structure of the two isobars exemplifies the challenge of this undertaking, with only upper limits established at this point. The large magnetic field behind the chiral magnetic effect may also have a measurable effect on the polarization of hyperons. While not yet showing sensitivity to the magnetic field, hyperon polarization from the plasma's large vorticity has been successfully measured (Section 3.1.5).

The observed sensitivity of heavy-ion collisions to the nuclear structure is one of many examples that highlight the interdisciplinary nature of heavy-ion collisions (Section 3.5). Studies of ultra-peripheral collisions have made a number of connections with other fields, including with the physics of the future Electron-Ion Collider. A joint interest in dense nuclear matter and relativistic fluids is also fostering close collaborations between the heavy-ion and astrophysics communities. Additional interdisciplinary collaborations include the community's involvement with machine learning, quantum computing, holographic studies of strongly-coupled systems, and more.

The progress accomplished since the last Long Range Plan is organized below into three broad categories. The "macroscopic" section covers work related to collectivity, flow, and the thermal and near-thermal properties of strongly-coupled nuclear matter. This covers hydrodynamic simulations of heavy-ion collisions, including the initial conditions used for these simulations, along with studies of the nuclear equation of state, the production of soft thermal electromagnetic probes by the plasma, and studies of chirality and vorticity. The "mesoscopic section" focuses on the limits of collectivity in nuclear collisions: evidence of collectivity in collisions of small nuclei and the evolving understanding of the applicability of hydrodynamics in lower multiplicity systems. The thermalization of systems in the early stage of heavy-ion collisions is also discussed, and the related topic of jet wake thermalization closes this subsection. The final "microscopic" section transitions from a macroscopic description of strongly-coupled quark-gluon plasma to a microscopic description of particles interacting with the plasma and other particle production. Jet physics represents a major part of this section, including the theory of parton-plasma interactions, jet substructure as well as light and heavy quark jet observables. Heavy quarks and their dynamical evolution in the plasma are further discussed. Also included in this section are the production of electroweak bosons, the study of the exotic hadronic bound states, and the rich physics of ultra-peripheral collisions. This same breakdown of topics is used in the future prospects section. The facilities section describes how the facilities have contributed to the progress to date as well as how the current and future upgrades including the newly constructed sPHENIX experiment recommended in the previous Long Range Plan will contribute to the next decade of progress and beyond.

While not a complete list, some of the key objectives of the hot QCD community in the next decade include:

- Continue the community's pioneering work on understanding the foundation of relativistic fluid dynamics, the limits of its applicability in low multiplicity or far-from-equilibrium systems, and the connections of these topics with attractors;
- Further constrain the location of a QCD critical point and study the phase diagram at high baryon chemical potential;
- Explore innovative ways to experimentally observe the chiral magnetic effect and chiral symmetry restoration;
- Use thermal photons and dileptons to probe the early stages of large and small system collisions;
- Determine the origin of collectivity in small systems;

- Utilize measurements of the jet-induced medium response to further our understanding and theoretical description of the jet-medium interface;
- Advance our understanding of the jet fragmentation process and its modification in heavy-ion collisions through detailed jet substructure measurements.
- Utilize new heavy-quark measurements to determine the heavy-quark diffusion coefficient and its temperature dependence.
- Improve the description of the three-dimensional structure of the initial state and its connection to the evolution of the produced QGP in heavy-ion collisions.

The summary, Sec. 6, describes the resources needed to address these questions in the next several years. These needs align well with the recommendations resulting from the Joint Hot/Cold QCD Town Hall meeting.

### 3 Progress since the last Long Range Plan

#### 3.1 Macroscopic: collectivity, flow and thermal properties

##### 3.1.1 The hydrodynamic limit of QCD: collectivity, flow and transport coefficients of quark-gluon plasma

Through long-standing efforts from both theory and experiment, the field of heavy-ion collisions is at the state of the art in terms of developing, testing, and simulating relativistic viscous fluid dynamics [11–13]. Since the last long-range plan, significant progress has been made in understanding the initial state immediately after two heavy ions collide, extracting transport coefficients at vanishing baryon densities, precisely reproducing experimental data, and the nature of collective flow in small systems, the development of relativistic spin hydrodynamics, the theoretical description of a multi-component relativistic fluid, and coupling hydrodynamics to jets and hadronic interactions. Because of these advances in relativistic viscous hydrodynamics, it has paved the way for new discoveries such as interdisciplinary connections through nuclear structure [14–18], out-of-equilibrium effects in neutron star mergers [19, 20], cold atom quantum analogs of the quark-gluon plasma (QGP) [21, 22], and statistical analysis techniques [23]. Below we will outline the developments in the field over the last 7 years and then we will explore open questions and new opportunities.

##### Standard Model of Heavy-ion collisions

Figure 1 provides a schematic demonstration of the “standard model” of heavy-ion collisions, that has been developed over a number of decades<sup>1</sup>. Radial flow occurs due to a greater pressure at the centre of the QGP compared to the outskirts, and this leads to a common velocity field outwards. The rate of the hydrodynamic expansion is influenced by the QGP’s bulk viscosity ( $\zeta/s$ ), which is its resistance to volume growth. Anisotropic flow is the result of a directional dependence to these pressure gradients. This occurs due to spatial anisotropies in the initial state. These arise if the collision zone is almond shaped (at  $b > 0$ ), or due to the lumpiness of the initial state. Such spatial anisotropies are converted to momentum anisotropies via the hydrodynamic response. This is influenced by the QGP’s shear viscosity ( $\eta/s$ ), which quantifies the resistance to fluid deformation.

A key development during recent times was the democratization of initial state models that can reproduce experimental data. The geometrical shape of the impact region of two colliding heavy ions can be quantified through a series of eccentricities

$$\mathcal{E}_{n,m} \equiv -\frac{\int r^m e^{in\phi} \rho(r, \phi) r dr d\phi}{\int r^m \rho(r, \phi) r dr d\phi} \quad (1)$$

wherein the indices  $n, m$  correlate various harmonics such that  $n = m = 2$  is the elliptical eccentricity and  $n = m = 3$  is the triangular eccentricity. Large pressure gradients (that appear due to the geometrical shape of the initial state) lead to flow such that over time an elliptical shape in the initial state is transformed into an elliptical shape in momentum space, which is possible to measure experimentally using azimuthal anisotropies or otherwise known as collective flow harmonics  $V_n$ . Careful studies using Pearson coefficients [24] have determined that linear response ( $V_n \sim \kappa_n \mathcal{E}_{n,n}$  where  $\kappa_n$  is some constant that encodes medium effects) is the predominant contribution to  $V_n$ , especially in central collisions. Because of linear response in certain regimes, one can directly compare ratios of eccentricities e.g.  $\frac{v_n\{4\}}{v_n\{2\}} \sim \frac{\varepsilon_n\{4\}}{\varepsilon_n\{2\}}$  to experimental data excluding a number of initial state models [25, 26] and providing a clear benchmark for models to pass. However, in peripheral collisions [27], low beam energies [28], and in small systems, the non-linear response of the final flow harmonics to the initial state [29] as well as out-of-equilibrium effects [30] begin to dominate. Now open-source codes that pass benchmarks of multi-particle cumulant ratios of eccentricities (e.g. T<sub>R</sub>ENTo [31] and IP-Glasma [32]) exist, such that the entire community has access to initial conditions

<sup>1</sup>This figure was inspired by illustrations from Chun Shen.

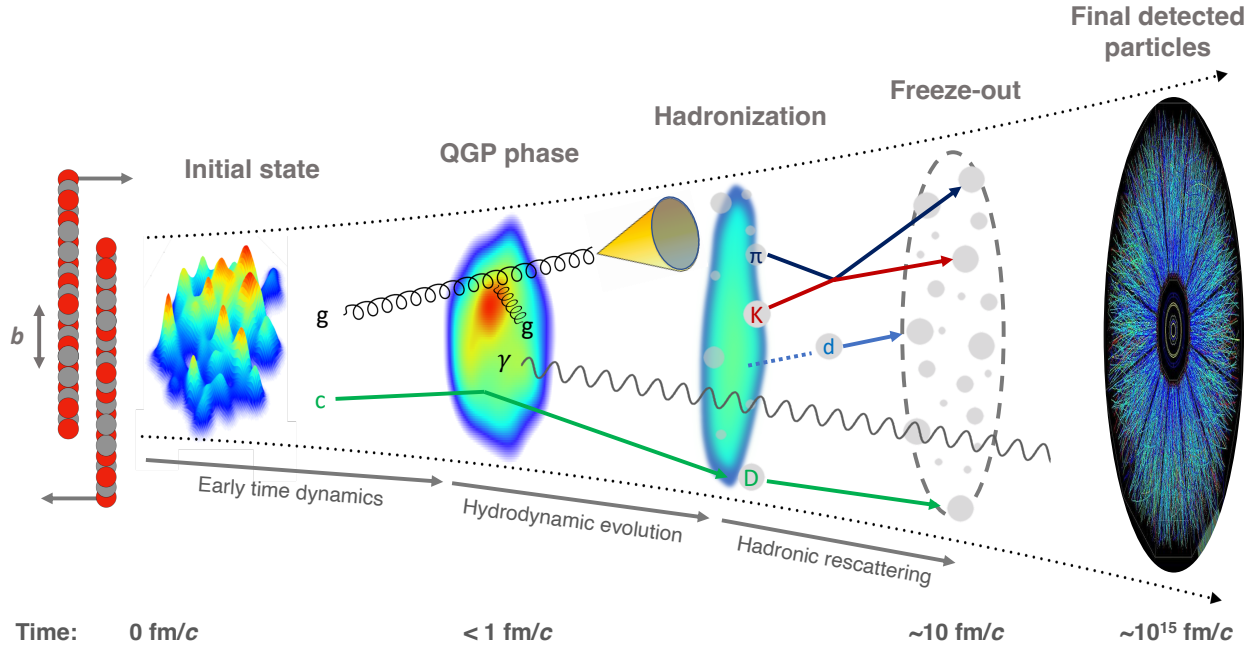


Figure 1: An illustration of different stages in a heavy-ion collision. The event display at the final stage is an iconic picture from the STAR experiment at RHIC.

that can reproduce experimental data. This has significantly reduced uncertainty in the extraction of transport coefficients and allows physicists to study questions that require greater precision than was previously possible.

Due to the far-from-equilibrium nature of the initial state in heavy-ion collisions, it is possible that the energy-momentum tensor from the initial state,  $T_0^{\mu\nu}$ , cannot be used directly input into hydrodynamics. At finite densities this is further complicated by out-of-equilibrium currents for initial baryon  $B^\mu$ , strangeness  $S^\mu$ , and electric charge  $Q^\mu$ . Hydrodynamics is applicable in the limit when the system has a large separation of scales. For example, the small scale,  $l$ , of a pond relates to the interactions of individual  $H_2O$  molecules whereas the large scale,  $L$ , of a pond is simply the size of the pond. Hydrodynamics is applicable when  $l \ll L$ . In heavy-ion collisions (especially for the initial state), it is not as clear that  $l \ll L$  and, therefore, it is generally believed that a pre-equilibrium stage exists in heavy ions where some dynamics occur until time  $\tau_{hyd}$  such that the initial energy momentum tensor,  $T_0^{\mu\nu}$ , is evolved in time until an energy momentum tensor is reached that is more compatible with hydrodynamics,  $T_{hyd}^{\mu\nu}$ . There are a number of strong theoretical arguments which highlight the need for a pre-equilibrium stage such as the violation of causality and stability if  $T_0^{\mu\nu}$  is applied directly to hydrodynamics [33, 34], the relation between  $\tau_{hyd}$  to the  $R_{AA} \times v_2$  puzzles in jets, and in order to handle large momentum-space anisotropies in the local rest frame [35]. These physics topics are covered in more detail in other sections, discussing the many open questions and future opportunities to explore, especially as one begins to explore jet-medium interactions and their influence on hydrodynamics (Sections 3.3 and 3.2.4) and far-from-equilibrium systems that are relevant to ultra-small systems (Section 3.2.1), such as those presumably created in collisions involving very small nuclei such as protons or deuterons.

The backbone of heavy-ions simulations is relativistic viscous hydrodynamics wherein a variety of 2+1D and 3+1D codes exist that incorporate shear and bulk viscosity [36–42] and are beginning to incor-

porate finite baryon densities [43, 44] and even strangeness and electric charge [45–48]. Then relativistic viscous hydrodynamic equations of motion have the general form of [49]

$$\tau_X \dot{X} + X = -(\omega + \frac{\tau_X}{2} X)\theta + \text{2nd order terms} + \text{coupling terms} \quad (2)$$

where  $X = \pi^{\mu\nu}, \Pi, n^\mu, \dots$  for the shear stress tensor, bulk pressure, and the diffusion currents associated with baryon number, strangeness, and electric charge, which have the associated first order transport coefficients of shear viscosity  $\eta$ , bulk viscosity  $\zeta$ , and charge diffusion matrix  $\kappa_{ij}$  where  $ij$  can be a combination of multiple conserved charges. These first-order transport coefficients have been studied quite extensively in a variety of theoretical frameworks. Due to the fermion sign problem [50], one cannot currently calculate these transport coefficients from lattice QCD but it is possible using perturbative QCD. Using these perturbative QCD calculations,  $\eta/s$  has been calculated for vanishing baryon densities [51] at next-to-leading order and at finite baryon densities  $\eta T/(\varepsilon + p)$  has been calculated at leading log [52] (note that  $\varepsilon + p = sT$  for vanishing densities such that  $\eta T/(\varepsilon + p)$  simplifies to  $\eta/s$  at  $\mu_B = 0$ ). In the future, it may be possible to calculate  $\eta/s$  directly from quantum computing. In the meantime, there is interest in developing quantum algorithms in order to calculate  $\eta/s$  directly from Quantum Chromodynamics (QCD) [53]. Unlike  $\eta/s$ , bulk viscosity  $\zeta/s$  is not possible to calculate within a conformal field theory and is precisely most relevant in the extremely non-perturbative regime around the QCD phase transition. Thus, it is not possible to calculate  $\zeta/s$  in the cross-over region from perturbative QCD, and other approaches are required. Recent calculations of bulk and shear viscosity both at  $\mu_B = 0$  and at finite  $\mu_B$  from other theoretical approaches include non-conformal holography [54], hadron resonance gas (HRG) model [55–59], transport theory [60, 61], Color String Percolation Model [62], linear sigma model [63], quasi-particle models [64, 65], or QCD-motivated alternatives [51, 66–68]. In the cross-over phase transition, relevant at vanishing baryon densities, then one expects a continuous matching between these transport coefficients in the hadron gas phase to the QGP phase [69]. Thus, calculations of  $\eta$  and  $\zeta$  within a hadron resonance gas also are of extreme interest and it appears that it is only possible to reproduce the extremely small minimum of  $\eta/s$  (from phenomenological approaches) or a peak in  $\zeta/s$  if sufficiently many hadrons exist and they are also very strongly interacting [70]. Transport coefficients associated with diffusion,  $\kappa_{ij}$ , have many other subtleties that will be explored further later on and also in Section 5.1. However, we note that even at the LHC and top RHIC energy, it may be possible to constrain baryons, strangeness, and electric charge diffusion using charge fluctuations due to gluons splitting into quark anti-quark pairs [71].

After the fluid has expanded and cooled sufficiently to fall below the QCD (crossover) phase transition, one must switch from a fluid into a gas of interacting hadrons. Generally, simulations rely on the Cooper-Frye approach [72] wherein one uses a Fermi-Dirac distribution to account for equilibrium  $f_{eq}$  and out-of-equilibrium corrections from shear viscosity  $\delta f_\eta$ , bulk viscosity  $\delta f_\zeta$ , and diffusion  $\delta f_{\kappa_{ij}}$  such that

$$f = f_{eq} + \delta f_\eta + \delta f_\zeta + \delta f_{\kappa_{ij}} \quad (3)$$

which can be used to calculate the particle spectra for each hadron species. Typically groups sample over this spectrum (at finite densities conservation of baryons, strangeness, and electric charges is important to consider) to produce particles that are then fed into hadronic afterburners like SMASH [73] where the particles first undergo chemical freeze-out, followed by kinetic freeze-out. From the final particle spectra after kinetic freeze-out one can then obtain collective flow observables that can be compared directly to experimental data.

This standard model of heavy-ion collision simulation setup is not just for soft observables, though. These hydrodynamic backgrounds are then used to produce jets, heavy flavor, or electromagnetic probes as well. In fact, it has been shown that subtle details in hydrodynamics as in the shear viscosity, using event-by-event simulations, or varying  $\tau_{hydro}$  can affect jets and heavy flavor observables. Recently, groups are taking

this a step further and fully incorporating jets into the hydrodynamic simulations using source terms that dump energy into the medium (see Section 3.2.4). Such approaches provide a fantastic opportunity to study far-from-equilibrium physics in the dense medium as well as multiscale problems across the entire range of momentum. Hydrodynamic predictions have been successful at reproducing collective flow in small systems and even making predictions [74, 75] for the PHENIX small system scan [76].

Over the past decade, one intriguing puzzle has arisen in the field of relativistic viscous fluid dynamics. What is the small droplet of the QGP and at what point does the fluid dynamic picture break down? In systems as small as proton-ion, proton-proton, and even  $\gamma^*$ -ion signatures of the QGP have appeared for collective flow, strangeness enhancement, and heavy flavor flow. However, the energy loss of high  $p_T$  particles has puzzled theorists and experimentalists alike (see Sec. 3.3). On the theoretical side, progress has been made in understanding these tiny droplets of fluid. It has been found that the pre-equilibrium phase can play a crucial role [30, 41, 77–79], the new for sub-nucleonic fluctuations have been necessary to describe certain flow observables [80–82], and a new core-corona approach wherein the interior of QGP is treated as a fluid but the exterior is treated either as jet-like or via hadronic interactions [83, 84] (especially important for strange particles).

Another direction that relativistic viscous hydrodynamics has taken is to explore large baryon densities that are relevant for the Beam Energy Scan (and more specifically at low beam energies). At low beam energies, the initial conditions become full 3-dimensional and may not reach hydrodynamization at a single initial time. Thus, groups have developed 3D initial conditions with baryon stopping with strings [85] or used hadron transport models [47]. Then, hydrodynamics must include the conservation of baryon number that also leads to a finite baryon diffusion, which has been recently implemented in a number of models [43, 44]. Meanwhile, groups have derived the theoretical framework for understanding critical fluctuations with hydrodynamics [86–97], termed “Hydro+” [98], and have applied this framework to low-dimension hydrodynamic toy models [99]. Studies in these low-dimensional hydrodynamic toys models have found interesting connections to out-of-equilibrium effects that may lead to potential signatures of the QCD critical point [100–102], but they must be tested first in more realistic simulations. However, a number of further steps are required in order to search for the QCD critical point or other interesting phase structures, which will be discussed in Section 5.1.

### Collective flow Observables

Since the previous Long Range Plan, a number of measurements sensitive to the hydrodynamic response have entered the precision era. The uncertainties associated with some of these bulk observables are typically on the order of a percent in heavy-ion collisions - for a recent review of such observables at the LHC, see here [103]. These measurements are therefore now used to provide strong constraints to the medium properties relevant for the studies of heavy-flavor and jet interactions in the QGP. A hallmark of the hydrodynamic response is the mass ordering observed for the  $p_T$  dependence of elliptic flow of various hadron species in the light flavor sector. Figure 2 shows the most recent measurements in Pb+Pb collisions at the LHC. The corresponding measurements are simultaneously sensitive to elliptic and radial flow, with elliptic flow leading to finite  $v_2$  values, and radial flow inducing a mass splitting at a fixed  $p_T$ . Therefore, these measurements constrain both  $\eta/s$  and  $\zeta/s$  respectively. The hydrodynamic predictions shown from T<sub>R</sub>ENTo+VISHNU are based on a Bayesian analysis of separate observables in the soft sector. They describe the mass ordering extremely well at low  $p_T$ . A divergence is observed for  $p_T > 1.5$  GeV/c, where non-equilibrium effects start to contribute. The clearest manifestation of these effects is observed via the baryon/meson grouping of  $v_2$  at higher  $p_T$ , which can be explained by quark coalescence processes. Identified light hadron flow measurements have also been performed for a variety of collision systems recently. At RHIC, these include collisions of Cu+Au at  $\sqrt{s_{NN}} = 200$  GeV [104] and U+U at  $\sqrt{s_{NN}} = 193$  GeV [105], while at the LHC these include Xe+Xe at  $\sqrt{s_{NN}} = 5.44$  TeV [106]. They have also been explored for higher orders of anisotropic flow, with examples from RHIC for Au+Au collisions at  $\sqrt{s_{NN}} = 200$  GeV [107], and

Pb+Pb collisions at the top LHC energy [108, 109].

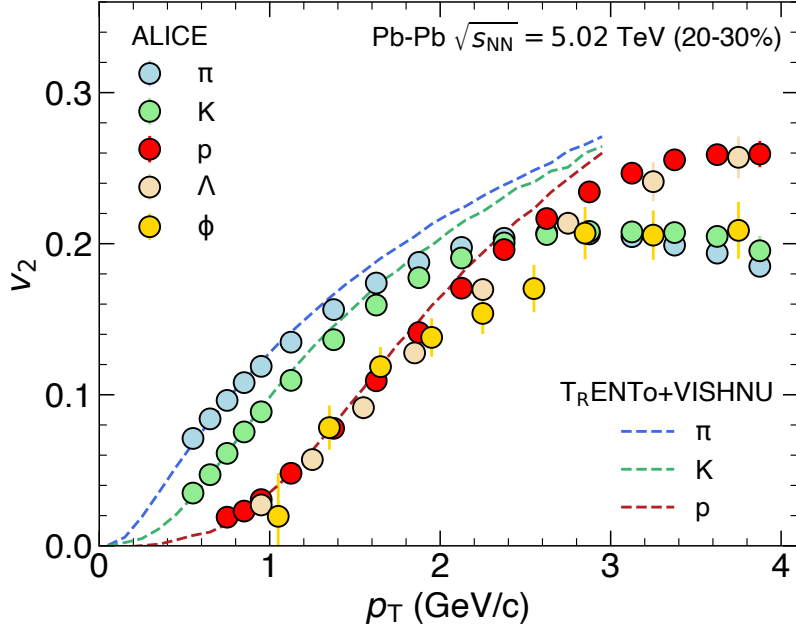


Figure 2: The  $p_T$  dependence of elliptic flow in Pb+Pb collisions at the LHC for various particle species. The data are from the ALICE experiment [108]. The curves represent estimations extracted from T<sub>R</sub>ENTo+VISHNU based on a Bayesian analysis that determines the optimal hydrodynamic parameters from other observables [23].

A key example of more differential endeavors regarding the investigations into hydrodynamic response, pursued since the last Long Range Plan, is given by measurements of Symmetric Cumulants (SC( $k, l$ )). These extend the study of the individual flow amplitudes  $v_n$  at low  $p_T$  to correlations between event-by-event fluctuations of flow coefficients [110–114]. Hydrodynamic calculations show that while  $v_2$  and  $v_3$  exhibit an approximately linear dependence on the corresponding eccentricities  $\epsilon_2$  and  $\epsilon_3$ , respectively, the higher order  $v_n$  coefficients (i.e., for  $n > 3$ ) have also non-linear contributions from  $\epsilon_2$  and  $\epsilon_3$  in addition to the linear ones from  $\epsilon_n$  [115–118]. These observations lead to non-trivial correlations between different flow coefficients which result in new and independent constraints on the initial conditions and  $\eta/s$ . The left panel of Figure 3 presents the centrality dependence of correlations between  $v_n$  coefficients (up to the 5<sup>th</sup> order) from Symmetric Cumulants, which are defined as:

$$SC(k, l) \equiv \langle v_k^2 v_l^2 \rangle - \langle v_k^2 \rangle \langle v_l^2 \rangle \quad (4)$$

The results shown are for Pb+Pb collisions at  $\sqrt{s_{NN}} = 2.76$  TeV [119, 120]. The correlations among different flow coefficients depend on harmonic, as well as collision centrality [120]. Positive values of SC(4,2), SC(5,2), and SC(5,3) and negative values of SC(3,2) and SC(4,3) are observed for all centralities. These indicate that event-by-event fluctuations of  $v_2$  and  $v_4$ ,  $v_2$  and  $v_5$ , and  $v_3$  and  $v_5$  are correlated, while  $v_2$  and  $v_3$ , and  $v_3$  and  $v_4$  are anti-correlated. Furthermore, the lower-order harmonic correlations are much larger than the higher-order ones. Measurements from ATLAS and CMS for Pb+Pb collisions at the LHC [122, 123], and STAR for variety of Au+Au collision energies [124], show similar trends. The SC observables are compared with EKRT [121] and T<sub>R</sub>ENTo+VISHNU [23] predictions in the right panel of Figure 3. The EKRT calculations are shown for two temperature-dependent  $\eta/s$  parameterizations that provide the best description of RHIC and LHC  $v_n$  data: the constant  $\eta/s = 0.2$ , and “param1” [121].

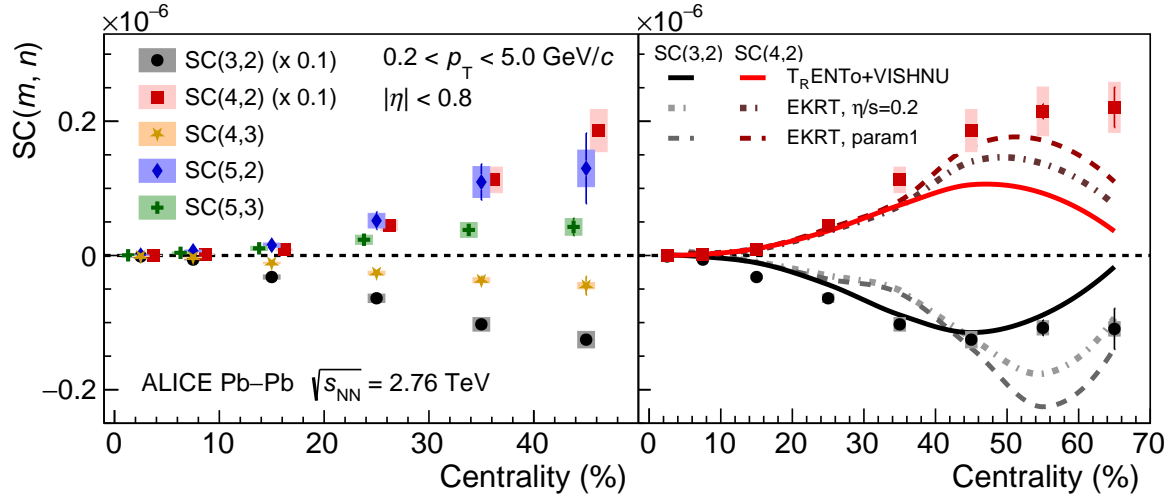


Figure 3: Centrality dependence of event-by-event flow harmonic correlations in Pb+Pb collisions at  $\sqrt{s_{\text{NN}}} = 2.76$  TeV [119, 120] compared with various hydrodynamic calculations [23, 121].

The “param1” parameterization is characterized by a moderate slope in the temperature dependence of  $\eta/s$  which decreases (increases) in the hadronic (QGP) phase and the phase transition occurs around 150 MeV. The measurements of SC(3,2) and SC(4,2) are not described simultaneously in each centrality interval by the EKRT calculations. However, such a comparison does demonstrate the sensitivity of SC( $m, n$ ) to the temperature dependence of  $\eta/s$  - the EKRT predictions are clearly different for the two parameterizations. Measurements of SC(4,2) are better described by the T<sub>R</sub> ENTo+VISHNU predictions for Pb+Pb collisions at  $\sqrt{s_{\text{NN}}} = 2.76$  TeV, however this is not the case for SC(3,2). These predictions utilize the same hydrodynamic parameters as those shown in Figure 2. Hydrodynamic calculations describe a wide variety of additional experimental results, which reveal many facets of the QGP dynamical evolution. Such results include the energy dependence of  $\Lambda$  global polarization values [125–127], and  $\Lambda$  longitudinal polarization measurements at RHIC and the LHC [128, 129]. These will be discussed further in Section 3.1.5. They can also describe measurements of higher-order flow coefficients (up to  $v_8$ ) [130, 131], non-linear contributions to higher-order flow coefficients [132, 133], and symmetry plane correlations [132, 134, 135]. All of these results are new with respect to the last Long Range Plan. On the other hand, for reasons subject to much theoretical attention, hydrodynamic predictions cannot describe measured anisotropic flow coefficients at LHC energies in ultra central Pb+Pb collisions to the same degree of accuracy as mid-central Pb+Pb collisions. This is referred to as the “ultra central flow puzzle” [136], and persists even with the most state of the art hydrodynamic models [137]. In addition, hydrodynamic calculations cannot describe balance-function widths [103, 138], which might be explained by charge diffusion effects not implemented in these calculations. The differences with respect to the data can therefore provide a crude measure of charge diffusion, another key QGP transport parameter.

Nonetheless, the success of hydrodynamic models in describing a wide variety of experimental observables implies that the system is strongly coupled at momentum scales corresponding to the QGP temperature, as hydrodynamics describes the evolution of the QGP in terms of a liquid. The question then becomes quantitative – how strong is the coupling – and values of the shear ( $\eta/s$ ) and bulk ( $\zeta/s$ ) viscosities per entropy density play a central role in addressing this question. In the strong-coupling picture, both



transport properties  $\eta/s$  and  $\zeta/s$  are proportional to the shear and bulk relaxation times. As the initial state is highly non-uniform, this leads to large non-equilibrium shear and bulk pressures at early times. The shear and bulk relaxation times determine how quickly the system can ease these pressures and develop flow – if the coupling is large, these times will be small, which corresponds to small values of  $\eta/s$  and  $\zeta/s$ , and vice versa. Measurements from a suite of soft sector observables at RHIC (e.g. [142–144]) and the LHC

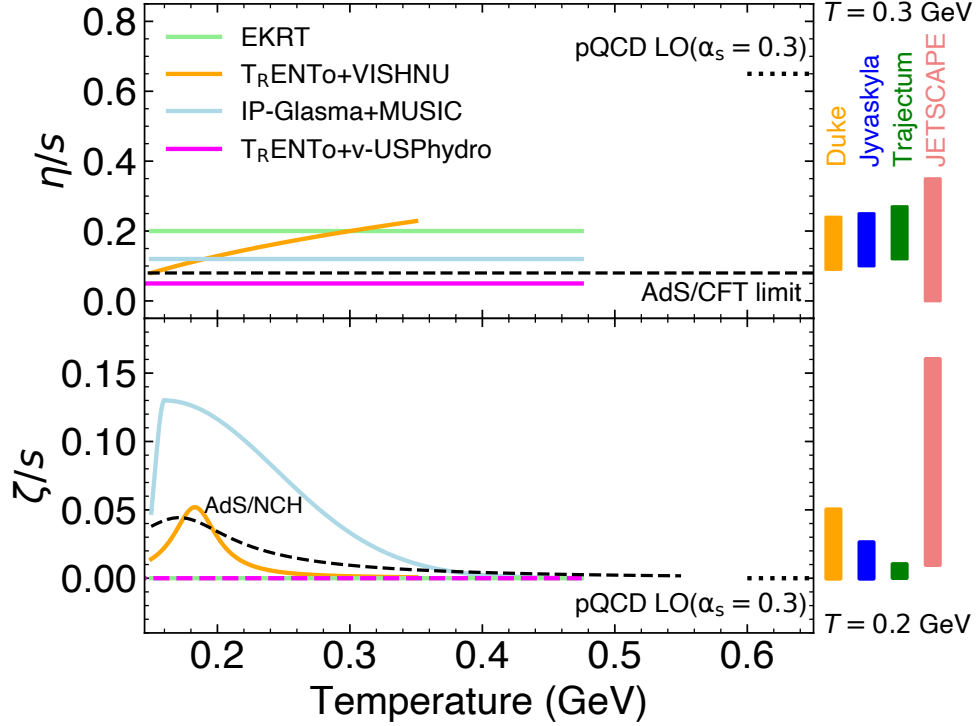


Figure 4: The temperature dependence of the shear (top panel) and bulk (bottom) viscosities over entropy density in the QGP phase constrained by RHIC and LHC measurements from various hydrodynamic models described in the text. Limits from pQCD [139], AdS/CFT [140], and AdS/Non-Conformal Holographic [141] approaches are also shown. The ranges on the right of the plot represent 90% posterior intervals from the Bayesian analyses. The figure is taken from elsewhere [103].

(e.g. [145–149]) have allowed for an exploration of the temperature dependence of  $\eta/s$  and  $\zeta/s$  in heavy-ion collisions.

Figure 4 compares these dependencies for four hydrodynamic model chain calculations constrained by RHIC and LHC data. Regarding  $\eta/s$ , many other fluids exhibit a temperature dependence for  $\eta/s$ , with a minimum occurring at the phase transition temperature between the gas and liquid phases. Whether such a temperature dependence exists for the QGP phase is an open question for the temperatures probed by heavy-ion collisions, as demonstrated in the top panel of Figure 4. The models utilize either an independence (IP-Glasma+MUSIC [150] and EKRT [121]), or a weak dependence ( $T_{\text{RENTO}}+\text{VISHNU}$  [23]). All provide a reasonable description of anisotropic flow measurements. The corresponding shear relaxation time range is  $\tau_{\pi} = 0.15\text{--}0.40$  fm/c at  $T = 0.5$  GeV, which implies that spatial anisotropies from the initial state are rather quickly developed into momentum anisotropies in the QGP phase. Two coupling limits are shown: an AdS/CFT limit which is calculated for infinite coupling, and a pQCD limit, which is determined in leading order for  $\alpha_S = 0.3$ . In the weak-coupling picture,  $\eta/s$  is inversely related to the coupling strength – therefore the  $\alpha_S$  chosen corresponds to the strongest possible coupling (therefore the lowest  $\eta/s$ ) in that scheme. It is

clear that the extracted  $\eta/s$  values are closer to the infinite-coupling limit. Nonetheless, it should be pointed out that next-to-leading-order corrections for the pQCD determination of  $\eta/s$  are very large [51]. The values of  $\eta/s$  from the QGP are roughly four times smaller than for Helium after it transitions to a superfluid [151].

The constraints on  $\zeta/s$  from RHIC and LHC measurements are shown in the bottom panel of Figure 4. Predictions from an infinitely-coupled AdS Non-Conformal Holographic approach (AdS/NCH) are also shown for comparison. As the applicability of Conformal Symmetry regarding the strong potential assumed in the AdS/CFT scheme at temperatures close to the  $T_{pc}$  is expected to break down, an alternative approach is needed to determine  $\zeta/s$ . The breaking of conformal symmetry leads to  $\zeta/s$  rising near  $T_{pc}$  (it is zero otherwise). This approach was also used to reevaluate the  $\eta/s$  in the limit of infinite coupling at all temperatures and was found to also give  $1/4\pi$ , which suggests this limit is universal. Its prediction that  $\zeta/s$  should depend strongly on the temperature in this region is utilized for the T<sub>RENT</sub>o+VISHNU and IP-Glasma+MUSIC models. The high-temperature pQCD limit for  $\zeta/s$  is close to 0, which appears to apply for all the models shown at temperatures above 0.4 GeV. This then implies that bulk pressures in the initial state are washed out in the QGP phase even more quickly than the shear pressures e.g.  $\tau_\pi < 0.1$  fm/c for IP-Glasma+MUSIC at  $T = 0.4$  GeV.

Finally, the posterior distributions for  $\eta/s$  and  $\zeta/s$  have been evaluated using Bayesian parameter estimation techniques on RHIC and LHC data. They have been carried out by the Duke [23], JETSCAPE [152], Trajectum [153], and Jyväskylä [154] groups. These are shown on the right of Figure 4, at  $T = 0.3$  GeV for  $\eta/s$  and  $T = 0.2$  GeV for  $\zeta/s$ . The size of these posterior ranges is influenced by the prior ranges and data sets included. For example, the JETSCAPE prior ranges were larger than those by the Duke and Trajectum groups and yielded a larger upper limit for  $\eta/s$ . The Jyväskylä group used an even larger prior range, but included measurements of Symmetric Cumulants. As discussed, these highly constrain the temperature dependence of  $\eta/s$ , and therefore reduce the upper limit. Generally, the  $\zeta/s$  ranges differ more than the  $\eta/s$  ranges for all the Bayesian analyses. The JETSCAPE group also found that the duration of the pre-equilibrium phase has a strong impact on the extracted viscosity transport parameters. This is clearly demonstrated by the v-USPhydro chain [155]; the hydrodynamic evolution starts without any pre-equilibrium phase, and therefore requires low values of  $\eta/s = 0.05$  and  $\zeta/s = 0$  in order to develop enough flow to describe LHC data [156]. Those values are also shown in Figure 4 in both panels.

### 3.1.2 Mapping the QCD phase diagram

At high temperatures and vanishing net-baryon density, the QGP-hadron transition is understood to be a smooth crossover based on lattice QCD calculations [157]. The most recent result for the transition temperature is  $T_C = 158.0 \pm 0.6$  MeV [158], in agreement with the previously quoted  $T_C = 156 \pm 1.5$  MeV [159]. Due to the fermionic sign problem, it is currently not possible to perform lattice simulations of QCD thermodynamics at finite baryon density. For this reason, the knowledge of the QCD phase diagram and equation of state from first principles is limited to small densities. The transition temperature as a function of baryon chemical potential  $\mu_B$  can be parameterized as a Taylor series, of which we currently know the 0-th, 2-nd and 4-th order coefficients with high precision [158, 159]. Model studies indicate that a first-order phase boundary is expected at large net-baryon density [160, 161]. If this is the case, then there is a QCD critical point, separating the first-order phase boundary and the smooth crossover. The state-of-the-art lattice calculations on the QCD transition line predict that the chiral crossover region extends to a finite chemical potential  $\mu_B/T \leq 2$  [158, 162], see Figure 5. Recent results on the Equation of State hint that this region might extend up to  $\mu_B/T \sim 3-3.5$  [163, 164]. Due to the current lattice QCD limitations, experimental measurements are essential to answer the question on the existence of the QCD critical point.

The Beam Energy Scan (BES) program at RHIC, colliding heavy nuclei at the center-of-mass energy range  $\sqrt{s_{NN}} = 3-200$  GeV, was initiated in 2008 in order to search for the QCD critical point and study

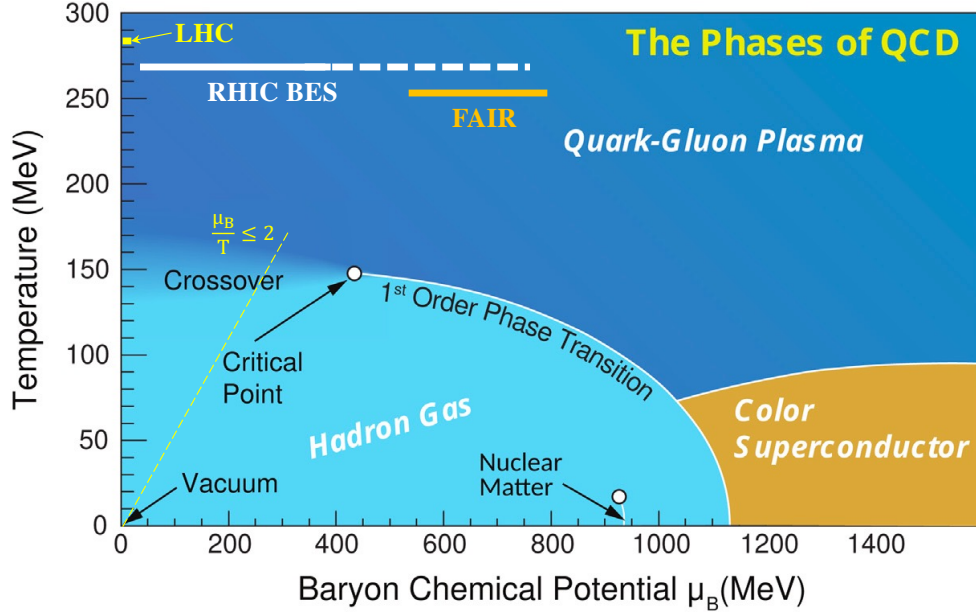


Figure 5: Sketch of the QCD phase diagram, incorporating a conjectured critical endpoint and first-order transition regime. The yellow line indicates the smooth crossover region up to  $\mu_B/T \leq 2$ . The coverage of the LHC, the RHIC-BES including the fixed target program (dashed line), and the future CBM Experiment at FAIR, are indicated at the top of the figure.

the nuclear matter equation of state at high baryon density [165, 166]. The BES phase-I (BES-I) program was conducted during 2010–2014 covering collision energies between 200 and 7.7 GeV (solid white line in Figure 5). The second phase of BES (BES-II) took place during 2019–2021 focusing on the center-of-mass energy range  $\sqrt{s_{NN}} = 3 - 19.6$  GeV. While data in the energy range 19.6 – 7.7 GeV were collected in the collider mode, the fixed target mode was also used to collect data over the energy range 3 – 13.1 GeV (dashed white line in Figure 5). In the overlap energy range, the event statistics from BES-II are improved by a factor of 20 to 40 compared to that of BES-I. Figure 6 summarizes the datasets collected at BES-I and BES-II including both collider and fixed target modes in different collision center-of-mass energies and their corresponding  $\mu_B$  values.

Experimental measurements have been focusing on searching for the evidence for the dominance of the QGP phase and the hadronic phase at different collision energies. All of the BES-I data have been analyzed and most of the results are published. While the first set of BES-II data, particularly at lowest energy at RHIC (3 GeV), was recently published and started to shed new insights into the understanding of the QCD phase structure at high density region. These observations include: (i) Jet Energy Loss: High momentum hadrons and fully reconstructed jets are unique probes for early-time QGP dynamics in heavy-ion collisions. The strong suppression in the leading hadron  $R_{AA}$  at  $p_T \geq 5$  GeV/c, a signature of the formation of the QGP in central Au+Au collisions at  $\sqrt{s_{NN}} = 200$  GeV, was found to be gradually increased and to even become larger than unity in Au+Au central collisions when energy is lower than 19.6 GeV [167]. (ii) Partonic Col-

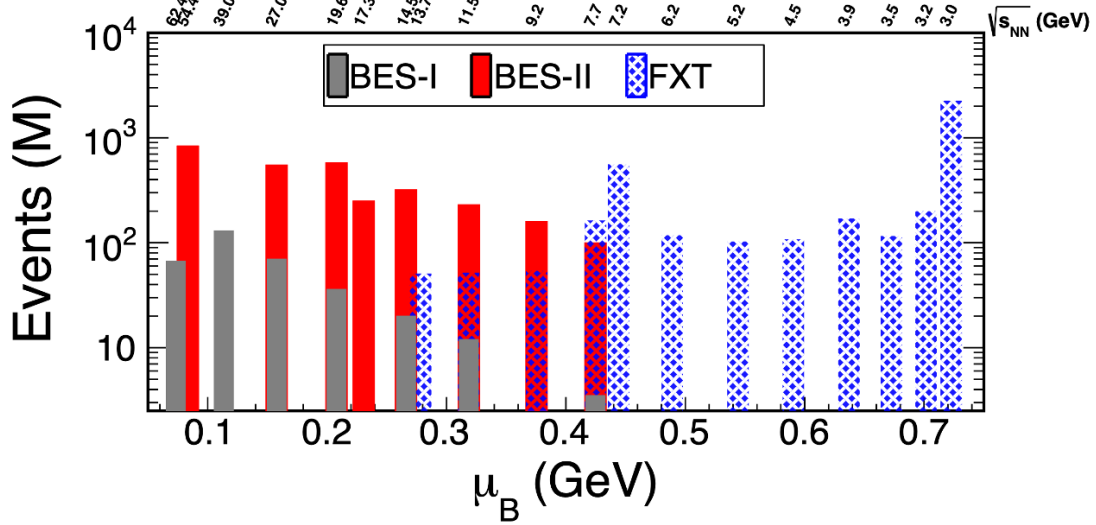


Figure 6: Recorded BES-I collider (grey bars), BES-II collider (red bars) and fixed target (blue hatched bars) datasets at different collision energies and their corresponding  $\mu_B$  values.

lectivity: Collective observables such as  $v_1$  and  $v_2$  are widely used for studying properties of the hot and dense medium created in high-energy nuclear collisions. The number of quark scaling found in the  $v_2$  for all hadrons, the fingerprint of the QGP, has been found to persist down to the 7.7 GeV Au+Au collisions [168]. This implies that the partonic activities remain to be dominant at these high-energy collisions. (iii) Critical Fluctuation: Higher order non-Gaussian cumulants of particle multiplicities and their ratios are expected to be sensitive to the existence of the critical point and phase boundary [169, 170]. The cumulants of net-proton protons (a proxy for net-baryons [171]) from top 5% central 200 GeV Au+Au collisions,  $C_6/C_2$ ,  $C_5/C_1$ , and  $C_4/C_2$ , are all found to be consistent with lattice QCD predictions of a smooth crossover chiral transition [162, 172–175]. In Au+Au collisions at 3 GeV, on the other hand, hadronic interactions are evident from the measurements of proton distributions, collective flow, and strangeness productions [176–178]. These results imply that the QCD critical point if it exists, can only be experimentally detected in heavy-ion collisions at energies  $\sqrt{s_{NN}}$  between 3 and 20 GeV.

Figure 7 shows recent results on the fourth-order net-proton (filled red circles) and proton (open squares) moments in central Au+Au collisions from the RHIC BES [172, 176, 179], compared to several model predictions. The thin red and blue dot-dashed lines are expected from a qualitative prediction due to critical behavior [180], even though recent quantitative results pointed out that the possibility of observing the dip depends on the distance of the freeze-out line from the critical point [181]. The hadronic transport model UrQMD [182, 183] (gold band) and a thermal model with canonical ensemble [184] (red dot-dashed line) represents a non-critical dynamic baseline. The RHIC BES-I data is inconsistent with the monotonic predictions of non-critical models at the  $3.1\sigma$  level [172, 176]. RHIC BES-II results will provide significantly improved statistical precision (and likely reduced systematic uncertainties) measurements, as indicated by the green band in the figure. The extended acceptance and particle identification to a larger rapidity region (from  $|y| < 0.5$  to  $|y| < 0.8$ ) will allow a more systematic investigation of the nature of these fluctuations.

The equation of state of QCD from first principles is currently known up to  $\mu_B/T = 3$  from a resummed Taylor expansion [163] and up to  $\mu_B/T = 3.5$  from an alternative expansion scheme which was recently proposed in Refs. [164, 187]. These results are obtained at either  $\mu_Q = \mu_S = 0$ , or for

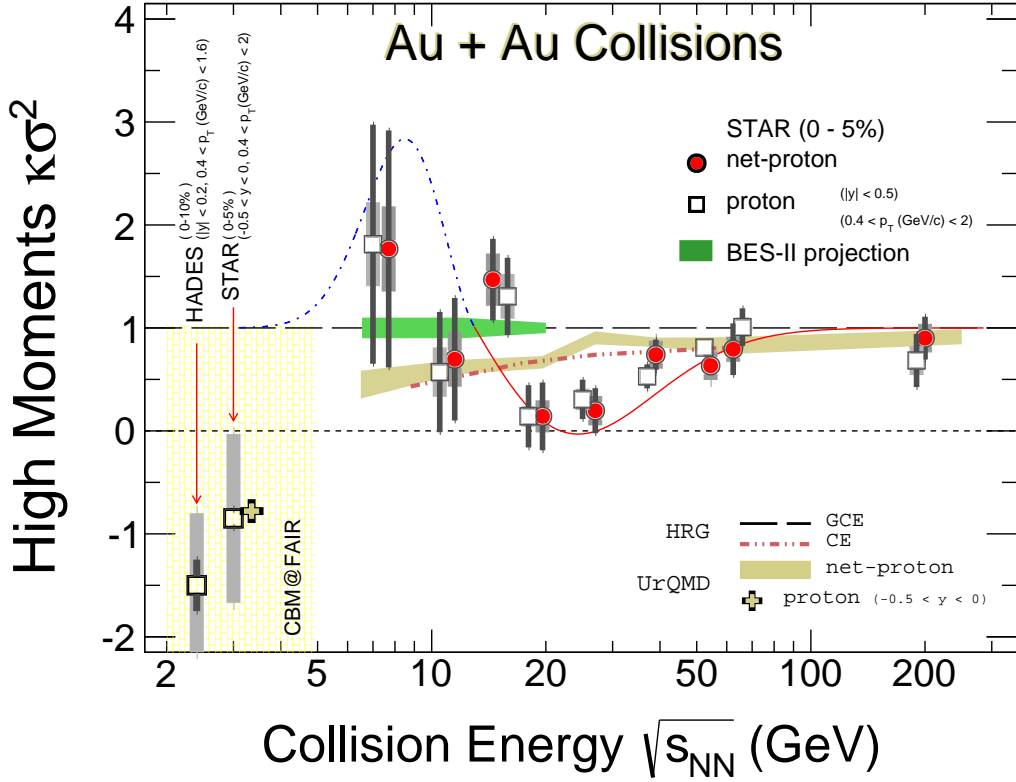


Figure 7: Energy dependence of the net-proton (filled circles) and proton (open squares) high moments from central Au+Au collisions at RHIC BES [176, 185, 186]. For comparison, model results from the HRG model based on both Canonical Ensemble (CE) and Grand-Canonical Ensemble (GCE) [184], and transport model UrQMD [182, 183] are also shown. The energy range covered by the CBM experiment is shown as the yellow hatched area. The non-monotonic curve indicates the qualitative shape of the contribution of critical fluctuations [180].

$\mu_Q$  and  $\mu_S$  as functions of  $\mu_B$  and  $T$  such that they satisfy the phenomenological conditions  $\langle n_S \rangle = 0$  and  $\langle n_Q \rangle = 0.4\langle n_B \rangle$ . A full, four-dimensional Taylor-expanded equation of state in the  $T, \mu_B, \mu_S, \mu_Q$  parameter space is available in the range  $\mu_B/T < 2$  [188, 189]. Extensions beyond these  $\mu_B$  ranges are works in progress and currently limited due to the fermionic sign problem.

Although neither the strength nor  $\mu_B$  value for the deconfinement and chiral phase transitions have been pinpointed at low temperatures, since the last long-range plan was written, significant progress has been made in understanding the equation of the state of dense matter. This advance came as a result of low-energy laboratory experiments and astrophysics observations, combined with a large theoretical effort from the nuclear physics and astrophysics communities. As a result, it was understood that dense matter is neither entirely soft nor stiff (as previously discussed) but presents nuances that can be translated into the structure in the (effectively) zero-temperature speed of sound [190–193].

First, from nuclear physics, there are indications that the symmetry energy of matter around saturation density is not large [194–196] (although controversy still exists [197–199]). This means that isospin-asymmetric matter, although stiffer than isospin-symmetric matter, is still relatively soft at low densities. This is corroborated by electromagnetic and gravitational-wave observations of intermediate-mass neutron stars, that point to small stars [200–203] with lower tidal deformability [204]. On the other hand, electro-

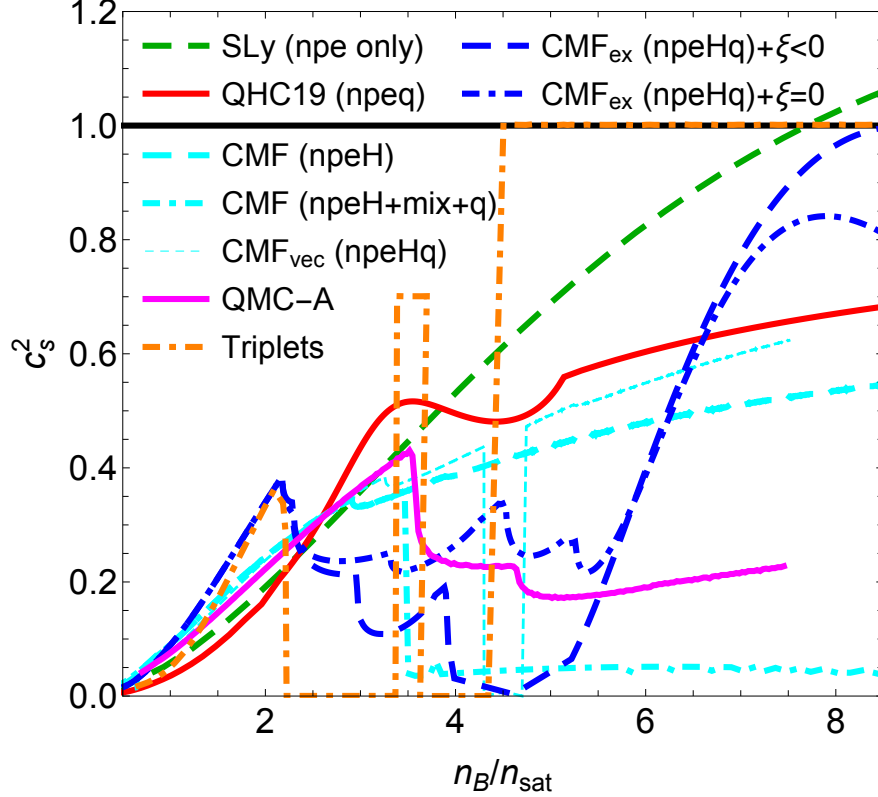


Figure 8: Comparison of the speed of sound squared calculated from state-of-the-art dense-matter models including different compositions and reproducing different-order phase transitions. Figure from Ref. [210]

magnetic [205,206] and possible gravitational-wave observations of massive stars [207] point towards a stiff equation of state at large densities. Finally, at asymptotically large densities, perturbative QCD predicts that the conformal limit is recovered from below, pointing once more to a soft equation of state [208]. Perturbative QCD results can be extrapolated to lower densities, providing a limit for the stiffness of the equation of state all the way down to a few times saturation density [209].

Together, these results show that either the degrees of freedom [192, 208, 211–216], symmetries [217, 218], or interactions [219–224] are changing within the relevant portion of the QCD phase diagram, implying a phase transition of some order at zero temperature, as shown in Figure 8. Besides the purely nucleonic Sly equation of state, all the others shown in the figure present a phase transition, either of the first order, with the speed of sound going all the way to zero, or higher order, including a mixed phase with very low speed of sound. These state-of-the-art dense-matter models present different compositions (including hyperons, negative parity states, and quarks) and symmetries (including chiral symmetry and different pairing schemes).

At finite temperature, meaning tens of MeV’s in order to modify significantly the properties of hadrons, dense matter beyond a couple of times saturation density has not been yet experimentally probed. This is because such conditions can only be found in supernova explosions (and within the first minute of life of proto-neutron stars) and in neutron star-mergers. So far, although much theoretical work has been laid [225–233], no neutrinos have been detected from supernovae in our neighborhood, and the post-merger part of gravitational-wave signals from neutron star mergers has not yet been detected by LIGO and Virgo detectors.

### 3.1.3 Thermal photons/dileptons

Heavy-ion collision experiments conducted at the Relativistic Heavy Ion Collider (RHIC) and the Large Hadron Collider (LHC) create an environment at a temperature of a trillion degrees, to study the property of dense nuclear matter. Electromagnetic (EM) probes, such as direct photons and dileptons ( $e^+e^-$  and  $\mu^+\mu^-$  pairs) are recognized as valuable messengers in relativistic nuclear collisions [234, 235]. Because photons and dileptons interact only electromagnetically, they can penetrate the medium, carry almost undistorted dynamical information, and report on conditions existing at their production point. Such probes are sensitive to the early stages of the collision system, to thermal and transport properties of the quark-gluon plasma (QGP), and the dynamical evolution proceeding from the cross-over regions to the hadronic phase [236–249]. In addition, dilepton invariant mass spectrum is the only observable that can measure the in-medium spectral function of hadrons, and its relation to chiral symmetry restoration [250, 251].

#### *Electromagnetic radiation in and out-of-equilibrium*

Electromagnetic emission rates from the QGP are directly related to the electromagnetic current-current correlation function [252, 253],

$$d\Gamma_k = \frac{d^3k}{(2\pi)^3 2k} \sum_{a=1,2} \epsilon_{(a)}^\mu(k) \epsilon_{(a)}^\nu(k) \int d^4x e^{-ik \cdot x} \langle J_{em,\mu}(0) J_{em,\nu}(x) \rangle, \quad (5)$$

where  $\epsilon_{(a)}^\mu(k)$  is the polarization vector. The current-current correlation function in Eq. (5) encodes the response of QGP to electromagnetic fields. It is directly related to quarks, the electric charge carriers in the QGP, and indirectly related to gluons which interact with quarks during photon emission processes. In thermal equilibrium, the EM current-current correlator can be related to the vector spectral function and the photon emission rate can be written as

$$k \frac{d\Gamma_k}{d^3k} \propto \frac{\alpha_{EM}}{\pi^2} n_B(k) \rho_v(k, \vec{k}). \quad (6)$$

With the same vector spectral function, the equilibrated dilepton production rates are

$$\frac{d\Gamma_{l+l-}(\omega, \vec{k})}{d\omega d^3\vec{k}} \propto \frac{\alpha_{EM}^2}{\pi^3 M^2} n_B(\omega) \rho_v(\omega, \vec{k}), \quad (7)$$

with  $M^2 \equiv \omega^2 - k^2$ . This EM vector spectral function  $\rho_v(\omega, \vec{k})$  in the QGP phase has been calculated using both perturbative QCD (pQCD) and non-perturbative lattice methods. Theoretical progress on the pQCD calculations has yielded full next-to-leading (NLO) EM spectral functions for both real ( $M = 0$ ) photons [254] and virtual photons, which subsequently decay into dileptons [255–257]. The NLO rates allow for comparisons and connections with non-perturbative approaches [258, 259]. Ref. [258] showed the remarkable agreement between NLO pQCD calculations of EM spectral functions and lattice QCD results [260, 261]. These advancements in computing the QGP EM spectral function provide carrying out reliable phenomenological studies with the RHIC and LHC experiments.

In the hot hadronic phase, the in-medium modifications of the vector spectral function in the hadronic phase, which has a direct connection to chiral symmetry restoration during the phase transition, have been studied extensively with hadronic many-body theories [262, 263].

The dynamically evolving QGP does not stay in thermal equilibrium, and the local momentum anisotropy of the plasma generates viscous corrections to photon emission rates. These out-of-equilibrium corrections to the EM emission rates are important for phenomenological studies. Calculations at the leading order of strong coupling  $\alpha_s$  were carried out for two-to-two scattering channels [241, 245, 264–267] and

inelastic channels with bremsstrahlung and pair annihilation processes with Landau-Pomeranchuk-Migdal (LPM) effects [268,269]. The viscous corrections to the dilepton emission rates were computed [270–274].

### *Thermal EM probes – the QGP multi-messenger*

Because the momentum distributions of photons and dileptons can carry dynamic information about their production points, they are excellent diagnostic probes to infer the dynamical evolution of QGP in relativistic nuclear collisions.

#### •*Thermometer and Chronometer*

Real and virtual photons are useful tools for experimentally accessing the temperature of the QGP created in heavy-ion collisions [275,276]. The yields of photons are directly proportional to the space-time volume and the average temperature of the hot QGP matter [277,278]. The dilepton yields in the low invariant-mass region showed a strong correlation with the fireball lifetime [279,280].

The slopes of the photon and dilepton spectra encode temperature information of the collision system. Direct photon  $p_T$ -spectra have been measured by the PHENIX, STAR, and ALICE Collaborations in heavy-ion collisions at the top RHIC and LHC energies [281–283]. The low  $p_T$  part of the spectra can be well characterized by their inverse logarithmic slope  $T_{\text{eff}}$ . The PHENIX Collaboration reported  $T_{\text{eff}} = (239 \pm 25^{\text{stat}} \pm 7^{\text{sys}})$  MeV for 0-20% Au+Au collisions at  $\sqrt{s_{\text{NN}}} = 200$  GeV [281] and the ALICE Collaboration found  $T_{\text{eff}} = (304 \pm 11^{\text{stat}} \pm 40^{\text{sys}})$  MeV in 0-20% Pb+Pb collisions at  $\sqrt{s_{\text{NN}}} = 2.76$  TeV [282]. The ALICE measurement of direct photon production at  $\sqrt{s_{\text{NN}}} = 2.76$  TeV constraint to the  $p_T < 4$  GeV/ $c$  region is shown on the left panel in Figure 9 with comparison to the current theoretical models. Quantitative studies [284,285] have shown that thermal photons emitted from  $T > 300$  MeV during early stages of the evolution were reflecting their local temperatures while those from  $T < 250$  MeV received significant blue-shift from the hydrodynamic flow. Therefore, the measured effective temperatures set strong constraints on hydrodynamic evolution. A solid extraction of the initial temperature of the collision system requires detailed comparisons between experimental data and dynamical model simulations.

On the other hand, thermal dilepton invariant-mass spectra are free from blue-shift flow contamination. The authors in Ref. [280] demonstrated that the slope of the dilepton spectrum in the intermediate mass region (IMR),  $1.5 \text{ GeV} < M < 2.5 \text{ GeV}$ , could provide temperature information about the collision system. However, Ref. [242] shows that the local momentum anisotropy of the quarks can lead to small but non-negligible corrections to the slope of the dilepton spectrum. In addition, Refs. [280,287–289] showed that dilepton invariant-mass spectra were valuable tools to probe the properties of the baryon-rich fireball in the RHIC Beam Energy Scan (BES) program. The right panel in Figure 9 shows the recent STAR measurement of the low mass region enhancement when compared to the cocktail sum of different decay production in three different collision energies. The comparison to the model calculations are all consistent with the scenario of in-medium broadening of the  $\rho$  meson, together with previous measurements providing an order of magnitude range in collision energy. Recently, phenomenological studies of dilepton invariant-mass spectra have been carried out in heavy-ion collision at HADES energies [290–292]. In such a baryon-rich environment, the interactions with the excess of baryons play a crucial role in EM emissions. The average temperature information has been extracted by HADES Collaboration [293].

#### •*Constraining out-of-equilibrium QGP dynamics*

The large expansion rates in relativistic heavy-ion collisions drive the system away from thermal equilibrium during its evolution. Out-of-equilibrium dynamics leave their fingerprints on the electromagnetic observables.

Effects on thermal photon emission owing to locally anisotropic particle distributions were investigated in Ref. [237,264,294–296]. The related phenomenological impacts were studied in Ref. [75,241,244,245,295,297,298]. Effects from bulk viscosity were recently studied Ref. [40,265,299,300]. The inclusion



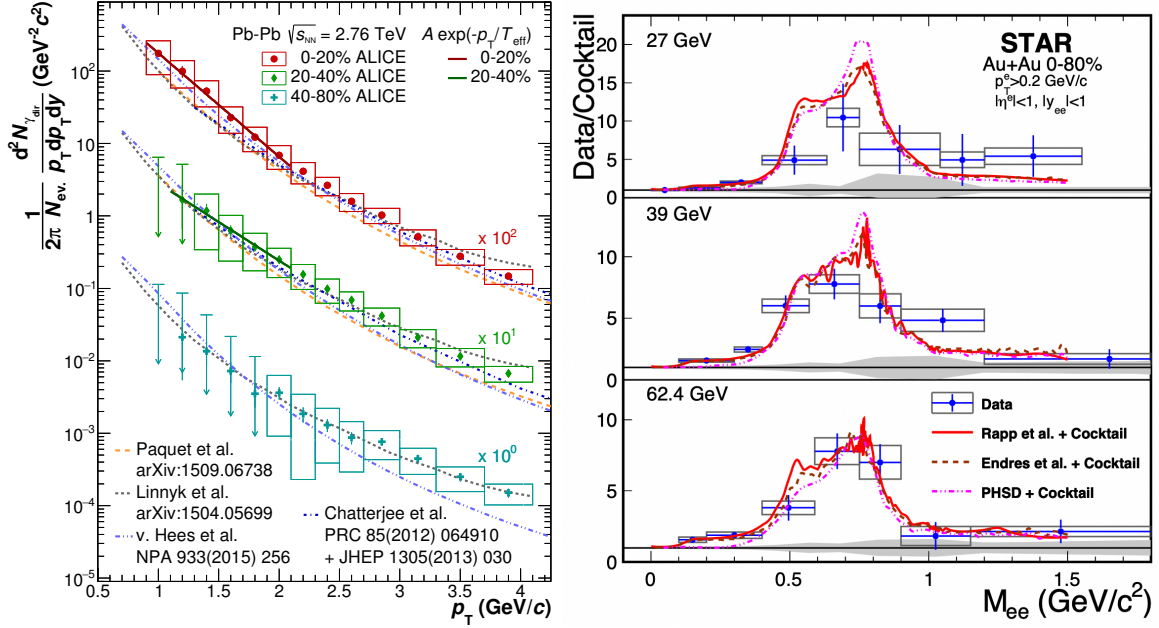


Figure 9: Left panel: The direct photon spectra from the ALICE experiment in Pb+Pb collisions in three different centrality classes compared with three different model calculations. Figure from Ref. [282]. Right panel: STAR result on the dilepton invariant mass divided by the expected background from the cocktail simulation at three different collision energies. The cocktail contributions from  $\omega$  and  $\phi$  mesons have actually been removed. Figure from Ref. [286].

of a non-vanishing bulk viscosity near the phase transition generates extra entropy production and increases the space-time volume in the late hadronic phase by about 50%, which allows more thermal photon radiation [299]. Another consequence of including bulk viscosity is reducing the hydrodynamical radial flow at the late stage of the evolution, which weakens the blue shift of the thermal photon spectrum compared to the simulations without bulk viscosity. Both effects together increase the thermal photon yields in the low  $p_T$  regions and shift the peak of the direct photon  $v_2(p_T)$  towards the low  $p_T$  regions [299].

Dileptons have also been shown to be a clean and sensitive probe of the out-of-equilibrium dynamics of the system [242, 247, 301]. Recent studies have demonstrated that, compared to hadronic observables, the thermal dilepton spectrum and its flow anisotropy show a larger sensitivity to the early time dynamics, to the system's shear stress tensor  $\pi^{\mu\nu}$  and bulk viscous pressure  $\Pi$ , to the temperature dependence of shear viscosity  $\eta/s(T)$ , and even to the choice of the second order transport coefficient  $\tau_\pi$  [272–274].

#### •Diagnosing early-stage chemical equilibrating QGP

The hot QGP emits photons and dileptons during its entire evolution. The early stage of heavy-ion collisions is overpopulated by gluons. The chemical evolution of QGP leaves its signatures at high  $p_T$  photon spectra and  $M > 1$  GeV in dilepton invariant-mass spectra. Because the EM emission rates are directly related to the quarks in QGP, the yields of high  $p_T$  photons and large invariant-mass dileptons carry information about chemical equilibration dynamics [246, 300].

One interesting way of studying the direct photon production is discussed in [302, 303], where the charged hadron multiplicity of the system is proportional to the temperature and size of the system. At the same energy, the centrality closely correlates with the size, while at the same centrality, the collision energy would correlate with the temperature and lifetime of the system. Figure 10 shows the recent results from PHENIX, where the important point is that A+A data from different centralities and a wide range of collision

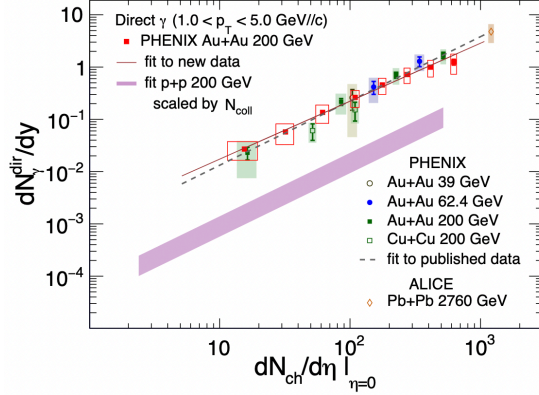


Figure 10: The direct photon yield compilation from the large collisions systems from PHENIX and ALICE as a function of the event multiplicity, figure from [303].

energies can be empirically described in terms of  $dN_{ch}/d\eta$  with just two parameters, suggesting some fundamental commonality in the underlying physics. There seems to be no qualitative change in the photon sources and their relative contributions for different collision centrality or collision energy. This scaling behavior shows that the direct photons emit from the (3+1)D space-time volume of the collisions while hadrons only emit from the final freeze-out surface. The measurement includes all non-prompt photons which would include all electromagnetic radiation from non-perturbative QCD processes.

•*Thermal emission signatures from small QGP droplets*

Unraveling the collective origin of small collision systems has been a hot topic in our field. If there were a hot and nearly thermal-equilibrated QGP medium produced in these collisions, the QGP droplet would radiate thermal photons and dileptons and enhance the measured spectra for these EM probes [304]. Systematic calculations have been carried out as a function of collision system size to study the hadronic observables and direct photon production as the same time [75, 277, 300, 305, 306]. The theory predicted thermal enhancement of direct photon at low  $p_T$  was consistent with the PHENIX measurements.

•*Photon emission in the dilute hadronic phase*

The photon emissions from the hadronic bremsstrahlung processes in the dilute phase were found to be important to explain the large excess of direct photon spectra measured by the PHENIX Collaboration at the RHIC [307]. Such out-of-equilibrium photon emission in the dilute hadronic phase was recently studied via a systematic comparison between photon emission from the hydrodynamic medium at low temperature and microscopic production from hadronic transport model SMASH [308]. One finds consistent results from photon  $p_T$  spectra from the two approaches. The photon elliptic flow is larger from the transport model than that from the near-equilibrium hydrodynamic description. A more comprehensive description requires the dynamical models to include additional photon emission processes from baryonic channels [309]. These processes are expected to play an important role in heavy-ion collisions in a baryon-rich environment at Beam Energy Scan energies.

•*Probing the nature of hadron-QGP phase transition at high baryon density*

Unlike the yields of hadronic particles, photons and dileptons production are correlated to the total space-time volume of heavy-ion collisions. Recent studies show that dilepton production can serve as a signature for the first-order phase transition [310, 311]. The fireball space-time volume will increase if the system goes through a first-order phase transition compared to that of a smooth cross-over situation. A

factor of 2 enhancement in dilepton yields was predicted from model calculations for Au+Au collisions at the  $E_{\text{lab}} = 1 - 10 \text{ GeV}$ .

### 3.1.4 Initial condition

#### 3.1.4.1 Challenges towards understanding the heavy-ion initial condition

The study of the initial stages of heavy-ion collisions is of paramount interest to the community of high-energy nuclear physics. This interest ranges from a better understanding of the wave functions of the colliding nuclei to the description of the early pre-equilibrium stage that is formed immediately after the collisions. The initial condition is followed by the QGP that is describable by effective kinetic theory or fluid dynamics. Therefore, any limitations in our knowledge of the initial condition contribute to uncertainties in the fluid-dynamic description of the matter formed in heavy-ion collisions and the interpretation of final state observables [150].

There are two dominant sources of uncertainties related to the initial condition. First, we have limited knowledge of the wave functions of the colliding ions in terms of 1) the nuclear structure, deformation parameters, and neutron skin and 2) the spatial, momentum, and collision energy dependence of the parton distributions of the colliding ions. Some of these quantities can be constrained through independent measurements. For example, constraints on nuclear structure come from measurements performed in low-energy nuclear physics experiments. The distribution of the partons inside a colliding proton or ion as a function of Bjorken- $x$  and momentum transfer ( $Q^2$ ) can be constrained using electron-proton/ion scattering at HERA [312], recently using ultra-peripheral collisions and, at the future EIC (see Section 3.4.6). However, uncertainties arise due to limited available data on nuclear parton distribution and we lack control over the kinematics of the heavy-ion initial state. We normally resort to theoretical frameworks such as QCD evolution equations such as BFKL, DGLAP, or JIMWLK that can extrapolate the parton distributions to the desired regions of the  $x - Q^2$  landscape [313–317].

The second source of uncertainty of the initial condition is associated with incorporating sources of initial-state fluctuations at different lengths scales and the description of the pre-equilibrium phase of matter formed immediately after the collisions. For theoretical modeling of heavy-ion collisions, initial-state models are expected to predict the initial full energy-momentum tensor that is input to fluid-dynamic simulations. No direct measurement can provide insights about this early phase of collisions as final-state effects always complicate the interpretation. Modeling of small collision systems have indicated that incorporating sub-nucleonic hot spots constrained by the HERA data [80] as well as pre-equilibrium flow play an important role in the description of the experimental data [41, 318]. However, discerning the relative contribution of the sub-nucleonic hot spots and flow in pre-hydrodynamic phase is experimentally challenging.

Over the years, attempts have been made to address these issues and to come up with the best possible solution description of the heavy-ion initial state. The commonly-used MC-Glauber model distributes the initial nucleons in coordinate space and uses various choices of energy or entropy deposition schemes to provide the necessary initial conditions. One example of such a scheme is the wounded nucleon model that involves free parameters that can be constrained by data-model comparison or Bayesian analysis with global data. In turns MC-Glauber description already provides the necessary lumpiness of the initial state to describe the most commonly used experimental measurements of flow harmonics ( $v_n$ ). If the kinematics of collisions are such that the colliding ions can be described as saturated sheets of gluonic matter one can use more sophisticated models of the initial state such as IP-Glasma. With inputs from HERA data on the gluonic profile of the proton, IP-Glasma can construct initial color-charge distribution inside the colliding nuclei. It then simulates the collisions of the color fields due to such color charges and also the evolution of the pre-equilibrium matter after the collisions. The spatial inhomogeneities at various length scales (down to inverse of nuclear saturation scale  $1/Q_s^2(x)$ , the intrinsic momentum space correlations of the gluons),

and the flow of the pre-equilibrium matter are dynamically generated in this framework. The output of IP-Glasma, such as the full stress-energy tensor corresponding to a given value of the number density of gluons can be coupled directly to a fluid-dynamic simulation [150]. The IP-Glasma model has been quite successful in describing bulk observables over a wide range of collision systems [319]. Such success of the IP-Glasma model can be attributed to its predictive power of the right correlation between transverse initial-state spatial anisotropy and gluon multiplicity. The IP-Glasma model combined with the RHIC data on deformed U+U collisions provided the stepping stones for the development of the TRENTO model which parametrizes the initial energy/entropy distribution in terms of the nuclear thickness function [31]. Due to its intrinsic simplicity and flexibility, TRENTO is one of the most widely used initial-state models and a common tool for Bayesian analyses.

### 3.1.4.2 Understanding the three-dimensional structure of the initial state

The success of the IP-Glasma or TRENTO is associated with the right description of the transverse profile of the initial energy density distributions. Since the last long-range plan, the development of the initial state has been focused on a deeper understanding of the three-dimensional structure of the initial state that remained largely unexplored. It turns out the measurements of pseudorapidity decorrelation of event planes and flow harmonics are ideal probes to constrain the three-dimensional initial state of heavy-ion collisions. The cartoon in Figure 11 (left) demonstrates how the initial-state longitudinal fluctuations and fluid dynamical response of the medium formed in HICs can lead to decorrelations of the harmonic anisotropies planes  $\Psi_n$  at different pseudorapidity. Such effects are often referred to as torque or twist of the event shape [320–322] that eventually leads to a breaking of longitudinal/boost/rapidity invariance. Depending on whether the initial state is determined by gluon saturation or the wounded nucleon model the effect of such de-correlation will be different. If the initial state is described by gluon saturation, as simulated by the 3D-Glasma model, the breaking of boost invariance is determined by the QCD equations (BK, JIMWLK) which predict the evolution of gluons in the saturation regime. The typical rapidity scale is over which boost invariance is broken depending on the strong coupling constant and the gluon saturation scales  $\Delta y \sim 1/\alpha_S(Q_s^2)$ . On the other hand if one expects the initial state is described by the wounded nucleon model the trivial scale controlling the breaking of boost invariance will be different. There is a trivial scale of decorrelation determined by the beam rapidity  $\Delta y \sim 2Y_{\text{beam}}$  – simply because the orientation of the harmonic anisotropy planes in the target and projectile fragmentation regions are different. With the decrease of collision energy, one expects  $Y_{\text{beam}}$  to change and therefore a stronger breaking of boost invariance is expected. In order to explore this effect, one needs to go beyond the conventional two-particle azimuthal correlations over a narrow window around mid-rapidity. Several promising observables have been proposed to study this effect, Figure 11 shows one which can be expressed as  $r_n(\eta_a, \eta_b) = V_{n\Delta}(-\eta_a, \eta_b)/V_{n\Delta}(\eta_a, \eta_b)$  that measures the de-correlation of flow vectors while going from  $-\eta_a$  to  $\eta_a$  using reference particles taken from  $\eta_b$  [323]. Here,  $V_{n\Delta}(\eta_a, \eta_b)$  is the Fourier coefficient calculated with pairs of particles taken from different pseudorapidity regions  $\pm\eta_a$  and  $\eta_b$ . In order to remove the trivial effect of de-correlation due to beam rapidity the x-axis of the plot is scaled by  $Y_{\text{beam}}$ . Data from CMS collaboration [323] are compared to 3D-Glasma models of saturation [324] and wounded nucleon model [325]. At RHIC predictions from both gluon saturation [326] as well as 3D-Glauber calculations with valence quarks and rapidity loss fluctuations [85] are available that remain to be tested. Further studies indicate that when scaled by the beam rapidity the ATLAS data [327] for  $\sqrt{s_{NN}}=2.76$  and 5 TeV fall on top of each other but due to large uncertainty it is not possible to see if RHIC data deviates from such scaling. Hydrodynamics models with 3D initial state from AMPT initial conditions [322] have been compared to data on Figure 11 that predict stronger decorrelations for RHIC measurements at 200 GeV. In summary, it is essential to incorporate the rapidity dependence of initial energy density to perform a full 3+1 dimensional hydrodynamic simulations. Other than the aforementioned models, the same has been performed by initializing the hydrodynamic simulations with inputs from UrQMD [328], AMPT [329] and

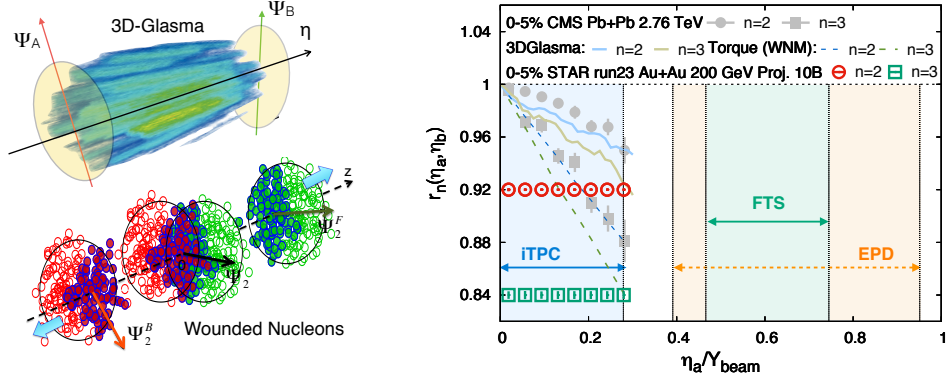


Figure 11: (Left) A cartoon depicting the de-correlation of event planes in the longitudinal direction of collision, based on the gluon saturation model 3D-Glasma [324] and the wounded nucleon model [320,333]. Both models predict the breaking of boost invariance, but at different scales. (Right) The longitudinal de-correlation of the elliptic anisotropy plane as a function of pseudorapidity, in units of beam rapidity. The colored regions show that current and future capabilities at STAR (with iTPC+EPD+FST) can extend such measurements with good precision by covering up to 60% of the beam rapidity at 200 GeV. As  $Y_{\text{beam}}$  decreases at lower (BES-II) energies, a wider longitudinal extent can be measured.

EPOS [330] initial conditions. The other models that include the rapidity dependent initial conditions are the strong coupling based Holographic initial conditions that employ AdS/CFT to match with hydrodynamic simulations [331, 332].

The BES-II and forward upgrades of the STAR experiment include the Even Plane Detector and the Forward Tracking Systems improve these measurements with greater precision and over a wider range of  $\eta/Y_{\text{beam}}$  extend these measurements up to about 60% of the beam rapidity at the top RHIC energy where  $Y_{\text{beam}} = 5.36$  as shown by the yellow and green bands in Figure 11 (right). With the decrease of collision energy the value of  $Y_{\text{beam}}$  decreases thereby covering an even wider longitudinal extent of the initial state. This way it will be possible to map the 3D structure of the initial state.

The de-correlations of the event plane can also be probed by measurements of mixed harmonic correlations of reaction planes. Such correlations have been measured by the STAR collaboration in Ref [334] using the relative pseudorapidity dependence of the three-particle correlator

$$C_{m,n,m+n}(\eta_a, \eta_b, \eta_c) = \langle \cos(m\phi_1(\eta_a) + n\phi_2(\eta_b) - (m+n)\phi_3(\eta_c)) \rangle$$

with BES-I data. In the limited (currently available) acceptance at STAR, a small but significant decorrelation of the event planes was already observed [334] and a hint of stronger decorrelations at lower energy was also observed. The origin of such decorrelations by analyzing the BES-II data that includes the wider acceptance of the iTPC detector. The future measurements of rapidity correlations at RHIC and LHC will extend our knowledge beyond the conventional two-dimensional (rapidity-invariant) picture of the initial state and help to constrain the rapidity evolution of the gluon densities inside colliding hadrons or nuclei.

Another observable studied by the ATLAS collaboration to study the three-dimensional structure of the initial state is the two-particle correlation function in pseudorapidity  $C(\eta_1, \eta_2)$  [335]. The coefficients  $a_{n,m}$  of the correlation function decomposed in terms of Legendre polynomials can be used to constrain the scale over which longitudinal invariance is broken [85, 336, 337]. The coefficients  $a_{1,1}$  measured in p+p collisions have been argued to constrain the intrinsic fluctuations of the saturation scale inside a proton [338].

One of the direct consequences of the breaking of longitudinal invariance is the creation of vortical structure in the initial stages of collisions. Such a vorticity of the medium is transferred to the spin polar-

ization of hadrons and has been measured in experiment. The polarization of hyperons is a novel probe of 3D initial state as they can help extract information such as the gradient of the fluid velocity that were not accessible before. Measurements of the global polarization of hyperons of different masses such as  $\Lambda$ ,  $\Xi$  and  $\Omega$  that have different formation times can provide the dynamics evolution of the velocity fields of the medium created in heavy-ion collisions. More discussion on this can be found in the later sections of this document.

### 3.1.4.3 Initial state of conserved charge distributions and baryon stopping

At lower energy collisions, the initial state is intimately related to understanding the nucleon wave function in the nucleus, in particular, the momentum distribution and short-range correlations of the nucleons confined in a nucleus [339, 340]. In addition, knowledge of baryon transport and beam fragmentation is also needed for a complete picture of the initial state at lower energy. The three-dimensional structure of the initial state becomes more important at lower collision energies. Due to limited constraints from experimental data, the initial state of heavy-ion collisions at lower energy is poorly understood. This limits the modeling of heavy-ion collisions at lower energy and the interpretation of measurements from the RHIC BES program, which is dedicated to the search for the onset of the first-order phase transition and QCD critical point.

The promise of the BES program is predicated upon the ability to create a Quark Gluon Plasma that can be doped with baryons in heavy-ion collisions. This enables us to walk along the chemical potential axis of the QCD phase diagram. For experiments, this boils down to the measurements of finite baryon asymmetry in the central rapidity region of the collisions where observables sensitive to the first-order phase transition and QCD critical point are also measured (see the section on the QCD critical point). In addition, we must have the ability to achieve a lever arm to vary the baryon asymmetry by changing the collision energy so that a wide range of the chemical potential axis can be scanned. The question is what is the dynamics that controls the initial density-distribution of the net-baryons in heavy-ion collisions. Since the net-baryon number cannot be created in the system and must come from the colliding target and projectile, a question is raised related to the understanding of the microscopic mechanism that makes baryons shift from the target and projectile rapidity to the midrapidity [341]. The observation of substantial baryon asymmetry in the central rapidity (mid-rapidity) region both at RHIC [142, 342, 343] and at LHC energies ( $\sqrt{s_{NN}} = 900$  GeV) [344, 345] is indeed a puzzling feature of heavy-ion collisions. Thus far, no approach from first principles has been able to explain this feature of the data. About three decades ago, it was argued that the question of how a baryon is stopped may be related to what is the true carrier of the baryon quantum numbers. In a conventional picture, valence quarks carry baryon quantum number in a nucleus. At sufficiently high energies, it is expected that these valence quarks will pass through each other and end up far from mid-rapidity in the fragmentation regions [346, 347]. However, the global data on net-proton yields at midrapidity from the Alternating Gradient Synchrotron (AGS) [348], the Super Proton Synchrotron (SPS) [349], RHIC [142, 342, 343], and LHC [147], as shown in Figure 12, indicate non-zero baryon stopping. The data also show that, for all centralities in heavy-ion collisions, the mid-rapidity net-baryon density follows an exponential distribution  $A \exp(-\alpha_B \delta y)$  with the variable  $\delta y = Y_{\text{beam}} - Y_{\text{cm}}$  and an exponent  $\alpha_B$  ranging from 0.65-0.67. Other ways of characterizing the substantial baryon asymmetry observed in collisions include studying the average rapidity loss [350] or the  $\bar{p}/p$  ratio [344, 345, 351]. Over the years, due to a lack of fundamental understanding, initial-state models of heavy-ion collisions have parametrized baryon stopping to reproduce experimental data.

A recent modeling of heavy-ion collisions indicates that the inclusion of the baryon junction is essential for describing net-proton density at RHIC [352]. Clearly some of the earlier implementations of baryon junctions (for example, the HIJING/B [344, 353], HIJING/B $\bar{B}$  [354]), which attempted to match the earlier experimental data with certain parameter tunes, do not reproduce the experimental results presented

in Figure 12. The idea that the flow of the baryon number can be traced by the flow of a non-perturbative Y-shaped configurations of gluon fields, called baryon-junctions, rather than valence quarks was proposed in Ref [346]. Such junctions are the only possible gauge invariant structure of the baryon wave function, and have been widely studied in Lattice QCD [355,356]. The gluon junctions as baryon carriers can lead to significantly larger baryon-stopping at mid-rapidity compared to that of quarks and could resolve the puzzle. Recently, a few experimental observables have been proposed to test such ideas [341]. In the next half a decade we might be able to have a much better understanding of the initial-state physics that describes the phenomenon of baryon stopping from first principles (see more in the ultra-peripheral collisions section).

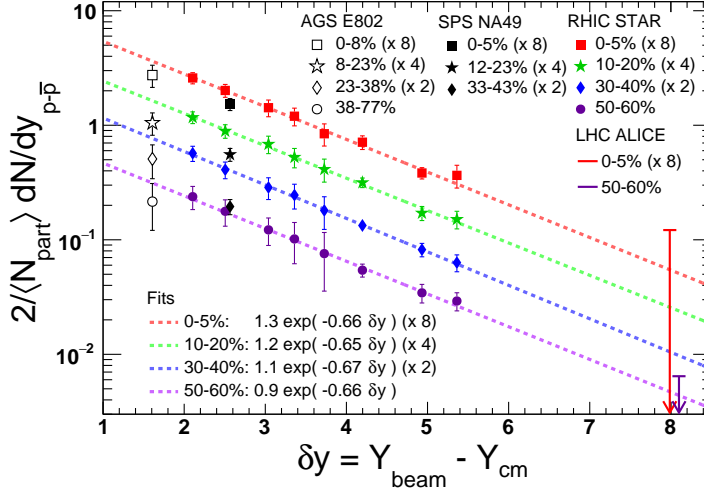


Figure 12: Exponential dependence of midrapidity ( $y \approx 0$ ) baryon density per participant pair in heavy-ion collisions with  $Y_{\text{beam}}$  which is equal to the rapidity difference between beam and detector midrapidity ( $\delta y$ ) [142, 147, 342, 343, 348, 349]. An exponential fit function of  $A \times \exp(-\alpha_B \delta y)$  is also included.

#### 3.1.4.4 Imprints of nuclear structure on the collective effects:

The 2015 NSAC long-range plan points out that there is an important advantage of colliding nuclei of different shapes, such as uranium, copper or gold. In such collisions, one can measure observables that are related to collectivity and see the imprints of the initial-state geometry and fluctuations. Over the past seven years, measurements at RHIC and the LHC have revealed that bulk observables in relativistic heavy-ion collisions are very sensitive to nuclear shape and nuclear radial profile. Leveraging the knowledge of nuclear structure from low-energy experiments, we then have a new tool to independently probe and constrain the initial condition of heavy-ion collisions.

The complications of the final-state effects can be largely eliminated if one considers collisions of systems with similar mass but different structural properties, which are well-known for many stable isotopes. These properties can be characterized, for instance, by parameters of a deformed Woods-Saxon distribution such as quadrupole deformation,  $\beta_2$ , octupole deformation,  $\beta_3$ , triaxiality  $\gamma$ , half-width radius,  $R_0$ , and surface diffuseness,  $a_0$ . In particular, we focus on the ratio of a given observable  $\mathcal{O}$  in collisions of isobars  $X$  and  $Y$ , and ask:  $\mathcal{O}_{X+X}/\mathcal{O}_{Y+Y} \stackrel{?}{=} 1$ . Any significant departure from unity must originate from the structural differences. Based on a Taylor expansion, numerical simulations show that isobar ratios can be

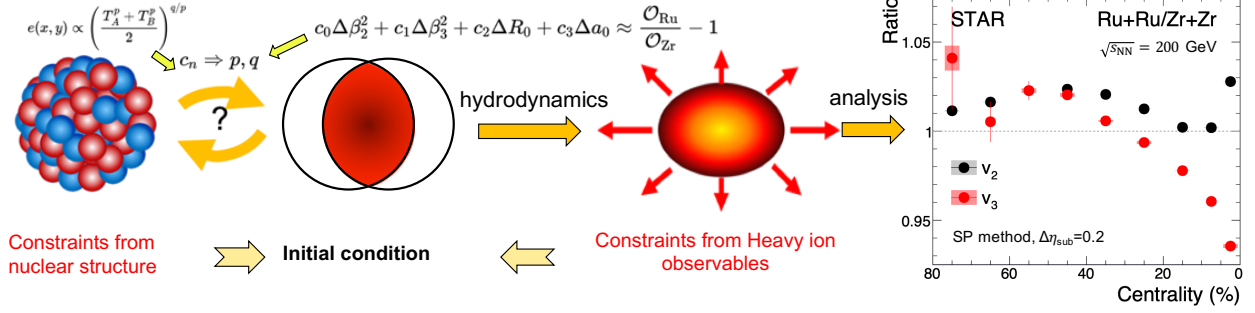


Figure 13: Impact of isobar-like collisions on the initial condition of QGP. Better control on the initial condition can be achieved by exploiting the constraints from both the ratios of final-state observables ( $v_2$  and  $v_3$  on the right side) [357] and the nuclear structure knowledge (left side). The left formula is a generic Ansatz for the initial energy of the system [358, 359], parametrized from the thickness functions of two nuclei,  $T_A$  and  $T_B$ . The parameters  $p, q$  can be constrained from  $c_{\mathcal{O},n}$  in Eq. 8.

approximated by [360–362]:

$$\frac{\mathcal{O}_{X+X}^{\text{ini}}}{\mathcal{O}_{Y+Y}^{\text{ini}}} \approx \frac{\mathcal{O}_{X+X}}{\mathcal{O}_{Y+Y}} = 1 + c_{\mathcal{O},1}(\beta_{2,X}^2 - \beta_{2,Y}^2) + c_{\mathcal{O},2}(\beta_{3,X}^2 - \beta_{3,Y}^2) + c_{\mathcal{O},3}(R_{0,X} - R_{0,Y}) + c_{\mathcal{O},4}(a_{0,X} - a_{0,Y}), \quad (8)$$

where  $\mathcal{O} \equiv p(N_{\text{ch}}), v_n$ , or  $\langle p_T \rangle$  are related to corresponding initial-state estimators,  $\mathcal{O}^{\text{ini}}$ , such as  $\epsilon_n$  for the  $v_n$ . The parameters  $c_{\mathcal{O},1}$  to  $c_{\mathcal{O},4}$  are found to be insensitive to final state effects [363, 364], and hence reflect directly the response of the initial condition to changes in the nuclear structure parameters (see Figure 13). From the experimentally measured isobar ratios on the left-hand side and known nuclear structure differences on the right-hand side, the  $c_{\mathcal{O},n}$  can be determined directly. Relations similar to Eq. (8) are also established for higher-order observables, such as  $\langle v_2^2 \delta p_T \rangle \sim a - b\beta_2^3 \cos(3\gamma)$  [365]. Therefore, isobar ratios offer a new tool to constrain the initial condition by exploiting nuclear structure information.

The impact of nuclear shapes on flow observables has been observed in isobar-like comparisons between  $^{238}\text{U}+^{238}\text{U}$  and  $^{197}\text{Au}+^{197}\text{Au}$  at RHIC [17, 366] and between  $^{129}\text{Xe}+^{129}\text{Xe}$  and  $^{208}\text{Pb}+^{208}\text{Pb}$  at the LHC [16, 367, 368]. The most striking evidence, however, was recently obtained from  $^{96}\text{Ru}+^{96}\text{Ru}$  and  $^{96}\text{Zr}+^{96}\text{Zr}$  collisions at RHIC [357]. Ratios of more than ten observables have been measured, all displaying distinct and centrality-dependent deviations of up to 30% from unity, two of which are reported in the right panel of Figure 13 [369]. The ratios in central collisions are mostly impacted by deformation, while in mid-central collisions they are impacted by  $R_0$  and  $a_0$  [362, 363, 370, 371]. The behavior of  $v_3$  and  $v_2$  suggests a large  $\beta_{3,Zr}$ , not predicted by mean field structure models [372]. As argued above, such rich and versatile information provides a new type of constraint on the initial condition.

### 3.1.5 Chirality and vorticity in QCD

Gauge fields describe the fundamental interactions in the Standard Model of particle physics. Gauge field configurations with nontrivial topology, such as instantons and sphalerons, are known to play crucial roles in many important phenomena, from matter-anti-matter asymmetry of today's universe to nonperturbative structures of the QCD vacuum. Their presence is however elusive for experimental detection. A novel approach for accessing such topological structures is to look for the Chiral Magnetic Effect (CME) in heavy-ion collisions. The CME predicts an electric charge separation along the large magnetic fields created at early times in these collisions, given the presence of nonzero quark chirality which in turn is a direct consequence of gluon topological fluctuations. Probing the CME signatures provides a unique way to explore the phenomenological roles of the quantum anomaly that connects quark chirality with gluon topology. In addition,



the observation of the CME could provide important evidence for the chiral symmetry restoration at high temperature — a fundamental feature of QCD theory.

Since the initial measurements published by STAR in 2009 with the first hint of possible CME signal, extensive theoretical studies as well as enthusiastic experimental search at both RHIC and LHC have been conducted. The key issue for an unambiguous detection of CME is a rather small signal embedded in a very large contribution from bulk background correlations. As noted in the 2015 Hot QCD White Paper: “*While there have been hints of the CME in experiments, conventional explanations of these data exist as well.*” Since then, substantial progress has been achieved in addressing this challenge.

On the theoretical front, the critical need was clearly identified in the 2015 Hot QCD White Paper: “*Quantifying the predictions regarding signatures of quantum anomalies is crucial. This requires inclusion of the anomalies into the standard hydrodynamic framework.*” Such a goal has been achieved through the development of EBE-AVFD (event-by-event anomalous-viscous fluid dynamics) [373, 374] as part of the Beam Energy Scan Theory (BEST) Collaboration project [1]. This comprehensive framework provides the quantitative simulations of CME transport on top of realistic bulk hydrodynamic evolution and implements relevant background correlations. It has now been widely used for studying anomalous transport, and in particular, adopted as an essential tool for developing, calibrating and interpreting various experimental observables [375–379].

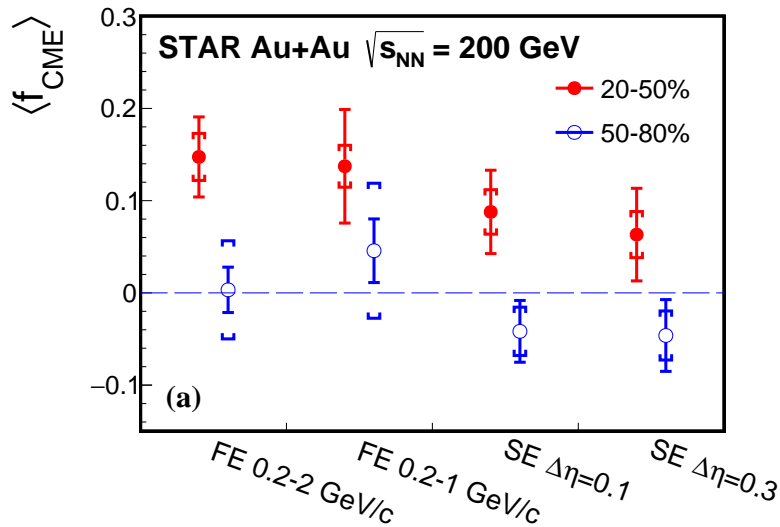


Figure 14: The CME signal fraction  $\langle f_{\text{CME}} \rangle$  after flow-background removal signal in 50–80% (open markers) and 20–50% (solid markers) centrality Au+Au collisions at  $\sqrt{s_{\text{NN}}} = 200 \text{ GeV}$ , extracted by various analysis methods (FE: full-event, SE: sub-event) and kinematic cuts. Error bars show statistical uncertainties; the caps indicate the systematic uncertainties. Figure from [380].

On the experimental side, a number of new methods and observables have been developed, aiming at the extraction of possible signals and separation of background correlations. By utilizing event-shape engineering approach as well as comparison with small colliding systems, the CMS and ALICE Collaborations have put stringent limits on the existence of CME at LHC energies [381–384]. On the other hand, the latest measurements from the STAR Collaboration using a variety of analysis methods [380, 385, 386] indicate a nonzero CME signal in 200 GeV Au+Au collisions at RHIC, albeit with still limited statistical significance. Fig. 14 shows an example of the finite signal fraction  $\langle f_{\text{CME}} \rangle$  at  $1 \sim 3\sigma$  level for 20–50% centrality [380], extracted from the overall charge-dependent azimuthal correlations by exploiting the azimuthal fluctuations of the magnetic fields [387] and comparing measurements relative to spectator versus

participant planes [388, 389]. Another significant step for the CME search was taken by completing the isobar collision experiment at RHIC, where data for several billions of events were recorded for each of the Ru+Ru and Zr+Zr colliding systems. Collisions of such isobar pairs were expected to produce identical bulk flow backgrounds while generating different CME signals due to differing magnetic field strength arising from their respective nuclear charges. A rigorous blind analysis procedure was developed and completed by the STAR Collaboration [390], with the results announced in 2021 [357]. The unprecedented high precision achieved in the isobar data analysis was able to decisively reveal the few-percent level of difference in the bulk properties (such as multiplicity and elliptic flow in the same centrality class) of Ru+Ru and Zr+Zr systems, thus pointing to a non-negligible variation of background correlations between them and complicating their comparative analysis. A recent attempt to account for such observed bulk differences and identify appropriate baseline (zero-signal scenario) for isobar comparison has revealed a potential signal fraction at a few percent level [391], which however may be vulnerable to various uncertainties such as nonflow effect [392]. Clearly, a final conclusion on the CME search from isobar collisions will require further experimental analyses as well as theoretical studies.

While the CME pertains to novel spin transport under magnetic fields, the spin degrees of freedom could also respond nontrivially to macroscopic fluid motions with large vorticity fields. One of the major discoveries since the last Long Range Plan is the observation of hyperon global spin polarization by STAR Collaboration [125], opening a new direction of investigation in the field. See recent reviews in e.g. [393–395]. When two nuclei collide with each other, especially in non head-on collisions, the system carries a large orbital angular momentum, of the order of  $L \sim 10^5 \hbar$ , which is partially transferred to the created medium. Particles produced in the collisions are “globally” polarized on average along the initial orbital angular momentum direction [396–398]. Under the assumption of local thermal equilibrium, the polarization  $\mathbf{P}$  can be determined by the local vorticity of the fluid  $\boldsymbol{\omega}$  [398]. In a non-relativistic limit, the polarization is simplified as [399]

$$\mathbf{P} \approx \frac{(s+1)}{3} \frac{(\boldsymbol{\omega} + \mu \mathbf{B}/s)}{T}, \quad (9)$$

where  $T$  is the temperature,  $s$  and  $\mu$  are the spin and magnetic moment of the particle, and  $\mathbf{B}$  is the magnetic field whose direction coincides with the direction of  $L$ , i.e., perpendicular to the reaction plane. A more general expression of the above equation that is relativistically covariant and properly in terms of thermal vorticity can be found in e.g. [400]. More recently it has been found that the spin polarization is also sensitive to the so-called thermal shear tensor contribution arising from the linear and symmetric part of the hydrodynamic field gradients [401, 402], which induces nontrivial local spin polarization patterns while leaves the global spin polarization unchanged.

Global polarization of  $\Lambda$  hyperons was first observed in the beam energy scan of Au+Au collisions [125] and later confirmed at  $\sqrt{s_{NN}} = 200$  GeV with more differential measurements [126]. As shown in Fig. 15 (left),  $\Lambda$  global polarization shows the collision energy dependence where a larger signal is observed when decreasing the collision energy — a nontrivial trend that could be understood from the predicted beam energy dependence of average vorticity in these collisions [403]. The data are in good agreement with theoretical calculations, such as hydrodynamics, transport model, and chiral kinetic theory. This reveals that the QGP is the most vortical fluid ever observed, of the order of  $\omega \sim 10^{21} \text{ s}^{-1}$ . Recent measurements at STAR fixed-target and HADES experiments [404, 405] show the largest polarization at a few GeV, which is close to the  $\Lambda$  production threshold and in which lower energies the system would be dominated by hadronic interactions rather than partonic interactions. At LHC energies, the signal is expected to be small and current results are consistent with zero [127].

As indicated in Eq. (9), there could be a contribution from the magnetic field which leads to larger polarization of  $\bar{\Lambda}$  than that of  $\Lambda$  due to the sign of  $\mu$ . In other words, one could probe the later-stage magnetic field with this measurement [399, 406, 407] which will be an important input for theoretical predictions of the

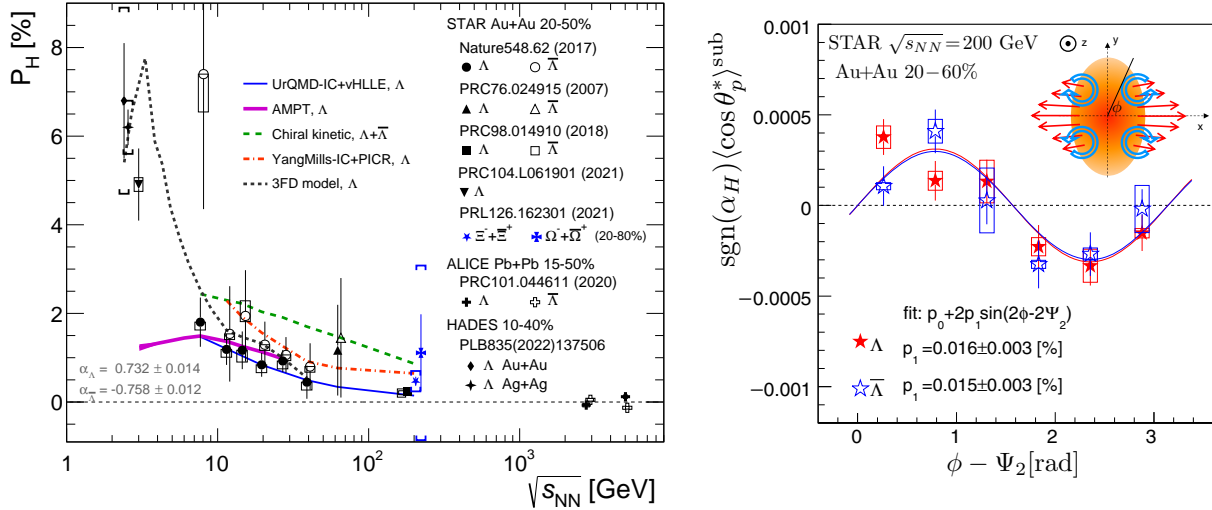


Figure 15: (Left) Hyperon global polarization as a function of collision energy, compared to various theoretical calculations. (Right) Polarization along the beam direction,  $\langle \cos \theta_p^* \rangle \approx \alpha_H P_z / 3$ , as a function of azimuthal angle for  $\Lambda$  and  $\bar{\Lambda}$  hyperons in Au+Au collisions at  $\sqrt{s_{NN}} = 200$  GeV.

CME signal, although there are other possible mechanisms to make such a difference [408–411]. Current measurements show a hint of the difference at lower energies but the difference is not significant. The possible difference between  $\Lambda$  and  $\bar{\Lambda}$  and the energy dependence in lower energies are being investigated with high statistics data collected during BES-II program at RHIC.

Recently, STAR also measured global polarization of multistrangeness such as  $\Xi$  and  $\Omega$  hyperons at  $\sqrt{s_{NN}} = 200$  GeV [412]. It is of great importance to confirm the global polarization and vorticity picture using different particles with different spins and/or magnetic moments to better understand the polarization mechanism in heavy-ion collisions. The uncertainties need to be reduced with future measurements but there seems to be a hint of a hierarchy in global polarization, i.e.,  $P_\Lambda < P_\Xi < P_\Omega$ , qualitatively consistent with a predicted mass-ordering effect [413]. Measurement of non-zero  $P_\Omega$  also helps to determine the sign of unmeasured decay parameter  $\gamma_\Omega$  [414].

Richer vortical structures due to density fluctuations coupled with the system collective expansion have been predicted [415–418]. In heavy-ion collisions, elliptic flow has been extensively studied and known as a consequence of stronger expansion into the reaction plane angle, which was predicted to lead the polarization along the beam direction  $P_z$  changing the sign depending on azimuthal angle. Such a local polarization was observed by STAR at RHIC [128] and later by ALICE at the LHC [129]. Figure 15 (right) shows  $P_z$  ( $\approx 3 \langle \cos \theta_p^* \rangle / \alpha_H$ ) as a function of azimuthal angle relative to elliptic flow plane angle ( $\Psi_2$ ). A quadrupole pattern of the polarization was observed which is consistent with the expectation from elliptic flow (see a cartoon inside the figure) and the blast-wave model with parameters determined by the fits to  $p_T$  spectra and HBT measurements [128, 417]. However unlike the case for the average global polarization, many theoretical models fail to describe the data of  $P_z$ , implying a possible lack of understanding the origin of the polarization and importance of non-equilibrium dynamics of spin in heavy-ion collisions. The latest studies in [401, 402] suggest that the inclusion of the thermal shear contribution to spin polarization could be important for explaining the data. A more quantitative investigation in [419] finds that the resulting longitudinal polarization results differ between two proposed implementations of the thermal shear terms and also depend upon the hydrodynamic initial conditions.

The polarization measurement of strongly decaying particles is more difficult but one can measure the

00<sup>th</sup> element of the spin density matrix  $\rho_{00}$  of vector mesons [420], which represents the probability to have spin projection onto the polarization axis to be zero. The deviation of  $\rho_{00}$  from  $1/3$  indicates spin alignment of vector mesons. Global spin alignment of  $\phi$  and  $K^{*0}$  mesons has been measured both at RHIC [421] and the LHC [422] and significant deviation from  $1/3$  was observed;  $\rho_{00} \sim 0.2-0.3$  ( $< 1/3$ ) for  $K^{*0}$  at the LHC and  $\rho_{00} \sim 0.36$  ( $> 1/3$ ) for  $\phi$  in lower energies at RHIC. These large deviations cannot be explained by the vorticity picture and possible explanation might be a strong force field as proposed in Refs. [423–425] which needs further investigation.

## 3.2 Mesoscopic: emergence of the quark-gluon plasma and approach to equilibrium

### 3.2.1 Small Collision Systems

Systems of different sizes and shapes, such as p+p, p+A, d+A, and  $^3\text{He}+A$  present challenges and opportunities for the study of mesoscopic QCD matter. In such systems the thermalization process has a significant impact on flow observables, offering a unique experimental window into the evolution of the QCD system from a quantum wave function to a hydrodynamically expanding quark-gluon plasma [426]. It is this transition and its rich non-Abelian many-body dynamics that we wish to briefly review and explore further both theoretically and experimentally.

The initial wave function of the system is characterized by its mean and fluctuations, and these initial-state fluctuations can yield measurable correlations in the final state [11]. Characterizing the fluctuation of the incoming particles (such as the fluctuation in the proton radius) is interesting in its own right, and is essential if the dynamics of the initial state are to be disentangled from the flow-like correlations built up by the many-body response of the system in its approach to equilibrium. Addressing this concretely is possible due to advances in experimental measurements and probes, and theory and simulation.

This section is structured as follows. First, in Section 3.2.2 we will review the measurements, and discuss a variety of new probes which can concretely characterize initial state fluctuations, both in rapidity and in the transverse plane. Ultimately, these experimental inputs will be the basis for numerical simulations that describe the system's thermalization process in detail. Since the last Long Range Plan, there has been enormous progress in understanding the transition to hydrodynamics both at weak and strong coupling from simulations. Indeed, there are features of the transition to hydrodynamics that are seemingly universal, and independent of the coupling. This is reviewed in Section 3.2.3. The challenge is to use the detailed experimental probes as a function of system size, together with advances in theory and simulation that incorporate these universal features, to provide a comprehensive picture of thermalization and the onset of hydrodynamics in small systems. Section 3.2.4 describes the connection between the interplay between the medium and hard probes.

### 3.2.2 Small systems & small size limit of the QGP

In the last decade, the experimental exploration of small collision systems has brought a paradigm shift in the understanding of hot QCD. Previously, proton-nucleus or deuteron-nucleus collisions were considered to be control experiments with no QGP formation that provide opportunities to study how cold nuclear matter in the initial state affects final-state observables. Proton-proton collisions are usually used as a reference baseline to quantify the nuclear effects. Most notably, the absence of suppression in the production of high- $p_T$  hadrons and in back-to-back di-hadron correlations in d+Au collisions at RHIC solidified the discovery of jet quenching in heavy-ion collisions [427–430]. The subsequent discovery of long-range correlations ("ridge") in particle productions in high-multiplicity p+p [431] and pPb [432–435] collisions at the LHC came as a surprise. At RHIC, reanalysis of previously recorded d+Au data [436–438] revealed that long-range angular correlations are also present in d+Au collisions at 200 GeV. In nucleus-nucleus (A+A) collisions the ridge is associated with the anisotropic collective expansion of QGP resulting from anisotropies in the initial collision geometry, which are subsequently transferred to the azimuthal distributions of the produced particles. If the ridge in p+p and p/d+A collisions is of the same origin as in A+A collisions, then the formation of small QGP droplets cannot be excluded in small systems and their role as control experiments has to be re-examined.

Following the initial discoveries, a vigorous experimental exploration ensued testing most every aspect of the bulk system dynamics associated with QGP formation in large systems (reviews can be found in Refs. [439–441]). The LHC experiments collected new pPb data at 8.16 TeV to complement the 2013 and 2016 data sets at 5.02 TeV. The higher collision energy gave access to higher multiplicities than previously

experimentally accessible. At LHC, high-multiplicity p+p collisions have been studied at several center-of-mass energies ranging from 2.76 TeV to 13 TeV. In 2014-2016 RHIC conducted a geometry scan with p/d/<sup>3</sup>He+Au collisions [76, 442–444] at 200 GeV providing means to test if the initial geometry is reflected in the final-state particle distributions. Additionally, a beam energy scan (200, 62.4, 39, and 19.6 GeV) with d+Au collisions [443, 445] was performed to investigate if the apparent collectivity turns off at lower collision energy. The geometry and beam energy scan with small systems comprised a major part of the last three years of the PHENIX experimental program. Since then, additional d+Au and O+O collision data at 200 GeV were collected by the STAR experiment in 2021 with the addition of a dedicated event-plane detector covering the pseudorapidity region of  $2.2 < |\eta| < 5.2$  and extended coverage in the TPC to  $|\eta| < 1.5$ . The LHC experiments utilized ultra-peripheral collisions (UPC) in Pb+Pb [446] and p+Pb [447] to examine if there are signs of collectivity in photon-nucleus and photon-proton collisions. Two-particle correlations were also studied in archived data from hadronic Z-boson decays in  $e^+e^-$  collisions measured by ALEPH at LEP [448], and in hadronic  $e^+e^-$  annihilation events at 10.52 GeV off-resonance from the  $\Upsilon(4S)$  state with the Belle experiment at KEKB [449], as well as in archived deep inelastic scattering events from e+p collisions with Zeus at HERA [450].

The collective behavior is characterized with single-particle azimuthal anisotropies that are quantified by  $n^{\text{th}}$ -order Fourier coefficients, or flow harmonics,  $v_n$ . There are different methods of measuring the flow harmonics that have different sensitivity to event-by-event flow fluctuations and to nonflow correlations that arise from resonance decays, Bose–Einstein correlations, and jet production. To reduce short-range nonflow correlations in the two-particle correlation analyses the particles are separated by rapidity gaps. By construction, the multi-particle cumulant measurements suppress nonflow by subtracting off lower order correlations. Measurements of  $v_2$  with multi-particle correlations in pPb [451–454] and in p+p [455–457] collisions at the LHC established that the observed long-range correlations are a collective phenomenon. At RHIC, up to 6-particle cumulants were studied in d+Au collisions at 200 GeV [445], and also found to agree with expectations for hydrodynamic behavior both in the measured values with 2-, 4-, 6- particles and the expected relation between the cumulants and the event-by-event flow fluctuations. Going down in energy the multi-particle measurements are more challenging as the multiplicity is reduced and nonflow correlations are more difficult to suppress. Nevertheless, real-valued  $v_2\{4\}$  were observed down to the lowest center-of-mass energy measured in d+Au collisions, indicating that collective effects may persist. Figure 16 shows the measurements of  $v_2$  using two- and multi-particle correlations from ALICE, ATLAS, and CMS collaborations from p+Pb collisions at 5.02 TeV, and the PHENIX collaboration in d+Au collisions at 200 GeV.

Another feature of the collectively expanding QGP in large systems is the mass dependence of the particle spectral shapes and the  $v_n$  coefficients. These features have also been seen in small systems and studied extensively with light-flavor hadrons [459–466]. Surprisingly, open-charm hadrons and even  $J/\psi$  also exhibit collective behavior in both pPb and in p+p collisions, while there is no clear evidence of bottom hadron flow in these systems [467–471].

Testing the response of the final-state particle production to the initial geometry motivated the geometry scan with p/d/<sup>3</sup>He+Au collisions at RHIC [472]. The three different projectiles provide initial geometries that have different elliptic and triangular eccentricities that can be probed in the final state with measurements of the second and third harmonics  $v_2$  and  $v_3$ . The PHENIX measurements [76, 442–444] shown in Figure 17 indicate that the final-state particle distributions retain memory of the initial-state geometry as expected in viscous hydrodynamics [75, 473]. Recent STAR measurements [474], on the other hand, find  $v_3(p_T)$  values that are system-independent within the uncertainties suggesting that sub-nucleonic fluctuations may influence the initial eccentricities. Kinematic dependencies in the flow and nonflow correlations, as well as longitudinal decorrelations may contribute to the observed differences [475]. In the PHENIX analysis the nonflow correlations are suppressed by imposing a large separation in pseudorapidity

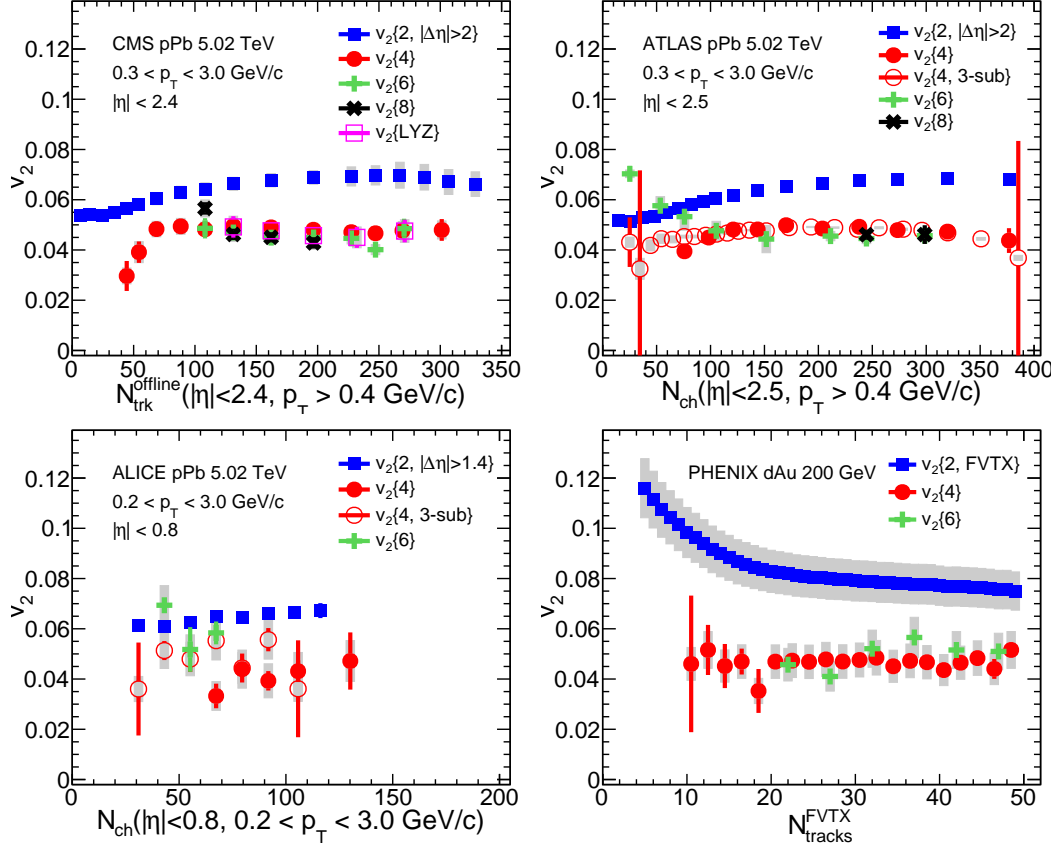


Figure 16: The measured  $v_2$  using two- and multi-particle correlations from CMS [455], ATLAS [458], and ALICE collaborations [457] in pPb collisions at 5.02 TeV, and PHENIX collaboration [445] in d+Au collisions at 200 GeV.

between the particles used to analyze flow and the event-plane detectors, the nonflow is estimated based on measurements in p+p collisions and included in the systematic uncertainties instead of being subtracted. The STAR measurements are performed in the range  $|\eta| < 0.9$  where nonflow correlations are large and are therefore subtracted. Nonflow correlations depend strongly on the particle separation in rapidity and nonflow estimates are challenging since there are significant model dependencies [476]. Large kinematic dependence in  $v_3$  values has also been observed by STAR in peripheral Ru+Ru and Zr+Zr [357] collisions. Another challenge is the fluctuations in rapidity. Because of this complication, which is becoming large in small systems, flow measurements in different rapidity windows do not have to agree. From a theoretical point of view characterizing these three-dimensional fluctuations is particularly important. Recent calculations [477] with  $(3 + 1)$ D framework combining a dynamic initial state with hydrodynamics and hadronic transport give a better description of the data. Further discussion has been given in Section 3.1.1. In the future, measurements of flow decorrelations at different rapidities, such as e.g. [135], with the upgraded STAR detector and in sPHENIX will be essential to a complete understanding of the dynamics.

Overall, the hydrodynamic description of the system evolution gives the most complete and quantitative description of the vast amount of experimental data collected with a variety of small collision systems spanning center-of-mass energies from 20 GeV to 13 TeV. However, certain features observed in the data are not unique to the hydrodynamic response to the initial-state pressure gradients. For example, momentum correlations in the initial state of the collision could persist into the final state as well. The relative contribu-

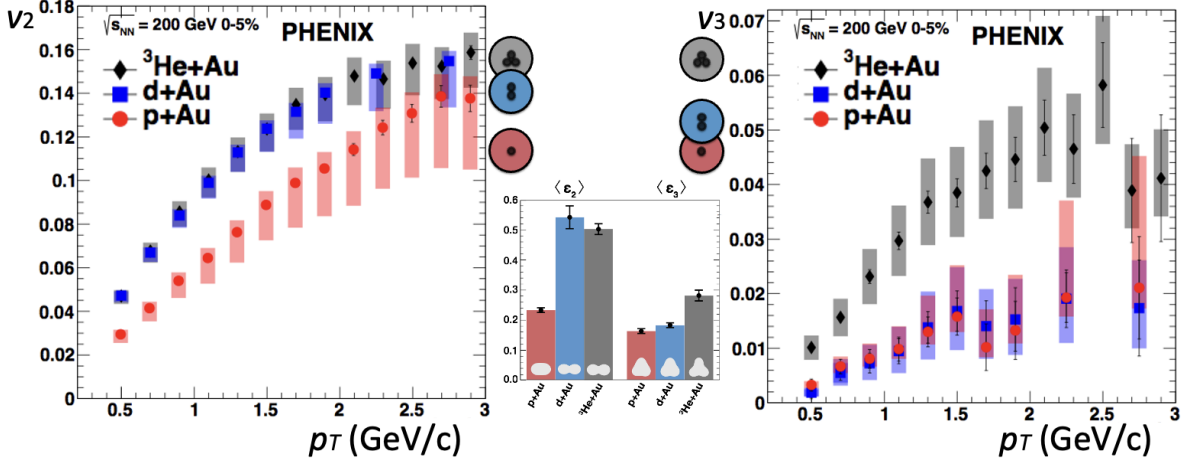


Figure 17: PHENIX measurements [76] of  $v_2(p_T)$  (left)  $v_3(p_T)$  (right) in  $\text{p}/\text{d}/^3\text{He}+\text{Au}$  collisions are compared to the initial spatial eccentricities (middle) calculated with the Glauber model.

tion to the final-state anisotropy is expected to become more important at low multiplicity and lower collision energy [478]. The correlations between  $v_n$  and mean  $p_T$  may provide means to distinguish initial-state momentum correlation effects [478] and hydrodynamic response [479]. The  $v_n$  and mean  $p_T$  correlations have been measured in  $\text{pPb}$  collisions by the ATLAS Collaboration [480], but the studied multiplicities may not be small enough to reveal any initial-state momentum correlations. Additionally, recent studies from the CMS collaboration [481] indicate that nonflow has to be carefully removed, since the theoretical models do not include these effects.

The observations of ubiquitous collective phenomena in large and small hadronic systems prompted searches for collectivity in photon-nucleus, photon-proton, and  $e^+e^-$  collisions. Significant nonzero flow coefficients are observed in  $\text{Pb}+\text{Pb}$  UPCs [446]. Calculations based on Color Glass Condensate [482] and full  $(3+1)\text{D}$  dynamical framework with 3D-Glauber+MUSIC+UrQMD [483] are both able to describe the data. In these models, the virtual photon in each UPC event is treated as a vector meson with a lifetime longer than the time of the interactions, therefore it is not a surprise to have flow in these calculations using meson-nucleus collisions. With the current multiplicity reach, no collective flow is observed in  $\text{pPb}$  UPC events [447]. If the photon-proton collisions are modeled as meson-proton interactions, it is possible that collective flow is revealed in  $\text{pPb}$  UPCs with future data sets that have larger statistical reach.

To account for collective effects in small systems string-based models, such as PYTHIA with color reconnections [484], the DIPSY rope hadronization [485], and the string-shoving [486], have been introduced and have demonstrated qualitative agreement with certain aspects of the data. The AMPT framework [487] based on parton transport also describes most of the collective observables well. A recent calculation in  $e^+e^-$  collisions with AMPT including string melting, parton scattering, hadronization and hadron re-scattering shows that a strong  $v_2$  can be created with two initial strings, while there is no observable signal of collectivity with one string [488]. The two-particle correlation measurements in  $e^+e^-$  collisions and deep inelastic  $\text{e}+\text{p}$  scattering do not indicate collective behavior [448–450]. The upcoming Electron-Ion Collider will provide new opportunities to explore collective phenomena in small systems.

### 3.2.3 Onset of hydrodynamics

There has been extraordinary progress in understanding the evolution of the system in the far from equilibrium situations relevant to heavy-ion collisions [489–492]. Significant developments have been made



towards understanding the emergence of hydrodynamic behavior in relativistic systems both in strong coupling [331, 493–501] and also in weak coupling/kinetic theory [78, 500, 502–520, 520–525]. Indeed, with the advent of hydrodynamic attractors [526], there is an emerging picture with which one can estimate the value of  $\tau_{\text{hydro}}$  where some form of hydrodynamics begins to apply at a given multiplicity see, for instance, Refs. [500, 510]. To illustrate and explain the main arguments behind these developments, here we consider a simple toy model of the QGP in terms of conformal kinetic theory [502, 503, 527] in the relaxation time approximation [528–531]. This type of approximation has provided powerful insights in the determination of the onset of hydrodynamic behavior in rapidly expanding systems [502, 503, 520, 529–532]. In fact, although the relaxation time approach may seem primitive, and the QGP is not a conformal system, many of the conclusions are expected to have a universal character as they reflect the competition between free streaming and dissipative dynamics of an approximately conformal system expanding longitudinally [533]. As we discuss below, the simple conformal kinetics captures the scaling behavior expected from QCD at weak coupling [534], and the scaling properties displayed by strongly coupled conformal theories based on the AdS/CFT correspondence [494]. Although below we focus on conformal systems for simplicity, we note that there has been recent evidence of the existence of hydrodynamic attractors for certain moments of the one-particle distribution function in non-conformal systems [535–537].

**Longitudinal Expansion.** Let us first assume the system undergoes homogeneous Bjorken expansion [538]. We consider a conformal medium, which essentially implies that the energy density,  $e$ , and the isotropic pressure,  $P$ , of the system are related via  $e = 3P$ . Furthermore, at finite temperature  $T$ , any dimensionful quantity scales with appropriate powers of  $T$  (for example,  $e \sim T^4$ ). For a Bjorken expanding system, conformality together with energy-momentum conservation,  $\partial_\mu T^{\mu\nu} = 0$ , gives

$$\frac{de}{d\tau} = \frac{e + P_L}{\tau}. \quad (10)$$

where  $P_L$  is the system's longitudinal pressure and  $\tau$  is the proper time. In first-order Navier-Stokes viscous hydrodynamics the longitudinal pressure takes the form  $P_L/e = \frac{1}{3} - \frac{16\eta/s}{9\tau T}$ , while second-order viscous corrections are of order  $(\eta/sT\tau)^2$  [490], where  $s$  is the entropy density and  $\eta$  is the shear viscosity. The hydrodynamic attractor concept [526] anticipates an all-order resummation of these terms into a constitutive relation of the form  $P_L/e = f(w)$ , where  $w(\tau) = \tau T_{\text{eff}}/(4\pi\eta/s)$  [489]. The effective temperature  $T_{\text{eff}}$  is defined through the non-equilibrium energy density and the equation of state,  $sT = \frac{4}{3}e = b_{\text{qgp}}T^4$ , where  $b_{\text{qgp}} \simeq 17.6$  is estimated from the lattice equation of state at high temperatures [539, 540]. Traditionally, hydrodynamics is expected to emerge when the Knudsen number, determined by the ratio between microscopic scales  $\ell$  (e.g., the mean free path of a gas) and macroscopic scales  $L$  associated with the spatial gradients of conserved quantities,  $\text{Kn} = \ell/L$ , becomes much smaller than unity. Here,  $w \sim 1/\text{Kn}$  so the hydrodynamic limit is valid at late times when  $w \gg 1$ , and corrections are organized in powers of  $w^{-1}$  (or, equivalently, in powers of  $\text{Kn}$ ). If the attractor constitutive relation is appropriate, the energy density takes the form [541]

$$\frac{e(\tau)\tau^{4/3}}{(e\tau^{4/3})_\infty} = \mathcal{E}(w). \quad (11)$$

Here  $(e\tau^{4/3})_\infty \propto (\tau s)_\infty^{4/3}$  normalizes the entropy in the system and  $\mathcal{E} \rightarrow 1$  at late times.

Numerous simulations in the relaxation time approximation [508–510, 513, 519, 520, 542], in complete QCD kinetic theory [78, 500, 504, 511, 512, 515], and the AdS/CFT correspondence [331, 494–501], show that the simple interpolating form of Eq. (11) captures the overall dynamics. The form of  $\mathcal{E}(w)$  is strongly constrained by its behavior at early and late times. At late times the entropy per rapidity  $(\tau s)_\infty$  is constant, while at early times  $\tau \rightarrow 0$  the energy per rapidity  $(\tau e(\tau))_0$  is constant, fixing the behavior  $\mathcal{E} \simeq C_\infty^{-1}w^{4/9}$  [541]. The constant  $C_\infty$  depends only very weakly on the theory and is approximately

unity. Simulations with QCD kinetic theory give  $C_\infty \simeq 0.87$ , while the AdS/CFT correspondence gives  $C_\infty = 1.06$  [494, 526].

The first phenomenological importance of the hydrodynamic attractor is that it determines the energy density with 20% accuracy during the initial stages from the measured charged particle multiplicity, almost irrespective of the underlying theory [541]. This level of precision can then significantly constrain models for the initial state, such as those built upon the color-glass condensate [543]. The second phenomenological importance of the attractor solution is that it provides a criterion for the onset of hydrodynamics, a criterion which has been validated in detailed studies. Specifically, the hydrodynamic gradient expansion becomes appropriate at a time  $\tau_{\text{hydro}}$  when  $w \simeq 1$  or larger. To translate this theoretical criterion into an experimental one, we first note that total entropy per rapidity in hydrodynamics is directly related to the hydrodynamic multiplicity [511]

$$\frac{dS}{dy} = b_{\text{hrg}} \frac{dN}{d\eta} \quad (12)$$

where  $b_{\text{hrg}} \simeq 8.3$  is determined by the particle content of the hadron resonance gas model and the lattice equation of state, and has a 15% uncertainty [511]. The temperature at late times is determined by the constant entropy or multiplicity  $dN_{\text{ch}}/d\eta \propto \tau T^3$  leading to

$$w \equiv \frac{\tau T}{4\pi\eta/s} = \frac{1}{4\pi\eta/s} \left( \frac{1}{N_0} \frac{dN_{\text{ch}}}{d\eta} \right)^{1/3} \left( \frac{\tau}{R} \right)^{2/3} \quad (13)$$

$$\equiv \chi \left( \frac{\tau}{R} \right)^{2/3}, \quad (14)$$

where we have defined the *opacity* of the system<sup>2</sup>

$$\chi = \frac{1}{4\pi\eta/s} \left( \frac{1}{N_0} \frac{dN_{\text{ch}}}{d\eta} \right)^{1/3}, \quad N_0 \equiv \frac{\pi b_{\text{hrg}}}{b_{\text{qgp}}} \simeq 6.68. \quad (16)$$

We note that the multiplicity factor  $N_0$  is primarily determined by the properties of the equation of state, which is known from lattice QCD. Consequently the uncertainties in  $N_0$  are only of order 20%. The system will have a strong hydrodynamic response if  $\tau_{\text{hydro}}/R \ll 1$  [78]

$$\frac{\tau_{\text{hydro}}}{R} = \frac{1}{\chi^{2/3}} \propto \frac{1}{\sqrt{dN_{\text{ch}}/d\eta}}, \quad (17)$$

which amounts to a requirement that the opacity is large  $\chi \gg 1$ . The final expression for the opacity is

$$\chi = \left( \frac{2}{4\pi\eta/s} \right) \left( \frac{dN_{\text{ch}}/d\eta}{54} \right)^{1/3}. \quad (18)$$

Figure 18 shows this opacity as a function of multiplicity and the range of systems explored in heavy-ion collisions.

**Transverse Expansion.** The attractor solution  $\mathcal{E}(w)$  for the energy density is valid before the transverse expansion begins. Viscous corrections in this regime are organized in inverse powers of  $w$ :

<sup>2</sup>There are several definitions of this type of opacity in the literature. In a conformal relaxation time approximation, an opacity  $\hat{\gamma}$  was defined from the transverse energy at time zero [522, 523, 544]. Using the attractor solution  $\hat{\gamma}$  can be related to the opacity defined here:

$$\chi = C_\infty^{1/4} \left( \frac{5\hat{\gamma}}{4\pi} \right)^{8/9} \simeq 0.432 \hat{\gamma}^{8/9}. \quad (15)$$

so that  $\chi = 1$  is  $\hat{\gamma} \simeq 2.6$ .

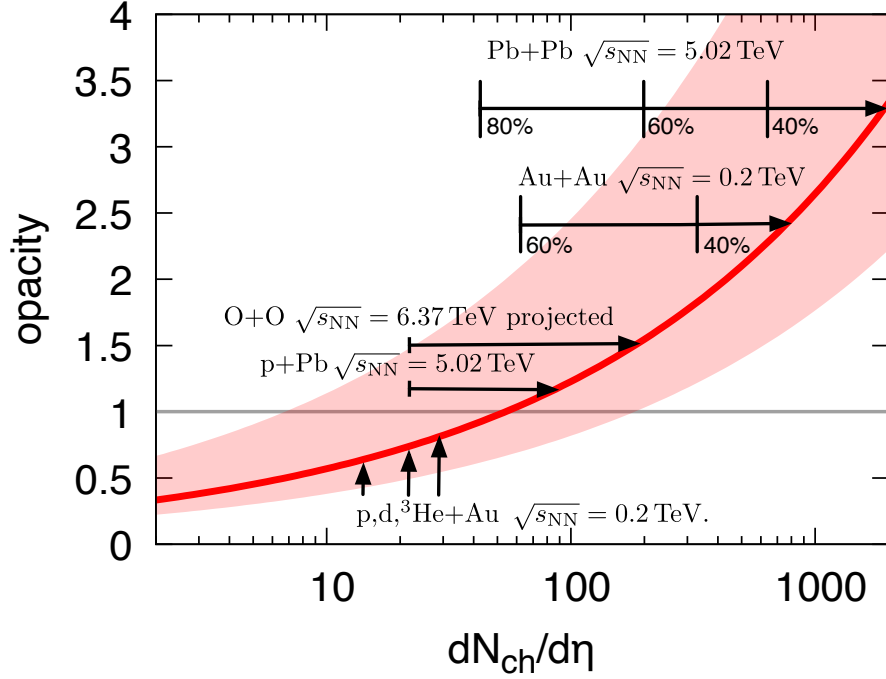


Figure 18: The opacity,  $\chi$ , as a function of multiplicity defined in Eq. (18). (See Eq. 15 for relations to alternate definitions). Hydrodynamics is a valid approximation for  $\chi \gtrsim 1$ . The solid line is for  $\eta/s = 2/4\pi$ , and the band indicates the range  $\eta/s = (1 \leftrightarrow 3)/4\pi$ , with  $\eta/s = 1/4\pi$  corresponding to the top of the band. The multiplicity is shown for Pb+Pb at the LHC for a centrality range of 0-80% [545], and Au+Au at RHIC for a centrality range of 0-60% [546]. Projections for the O+O run at the LHC are taken from [547]. p+Pb data from the LHC are estimated from a recent analysis [548]. The multiplicity from the geometry scan at RHIC is taken from [549].

$$\mathcal{E}(w) = 1 + \frac{C_1}{\chi} \left(\frac{\tau}{R}\right)^{-2/3} + \frac{C_2}{\chi^2} \left(\frac{\tau}{R}\right)^{-4/3} + \dots \quad (19)$$

$$\Rightarrow 1 + \frac{C_1}{\chi} + \frac{C_2}{\chi^2} + \dots \quad (20)$$

At the boundary of applicability, when  $\tau \simeq R$ , the attractor  $\mathcal{E}(w)$  is only a function of  $\chi$ . Since the subsequent three-dimensional hydrodynamics must match with the attractor solution at early times, the transverse hydrodynamic response is only a function of the opacity  $\chi \propto (dN_{\text{ch}}/d\eta)^{1/3}$ , and viscous corrections to the transverse flow are organized in powers of  $1/\chi$  [550].

This has a number of consequences. First, since the opacity for a conformal system is only a function of multiplicity and not the radius, systems with different sizes but the same multiplicity should exhibit similar transverse flow. Experimentally, it is observed that at the same multiplicity the fluctuation driven  $v_2$  and  $v_3$  are the same in the p+Pb and Pb+Pb to 5% accuracy [432, 550]. This seems to corroborate the conformal assumptions [550], provided a minimal random cluster model (with the number of clusters proportional to the multiplicity) is adopted for the geometric fluctuations. We should emphasize here that there are corrections to the conformal characterization of the system, which remain to be fully clarified.

Additional corrections to the transverse response stem from the pre-equilibrium evolution and are not captured by hydrodynamics even for  $\chi \gg 1$ . They are of order  $\tau_{\text{hydro}}/R \propto 1/\chi^{3/2}$  and are suppressed

compared to the first viscous correction, which is of order  $1/\chi$  [522,544,551]. The non-equilibrium response modifies the initial conditions for hydro by an amount of order  $\tau_{\text{hydro}}/R$ . Conversely, for  $\chi > 1$  the non-equilibrium dynamics plays a prominent role and hydrodynamics is not clearly applicable.

### 3.2.4 *Medium response of partonic excitations*

Jets, the collimated spray of particles resulting from a hard scattering, are typically used to probe the medium properties at the microscopic level. However, the response of the QGP to the hard scattered parton provides insight at the mesoscopic level and into the interplay between soft and hard physics.

Medium response refers to the excitation of the medium caused by the jet-medium interaction and plays a non-negligible role in the transport of jet energy and momentum. In the jet-medium interaction, some jet momentum is transferred to medium constituents or recoil particles, which further propagate in the medium and interact with other medium constituents. These recoil medium constituents carrying some of the jet energy and momentum undergo the hadronization process mostly through coalescence and contribute to low-momentum hadrons spreading around the jet axis. Since these soft hadrons are correlated with the jet, they, in principle, should be considered as part of the jet and not be subtracted as a background. The uncorrelated background can be computed theoretically through simulations of the same events without the triggered jet and subtracted from the events with the jet. Experimentally, such background subtraction without affecting hadrons from the medium response is still a challenge.

The medium response not only contributes to the jet reconstruction and jet-correlated observables but is also closely related to some interesting phenomena related to the properties of the QGP medium. Since recoil medium constituents go through further interaction, this part of the jet energy and momentum they carry will be spread to more recoil and radiated partons leading to thermalization of the energy and momentum lost by the leading jet partons. Thus, the medium response can address a fundamental question in investigating the QGP properties: how do non-equilibrium partons equilibrate in a QGP heat bath? When a fluid gains energy and momentum from a source moving faster than the speed of sound, a conical-shaped shock wave, the so-called Mach cone, forms. The angle of the Mach cone is determined by the medium's sound velocity, while the shock wave's width is influenced by the shear viscosity [552]. The jet-induced medium response, therefore, also reflects the hydrodynamic transport properties of QGP. Furthermore, through the interplay between the jet-induced medium response and background flow, jets have the potential to distinguish among different possible global flow patterns of the background QGP fluid [553–555].

In some Monte-Carlo models of the in-medium jet shower, the medium response is implemented as the transport of recoil partons [556–561] in a linear Boltzmann transport approximation. In this recoil prescription, the energy-momentum exchange between the jet and the medium is mediated by 2-to-2 parton scatterings. The initial medium parton in these scattering processes is sampled from the thermal distributions. These medium partons, after the scattering, will propagate and interact with the medium just like other jet partons. The successive interactions between the recoil and the medium partons form a structural wake of recoils, which spreads like a Mach cone. In addition to jet-induced medium response in the form of the Mach-cone-like excitation, jet-medium interaction kicks the medium parton into a recoil particle and leaves behind the “holes” (Figure 19), leading to a diffusion wake in the medium.

The approximation of the recoil prescription breaks down when the energy of the jet shower parton drops to the typical energy scale for the thermal medium constituents. The number of recoil partons becomes large beyond the linear Boltzmann transport approximation. To extend the model's applicability to this regime, one can solve the full Boltzmann equations directly. In a static and uniform medium, one can complete some of the integrals over the relative angles among jet, medium and recoil partons analytically in the collision kernel and solve the reduced Boltzmann equations numerically [562, 563]. The solutions can illustrate the thermalization of recoiled partons and the formation of medium response, including the

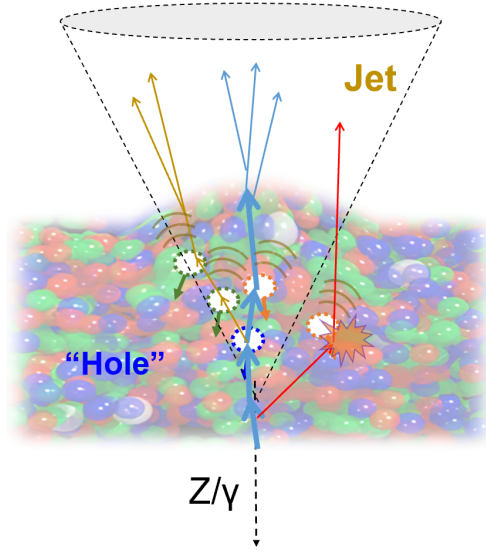


Figure 19: Illustration of a parton traversing the medium and forming a jet opposite a direct photon or Z boson.

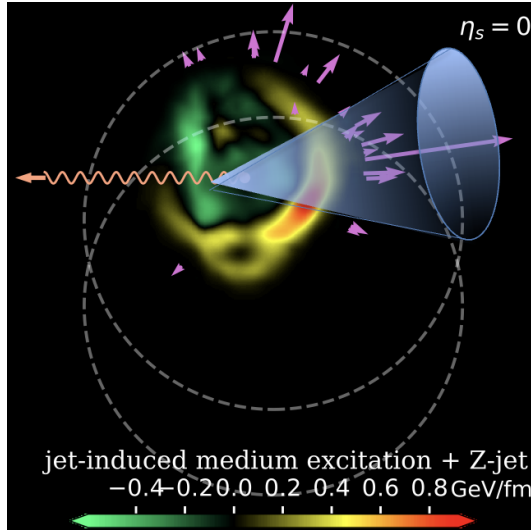


Figure 20: Mach cone induced by a Z-triggered jet.

diffusion wake. One can also apply the hydrodynamic description to the soft modes of jet energy-momentum transport together as well as the bulk dynamics of the medium [564–574]. This can be done by solving the hydrodynamic equation with the source term [554, 555, 575–582].

$$\nabla_{\mu} T_{\text{fluid}}^{\mu\nu}(x) = J^{\nu}(x). \quad (21)$$

Here  $T_{\text{fluid}}^{\mu\nu}$  is the energy-momentum tensor of the medium fluid including the thermalized part of jet energy and momentum, and  $J^{\nu}$  is the source term representing the space-time profile of the energy-momentum deposition from the non-thermalized part of jets from the jet transport. One can describe the jet propagation and hydrodynamic evolution of the medium response in a coupled jet transport and hydrodynamic model [555, 574, 577, 583] where the source term in the hydrodynamic equations comes from jet transport

in a medium whose evolution is governed by the hydrodynamic equations. The state of art approach is a concurrent simulation of the jet transport and hydrodynamic evolution coupled through a source term in the hydrodynamic equations constructed with partons from jet transport that are considered thermalized in the local medium [554, 577, 580, 583, 584]. The deposited energy and momentum propagate as a hydrodynamic flow of a Mach cone in the medium, which allows the final state bulk medium-derived hadrons to correlate with the jet. In the models, those jet-correlated medium hadrons are obtained at the same time as the hadrons in the whole bulk medium, without distinction, using the Copper-Frye formula [72] as in the conventional hydrodynamic models. One can calculate hadron yield from the medium response by subtracting the same hydro events without jets (Figure 20). Energy-momentum from the medium response including the energy-momentum depletion due to the diffusion wake should be included in the jet reconstruction and calculation of jet profiles and fragmentation functions. Since one cannot unambiguously separate soft hadrons from medium response and radiation in and around the jet direction, the depletion of soft hadrons due to the diffusion wake is a unique phenomenon related to jet-induced medium response. The jet-hadron correlations for soft hadrons in both azimuthal angle and rapidity are found to have some unique features due to transverse momentum broadening and diffusion wake in the medium response (Figure 21).

The medium response and medium recoil effects have been first studied by dijet missing transverse momentum measurements. Since then, the analyses of the jet-induced excitation included the broadening of the jet profile at a large radius [585], cone-size dependence of the jet suppression [586], and enhancement of low  $p_T$  particles in the jet fragmentation function [587] and jet-hadron angular correlation [588]. Moreover,  $Z/\gamma$  tagged jets are unique and clean probes because electroweak bosons do not participate in the strong interaction and serve as a tagger of the initial hard scattering. Measurements of  $\gamma$ -hadron correlations [589–591] have provided new insights into the medium response and medium recoil effects near the outgoing hard-scattered partons. Recently,  $Z$ -hadron correlations have also been carried out, with the motivation to search for the reduction of the associated yield near the  $Z$  bosons [592, 593].

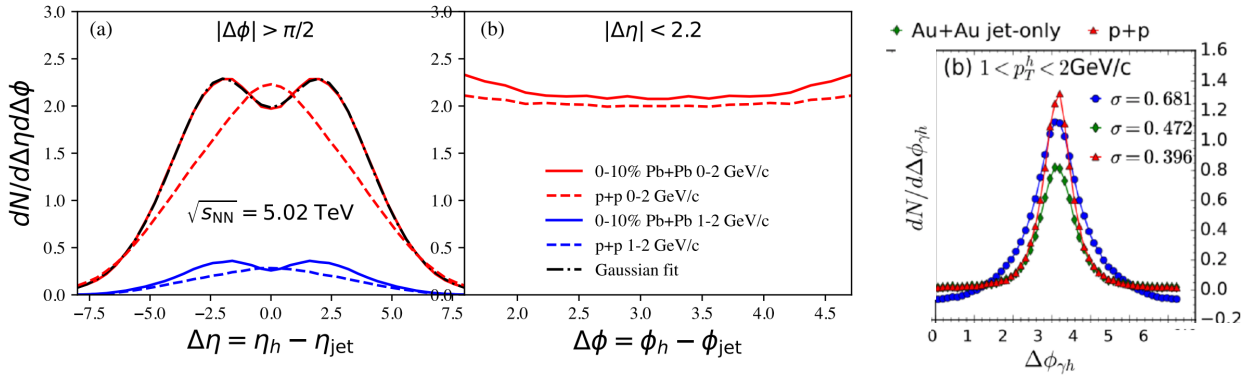


Figure 21: CoLBT model results on the  $\gamma$ -jet-hadron correlation in both azimuthal angle and rapidity.

### 3.2.5 Jet Modification in Small Systems

With the overwhelming evidence of collectivity in small systems, it is natural to explore other signatures of QGP formation such as the modification of hard jets. However, there are several caveats to such an exploration. In the simplest possible terms, the radiative energy loss of a hard parton in a dense (almost static) medium may be expressed using the BDMPS formula [594],

$$\Delta E \propto \hat{q}L^2. \quad (22)$$

Where,  $\hat{q}$  is the jet transport coefficient described in the subsequent subsection, and  $L$  is the length traversed by the parton. While more realistic expressions for energy loss in dynamical media will possess more dependencies, the basic fact remains that radiative energy loss of a hard parton is approximately proportional to the square of the length traversed by the hard parton.

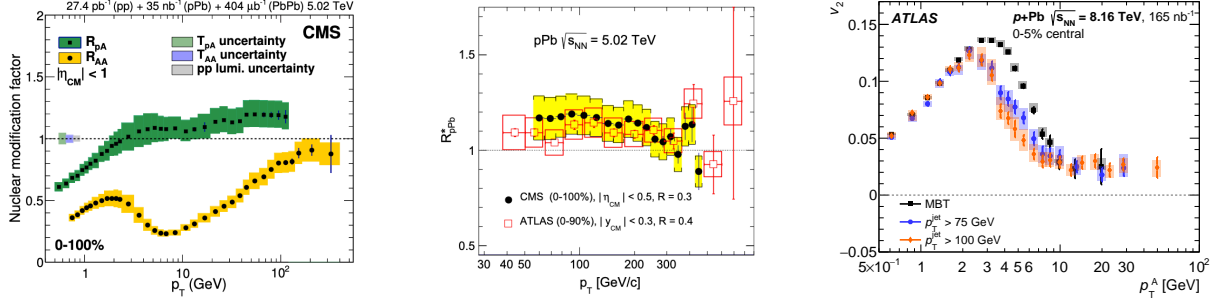


Figure 22: (Color online) Left panel shows the minimum bias nuclear modification for charged hadrons in  $p$ -Pb collisions ( $R_{pA}$ ) at 5.02 TeV, compared to the minimum bias  $R_{AA}$  in Pb-Pb collisions at 5.02 TeV. Center panel shows the  $R_{pPb}$  for jets in minimum bias collisions. The  $R_{pPb}$  in both the left and center panels are consistent with unity indicating no modification of jets or high- $p_T$  hadrons in the medium created in  $p$ -Pb collisions. The right panel shows the the second Fourier coefficient ( $v_2$ ) of the azimuthal anisotropy of high- $p_T$  hadrons in 0-5% most central collisions at 8.16 TeV. This figure suggests a remnant anisotropy, even at  $p_T \gtrsim 50$  GeV.

As a result, energy loss of hard partons is expected to drop rapidly with system size. In fact, the simplest scan with system size as observed in the centrality dependence of jet modification observables does reveal a pattern consistent with Eq. (22) (See Sect. 3.3.1 for details and plots). Following this line of inquiry, several studies of the nuclear modification factors of jets and high- $p_T$  hadrons, in minimum bias  $p$ -A collisions, have yielded results consistent with no modification [595] (See the left and center panel in Fig. 22). However, the hadron  $v_n$  at high  $p_T$  was measured to be non-zero [596,597] (right panel in Fig. 22). In A+A collisions non-zero  $v_n$  is interpreted as resulting from path-length dependent energy loss (see the right panel in Fig. 22). This has caused great interest in the exploration of other observables [598–600] that could be more sensitive to small amounts of energy loss. This has also raised the question: In how small of a system can jet suppression be observed? We will revisit this question in 5.3.1.

### 3.3 Microscopic I: Jets and leading hadrons

Collisions of protons and nuclei often engender hard scatterings with transverse momentum transfers  $\delta p_T \gg \Lambda_{QCD}$  which lead to the formation of hard partons, with energies  $E \gg Q$  the virtuality of the parton. At high enough energy, the virtuality  $Q$  is itself much larger than  $\Lambda_{QCD}$  ( $Q \gg \Lambda_{QCD}$ ). The decay of these hard partons occurs via the repeated emission of progressively softer partons. Due to the condition  $E \gg Q$ , the ensuing spray of partons is collinearly collated into jets of partons. It is important to note that a jet is defined by the jet-finding algorithm used to cluster the resulting fragmentation products into a jet. The large scales involved allow for the use of pQCD to calculate the cross section and various other properties of these jets [601–604].

As these jets traverse the dense QGP formed in heavy-ion collisions, they are modified [605]. The scattering in the medium leads to the production of more radiation from the jet, leading to more energy being radiated at larger angles, referred to as jet quenching [606–608]. Over the last two decades, there has been a tremendous amount of development in this field: At the start of the RHIC program, various formalisms, all based on pQCD were focused on the study of leading hadrons that emanated from the fragmentation of leading partons which suffered energy loss in the medium [609–612]. Over the first decade at RHIC, there arose a series of efforts to understand energy loss via the AdS/CFT conjecture [613], both for light [614,615] and heavy flavors [616]. With the onset of the LHC and the availability of high statistics jet and high- $p_T$  hadron data at very high energies (in the 100's of GeV), the focus has moved to a multi-stage process [617, 618] with an initial vacuum-like shower with a diminished coupling with the medium [619, 620], followed by the multiple scattering induced energy loss phase [607, 608, 611, 621].

In the period after the last Long Range Plan, the community has now moved far beyond the energy lost by the hard partons in the jet to a deep study of how the energy of various fragments of the jet is redistributed by the medium (jet substructure), to the reappearance of the energy in the medium from the recoil of the hard partons [556, 622–625], to the appearance of a wake of the jet in the soft medium [555, 575, 577, 578]. Likewise experimental results now include a wide range of observables beyond jets and leading hadrons, such as jet azimuthal anisotropy [626], groomed [627] and un-groomed [585] jet substructure, coincidence observables [628] etc.

The orders of magnitude increase in the number and statistical precision of jet measurements have opened up extensive theoretical possibilities in the field. It is now possible to compare different approaches to various experimental observables. To make this process rigorous each energy loss module should be constrained to employ the same initial state to generate both the hard and soft sectors, lose energy in an identical fluid simulation, and be subjected to the same hadronization routine. This can only be achieved using an event generator framework, where modules that simulate different aspects of a collision can be replaced in an extensive end-to-end simulation. Since the last Long Range Plan, such a framework called JETSCAPE is now available [2].

As an illustration of the abilities of such frameworks, we present recent results from JETSCAPE covering a wide range of jet, leading hadron, jet substructure and jet coincidence observables in the first subsection. Simulations carried out within these end-to-end generator frameworks typically do not contain the newest theories or exploratory approaches and still have not addressed the entirety of all jet based observables. As such, in the subsequent sections, each of these observables will be discussed in detail, highlighting new theoretical improvements, along with a discussion of experimental observables that have yet to be satisfactorily addressed by theory or simulation. The final subsection will address the somewhat new development of Bayesian analysis for jet based observables, and the ability to study the cross correlation between various parameters in data driven approaches.



### 3.3.1 Simultaneous results from end-to-end simulator frameworks

For years after the start of the RHIC and even the LHC program, (up to and including the last Long Range Plan) the *modus operandi* of most theorists, working in jet quenching, was to carry out calculations of individual observables. Since the onset of end-to-end simulation frameworks such as JETSCAPE, one can now focus on the calculation of *events*. Observables are built by combining final state particles from these events. One can also look at observables from intermediate states in the evolution, to directly see how different stages of the evolution initiate and change each observable.

In the following, we present recent results from JETSCAPE, where almost the entire range of jet based observables (with the exception of jet  $v_2$ ) was addressed by a single series of simulations [624, 625] with only two jet based parameters tuned to data at one energy and centrality. These parameters are the normalization of the jet transport coefficient  $\hat{q}$  and the transition scale  $Q_{SW}$ , between the high and low virtuality stages of a jet quenching simulation. The jet propagation is carried out on top of a pre-calibrated bulk simulation. The presented results used the T<sub>R</sub>ENTo model as the initial state for both bulk and jet evolution, followed by energy loss via a 2 stage (MATTER + LBT) simulation in a 2+1D (MUSIC) fluid dynamical simulation, followed by hadronization of the soft sector via Cooper-Fry and a Lund model based hadronization (Pythia) for the hard sector.

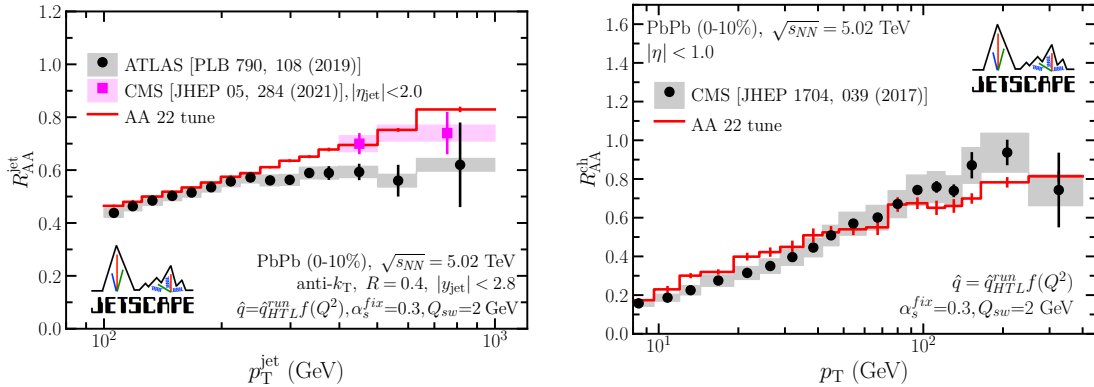


Figure 23: (Color online) Nuclear modification factor for inclusive jets (left) and charged-particles (right) in most central (0-10%) Pb+Pb collisions at  $\sqrt{s_{NN}} = 5.02$  TeV from MATTER+LBT simulations within JETSCAPE. The fit to these data from ATLAS and CMS set the two parameters  $\alpha_s^{\text{fix}} = 0.3$  and  $Q_{SW} = 2$  GeV. All JETSCAPE results below will use these parameters. (Left) Results for inclusive jet  $R_{AA}$  with  $R = 0.4$  and  $y_{\text{jet}} < 2.8$ , compared to ATLAS data [629] (black circles) and CMS data for  $\eta_{\text{jet}} < 2.0$  [586] (magenta squares). (Right) Results for charged-particle  $R_{AA}$  with  $\eta < 1.0$ , compared to CMS data [595].

In these calculations, MATTER [630, 631] simulates the high-virtuality stage with coherence effects weakening the coupling with rising off-shellness of the parton [619]. This is indicated with the factor  $f(Q^2)$ , which reduces with increasing  $Q^2$  [ $f(Q^2)$  is calculated from Ref. [619], *not* determined from data]. This factor is combined with a jet transport coefficient calculated using running coupling in leading order HTL effective theory [632]:

$$\hat{q}_{\text{HTL}}^{\text{run}} = C_a \frac{50.484}{\pi} \alpha_s^{\text{run}}(Q_{\text{max}}^2) \alpha_s^{\text{fix}} T^3 \ln \left[ \frac{2ET}{m_D^2} \right], \quad (23)$$

The lower virtuality phase is simulated with LBT [622]. The transition between MATTER and LBT is set at a  $Q = 2$  GeV by comparison with data. Both MATTER and LBT employ a similar recoil prescription where a parton is sampled from the local medium and then scattered off a jet parton. The recoil parton

becomes a part of the evolving jet, while the holes left by the incoming partons are subtracted from the final observables, if they lie within jet cones.

In Figs. 23, and 24 we demonstrate that the jet and leading hadron  $R_{AA}$  at all centralities from top LHC to top RHIC energies can be simultaneously described by the same simulation with no refitting of parameters between energy or centrality. Unlike the results from the prior JET collaboration [633], which required setting the normalization of  $\hat{q}$  at RHIC and LHC separately, current simulations from JETSCAPE only require the normalisation and the transition scale to be determined at one energy and centrality.

In Fig. 23, the normalization of  $\hat{q}$  determined by the parameter  $\alpha_S^{\text{fix}} = 0.3$ , and the transition scale  $Q_{\text{SW}} = 2$  GeV are set by comparing with the data on inclusive jets (left) and leading hadrons (right). In Fig. 24 (a) and (b) we show the comparison between simulation and ATLAS data [629] for  $R_{AA}$  of jets in semi-central events. These plots also demonstrate the effect of removing and not removing the holes created by the in-coming medium partons which are scattered into becoming a part of the jet.

In Fig. 24 panels (c) and (d), the centrality and collision energy dependence of the leading hadron suppression is demonstrated in comparison with data from semi-central LHC collisions at  $\sqrt{s_{\text{NN}}} = 5$  TeV and central collisions at 2.76 TeV. The collision energy dependence of jets is demonstrated with LHC and RHIC data in panels (e) and (f) of Fig. 24 respectively. Finally jets and charged pions at RHIC energies are compared with JETSCAPE simulations in panels (g) and (h) of Fig. 24, all of whose parameters were determined in Fig. 23.

The same set of simulations which generated all of the plots in Figs. 23-24, can now be reanalysed and compared to data on a variety of jet substructure observables. The utility of calculating events rather than observables allows for rigorous cross comparisons between observables as no new events are generated. In the following we present the simulation results for a handful of substructure observables,

In the top panel of Fig. 25, a distribution of the soft drop momentum fraction [634] variable  $z_g$  calculated using jets from the same simulation in Fig. 23 are compared with data from  $p$ - $p$  collisions measured by the ALICE experiment. The bottom panel presents the ratio of the distribution from quenched jets in  $Pb$ - $Pb$  collisions to that in  $p$ - $p$ . The experimental data indicate no modification of this distribution, which is also demonstrated by the theoretical simulation. In the figures, the red solid line represents the default calculation, while the green dashed line represents simulations where the coherence effect is removed, i.e., there is no weakening of the interaction with the virtuality of the hard parton.

In the top panel of Fig. 26, the corresponding angular distribution of the two prongs ( $r_g$ ) emanating from the soft drop procedure are presented. Measurements from ALICE are compared with predictions from JETSCAPE. The top panel represents the distribution in  $p$ - $p$ , while the bottom panel presents the ratio between the distribution of quenched jets in  $Pb$ - $Pb$  and those in  $p$ - $p$ . Unlike the case of the  $z_g$  distribution, the  $r_g$  distribution shows a clear narrowing of the angle between the two prongs formed as a result of the soft drop re-clustering procedure. Results including coherence effects, seem to be marginally better in comparisons with experimental data.

A clear separation between calculations including and not including coherence effects is seen in the plot of the  $R_{AA}$  as a function of  $r_g$  as presented in Fig. 27. This figure presents the nuclear modification factor for re-clustered jets that have passed the soft drop condition as a function of the angle between the eventual two prongs. The yellow band represents bins where the transverse momentum between the prongs is less than 1 GeV and therefore represent the non-perturbative region. In the region where pQCD based calculations should work, we see a clear preference for calculations which include coherence effects (red solid lines), as opposed to simulations without coherence effects (green dashed lines).

In the subsequent subsections, the current and exploratory aspects of the physics of inclusive jets, leading hadrons, jet substructure, jet coincidence and heavy flavor observables will be discussed in more detail. New theoretical directions will be identified, and experimental data without a satisfactory theoretical

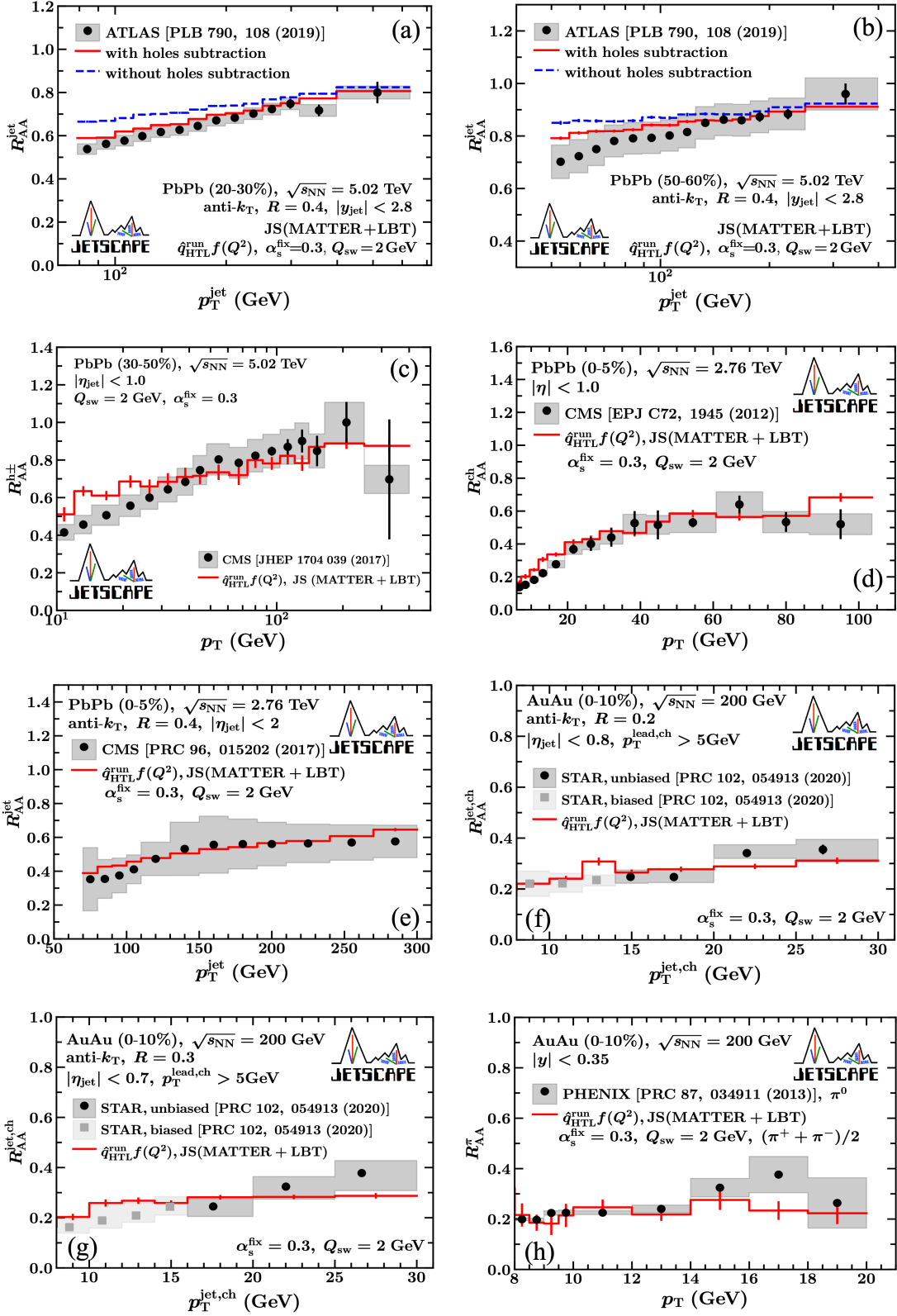


Figure 24: Red calculations have no further tuning after fitting inclusive jet  $R_{AA}$  and charged-particle  $R_{AA}$  at most central (0-10%,  $\sqrt{s_{NN}}=5.02$  TeV) Pb+Pb collisions and are compared to various measurements (black circles) across a variety of centrality classes, collision energies and species, and kinematic ranges.

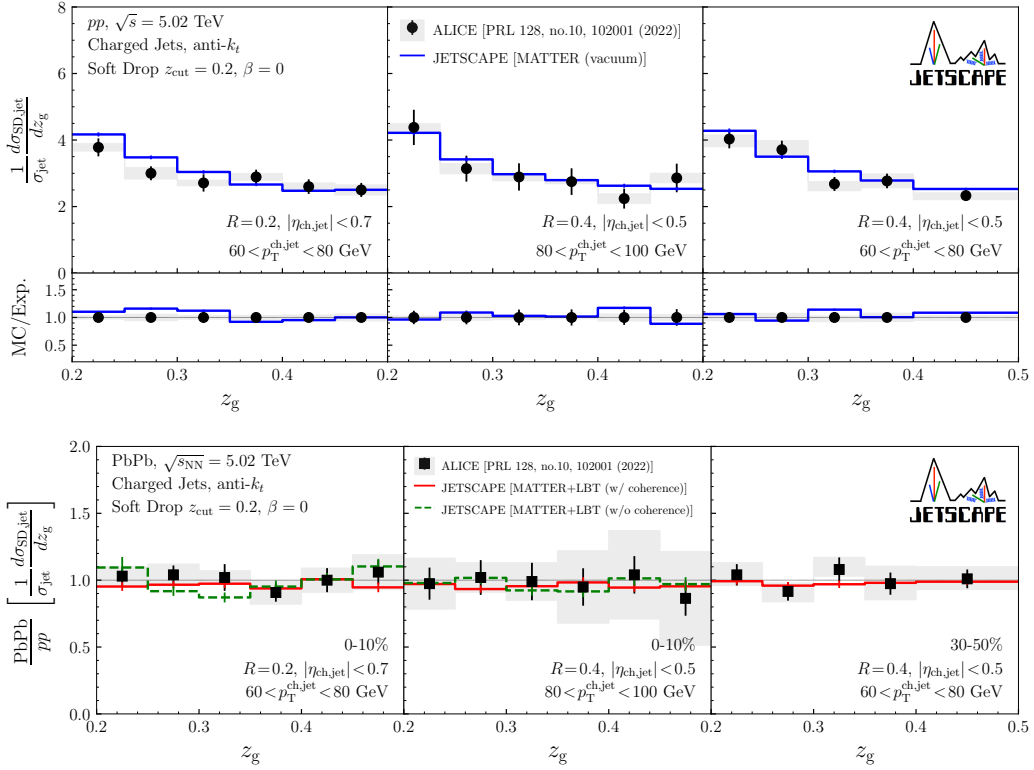


Figure 25: (Color online) (Top) Distributions of soft dropped jet splitting fraction  $z_g = \frac{\min[z_1, z_2]}{z_1 + z_2}$  for charged jets in  $p+p$  collisions at  $\sqrt{s} = 5.02$  TeV and the ratios for different jet cone size  $R$ , and  $p_T^{\text{ch,jet}}$  range. (Bottom) Ratios of  $z_g$  distributions for charged jets between Pb+Pb and  $p+p$  collisions at  $\sqrt{s_{\text{NN}}} = 5.02$  TeV for different centrality, jet cone size  $R$ , and  $p_T^{\text{ch,jet}}$  range. The lines show the results from JETSCAPE. The circles (top) and squares (bottom) with statistical error bars and systematic uncertainty bands are the experimental data from ALICE [627].

description explored. The current section will end with a discussion of aspects of Bayesian analysis for the hard sector of heavy-ion collisions. In the subsequent section, a discussion on non-jet based rare hard probes will be carried out.

### 3.3.2 Jet quenching theory

In a seminal (unpublished) work [605], Bjorken hypothesized that the formation of a quark-gluon plasma in high-energy hadronic collisions would be reflected in the suppression of jets due to collisional energy loss which was pointed out later to be negligible as compared to radiative parton energy [636] to cause the jet quenching phenomenon. Such parton energy loss can also lead to significant suppression of large  $p_T$  single inclusive hadron spectra as well as hadron spectra associated with a hard trigger (photon or hadron) as estimated within the HIJING Monte Carlo model [606, 637] and the pQCD parton model [638, 639]. This phenomenon was successfully observed in the early 2000s at RHIC in the quenching of high-energy single inclusive hadrons [640, 641], dihadrons [642] and  $\gamma$ -hadron spectra [643, 644]. A decade later, jet quenching was confirmed by the study of fully reconstructed jets at the LHC [645].

This remarkable discovery has spurred a lot of theory and experimental research activity in the past two decades with the objective of using jets as a multi-dimensional tool to probe the properties of the quark-

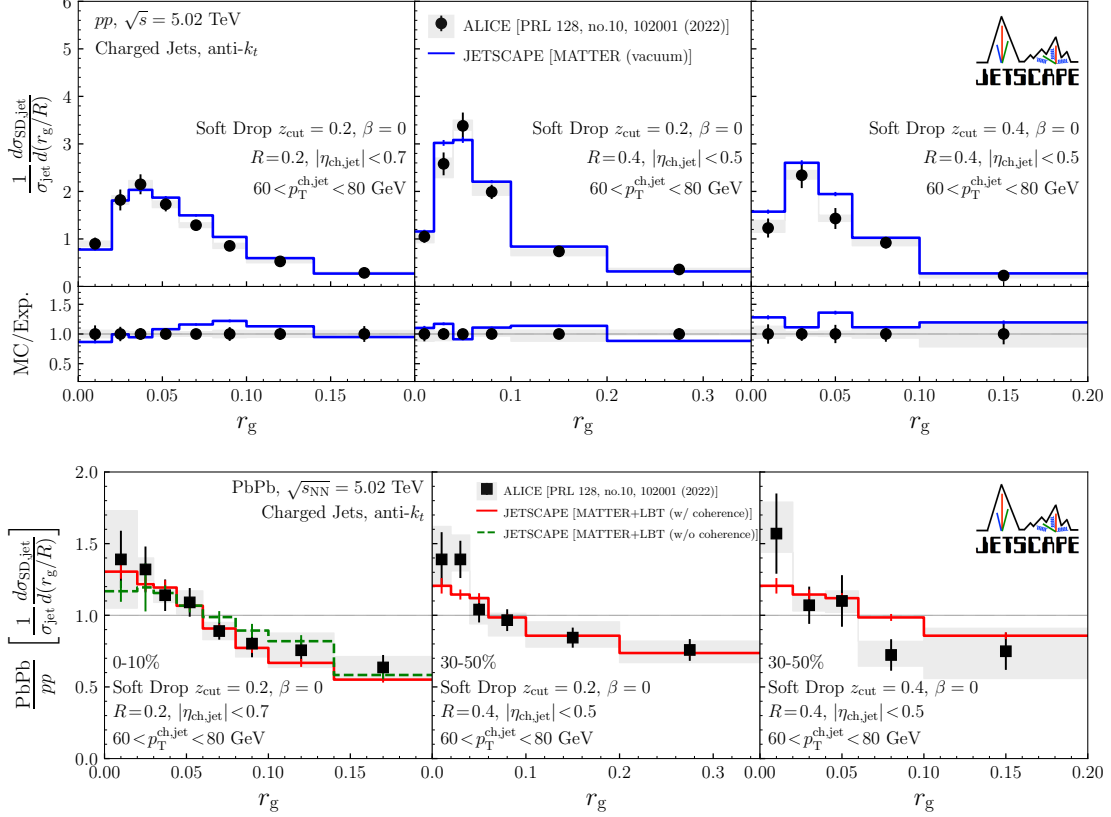


Figure 26: (Color online) (Top) Distributions of jet splitting radius  $r_g$  for soft dropped charged jets in  $p+p$  collisions at  $\sqrt{s} = 5.02$  TeV and the ratios for different jet cone size  $R$ , and  $p_T^{\text{ch,jet}}$  range. (Bottom) Ratios of  $r_g$  distributions for charged jets between Pb+Pb and  $p+p$  collisions at  $\sqrt{s_{\text{NN}}} = 5.02$  TeV for different centrality, jet cone size  $R$ , soft drop parameter  $z_{\text{cut}}$ , and  $p_T^{\text{ch,jet}}$  range. The lines show the results from JETSCAPE. The circles (top) and squares (bottom) with statistical error bars and the experimental data from the ALICE Collaboration [627], respectively. The bands indicate the systematic uncertainties of the experimental data.

gluon plasma at various length scales.

### Transverse momentum broadening and parton energy loss

The theory of jet quenching is based on transverse momentum broadening and parton energy loss [646–649]: a high-energy parton produced early in a heavy-ion collision through a hard scattering process, before the plasma has formed, will subsequently propagate through the hot deconfined matter and undergo multiple scattering whose effect is to i) increase the transverse momentum of the energetic parton via a diffusive process in transverse momentum space:

$$\langle k_{\perp}^2 \rangle \equiv \hat{q}L \quad (24)$$

where  $L$  is the medium length and  $\hat{q}$  the diffusion coefficient aka the jet quenching parameter that encodes the properties of the hot QCD matter. The general assumption is that the scattering centers are independent from each other. This is justified so long as the in medium mean free path is much larger than the correlation length, and, the parton's mean lifetime is shorter than the mean free path in the medium.

In addition to elastic processes, multiple scattering may trigger coherent gluon radiation [650] for

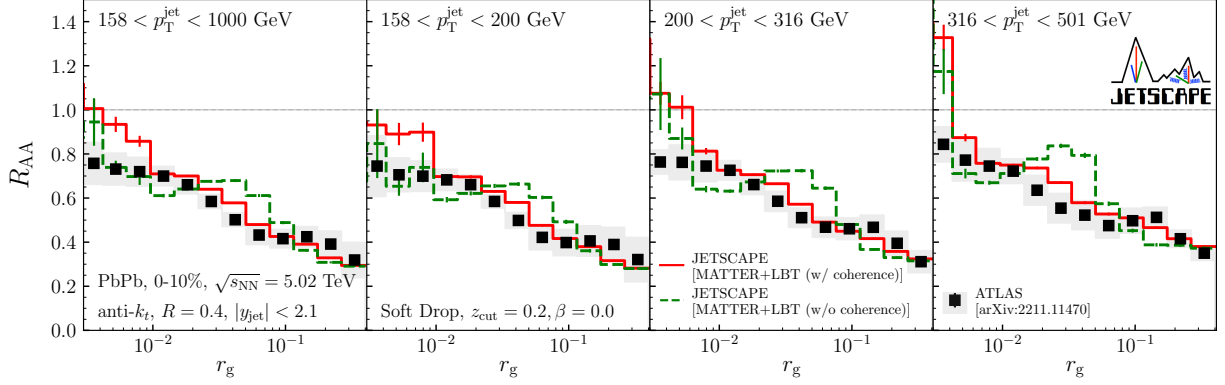


Figure 27: (Color online) Nuclear modification factor  $R_{AA}$  in 0-10% Pb+Pb collisions at  $\sqrt{s_{NN}} = 5.02$  TeV, as a function of  $r_g$  for jets with different  $p_T^{\text{jet}}$ . The solid and dashed lines with statistical error bars show the results from the same events generated from Fig. 23 with and without coherence effects, respectively. For comparison, the experimental data from the ATLAS Collaboration [635] are shown by squares with statistical errors (bars) and systematic uncertainties (bands). The yellow-shaded regions are the bins where the transverse momentum between the prongs is less than 1 GeV.

long-lived partons. Considering the dominant processes when the radiated gluon goes through coherent multiple scattering, the total radiated energy loss has quadratic path length dependence [594, 607, 609–611, 651, 652]. During this quantum coherence time  $t_f$  the radiated gluon accumulates a transverse momentum via diffusion  $k_f^2 \sim \hat{q}t_f$  which implies that  $t_f \equiv 2\omega/k_{\perp}^2 \sim \sqrt{\omega/\hat{q}}$  for massless partons.<sup>3</sup> Thus, the softer gluons in the soft radiation and multiple scattering limit have shorter formation times and therefore can be emitted quasi-instantly with constant rate

$$\omega \frac{d\Gamma}{d\omega} = \frac{\alpha_s C_R}{\pi} \sqrt{\frac{\hat{q}}{\omega}} \quad (25)$$

This rate is suppressed at large frequency due to the Landau-Pomeranchuk-Migdal (LPM) effect and its maximal suppression is reached at the gluon frequency  $\omega_c \equiv \hat{q}L^2$  and minimum angle  $\theta_c \equiv (\hat{q}L^3)^{-1/2}$ . While the light-flavor LPM effects have been calculated using Hard Thermal Loops (HTL) formalism [252, 611, 654, 655], thus providing HTL-resummed scattering and radiation rates, the same cannot be said for heavy flavors. However, the generalized HTL formalism to describe heavy flavor interaction with the QGP at lower virtualities has been devised by Caron-Huot [656]. For more complete phenomenological studies to be done, that formalism needs to be applied in earnest, resulting in LPM-resummed rates for heavy flavor scattering and radiation, akin to Refs. [611, 654, 655].

Early studies of high hadron suppression and jet quenching were based on single parton energy loss. However, a complete treatment of jet quenching requires going beyond this approximation. This will be discussed in what follows.

### Jet quenching and color decoherence

Jets are coherent multi-partonic systems that extend in time and space, which requires to go beyond single parton energy loss. The question of how these complex objects interact and lose energy to the plasma

<sup>3</sup>The gluon radiation process off heavy quarks is more intricate given the new scale introduced into the system, i.e. the heavy quark mass. In that case, the coherence time becomes  $t_f = \frac{2\omega}{k_{\perp}^2 + y^2 M^2}$  where  $y$  is the momentum fraction carried away by the radiated gluon and  $M$  is the mass of the heavy quark [653].

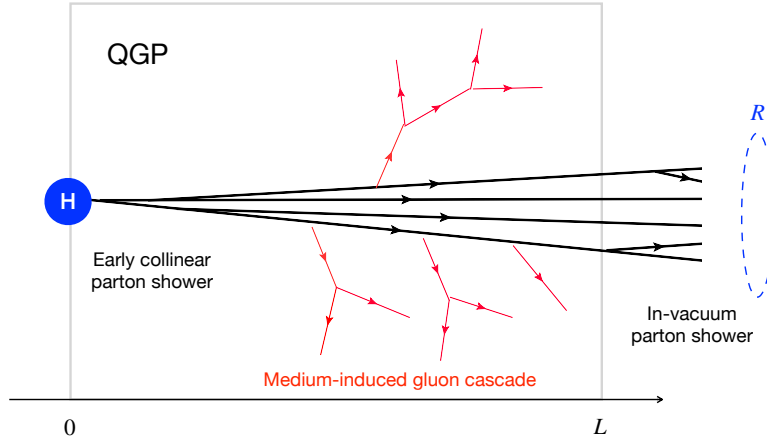


Figure 28: (Color online) Sketch of the different stages of jet evolution in the quark-gluon plasma (see description in the text).

and how their substructure is modified as a result of these final state interactions has been a central focus in the theory community.

There are three distinct stages to jet evolution in the QGP [657] (cf. Figure 28 for an illustration). The first stage corresponds to a hard and collinear parton cascade that forms due to the large virtuality associated with the hard scattering. This cascade develops early, mostly before energy loss processes take place [618, 658]. The high-virtuality stage may also acquire medium-induced correction such as discussed in Ref. [610, 653, 659]. For a single gluon radiation of energy  $\omega$  the time window associated with this stage is  $1/p_T R^2 \ll t \ll t_f \sim \sqrt{\omega/\hat{q}}$ . Or equivalently, in terms of transverse momentum  $Q^2 \equiv (p_T R)^2 \ll k_\perp^2 \ll k_f^2 = \sqrt{\omega\hat{q}}$ .<sup>4</sup> In the second stage copious medium induced radiation off the jet color charges produced in the first stage take place with constant rate inside the medium of size  $L$ . Medium induced radiation is followed by a gluon and quark cascade [660] that efficiently transports energy from fast color charges down to the plasma temperature scale where energy is dissipated [563, 661–663]. In the last stage the fast charges that escape the plasma continue fragmenting until their virtuality reaches non-perturbative scales where hadronization occurs. While focus herein is on describing the showering in the large-energy ( $E$ ) eikonal limit, there is work improving eikonal results by supplying sub-eikonal  $\mathcal{O}(1/E)$  corrections [664, 665]. Though some phenomenological implications of sub-eikonal effects have been studied in, e.g., [666, 667], in the future such studies would benefit to be implemented within more realistic multi-stage dynamical model describing jet propagation in a nuclear medium. The assumption that all medium-induced splittings in the shower are independent may be questionable for splittings with relatively large formation times. In this case, there may be quantum interference between subsequent splits (beyond what can be refactored in an effective  $\hat{q}$  parameters) that need to be carefully considered as explored in, e.g., Ref. [668–670]. Depending on the amount of interference between subsequent splits, it may be that Monte Carlo showering algorithms, akin to those discussed herein, need to be revised to take into account such effects to achieve higher precision computations.

An important feature of parton cascades is color coherence that plays a role beyond the leading order

<sup>4</sup>To include gluon radiation off heavy quarks in these ordered inequalities, the following substitution is needed:  $k_\perp^2 \rightarrow k_\perp^2 + y^2 M^2$ , with  $M$  the heavy quark mass and  $y$  the gluon momentum fraction. The other channel involving heavy quarks is their pair production through  $g \rightarrow Q + \bar{Q}$ . In that case, the transverse momentum conditions is modified according to  $k_\perp^2 \rightarrow k_\perp^2 + M^2$ , where  $M$  is the heavy quark mass.

of single gluon radiation and thus needs to be accounted for in parton shower energy loss. It is a quantum interference effect that suppresses gluon radiation with wavelength larger than the size of the emitting system: for instance, gluon radiation off of a quark antiquark in a color singlet state is suppressed at angles larger than the angle between the pair due to destructive interference leading to angular ordering of successive splittings. In the presence of a hot colored medium this property is expected to be altered as a result of rapid color precession of jet color charges [620, 671]. Color coherence also affects medium-induced radiation similarly. Energy loss of a quark-antiquark pair depends on the extent to which the medium resolves the individual colors charges [672]. If the antenna (quark-antiquark pair) opening angle is larger than the characteristic angle  $\theta_c \equiv (\hat{q}L^3)^{1/2}$  angle the medium resolves the pair and thus the latter loses energy as independent color charges with intensity proportional to  $2C_F$ , in the opposite scenario energy loss is proportional to the total charge of the pair which is either vanishing in the case off a single state or proportional to  $C_A$  in the case of gluon parent [673]. A remarkable consequence of color coherence is that a jet with opening angle smaller than the medium angular scale  $\theta_c \gg R$  loses energy as a single color charge given by the parent parton [658].

The study of the antenna system in the medium allowed to elucidate how the phase space of parton showers is affected by energy loss. As a phenomenological application, the physics of color (de)coherence was implemented at all order in perturbation theory in the leading logarithm approximation for inclusive jet spectrum and the corresponding nuclear modification factor [674] (cf. Figure 29). It was also shown to yield an excess of soft particles inside the jet in a study of the jet fragmentation function [618, 675]. Moreover, jet substructure observables were extensively studied to probe the resolution power of the medium [676–678]. The effect of the medium response is still to be investigated in these studies.

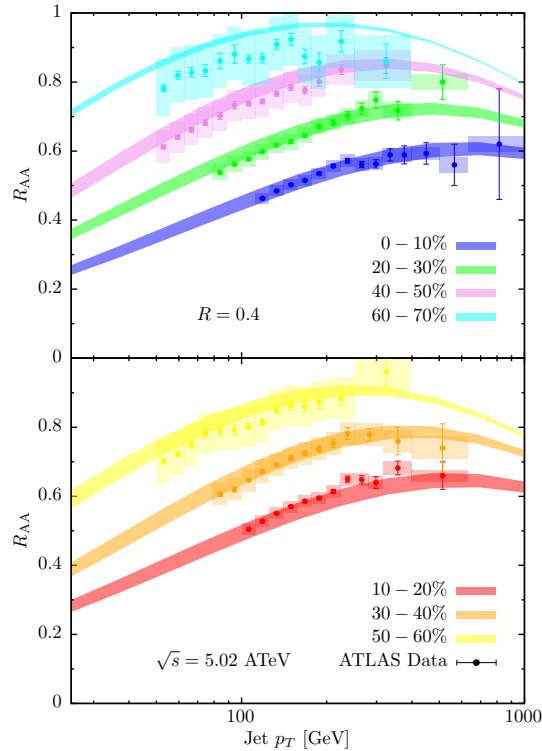


Figure 29: Analytic calculation of inclusive jet  $R_{AA}$  in Pb+Pb collisions at  $\sqrt{s} = 5.02\text{TeV}$ , compared to ATLAS data [629], for different centralities. It includes resummation of energy loss effects from hard, vacuum-like emissions occurring in the medium and color coherence effects [674].(Color online)



A lot of progress has been made recently to unify the various energy loss formalisms both analytically, with the so-called improved opacity expansion (IOE) [679,680], and numerically [681–683] paving the way for precision phenomenology in the future. A future prospect is to improve on the accuracy of such gluon cascades by systematically computing higher order corrections to medium-induced gluon splitting including full kinematics [668,669,684].

### Extractions of $\hat{q}$ , higher order and quantum corrections

It is now widely held that the transverse momentum jet transport coefficient  $\hat{q}$ , defined as the mean squared transverse momentum exchanged per unit length between a jet parton and the medium, encapsulates the dominant effect of the medium modification on a propagating jet. Thus,  $\hat{q}$  reveals properties of the medium that can be probed via the quenching of hard jets.

Calculations of jet observables, either via Monte-Carlo event generators or semi-analytical theoretical approaches, encode a range of assumptions within the form of  $\hat{q}$  used and its dependence on the temperature of the medium, the scale and energy of the hard parton etc. For example, if one assumed that the QGP could be described using leading order HTL [685,686], one would obtain the expression for  $\hat{q}$  in Eq. (23), assuming running coupling and that the energy of the jet far exceeds the temperature scale of the plasma [632]. This form, both with and without additional scale dependence (coherence effects), has been widely used in phenomenological comparisons between experiment and simulation where the  $\alpha_s^{\text{fix}}$ , the coupling at the medium scale is used as a fit parameter (see the plots in Sec. 3.3.1).

Along with the extractions of  $\hat{q}$  from comparison with data, there have been several attempts to calculate this from first principles. Next-to-leading order calculations of  $\hat{q}$ , entirely within the assumptions of HTL theory [687], indicate large corrections to the leading order formula of Eq. (23). There have been attempts to estimate the soft sector of  $\hat{q}$  using a effective 3-D theory on the lattice called Electro-static QCD (EQCD) [688]. While these represent small corrections to the LO formula at temperatures  $T \gtrsim 10T_C$ , they remain large corrections close to  $T_C$ .

In an alternative approach, one could drop the assumption of an HTL plasma and define  $\hat{q}$  using the operator product expansion [689] and extract  $\hat{q}$  from the leading operator in the expansion, yielding [690]:

$$\frac{\hat{q}}{T^3} \simeq \frac{4\pi\alpha_s}{N_C T^4} \langle F^{+j} F_j^+ \rangle_{T-V}. \quad (26)$$

In the equation above, the  $F^{+j} F_j^+$  represents the local color summed gluon field strength correlator. The subscript  $T - V$  indicates the thermal minus vacuum expectation. These operator products can now be calculated in Lattice-QCD. In Ref. [690], continuum extrapolated lattice calculations of  $\hat{q}$ , in both quenched and 3-flavor QCD, are presented in comparison with extractions from phenomenology, leading order HTL and EQCD calculations.

The results of such cross comparisons are presented in Fig. 30, where the results from the JET [633], and JETSCAPE [691] collaborations are compared with first principles calculations in Lattice-QCD [690], Leading order HTL [632], Electrostatic QCD [688], and a stochastic vacuum model at  $N_f = 0$  [692]. This plot represents the current state-of-the-art of our knowledge of the jet quenching parameter  $\hat{q}$ . The results from EQCD at temperatures below 0.5 GeV and next-to-leading order corrections to  $\hat{q}$ , within HTL perturbation theory are beyond the scale of the plot. All calculations tend to approach similar values at  $T \gtrsim 10T_C$ , with the obvious separation between the quenched ( $N_f = 0$ ) and 3-flavor QCD results.

In past few years, higher order quantum corrections to transverse momentum broadening were investigated. It was in particular shown that they are enhanced by a large double logarithm of the medium size, i.e.,  $\alpha_s \ln^2 L$  [661,693–695]. When resumed to all orders they result in an anomalous scaling of transverse momentum broadening that reflects a super diffusive behavior

$$\langle k_{\perp}^2 \rangle \sim L^{\gamma}, \quad (27)$$

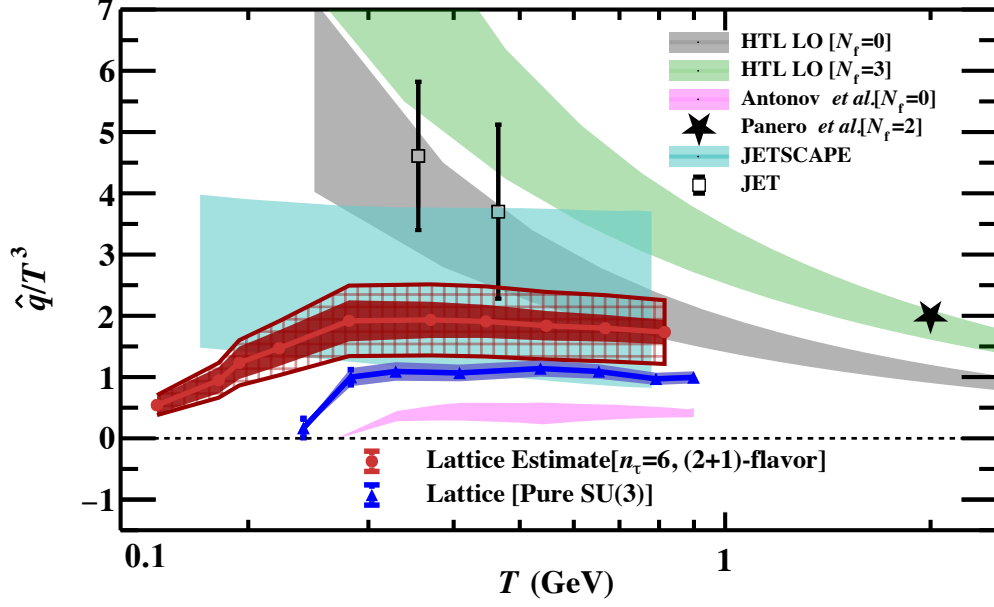


Figure 30: (Color online) Cross comparisons of the jet transport parameter  $\hat{q}$ , obtained from many different approaches [690]: Phenomenological comparisons with data from the JET and JETSCAPE collaborations, and first principles theoretical approaches from Lattice QCD, EQCD (Panero et al.), Hard thermal loop effective theory, and a stochastic vacuum model (Antonov et al.).

where  $\gamma \simeq 1 + 2\sqrt{\bar{\alpha}}$  and  $\bar{\alpha} \equiv C_A \alpha_s / \pi$ . In a recent series of articles a systematic approach was developed to compute higher order corrections and running coupling effects [696–699]. Note that this anomalous scaling is a consequence of the renormalization of the jet quenching parameter and its scale dependence in the non-linear regime of multiple scattering [694]. At very high momentum transfer the jet quenching parameter obeys the DGLAP evolution equation [700, 701]. One important outlook is to implement these quantum corrections to jet quenching observables that are currently based on the leading order formulation of  $\hat{q}$ .

While historically  $\hat{q}$  has been considered to have a temperature and momentum dependence, recent development suggests that its non-trivial virtuality dependence plays an important role in explaining experimental data [619]. The phenomenological implications of this virtuality dependence on heavy flavor quarks is investigated in the next section, while light flavors can be found in [624]. The virtuality dependence alone may not enough to fully explain heavy quark  $R_{AA}$  [702], and phenomenological study in Ref. [702] points towards further theory development to obtain not only a temperature ( $T$ )- and virtuality ( $Q^2$ )-dependent  $\hat{q}$ , but also a heavy quark mass  $M$ -dependent  $\hat{q}$ : i.e.,  $\hat{q}(T, Q^2, M)$ . As one goes towards lower virtualities, a momentum ( $p$ )-dependent  $\hat{q}$  should also be considered (e.g. Ref. [703], and reference therein), and is further affected by LPM-resummations.

### 3.3.3 Phenomenology of Hard Heavy Flavors

There has been wealth of phenomenological progress in simulating high-energy heavy flavor propagation within a nuclear medium incorporating many of the formal theoretical advances mentioned above. While the high-energy elastic  $2 \rightarrow 2$  scattering is common among many heavy-flavor energy loss formalisms [704, 705], the treatment of inelastic/radiative processes is where different phenomenological assumptions are used. The high virtuality portion of heavy quark energy loss in the QGP can be well described using

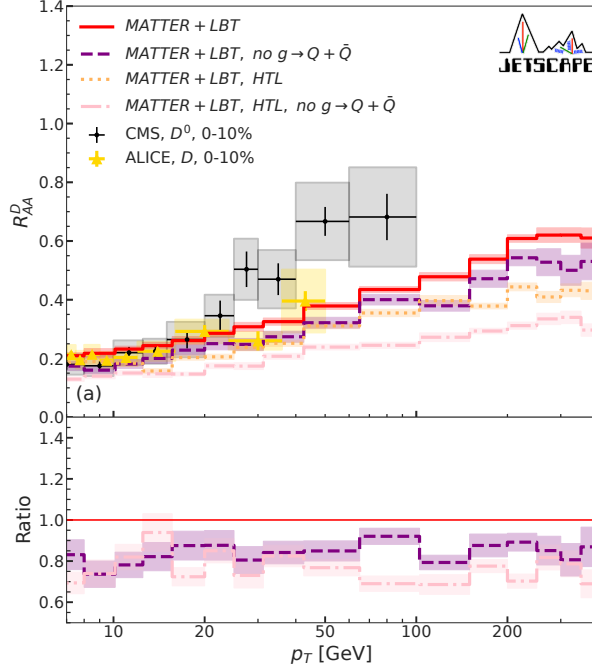


Figure 31: (Color online) Nuclear modification factor for D-mesons in  $\sqrt{s_{NN}} = 5.02$  TeV Pb+Pb collisions at the LHC at 0-10% centrality using a combination of higher-twist energy loss (MATTER) and linearized Boltzmann transport (LBT) [702]. For comparison, simulations with a virtuality-independent  $\hat{q}$  have the HTL designation in the legend. The dashed line in the ratio subplots divides MATTER+LBT no  $g \rightarrow Q + \bar{Q}$  to MATTER+LBT HTL, while the dotted-dashed line divides MATTER+LBT HTL no  $g \rightarrow Q + \bar{Q}$  to MATTER+LBT HTL.

the higher twist formalism<sup>5</sup>. At lower virtuality, there are many formalisms for heavy quark radiation. For instance, the Linearized Boltzmann Transport (LBT) approach [622, 709] uses higher-twist inspired radiation [653]; the approach developed at Duke [710–712] uses the improved Langevin dynamics and extends it within the Linear-Boltzmann-plus-Diffusion-Transport-Model LIDO [705, 713]; the Nantes approach use  $2 \rightarrow 3$  inelastic processes [714, 715]. While all these approaches made important contributions towards understanding how hard heavy flavor quarks interact with the nuclear medium, the most recent advance combining different energy loss formalisms together.

A recent comparison with experimental data has revealed that a multi-formalism/multi-scale approach is required to simultaneously describe light flavor observables from different  $\sqrt{s_{NN}}$  collision energies [619]. In particular, the combination of high-virtuality/higher-twist formalism with the low-virtuality effective Boltzmann transport, both of which are being further improved (as discussed in the previous section), revealed to be a fruitful combination. On the heavy flavor side, the need for a multi-scale approach was investigated for the first time in Ref. [702]. In that study, an important additional ingredient was the phe-

<sup>5</sup>For light flavor, the higher twist result can be shown to agree with the approach by Gyulassy-Levai-Vitev (GLV) [609, 706] as discussed in, e.g., Ref. [707]. However, the Djordjevic and Gyulassy [708] extension to the GLV formalism for heavy flavor has yet to be as thoroughly compared with the higher twist result.

nomenological inclusion of in-medium production of heavy-flavor via  $g \rightarrow Q + \bar{Q}$ , incorporated within the high-virtuality energy loss simulation, which was combined together with low-virtuality Boltzmann transport approach before comparing with data.<sup>6</sup> Heavy flavor pair production is most important for studies of charm energy loss, given that the gluon virtuality needed to produce charm quarks is the smallest among heavy quarks. Ref. [702] has found that dynamical charm pair production in the QGP plays an important role when describing D-meson, as depicted in Figure 31. In that simulation, a phenomenological light flavor  $\hat{q}(T, Q^2)$  was used to study the importance of having a virtuality dependent  $\hat{q}$ , given that the heavy flavor  $\hat{q}(T, Q^2, M)$  is not yet known. These results show that a multi-scale energy loss calculation of heavy flavors is needed. The multi-scale (heavy quark mass and virtuality) dependence of  $\hat{q}$  can be better assessed by investigating how D-meson  $R_{AA}$  changes as a function of centrality. Indeed, the amount of QGP that heavy quarks have to traverse is reduced in more peripheral collisions, affecting the balance between high-virtuality energy-momentum exchange relative to low-virtuality Boltzmann transport, as seen in Ref. [702]. The high-precision measurements planned by the sPHENIX Collaboration, as well as the upcoming higher-statistic measurement from the LHC, will be crucial in pinning down the full functional dependence of  $\hat{q}$ , using Bayesian model-to-data comparisons.

### 3.3.4 Jets, leading hadrons and coincidence measurements

One of the signatures of the jet quenching phenomenon is the suppression of high-momentum charged hadrons. There has been many measurements since the last Long Range Plan with increasingly higher precision [595, 718–724]. A general trend is observed across all measurements. These charged hadron measurements are complemented by those measuring the suppression of jets [586, 629, 645, 725–730]. There is a good agreement between different experiments for anti- $k_T$  jets with a distance parameter up to 0.4, with a slight tension at high  $p_T$ . The modification of jet also manifests itself in  $p_T$  balance of back-to-back jets for both inclusive dijets [731–736] and b dijets [725].

In recent years, there is an effort in different experiments to investigate the suppression of larger size jets up to a distance parameter of 1.0. It poses a nontrivial experimental challenge. Results for the larger jets may provide additional input to understanding the mechanism with which the high-energy parton interacts with the QGP. For example, if the size is big enough that color decoherence can be probed, a larger suppression may be observed; on the other hand, energy recovery of smaller jets will reduce the amount of suppression. The result reported by the CMS collaboration at high energy indicated that there is no strong dependence on the  $R_{AA}$  from 0.2 to 1.0 [586], as shown in the left panel of Figure 32. The situation at lower  $p_T$  is more interesting with ALICE reporting a new measurement showing a larger suppression of wide jets with a novel machine-learning based approach to jet reconstruction [737], while the ATLAS  $R_{CP}$  result [645] indicate a different trend, as can be seen in the right panel of Figure 32. It will be exciting for future measurements to resolve this apparent tension.

The energy loss of jets can also be established by measuring jets associated with a Z boson or a high energy photon [738–741]. Relative to the transverse momentum of the  $Z/\gamma$ , a smaller  $p_T$  of the jet is seen in heavy-ion collisions compared to the reference  $pp$  collisions, as shown in Figure 33. Events with these topologies are studied in more detail by looking into distribution of hadrons with respect to the Z boson [592, 593] or photon [591]. As can be seen in Figure 34, it is found that there is also an excess of particles on the same side as the Z. In addition to photons, jets and hadrons recoiling against a high-energy  $\pi^0$  has been studied at RHIC, indicating a broadening of jet shower and a modification of the acoplanarity distribution when compared to the PYTHIA baseline.

<sup>6</sup>A recent calculation [716, 717] has also explored the importance of heavy flavor pair production via  $g \rightarrow Q + \bar{Q}$  in a static medium with constant temperature. It would be interesting to investigate how these results change using a multistage energy loss in a dynamical medium.

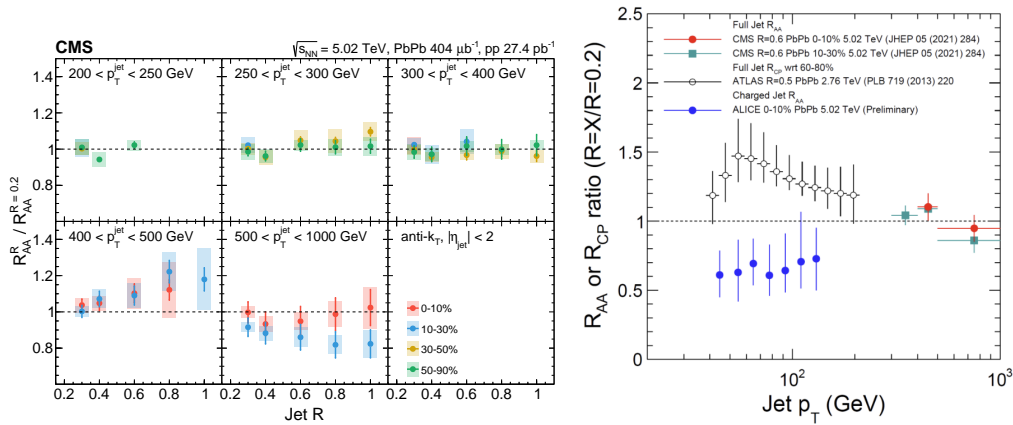


Figure 32: Jet  $R_{AA}$  measurements with large distance parameter as measured by CMS [586] (left) and ATLAS [645] compared to the machine learning extracted result from ALICE [737] (right).

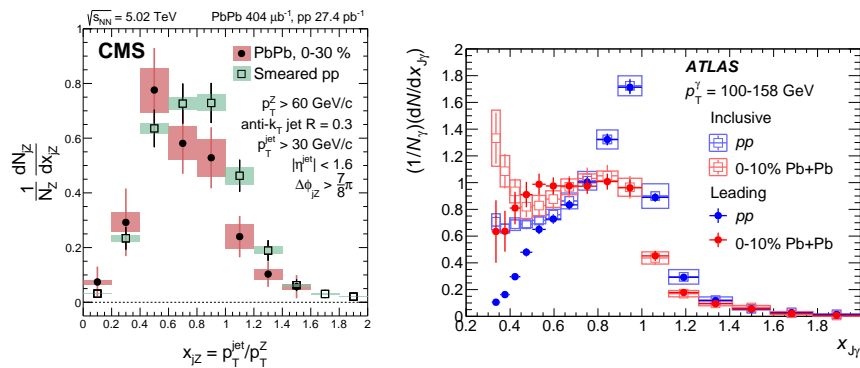


Figure 33: Example of measurements of jets balancing against a  $Z$  boson or a photon [738, 741].

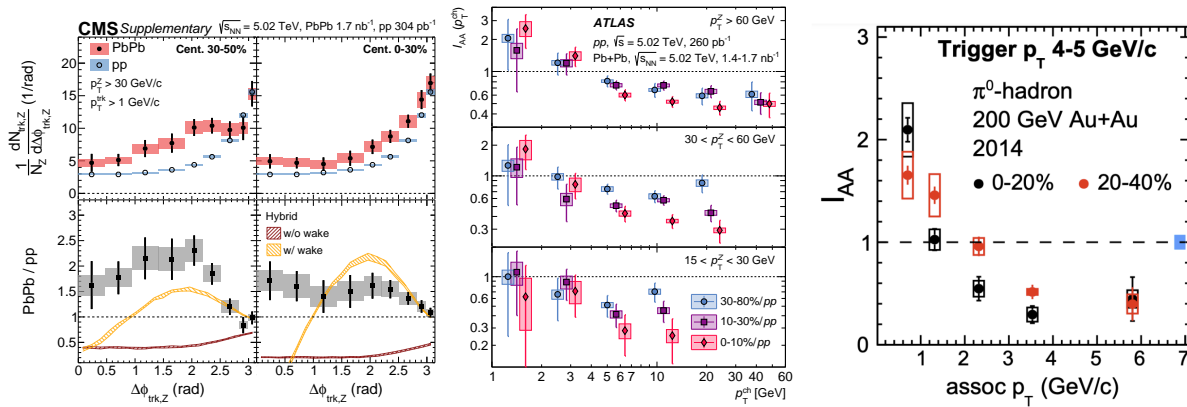


Figure 34: Example of measurements [591–593] of hadrons produced in association with a  $Z$  boson (left, middle), or a  $\pi^0$ .

Investigation of the distribution of hadrons inside jets provides insight on the jet quenching phenomenon. There has been a number of measurements on the fragmentation function of inclusive jets [587, 742–749], as well as  $Z$ /photon tagged jets [589, 750]. Together with the jet transverse momentum profile and jet-track correlation measurements [585, 588, 590, 628, 731, 751–757] it is observed that the energy of

the jet is transported away from the axis on average as soft particles, and it extends beyond  $\Delta R \sim 1.0$ .

Correlations between hadrons and jets are also further studied by classifying the leading dijet in the events in different  $x_j \equiv p_{T,2}/p_{T,1}$  bins [752]. It is found that the transverse momentum profile of the subleading jet in a less balanced configuration is more modified compared to its counterpart in a more balanced dijet configuration. Figure 35 shows jet and dijet  $v_n$  measurements [626, 758, 759] which correlate jet direction with all the hadrons in the event. A  $v_2$  signal is observed while  $v_3, v_4$  are consistent with zero within uncertainties.

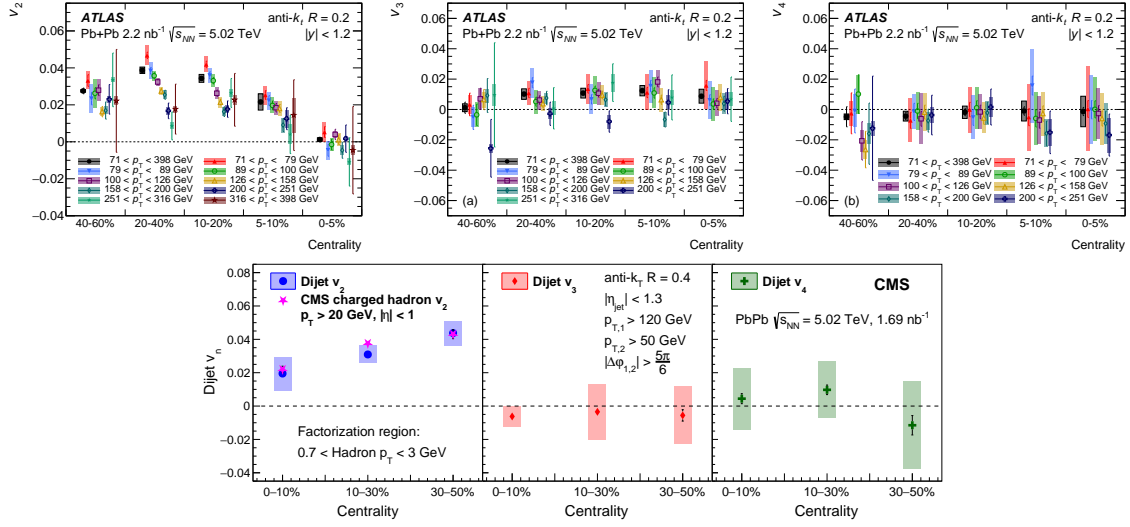


Figure 35: Jet and dijet  $v_n$  measurements [626, 758, 759] at the LHC.

### 3.3.5 Jet substructure

Jets play a crucial role in the study of QGP tomography [760, 761]. It was already realized in the 2015 Long Range Plan [762] that jets can serve as multi-scale probes of the medium due to their rich internal substructure which encodes information about the jet evolution at various energy scales [763]. Average jet properties such as the energy profile (jet shape) as a function of the distance from the jet axis, and longitudinal momentum carried by individual particles within jet (fragmentation function) were studied at both RHIC [591, 764–771] and the LHC [587, 589, 590, 627, 627, 742, 746, 747, 750, 756, 757]. The results showed that a fraction of the original jet’s energy was redistributed away from its axis due to jet-medium interactions and were carried predominantly by low energy particles. Jet substructure studies going beyond average quantities such as angularity [772, 773] and mass [774–776] were also performed to utilize the more differential phase space mapped out by per-jet substructure fluctuations. With sPHENIX as the new detector at RHIC, upgrades to STAR and the detectors at the LHC (ATLAS, CMS, ALICE and LHCb) were planned and carried out since the 2015 Long Range Plan to allow for precision jet substructure measurements in an environment where medium effects are expected to be significant. Therefore, we stand at the precipice of a quantitative jet substructure program aiming at elucidating the multi-scale, space-time evolution of jets and the QGP. This progress will depend on successful data-taking and the completion of the RHIC scientific mission in Runs 2023–2025, as well as utilizing the LHC Run 3 and Run 4 data for new high precision scans of the jet substructure phase-space.

The longitudinal and transverse momentum distributions of jet particles encode comprehensive information about the whole jet evolution history. This motivates an infinite class of jet substructure observables defined via inclusive sums of transverse momentum weighted angles among particles or jet axis to

arbitrary powers [777, 778]. On the other hand, motivated by the sequential gluon emissions predicted by theory, clustering algorithms define another class of jet substructure observables which are quantified by the information available in the clustering tree [779]. Both methods contain contributions from underlying events or even pileups in high-luminosity proton collisions which complicate the comparison with theoretical calculations. Therefore jet grooming to remove unwanted particles based on characteristic differences between signal jets and their backgrounds (typically soft and at large angles from the jet axis) needs to be performed. In addition, subtraction techniques based on clustering or per-particle identification were developed for high-multiplicity collisions such as in high-pileup proton-proton or central heavy-ion collisions [780, 781]. By removing sensitivities to soft particles, originally motivated by background mitigation purposes, one can design jet observables which are dominated by perturbative processes [634, 782]. These observables then offer a robust approach to probe the wide range of emission phase space [783] which are now being explored by the community.

With the rise of modern machine learning development concurrently with the 2015 Long Range Plan-period [784–787], jet substructure studies benefited from these powerful data analysis tools to extract the rich information contained in jets, deal with background corrections and detector effects. Frameworks to capture comprehensively jet information were proposed using different jet representations, including substructure observable bases [788–792] and also de-clustering tree branching history [779] as a bottom-up approach. This naturally extends conventional, single-variable jet modification studies to correlations among multiple jet features. In particular, the correlation between jet quenching and substructure was explored to investigate how jets with different topology or substructure would lose energy differently. Machine learning tools were directly applied on jet representations to extract modification patterns first in simulation-based studies [792–799]. Such efforts help not only define concrete observables to eventually test underlying jet quenching mechanisms in data, such as creating a direct connection to theory without the need for advanced methods, but also provide opportunities for searching modification patterns using data-driven methods.

To map out jet evolution in more detail therefore requires measurements of multiple jet observables in a high-dimensional space. The jet clustering tree which provides a splitting history has been actively utilized in recent experimental and theoretical studies. Measurements of the individual, subsequent branching are also in progress. We see that later branching and narrow-angle ones start to deviate from the expectation of perturbative parton splitting and show a more democratic momentum sharing [800, 801]. On the other hand, machine learning techniques to extract the full multi-dimensional correlation among different substructure observables are applied in a cleaner environment [802, 803]. It is promising to unfold multi-differential distributions in heavy-ion jet studies once we have experimental control over individual jet substructure observables. The necessity of precision in both experimental measurements and theoretical calculations will be an important aspect of the 2023 Long Range Plan.

As described earlier, groomed jet observables can reduce the impact of soft, wide-angle radiation which is theoretically more challenging to be described. Fully corrected data can therefore be compared to theoretical calculations with higher accuracy. In general, a jet substructure observable is defined as a sum over contributions from both hard and soft particles in a jet. By restricting the jet constituents that contribute to the observable, as is what is done in grooming, one can design substructure observables with sensitivities to specific subsets of jet constituents. Here we refer to hard jet substructure as those observables which have reduced sensitivities to soft jet particles, while soft jet substructure either retains or has enhanced sensitivity to soft particles.

### 3.3.5.1 *Hard jet substructure*

One of the first measurements for hard jet substructure at the LHC was the soft-drop groomed momentum sharing  $z_g$  [804]. It is defined as the momentum fraction of the first soft branch in the declustering satisfying

the condition,

$$z = \frac{\min(p_{T,1}, p_{T,2})}{p_{T,1} + p_{T,2}} > z_{\text{cut}} \left( \frac{R_{12}}{R} \right)^\beta \quad (28)$$

where 1, 2 label the two branches in the declustering tree and  $z_{\text{cut}}$  and  $\beta$  are the soft-drop parameters.  $R_{12}$  is the angle between the two branches and  $R$  is the jet radius. The groomed jet radius  $R_g$  is similarly defined as the angle between two such branches. There is less ambiguity in the origin of high-energy particles because they are primarily produced in hard scattering. These particles are more likely to survive soft-drop which removes wide-angle soft particles due to the angular-ordered declustering. Any observable based on the constituents of a groomed jet is potentially a hard jet substructure. However, it is also realized that the effect of grooming can differ among jets. For example, a jet with a large groomed jet radius would have little radiation removed, therefore retains the sensitivities to soft particles.

Figure 36 highlights three such jet substructure measurements and their impact on our understanding of QCD. The top left panel shows the distribution of the opening angle of the first hard splitting of jets at RHIC energies from the STAR experiment, compared to a NLL pQCD calculation in the shaded gray band [805]. The comparison suggests the necessity of higher order calculation and non-perturbative contribution in order to describe the data. The top right panel shows the ATLAS measurement [806] of the Lund plane for high-momentum jets at the LHC, with specific regions of the phase-space sensitive to hadronization or perturbative emissions. The ALICE collaboration utilized the jet clustering tree and compared the opening angle distributions of inclusive jets and jets tagged with the  $D^0$  meson. The dead-cone effect was observed in the suppression of narrow angle emissions as shown in the bottom panel of Figure 36.

Since the 2015 Long Range Plan, there has been significant progress on quantifying the modification of jets in their substructure. The primary goal is to correlate jet suppression to substructure and quantitatively discriminate between proposed jet quenching mechanisms. With substructure observables, one can identify characteristic scales which are sensitive to jet-medium interactions and the QGP's microscopic properties. Measurements of jet shapes and masses [775, 776] suggest a narrowing of the jet core, while soft contributions such as medium responses to jets can still affect significantly the outer jet regions. Modifications of hard jet substructure will inform us of the onset of jet-medium interaction in the whole jet formation process. These complementary measurements highlight the multi-faceted nature of medium recoils and jet quenching effects; the jet mass seems to favor less recoils whereas the shapes and fragmentation function require a larger contribution in order to fit the data. In looking more into the convolution of the varying scales within jets, the first application of groomed jet substructure observables in heavy-ion collisions was the measurement of the momentum fractions at the first hard emission which survives soft-drop. The left panel of Figure 37 presents the first such measurement of the  $z_g$  distribution from the CMS collaboration [804] at the LHC with  $z_{\text{cut}} = 0.1$  and  $\beta = 0$ . This measurement, along with the measurement of the groomed jet mass [776], showed small modifications which are consistent with suppression of hard emissions with  $z_g \sim 0.5$ . Little modification is seen when one imposes more stringent grooming criterion with a larger  $z_{\text{cut}}$  as in the measurement from the ALICE collaboration [627] (top right panel of Figure 37), or selects jets with a hard constituent ( $p_T > 2.0$  GeV) at RHIC by the STAR collaboration [767] (bottom right panel).

There has also been much progress recently on revisiting energy correlators and connecting them to advanced theoretical tools of calculating correlation functions [808, 809]. Since these energy correlators are cross sections of angles weighed by particle energies, they are insensitive to soft particles and belong to hard jet substructure. The small-angle behavior of energy correlators may give a robust probe of low energy QCD dynamics and hadronization [800, 801].

At the current stage, the study of hard jet substructure helped initiate a more robust, hopefully, understanding of jet evolution in both vacuum and medium. For quenched jets, we observe little modification of some hard jet substructures in a variety of measurements. This leads us to the investigation of soft jet substructure which may be more sensitive to medium-induced effects which we will discuss next.



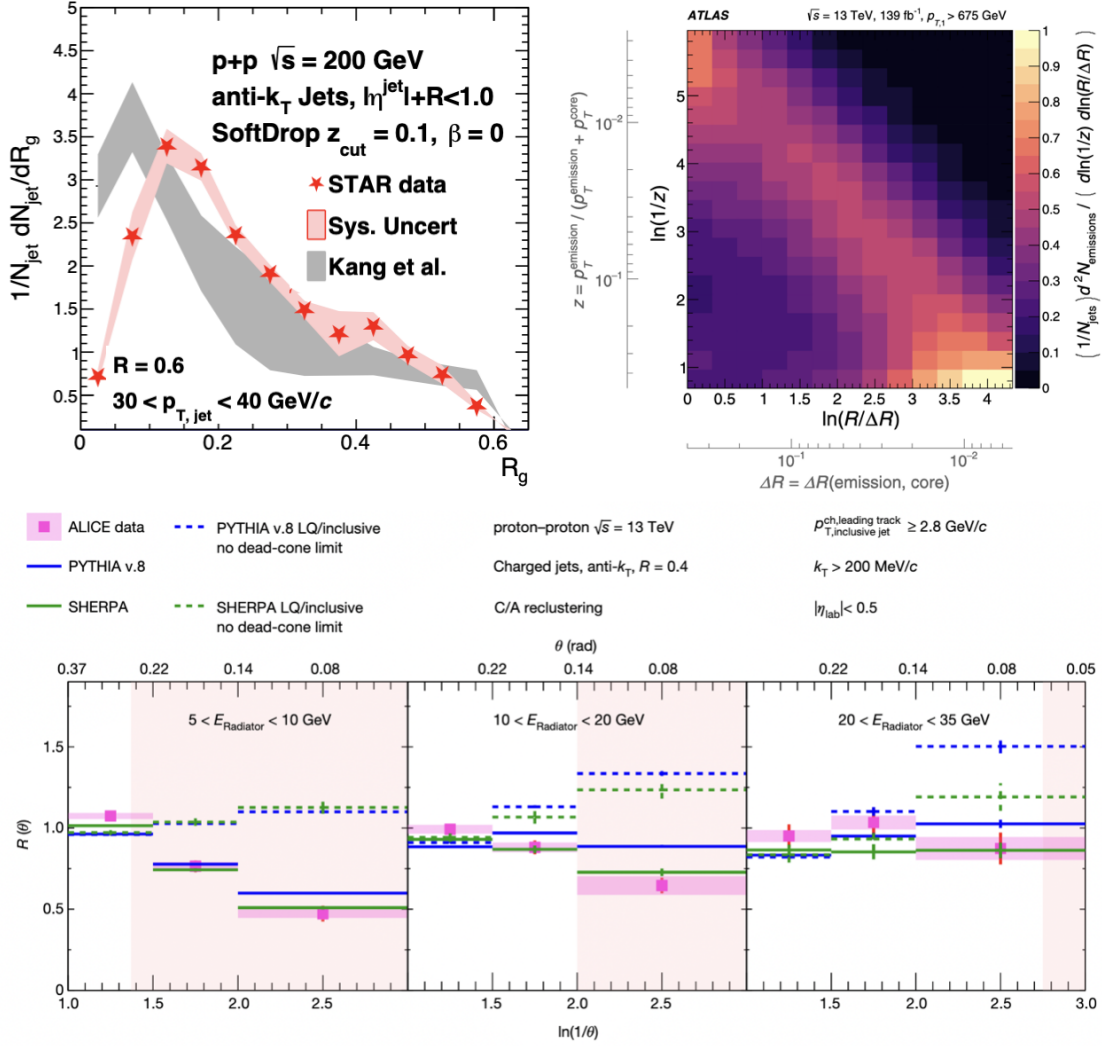


Figure 36: Top left: Groomed jet radius  $R_g$  distribution for jets at RHIC energies in the red markers compared to a pQCD calculation in the gray shaded region [805]. Top right: Fully corrected primary Lund plane for high-momentum jets at the LHC with the angle and momentum fraction as the coordinates [806]. Bottom: Observation of the dead-cone effect as a suppression of jets with small opening angle and tagged with a D0-meson, with varying emitter energies [807].

### 3.3.5.2 Soft jet substructure

Soft particles within a jet may be produced by a variety of sources such as vacuum-like or medium-induced soft emissions, correlated (typically referred to as medium recoil) and uncorrelated medium background particles. The quantitative description of these soft particles to disentangle their different origins is an active area of research.

Soft particles within jets generated due to medium interactions are evident from the excess of low-momentum particles, which are impacted by the heavy-ion background. There have recently been two approaches to study the correlation between the hard splitting angle and the degree of quenching at both RHIC and the LHC. Grooming techniques naturally introduce an angular observable at the selected hard splitting which was studied recently at the LHC as discussed in the previous section. By increasing the

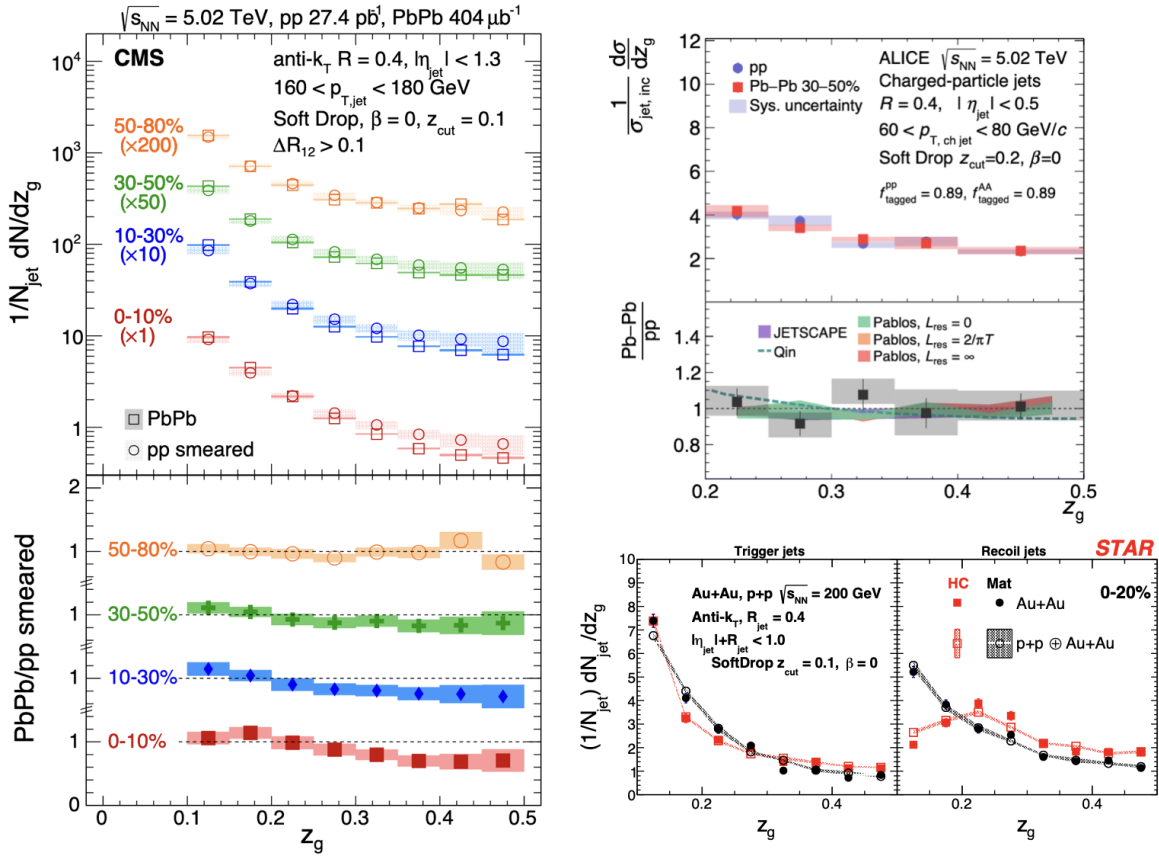


Figure 37: Left: CMS measurement [804] of the soft-drop  $z_g$  for high-momentum jets at the LHC with different centrality selections in Pb+Pb collisions, compared to the vacuum baseline (open markers). The bottom panel shows the ratio between Pb+Pb and p+p results. Top right: Normalized  $z_g$  distributions from the ALICE collaboration [627] with  $z_{cut} = 0.2$  for low energy jets at the LHC. The bottom panel shows the ratio with the vacuum baseline. No significant modification is observed even for the most central collisions. Bottom right: Measurements of the normalized  $z_g$  distributions for trigger (left panel) and recoil (right panel) jets from the STAR collaboration [767] for the most central Au+Au collisions compared to an embedded p+p&Au+Au baseline. Red markers represent the Hardcore di-jets and black markers represent the Matched di-jets.

value of  $z_{cut}$ , one reduces the impact of the heavy-ion background in the selection of the splitting. It can also introduce a bias toward a later splitting which can affect the discussion on the space-time picture of jet quenching. The first such studies were done at the LHC as shown in the left and middle panel of Figure 38 by measuring the nuclear modification factor as a function of the  $R_g$  for different jet momenta [635, 810]. Both measurements observe a variation of the quenching effects at an angular scale smaller than 0.1. Such a study has the potential to point towards studying coherence vs decoherence energy loss by probing the coherence length of the plasma. With the bias of later splitting introduced by a harder grooming criterion, such measurements are complementary to the ones performed at RHIC as shown on the right panel of Figure 38. Since the energy scale of jets at RHIC is significantly lower, a jet selection bias called the Hardcore selection is introduced which biases the surviving jets towards harder fragmentation in the recent STAR measurements [767]. The momentum asymmetry for these selected di-jet was measured differentially

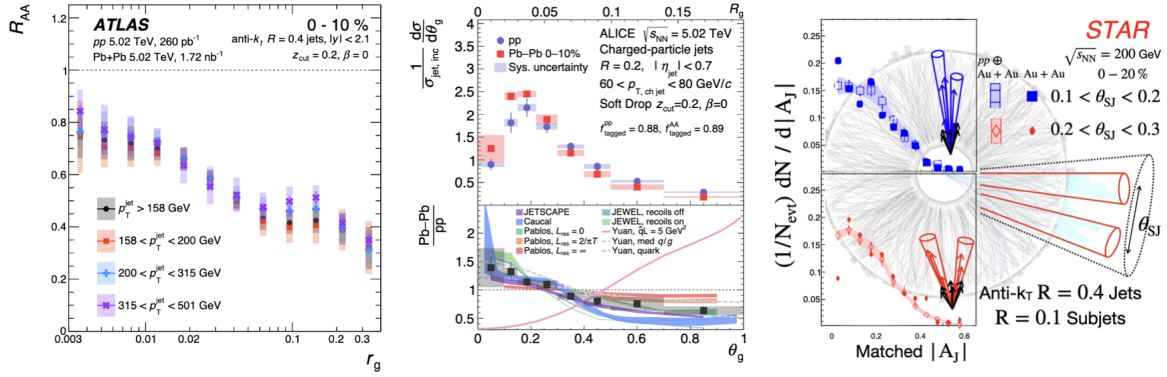


Figure 38: Left: Jet nuclear modification factor  $R_{AA}$  for most central events as a function of the soft-drop groomed jet radius  $R_g$  for varying jet momenta from the ATLAS collaboration [635]. Middle: Normalized distributions of the groomed jet radius  $R_g$  for jets from central heavy-ion collisions from the ALICE collaboration [810] compared to the vacuum baseline and theoretical calculations. Right: Di-jet momentum asymmetry at RHIC from the STAR collaboration [767] for selected di-jets with varying sub-jet opening angles in central Au+Au collisions compared to an embedded vacuum reference.

as a function of the opening angle of sub-jets with a momentum threshold as opposed to a momentum fraction requirement. The angular resolutions between  $0.1 < \theta < 0.3$  show similar levels of momentum asymmetry caused by the loss of low momentum particles leading to the quantification of energy loss from a single color charge with an unmodified splitting structure. These studies suggest a consistent understanding of jet energy loss for a particular, biased jet population via a broad selection of jet and event geometry in experiment.

A critical challenge in the study of soft jet substructure is to appropriately separate the signal from the background. The medium-induced emissions within the jet cone as well as correlated and uncorrelated medium radiations can all affect soft jet substructure. We have seen experimental evidence of the recovery of momentum balance, i.e. the lost energy from the jet can be recovered in the soft sector. The extent to which one needs to go further away from the jet axis to recover the lost energy is highly dependent on the type of jets considered in the study. For inclusive jets at the LHC, we have seen that one needs to go to almost the entire hemisphere. On the contrary, for hard-fragmentation triggered jets at RHIC the situation is significantly different, with the quenched energy being recovered within a relatively narrow jet cone.

### 3.3.6 Heavy-flavor tagged jets

Studying jets originating from heavy flavor quarks (charm and bottom) provides additional insights to the jet quenching mechanism in the QGP. Due to their larger masses, heavy quarks are expected to lose less energy due to gluon radiation than light quarks, known as the dead-cone effect [811]. Such a QCD-inspired effect has been confirmed experimentally by the ALICE collaboration in p+p collisions, as illustrated in Figure 36 [807].

Identification of heavy flavor jets experimentally usually employs two approaches: i) exploitation of the distinct properties of heavy flavor hadrons and their decay topology, e.g., longer decay length and larger mass compared to light favor hadrons; ii) tagging with fully reconstructed heavy flavor hadrons or their leptonic decay daughters.

As a reference for measurements of modifications to heavy flavor jets in the hot medium, nuclear

modification factors for  $b$ -jets [812, 813] and  $c$ -jets [814] have been measured in p+Pb collisions at  $\sqrt{s_{\text{NN}}} = 5.02$  TeV at the LHC, where a QGP of extended volume is not expected to be formed. The results are consistent with no significant modifications to the heavy flavor jet production in the cold nuclear matter.

Modifications to  $b$ -jet yield in heavy-ion collisions compared to p+p collisions have been measured by CMS and ATLAS collaborations [815, 816], where a strong suppression of the  $b$ -jet production rate is observed. To study the dependence of the medium-induced energy loss on parton's mass and color charge,

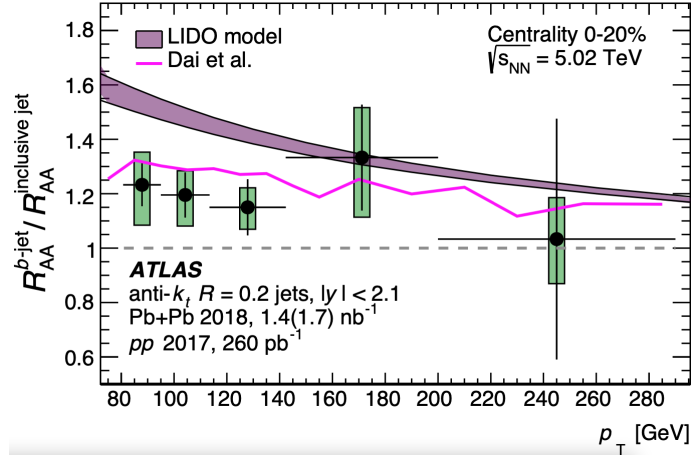


Figure 39: Ratio of  $b$ -jet  $R_{AA}$  to that of inclusive jets as a function of  $p_T$  in 0-20% Pb+Pb collisions at  $\sqrt{s_{\text{NN}}} = 5.02$  TeV [816].

Figure 39 shows the ratio of  $R_{AA}$  for  $b$ -jets and inclusive jets. The former contains contributions from gluons splitting into  $b\bar{b}$  pairs, and the latter is made up of jets mostly originating from light quarks and gluons. The ratio is consistently above 1, indicating that  $b$ -jets are less suppressed than inclusive jets. These results suggest that mass and color charge play an important role in determining the parton energy loss.

Substructures of heavy flavor jets are used to probe the jet quenching phenomenon in more detail. The left panel of Figure 40 shows the ratios of jet shape distributions, *i.e.* normalized transverse momentum profile of charged particles with  $p_T > 1$  GeV/c in jets, in central Pb+Pb and p+p collisions at  $\sqrt{s_{\text{NN}}} = 5.02$  TeV for  $b$ -jets (filled circles) and inclusive jets (open squares) [751]. For both types of jets, a redistribution of energy to larger distances from the jet axis is seen, and the effect is stronger for  $b$ -jets than for inclusive ones. Figure 40, right panel, shows the difference in  $\langle x_J \rangle$  as a function of centrality between Pb+Pb and p+p collisions at  $\sqrt{s_{\text{NN}}} = 5.02$  TeV for  $b$ -dijets (circles) and inclusive dijets (squares) [725]. Here,  $\langle x_J \rangle = \langle p_{T,2}/p_{T,1} \rangle$ , where  $p_{T,1}$  and  $p_{T,2}$  are the transverse momenta of leading and subleading jets in a dijet pair. In 0-10% central collisions,  $\langle x_J \rangle$  is shifted to a small value in Pb+Pb collisions compared to p+p collisions, indicating jet energy loss in the QGP. The amount of shift is compatible between  $b$ -dijets and inclusive dijets.

The  $c$ -jet substructure is studied by measuring the radial profile of the  $D^0$  mesons in jets, *i.e.* distribution of the distance between  $D^0$  mesons and the jet axis. Figure 41 shows the ratios of the  $D^0$  meson radial profiles in heavy-ion and p+p collisions at RHIC (left) and the LHC (right, middle panel) [817, 818]. At RHIC, the ratio in central collisions is consistent with unity within uncertainties for  $p_{T,D^0} > 5$  GeV/c and  $p_{T,\text{jet}} > 5$  GeV/c, while there is a hint of  $D^0$  mesons diffusing away from the jet axis in heavy-ion collisions at the LHC for  $4 < p_{T,D^0} < 20$  GeV/c and  $p_{T,\text{jet}} > 60$  GeV/c. The observation at the LHC is quantitatively different from charged particle radial distributions in inclusive jets, where a suppression is seen for  $p_{T,\text{trk}} > 4$  GeV/c and  $r > 0.1$  in Pb+Pb compared to p+p collisions [585].

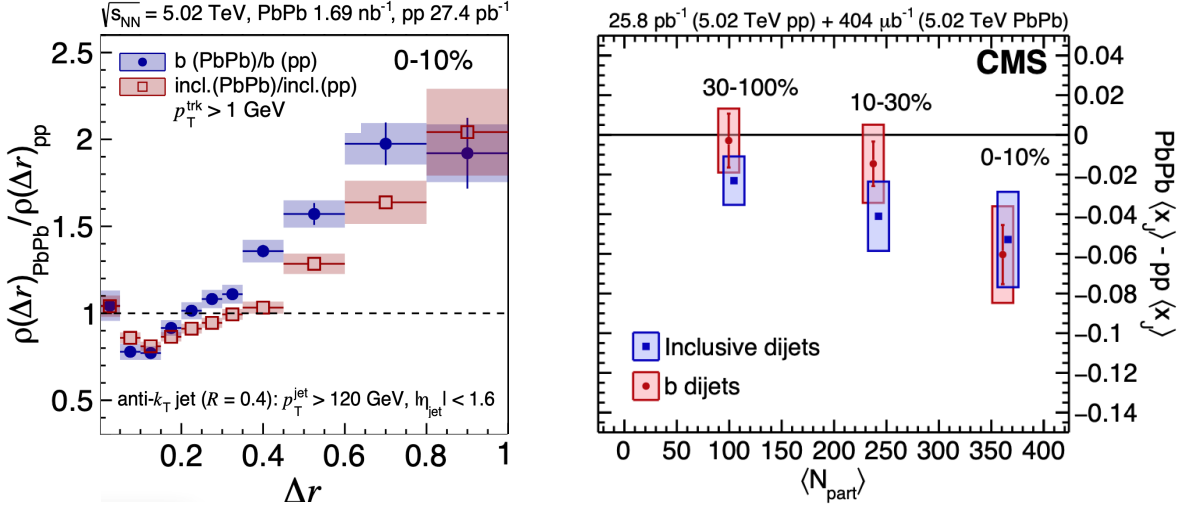


Figure 40: Left: ratio of jet shape distributions in Pb+Pb and p+p collisions at  $\sqrt{s_{\text{NN}}} = 5.02$  TeV for  $b$ -jets and inclusive jets [751]. Right: difference of dijet imbalance measured in Pb+Pb and p+p collisions at  $\sqrt{s_{\text{NN}}} = 5.02$  TeV for  $b$ -dijets and inclusive dijets [725].

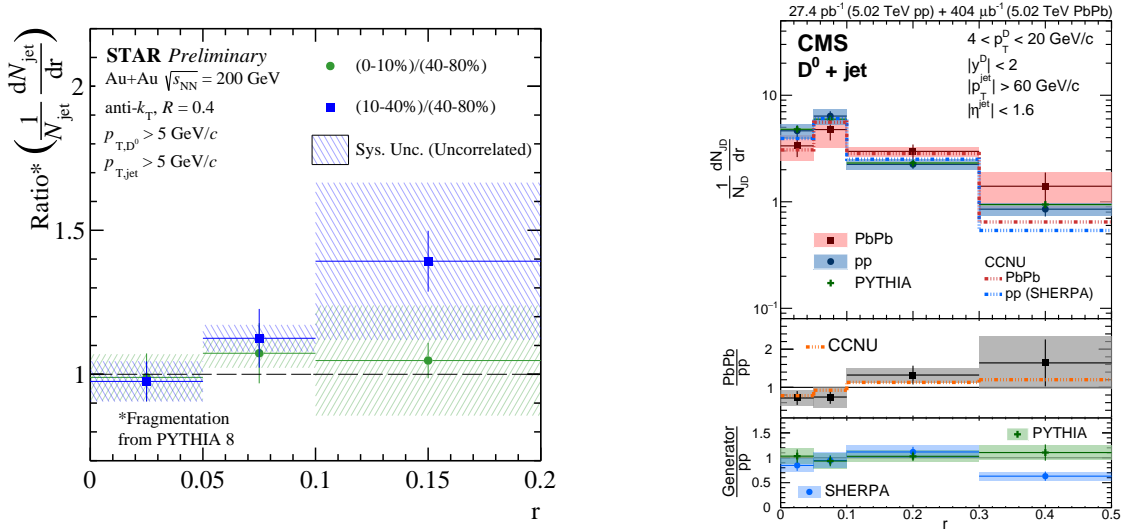


Figure 41: Measurements of the radial distribution for  $D^0$  mesons with respect to the jet axis at RHIC (left) [817] and the LHC (right) [818].

### 3.3.7 Bayesian methods for hard probes

With the proliferation of results in the hard sector in recent years described in this paper, analyses following a global parameter extraction approach have become increasingly important, in line with what was mentioned in the 2015 Long Range Plan. Due to the nontrivial dependence of QGP transport properties on the experimental observables, many different effects are often entangled in the measurements. A global analysis is well suited to extract the properties, for example (but not limited to) on the viscosities and  $\hat{q}$ , with precision and from increasingly larger set of measurements simultaneously. It is complementary to many other studies utilizing a smaller set of data to understand the properties of QGP. Many recent advances from the statistics community also allows rigorous and scalable analyses with well-controlled precision. One of the

popular approaches is the so-called Bayesian analysis approach [819–821]. In this approach, Bayesian statistics is used to describe the posterior probability density in the theory parameter space and thereby extract the “best-fit” parameters.

Bayes’ Theorem states that

$$P(\vec{\theta}|\vec{x}) = \frac{P(\vec{x}|\vec{\theta})P(\vec{\theta})}{P(\vec{x})}, \quad (29)$$

where the term  $P(\vec{\theta}|\vec{x})$  denotes the conditional probability density of theory parameter  $\vec{\theta}$  condition on experimental data  $\vec{x}$ , and is usually referred to as the “Bayesian posterior function.” The term  $P(\vec{x}|\vec{\theta})$  is the “Bayesian likelihood function”, and it is typically obtained through Monte-Carlo simulation methods where a set of events are simulated following a given input parameter set  $\vec{\theta}$  and subsequently analyzed to compare with experimental input. The computing cost to obtain the Bayesian likelihood function is nontrivial, and it is not computationally feasible to calculate for all possible input parameter  $\vec{\theta}$ . The common approach to this problem is to calculate the Bayesian likelihood function for only a selected set of parameter points (typically referred to as “design points”), and perform interpolation, for example with Gaussian process emulators [822], to obtain the function for the full parameter space. It has been observed that one can obtain reasonable performance with a much smaller number of design points compared to a naive grid-like approach where the number of points scales with the volume of the parameter space. Finally, a popular approach to analyze the Bayesian posterior function in recent work is to utilize Markov-Chain Monte-Carlo (MCMC) methods [823, 824] to obtain projected parameter density functions in one or two dimensions.

Many recent works [825–829] for the hard probes have been focusing on the extraction of the  $\hat{q}$  parameter and charm diffusion coefficient  $D_s$ . Even with the analysis methods to drastically reduce the computation cost needed, the computing requirement is still considerable. Therefore many recent results adopted the approach to separate the soft and the hard sector: the parameters corresponding to the bulk properties are taken as input to the calculation and are not treated as part of the target parameter space for the analyses. Many recent advances in the Monte-Carlo generators (for example the JETSCAPE/XSCAPE framework [2]) allow a more accurate description of a wider class of jet observables that are sensitive to treatment of the correlated medium response. For example the multi-staged approach employed by ref. [825, 826] attempts to describe the parton energy loss with the MATTER [830] and the LBT [622, 709] models each specialize in different ranges of parton virtuality, allowing more flexibility in the modeling of the jet quenching process. Xie et al [827] employed an information field [831–833] based approach in the extraction of the  $\hat{q}$  parameter to explore potential new ways to extract  $\hat{q}$  without an explicit functional assumption. Current analyses also highlighted a need for an improved experimental uncertainty reporting.

The scope of analyses is usually limited by the computational capacity. There has been a number of ongoing efforts to improve the current Bayesian analysis methods in the context of parameter extraction in heavy-ion physics, focusing on ways to reduce computational requirements for a similar performance. As an example, the active learning approach [834] iteratively includes new design points to maximally reduce uncertainties from the interpolation procedure. Approaches such as transfer learning [835] or multi-fidelity [836] utilize existing interpolated functions as the base either from related analysis or from lower fidelity models which do not cost as much to run. The full simulations then only need to capture the difference between the full model and the base model, thereby reducing computing needs. A sustained effort in research on methodology improvements is vital for the future physics program for global parameter extraction, where parameter spaces that are much larger than those probed in the current iteration of analyses need to be explored, and which would not be possible without significant improvement to the analysis method.

### 3.4 Microscopic II: Quarkonia, open heavy flavor, electromagnetics and bound states

#### 3.4.1 Theory: heavy flavor

From a theoretical perspective, heavy flavor probes provide a unique opportunity to learn about the in-medium QCD force and its manifestation in the binding of heavy quarks and in inelastic or elastic reaction rates involving heavy quarks. Below we discuss theory developments related open heavy flavor and quarkonia.

**Open Heavy Flavor.** In the deconfined QGP, heavy quarks produced at the initial stage of a heavy-ion collision propagate through the QGP, during which their momenta change and their energies are lost. By studying the nuclear modification factors in the production of open heavy flavor hadrons, we can probe how the QGP modifies the transport of heavy quarks and thus studying the QGP transport properties. Cold nuclear matter effects (CNM) such as the nPDF also affect the heavy flavor hadron production. Yields of different heavy flavor mesons and baryons are also sensitive to the hadronization mechanism, which can be studied in other collisions such as  $e^-e^+$ ,  $e^-p$  and  $p+p$  collisions. Hadronization, however, may be modified by the presence of hot medium, see e.g. Refs. [837, 838]. This is consistent with the lattice study of charm fluctuations and correlations [839] as discussed below.

At low transverse momentum, the dominant energy loss mechanism of heavy quarks is elastic scattering, while at high-transverse momentum, radiative energy loss becomes dominant. Radiative energy loss can be studied perturbatively and is similar to the energy loss of a high-energy parton, except for the finite mass effect. An effective description of heavy quark dynamics inside the QGP is based on a Langevin equation with diffusion and drag, as well as a radiation term added. The heavy quark diffusion coefficient encodes the QGP transport property that can be probed by studying open heavy flavor hadrons. The heavy quark diffusion coefficient has been studied perturbatively, nonperturbatively via AdS/CFT [840–843], lattice QCD methods [844–848], and the T-matrix approach which uses some input from lattice QCD [849, 850]. It was also determined from experimental data via Bayesian analysis [704, 828]. In the large heavy quark mass limit, the heavy quark diffusion coefficient is obtained from the spectral function of the chromoelectric field strength correlator [842, 851]

$$\kappa_{\text{fund}} = \frac{g^2}{3N_c} \text{Re} \int dt \langle \text{Tr}_c [U(-\infty, t) E_i(t) U(t, 0) E_i(0) U(0, -\infty)] \rangle_T, \quad (30)$$

where  $E_i$  is the  $i$ th component of the chromoelectric field and  $U$  denotes a timelike Wilson line in fundamental representation. There was significant progress made in the lattice QCD calculations using this approach [846–848, 852–854]. These calculations have been so far limited to quenched QCD. The results obtained by different methods and different groups are consistent and the lattice results hint toward a temperature dependence of the heavy quark diffusion coefficient. The mass suppressed contribution to the heavy quark diffusion coefficient that can be expressed in terms of chromo-magnetic field strength correlator [855, 856], was estimated very recently independently by two groups [852, 853], leading to the same result of 10 – 20% correction for bottom quark and 20 – 30% correction for charm quark compared to the case of infinitely heavy quark for temperature around  $1.5T_c$ . The first lattice calculation of the heavy quark diffusion coefficient in 2+1 flavor QCD appeared very recently [857]. Strictly speaking in QCD the heavy quark diffusion coefficient describes the diffusion of the conserved net heavy quark number, and by definition this diffusion coefficient only depends on the temperature. To understand the production of heavy flavor hadrons in heavy ion collisions one needs to introduce an effective momentum dependent diffusion coefficient in the Langevin dynamics [858]. In the zero momentum limit this effective diffusion coefficient reduces to the usual heavy quark diffusion coefficient that is defined in QCD. The effective heavy quark diffusion coefficient including its temperature and momentum dependence has been calculated non-perturbatively in the T-matrix approach [849, 850].

It was pointed out the charm fluctuations and charm baryon number correlations obtained on the lattice can provide information about the nature of charm degrees of freedom close to the QCD crossover [839]. Current lattice data hint toward the existence of charm mesons and baryons above the crossover temperature [839]. This was confirmed in calculation of the charm fluctuations and charm light quark flavor correlations within the T-matrix approach [859], which agree well with the lattice results. Within the T-matrix approach the in-medium spectral functions of the  $D$  meson in QGP have been obtained [859]. Furthermore, in-medium masses of charm mesons have been directly from lattice QCD meson correlation functions and it was found that corresponding masses may shift downward by about 1% close to the crossover [860].

**Quarkonium.** Quarkonia, bound states of  $c\bar{c}$  (charmonium) and  $b\bar{b}$  (bottomonium) pairs, have played a unique role in probing the properties of the QGP as they are sensitive to medium effects. Hot medium effects include plasma screening of the heavy quark-antiquark potential, dissociation and recombination. In different temperature regimes, these hot medium effects can be related to different transport properties of the QGP. Quarkonia of different sizes are affected differently by these hot medium effects and thus providing a powerful probe of the QGP properties at different scales. Quarkonium suppression in heavy ion collisions is also sensitive to the feed-down structure, e.g.,  $\psi(2S) \rightarrow J/\psi$ ,  $\Upsilon(3S) \rightarrow \Upsilon(2S) \rightarrow \Upsilon(1S)$  and  $\chi_b(1P) \rightarrow \Upsilon(1S)$ , as well as cold nuclear matter effects.

For quarkonium production at low transverse momentum, the description of quarkonium in-medium dynamics varies in different temperature regimes. Our understanding of quarkonium dynamics inside the QGP was greatly advanced by the application of the open quantum system framework (recent reviews can be found in Refs. [861–864]), since the last Long Range Plan.

An open quantum system is a system of interest coupled with an environment that is integrated out. The total Hamiltonian can be written as the sum of the system Hamiltonian, the environment Hamiltonian and their interaction  $H = H_S + H_E + H_I$ . The combination of the system and the environment evolve together unitarily and time-reversibly

$$\frac{d\rho(t)}{dt} = -i[H, \rho(0)], \quad (31)$$

where the initial density matrix is assumed to be factorized  $\rho(0) = \rho_S(0) \otimes \rho_E(0)$ . If we only focus on the time evolution of the system by tracing out the environment degrees of freedom, we will arrive at a non-unitary time evolution equation that is time-irreversible. For the application to quarkonium inside the QGP, the system contains heavy quark-antiquark pairs that can be either in the color singlet or the color octet, while the QGP serves as the environment. The QGP is usually assumed to be at thermal equilibrium with a temperature  $T = 1/\beta$  and thus  $\rho_E(t) = e^{-\beta H_E} / \text{Tr}(e^{-\beta H_E})$  is time independent.

The non-unitary and time-irreversible time evolution equation of the system can be greatly simplified in two limits. One limit is called the quantum Brownian motion limit, valid at high temperature and the other is the quantum optical limit, valid at low temperature. An intuitive illustration of these two limits is shown in Figure 42. Both the quantum Brownian motion limit and the quantum optical limit of quarkonium transport have been investigated in recent studies. In the quantum Brownian motion limit, the time evolution of the open system is described by a Lindblad equation [865–877], a non-unitary generalization of the Schrödinger equation. So far only the Lindblad equations for one heavy quark antiquark pair have been studied due to limited computing power, which can be improved by future developments of computing tools and machine learning techniques. In practice, many studies used the semiclassical limit of this Lindblad equation that corresponds to a Langevin equation. In the quantum optical limit, a Boltzmann equation for quarkonium dissociation and regeneration was derived by applying a Wigner transform to the density matrix and performing a gradient expansion [878, 879]. The Boltzmann equation that has been widely used in quarkonium phenomenology (see e.g. [880, 881]) is one approximation of the more general quantum approach. Motivated by the quantum approach, recent studies started to look into the interplay between the



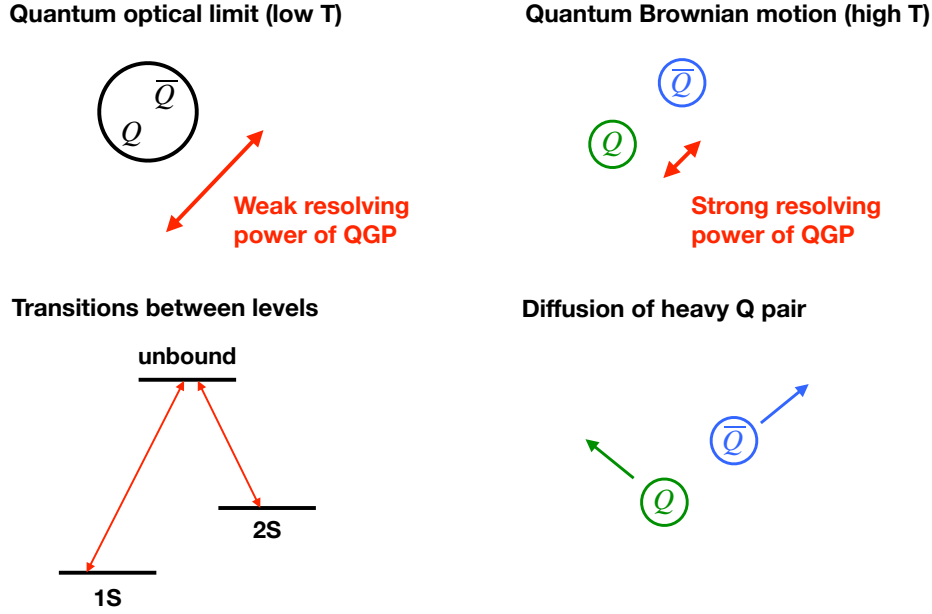


Figure 42: Intuitive illustration of the quantum optical (left) and the quantum Brownian motion (right) limits. At low temperature, the resolving power of the QGP is too weak to see the internal structure of a quarkonium state and the eigenstates of the quarkonium relative motion form a good basis for computation, in which the quarkonium in-medium dynamics is described by transitions between eigenstates at different energy levels. At high temperature, the resolving power of the QGP is strong enough to see the internal structure of quarkonium and the QGP is interacting with the heavy quark and antiquark almost independently. As a result, both heavy quarks diffuse, which leads to decoherence of the quarkonium wavefunction. (Figure courtesy of Xiaojun Yao.)

open heavy quark dynamics and the quarkonium dissociation and recombination processes, since both of them are part of the same density matrix. Some of these studies treat the open heavy quark dynamics as diffusion in a Langevin equation [869, 882]. Other studies constructed a coupled set of Boltzmann equations for open heavy flavors and quarkonia to study quarkonium thermalization and production [883–886]. In all these studies, both spatial and momentum correlations between the unbound heavy quark antiquark pair is accounted for in recombination. Boltzmann equations with dissociation and recombination have also been used to study  $X(3872)$  [887],  $B_c$  [888] and  $\Xi_{cc}$  [889] production in heavy ion collisions.

Important new theoretical developments that are obtained or motivated from using the open quantum system framework include: (1) the understanding of quarkonium dissociation as a result of quantum decoherence of the quarkonium wavefunction [890, 891]; (2) the microscopic construction of the recombination term that is on the same theoretical foundation as, and thus consistent with dissociation in both quantum and classical transport approaches [871, 872, 878, 879, 892, 893], which were absent in previous transport studies [894–906]; and (3) the construction of a novel transport coefficient for a heavy quark-antiquark pair entangled in color [879, 907], whose generalization to finite frequency also contains important information on quarkonium in-medium dynamics [879].

With these advances, our current understanding of low- $p_T$  quarkonium in-medium dynamics is as

follows: at high temperature, the  $Q\bar{Q}$  pair is unbound, each of the heavy quarks diffuses in the QGP, while interacting with each other via some real potential. The real potential only lasts for a short time period, which is related to the imaginary part of the potential. The diffusion dynamics is determined by the same transport coefficient  $\kappa_{\text{fund}}$  as in the open heavy flavor transport. As the QGP expands and cools down, color and spatial correlations between the  $Q\bar{Q}$  pair cannot be neglected any more, which affect the diffusive dynamics and the transport coefficient that is relevant becomes  $\kappa_{\text{adj}}$  and  $\gamma_{\text{adj}}$ , which are defined by

$$\kappa_{\text{adj}} + i\gamma_{\text{adj}} = \frac{g^2 T_F}{3N_c} \int dt \langle \mathcal{T} E_i^a(t) W^{ab}(t, 0) E_i^b(0) \rangle_T, \quad (32)$$

where  $W$  denotes a time-like Wilson line in adjoint representation. Finally, in the low temperature regime, quarkonium dynamics can no longer be described in the diffusion picture, rather, it is described in terms of transitions between different bound and unbound states. The QGP property that determines the rates of these transitions (dissociation and recombination) is given by the finite frequency generalization of  $\kappa_{\text{adj}}$ :

$$[g_E^{++}]^>(\omega) = \frac{g^2 T_F}{3N_c} \int dt e^{-i\omega t} \langle E_i^a(t) W^{ab}(t, 0) E_i^b(0) \rangle_T. \quad (33)$$

The difference between the fundamental and adjoint versions of the chromoelectric correlators is not in their representation, but in the operator ordering [908, 909]. At next-to-leading (NLO) order, the spectral functions of these two chromoelectric field correlators differ by a temperature independent piece [909–911]

$$\Delta\rho(\omega) = \frac{T_F g^4 (N_c^2 - 1) \pi^2}{3(2\pi)^3} |\omega|^3, \quad (34)$$

where  $\Delta\rho(\omega)$  denotes the difference between these two spectral functions. The most striking feature of Eq. (34) is the non-oddness in frequency. The sPHENIX program at RHIC will provide a unique opportunity to probe this object at finite frequency.

In practical calculations, the transition between different temperature regimes can be determined by lattice studies of correlation functions in Euclidean time, which are Laplace transforms of the spectral functions and can tell in-medium quarkonium masses and width as well as the corresponding melting temperatures, see e.g. Refs. [912, 913] for reviews. The main challenge of reconstructing the spectral functions from the lattice results on the correlation function is the limited extent of the Euclidean time direction,  $\tau < 1/T$ , with  $T$  being the temperature, and the limited number of temporal grid points  $N_\tau$ . The lattice calculations of the heavy flavor probes significantly matured since the last Long Range Plan. It was realized that to deal with the limited Euclidean time extent at  $T > 0$  in the study of bottomonium properties at high temperatures it is advantageous to use optimized meson operators that are mostly sensitive to the meson state of interest [914, 915]. Therefore, unlike in the previous lattice QCD calculations that used point-like meson operators and could not provide reliable information on the in-medium mass and width of different quarkonium states, now it is possible to directly obtain this information from lattice correlators. Using the above approach and 2+1 flavor  $N_\tau = 12$  lattices the in-medium masses and widths for  $\Upsilon(1S)$ ,  $\Upsilon(2S)$ ,  $\Upsilon(3S)$ ,  $\chi_b(1P)$  and  $\chi_b(2P)$  states have been estimated [914]. The mass shift with respect to the vacuum values turned out to be insignificant within the estimated errors, but the thermal width of different bottomonia states was found to increase with increasing temperature. Furthermore, the hierarchy of the thermal width of different bottomonium states appears to follow the hierarchy of their sizes [914].

The study of the complex  $Q\bar{Q}$  potential at non-zero temperature also requires the reconstruction of the spectral function of Wilson line correlation function. The position of the dominant peak in this spectral function defines the real part of the potential, while the width gives the imaginary part of the potential [916]. Lattice calculations with  $N_\tau = 12$  were performed very recently [917]. This calculation indicates that the

real part of the potential is not screened and is about the same as in the vacuum [917]. If confirmed by future lattice calculations with larger  $N_\tau$  this finding will make the revision of many models for quarkonium production in heavy ion collisions necessary. The imaginary part of the potential is quite sizable and increases with the temperature and with the separation between the quark and anti-quark [917]. It should be noted, however, that in lattice QCD one calculates the energy of a static quark anti-quark pair. This energy contains the energy of the static quark and anti-quark, as well as the interaction energy between the static quark and anti-quark. It is possible both of these components are temperature dependent but their sum turns to be temperature independent. This possibility was discussed in Refs. [896].

Finally, by studying spatial bottomonium correlation functions it is possible to provide constraints on the melting temperature of different bottomonium states. In general the relation of the spatial meson correlation function to the spectral function is quite involved (see e.g. Ref. [913]). However, at high temperatures it is easy to estimate the spatial correlation function corresponding to unbound heavy quark and anti-quark and compare it to the lattice result. Such comparison for the ground state bottomonium has been performed and it was found that for  $T > 500$  MeV the corresponding lattice meson correlator agrees with the one of unbound quarks. Thus the 1S bottomonium state melts for  $T > 500$  MeV [918]. A similar comparison for the  $\chi_b$  states indicates that these states will melt at  $T \simeq 350$  MeV [918].

### 3.4.2 Experiment: quarkonia

Along the progresses made from the theoretical side as detailed in the previous section, progresses on quarkonium measurements have also been made from the experimental side, which will be highlighted in the following.

One can quantify the CNM effects, including both initial and final state effects [919], experimentally by measuring quarkonium production in p+A collisions, in which a QGP of extended volume as that observed in heavy-ion collisions is not expected to be formed [920–935]. Figure 43 shows measurements of the nuclear modification factor ( $R_{pA}$ ) for  $J/\psi$  in p+Au collisions at  $\sqrt{s_{NN}} = 200$  GeV by the STAR experiment (left) [923] and for  $\Upsilon(1S)$  in p+Pb collisions at  $\sqrt{s_{NN}} = 5.02$  TeV by ATLAS (right) [927]. A clear

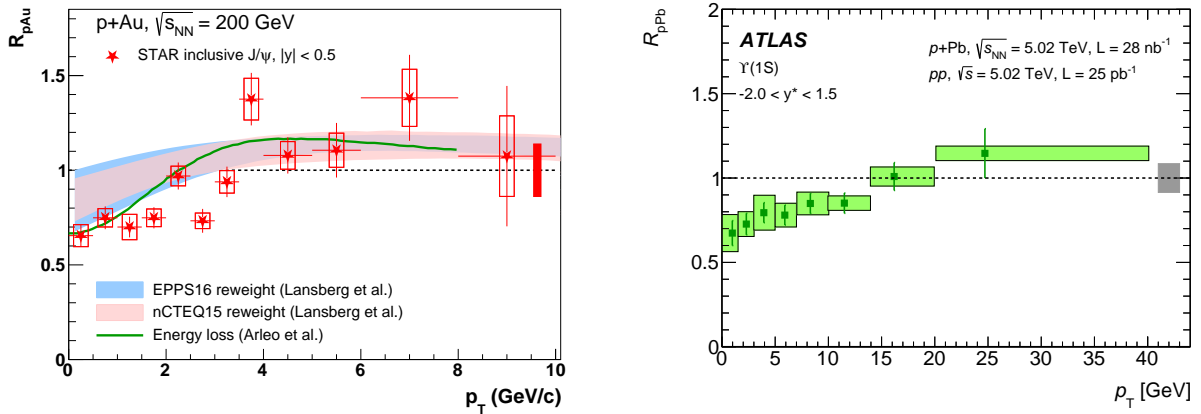


Figure 43: Measurements of  $R_{pA}$  as a function of  $p_T$  for  $J/\psi$  in p+Au collisions at  $\sqrt{s_{NN}} = 200$  GeV (left) [923] and for  $\Upsilon(1S)$  in p+Pb collisions at  $\sqrt{s_{NN}} = 5.02$  TeV (right) [927].

suppression of about 30% is seen at low  $p_T$ , which could mimic the dissociation effect and therefore needs to be taken into account when interpreting similar measurements in heavy-ion collisions. As  $p_T$  increases,  $R_{pA}$  also increases and becomes consistent with unity within uncertainties at high  $p_T$ . Theoretical calculations including latest nPDF sets [936, 937] or coherent energy loss [938], as shown in the left panel of

Figure 43, can qualitatively describe data. To further study the CNM effects, measurements of charmonia

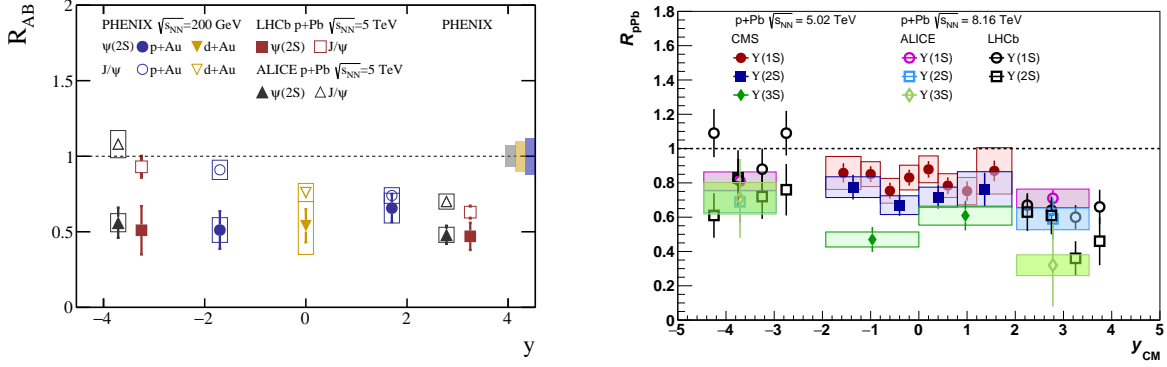


Figure 44: Charmonia (left) and bottomonia (right)  $R_{pA}$  as a function of rapidity [920, 922, 924–926, 930–932, 934].

( $J/\psi$ ,  $\psi(2S)$ ) and bottomonia ( $\Upsilon(1S)$ ,  $\Upsilon(2S)$ ,  $\Upsilon(3S)$ )  $R_{pA}$  as a function of rapidity are shown in the left and right panels of Figure 44, respectively. For charmonia [920, 922, 924, 925, 931, 932], the level of suppression for  $\psi(2S)$  is similar to that of  $J/\psi$  at forward p-going direction indicating the dominance of the initial-state effects, while  $\psi(2S)$  is more suppressed than  $J/\psi$  at backward A-going direction, which is likely resulted from final-state effects, such as comover breakup [939], that affect  $J/\psi$  and  $\psi(2S)$  differently. For bottomonia [926, 930, 934], all three  $\Upsilon$  states are suppressed across the probed rapidity range with the excited states more suppressed than the ground state, which again points at final-state effects.

Measurements of the  $J/\psi$   $R_{AA}$  as a function of charged particle multiplicity in heavy-ion collisions by NA50, STAR and ALICE are shown in the left panel of Figure 45 [103, 940, 941]. If the dissociation is the

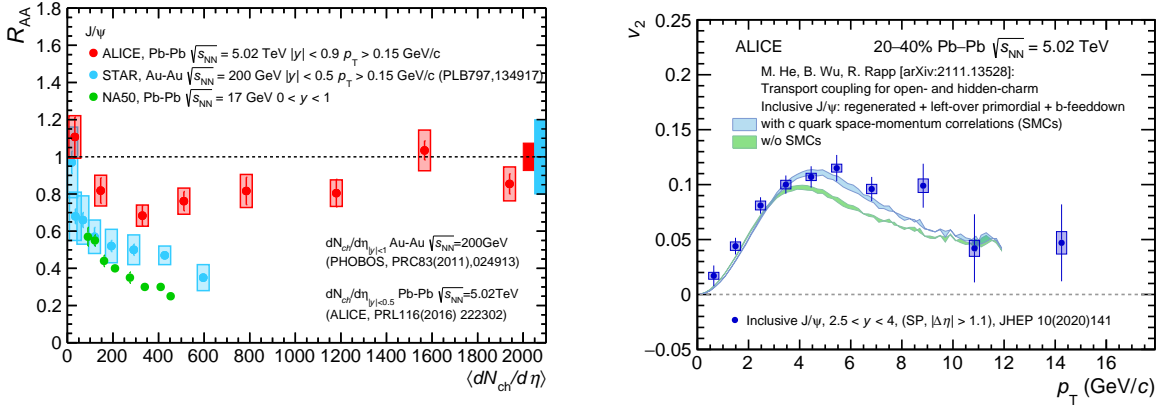


Figure 45: Left:  $J/\psi$   $R_{AA}$  at low  $p_T$  as a function of charged particle multiplicity in heavy-ion collisions by NA50, STAR and ALICE [103, 940, 941]; Right:  $J/\psi$   $v_2$  as a function of  $p_T$  in 20–40% Pb+Pb collisions  $\sqrt{s_{NN}} = 5.02$  TeV [942], compared with a transport model calculation [943].

only effect in play, one would expect a larger suppression in the  $J/\psi$  yield, and thus a smaller  $R_{AA}$ , in collisions of higher energy where a hotter QGP is expected to be formed *i.e.*, the  $J/\psi$   $R_{AA}$  should decrease with increasing collision energy [880]. However, the opposite is observed experimentally, which points to the increasing contribution of recombination at higher energy. At the LHC, the  $J/\psi$   $R_{AA}$  is also seen to increase from peripheral to central collisions, which is also likely caused by the enhanced recombination in central

collisions because of the larger number  $c\bar{c}$  pairs produced in these collisions. The right panel of Figure 45 shows  $J/\psi$   $v_2$  as a function of  $p_T$  measured in Pb+Pb collisions at  $\sqrt{s_{NN}} = 5.02$  TeV by ALICE. The  $J/\psi$   $v_2$  increases with  $p_T$  and reaches about 0.1 around  $p_T = 5$  GeV/c. The  $J/\psi$  mesons produced during initial hard scatterings are not expected to acquire significant flow through thermalization. Such a large  $v_2$  signal at low to intermediate  $p_T$  can only be explained by the dominance of regenerated  $J/\psi$  mesons inheriting the elliptic flow of the constituent charm quarks which likely have reached local thermalization in the QGP. Such a scenario is confirmed by the good agreement between data and a transport model calculation [943], shown in the right panel of Figure 45, in which  $J/\psi$  at low to intermediate  $p_T$  is mostly produced through recombination of diffusing charm and anti-charm quarks in the hydrodynamically expanding fireball. It becomes clear that both the dissociation and recombination contributions, besides other effects such as CNM effects and feeddown structure, are needed to provide a satisfactory explanation of  $J/\psi$  production in heavy-ion collisions from low to high energies.

The high-energy heavy-ion collisions at the LHC also open the door for measuring  $J/\psi$  at high  $p_T$ . The left panel of Figure 46 shows the ATLAS measurement of the prompt  $J/\psi$   $R_{AA}$  from 9 to 40 GeV/c compared to that of charged hadrons, which are seen to coincide each other above 12 GeV/c. One possible explanation is that high- $p_T$   $J/\psi$  is dominantly produced through parton fragmentation, and the suppression seen in the  $J/\psi$  yield is a reflection of the energy loss of the parent parton before fragmentation, the same mechanism responsible for high- $p_T$  charged hadron suppression. The parton energy loss mechanism could

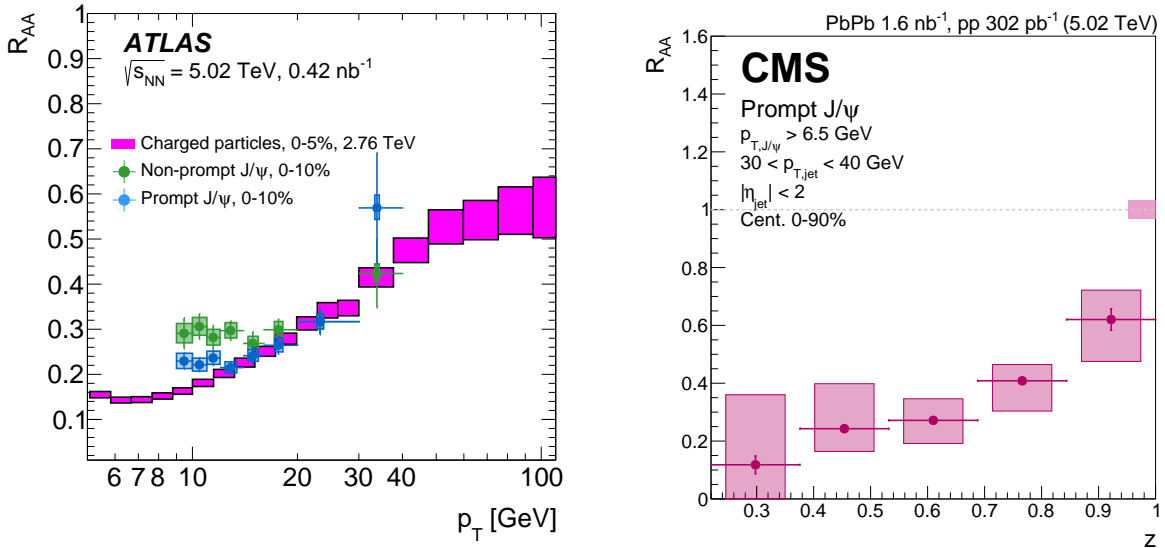


Figure 46: Left: comparison of  $R_{AA}$  as a function of  $p_T$  for high- $p_T$  prompt  $J/\psi$ , non-prompt  $J/\psi$  and charged hadron [944]. Right:  $R_{AA}$  of  $J/\psi$  mesons contained in jets as a function of the jet momentum fraction carried by the  $J/\psi$  [945].

also explain the finite  $v_2$  observed for  $J/\psi$  above 10 GeV/c, as shown in the right panel of Figure 45, by invoking its path-length dependence. This idea is further explored by the CMS experiment by studying high- $p_T$   $J/\psi$  contained in jets [945, 946]. It was found that about 85% of  $J/\psi$  with energies above 15 GeV within the rapidity range of  $|\eta| < 1$  are contained in jets, *i.e.*, there are hadronic activities nearby the  $J/\psi$ , with energies above 19 GeV in p+p collisions at  $\sqrt{s} = 8$  TeV. This observation corroborates that high- $p_T$   $J/\psi$  is dominantly produced during parton fragmentation. The right panel of Figure 46 shows that the level of suppression for high- $p_T$   $J/\psi$  yields in jets increases with decreasing  $z$ , the fraction of jet  $p_T$  carried by  $J/\psi$ . Theoretical calculations based on leading power non-relativistic QCD show that the fraction of directly

produced  $J/\psi$  from gluon fragmentation varies between 70-90% from 10 to 100 GeV/c [947]. This opens the door for obtaining an enriched sample of gluon-initiated jets by tagging with high- $p_T$   $J/\psi$ , which can be used to study gluon energy loss mechanism and compared to quark-initiated jets.

The full power of utilizing quarkonium suppression to infer the transport and thermodynamic properties of the QGP arises from the ability to measure quarkonia of different sizes. Figure 47 shows the  $R_{AA}$  (filled symbols) of charmonia ( $J/\psi$ ,  $\psi(2S)$ ) and bottomonia ( $\Upsilon(1S)$ ,  $\Upsilon(2S)$ ,  $\Upsilon(3S)$ ) in heavy-ion collisions at RHIC (left) and the LHC (right) as a function of the binding energy, compared to corresponding measurements in p+A collisions (open symbols) [922, 928–930, 941, 948–953]. Here, the binding energy is

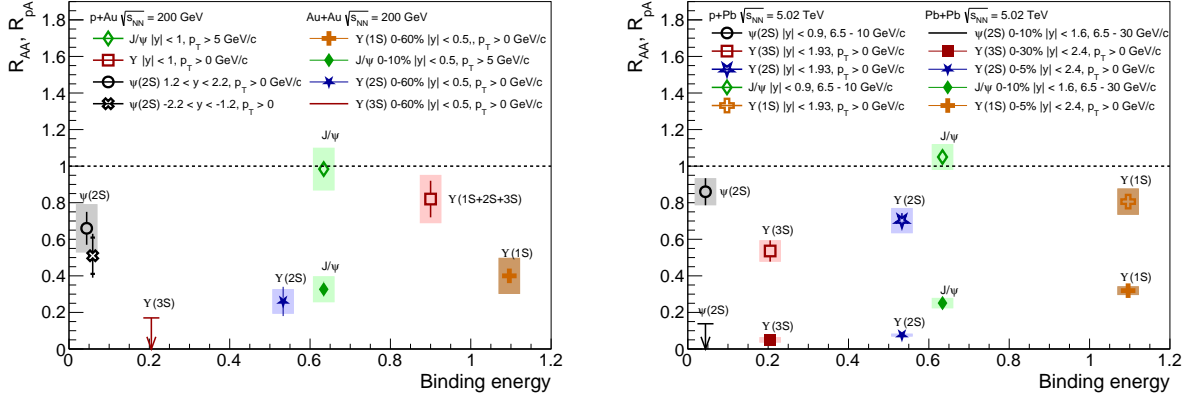


Figure 47: Quarkonium  $R_{AA}$  (filled symbols) and  $R_{pA}$  (open symbols) as a function of binding energy measured at RHIC (left) and the LHC (right) [922, 928–930, 941, 948–953].

calculated as the difference between twice the lightest heavy quark meson mass and the quarkonium mass. For charmonia, measurements above 5 (6.5) GeV/c are shown at RHIC (LHC) to minimize complications from CNM effects and recombination, except that the  $\psi(2S)$   $R_{pA}$  for 200 GeV p+Au collisions is shown for  $p_T > 0$  GeV/c which is the only available measurement at RHIC. A suppression of the bottomonium states is seen in p+A collisions, while high- $p_T$   $J/\psi$  is not. In heavy-ion collisions, a sequential suppression pattern depending on the binding energy is clearly seen, in line with the expectation that more loosely bound states are more likely to be dissociated in the QGP. Such a sequential suppression pattern also points to the importance of accounting for the feeddown contributions from excited states to ground states, which are included in the experimentally measured yields, when interpreting these data. A comprehensive comparison to model calculations, which include all the effects that affect the measured quarkonium yields, is needed to extract the QGP properties.

### 3.4.3 Experiment: open heavy flavor

Some of the requirements needed for the quark-gluon plasma characterization are: i) the medium needs to have a relatively large volume; ii) the probe needs to be formed and not shower in the vacuum before the QGP formation; and have different mass and momentum scales. Relativistic heavy-ion collisions produce QGP with volumes on the order of the size of the colliding nucleus. Heavy quarks (charm and bottom) have a formation time  $< 0.07$  fm/c, way before the formation of a thermalized QGP which is supposed to take between 0.3 and 1.5 fm/c [954]. The energy that a quark loses when crossing the QGP medium depends on its mass  $m_q$ . The gluon radiation formed when an incident quark crosses the QGP medium has a cone with minimum angle  $\theta = m_q/E_q$ , meaning that the dead radiation cone is larger for heavy quarks [811].

Heavy quarks are predominantly formed from gluons in high-energy collisions. At RHIC energies flavor excitation and pair creation are the dominant processes as indicated in measurements of muon pairs

from heavy flavor decays measured by PHENIX [955]. Gluon splitting is dominant at LHC energies.

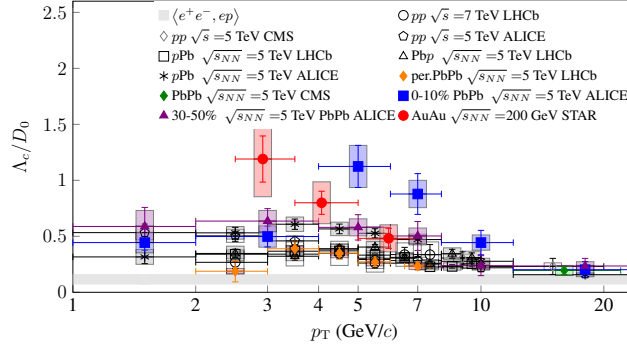


Figure 48:  $\sigma(\Lambda_c)/\sigma(D^0)$  ratio measured in  $e^+e^-$  [956–958],  $ep$  [959,960],  $p+p$ ,  $p+Pb$ ,  $Au+Au$  and  $Pb+Pb$  collisions [961–967].

One of the most interesting recent observations is the modification of the charm fragmentation fraction observed in  $pp$  collisions when compared to  $e^+e^-$  and  $ep$  collisions as indicated in the study performed by the ALICE collaboration [968]. The modification infers the enhancement of charmed baryons which is compensated with a suppression of charmed mesons. This effect is also observed between  $pp$  and heavy-ion collisions where the total  $D^0$  cross-section per binary collision measured by STAR is not conserved in  $Au+Au$  collisions [969], despite the expected conservation of the number of charm quarks observed in semi-leptonic decays [970]. The  $\Lambda_c$  baryon enhancement relative to  $D^0$  mesons was observed in several collision systems by several experiments at LEP, DESY, RHIC and LHC as shown in Figure 48. The  $p_T$  integrated results obtained from  $e^+e^-$  [956–958] and  $ep$  [959,960] are consistent and shown in the figure as an average with the uncertainty band covering the combined statistical and correlated uncertainties. The  $\Lambda_c/D^0$  yield ratio is systematically larger in hadronic collisions. One of the most successful descriptions of the baryon enhancement is color reconnection [484] where the underline partons in the proton contribute to the hadron formation. In large systems, such as central  $Au+Au$  and  $Pb+Pb$  collisions, hadron coalescence inside QGP further enhances charmed baryon fractions [971]. The same effects may also happen with bottom quark fragmentation. Other baryon formations are expected to be further studied. First studies on  $\Lambda_b/B^0$  fractions were reported by LHCb in  $pPb$  collisions [972]. The observation of more exotic baryons, such as  $\Omega_{cc}$  and charmed tetraquarks (Section 3.4.4), are on target for the Run3 LHC.

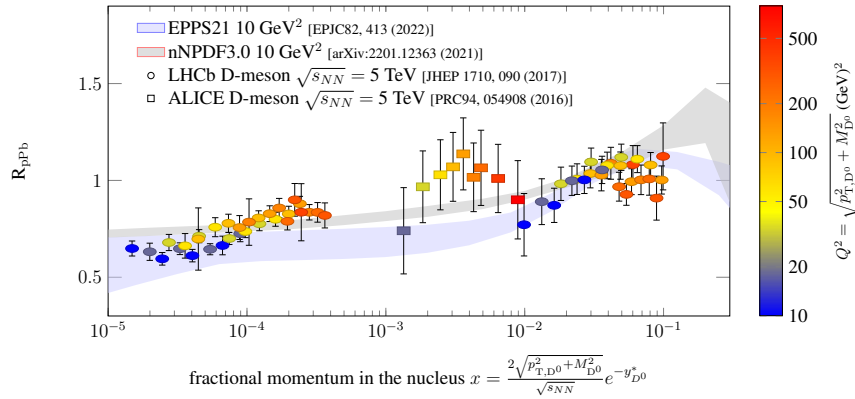


Figure 49: Partonic momentum fraction dependency of  $D^0$  nuclear modification factor in  $pPb$  collisions obtained by LHCb [973] and ALICE [974] along with the most recent nuclear parton distribution functions.

At the same time, heavy flavor yields can be modified by initial effects in the nucleus such as nuclear shadowing, initial state energy loss and gluon saturation effects. A recent overview of initial-state effects can be found in [975]. Heavy flavor nuclear modification factor in p(d)+A collisions has been measured at RHIC and LHC. Figure 49 shows the extension of the fractional momentum  $x$  of  $D^0$  meson nuclear modifications measured at LHC. The fraction of the proton longitudinal momentum  $x$  is an approximation assuming a  $2 \rightarrow 1$  process. The new set of data coming from the forward coverage of LHCb are responsible to finally provide a constraint to the nuclear PDFs at small- $x$  and small momentum transfer  $Q^2$  region as also shown in Figure 49.

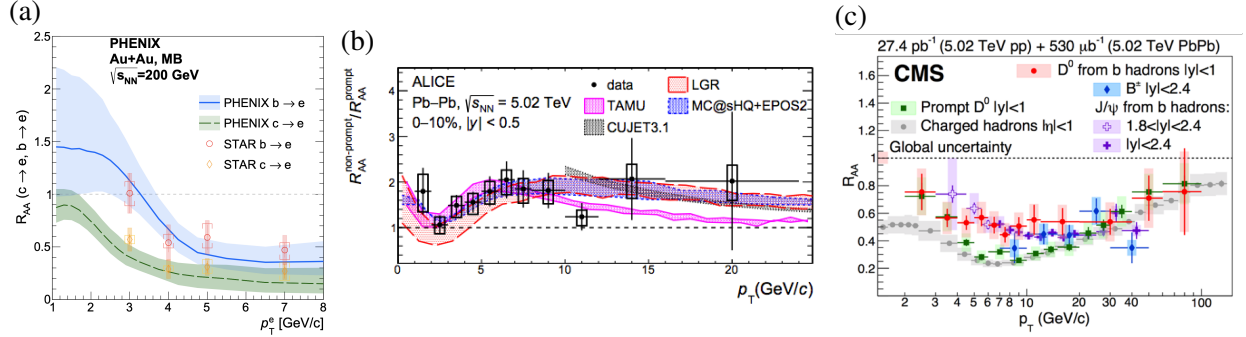


Figure 50: Nuclear modification factor of charm and bottom hadrons: (a) Electrons from semi-leptonic decays of charm and bottom hadrons measured by PHENIX [976] and STAR [977]. (b) Non-prompt (from B-meson decays) over prompt  $D^0$  nuclear modification factor ratio in Pb+Pb collisions from ALICE along with models [978]. (c) Light hadron (charged hadron), charm hadron (prompt  $D^0$ ) and bottom hadrons (non-prompt  $D^0$ , non-prompt  $J/\psi$  and B-mesons) nuclear modification factor in Pb+Pb collisions from CMS [979].

Systematic evidence for a mass hierarchy on the quark energy loss in QGP  $\frac{dE_{ud}}{dx} > \frac{dE_c}{dx} > \frac{dE_b}{dx}$  have been presented by experiments at RHIC and LHC in a variety of channels [969, 976–980] as summarized in Figure 50. Most nuclear modifications differences between  $c$  and  $b$  quarks happen in the intermediate  $p_T$  and reduce or vanish at high  $p_T$ . This is one of the major experimental accomplishments in the field of Hot QCD thanks to the investment in silicon vertex detectors which enable these measurements. New horizons were opened with the first observation of top quarks in Pb+Pb collisions by CMS [981]. The measured cross-section is consistent with binary  $pp$  scaling.

Relative abundances of  $D^0$ ,  $D^\pm$  and  $D^{*+}$  are unmodified as observed by ALICE [982], except strange D-meson yield  $D_s^+$  which is enhanced in Au+Au and Pb+Pb collisions at RHIC and LHC when compared to other D-mesons as reported by STAR [983] and ALICE [984]. Similar enhancement is also observed for  $B_s^0$  in Pb+Pb collisions as measured by CMS [985]. However, no apparent strangeness enhancement is observed in small systems as reported by ALICE [986]. The results suggest a hadron recombination in the QGP medium created in these collisions. Similar effects would also cause the enhancement of  $B_c$  mesons formed by a charm and a bottom quark, an unlikely formation in  $pp$  hard scattering processes but favored in QGP.

Preliminary results from PHENIX [990] and STAR [991] with electron decays indicate both charm and bottom quarks flow with the bulk medium. The elliptic flow parameter  $v_2$  reduces with the mass of the quark constituent. Elliptic  $v_2$  and triangular flow  $v_3$  of  $D^0$  have been measured by STAR [988] [992](prelim.), ALICE [982] and CMS [989] (Figure 51-c). The elliptic flow of  $D^0$  scales with light hadrons when the number of valence quarks and the quark mass dependence is accounted for as seen in Figure 51-b. The observed combination of  $R_{AA}$  and flow parameters is combined with current phenomenology models to



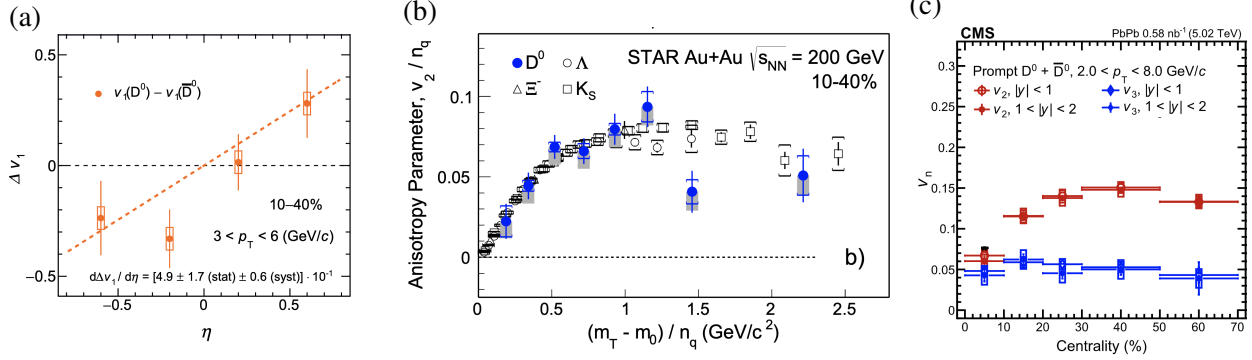


Figure 51: (a)  $D$ -meson direct flow charge asymmetry measured by ALICE [987]. (b)  $D^0$  elliptic flow over number of valence quarks compare lighter hadrons measured by STAR [988]. (c) Centrality and rapidity dependence of  $D^0$  elliptic and triangular flow from CMS [989].

determine the heavy flavor transport in QGP. The spatial diffusion coefficient  $2\pi D_s T_c$  has been constrained using RHIC and LHC data as summarized in Figure 52 along with lattice and transport model calculation efforts.

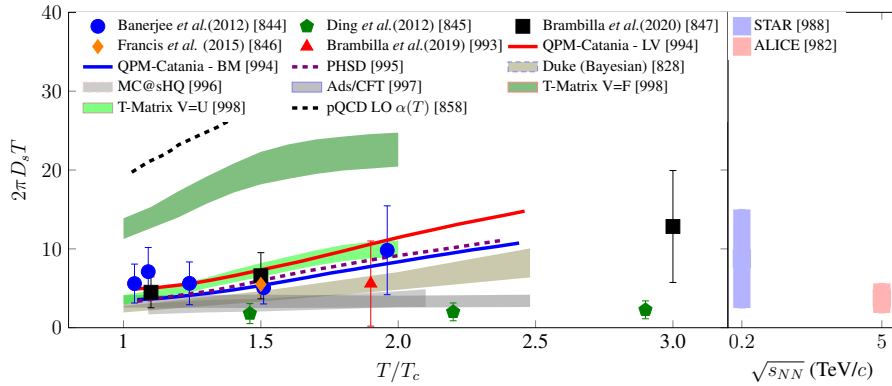


Figure 52: Spatial diffusion coefficient  $2\pi D_s T$  obtained from lattice computations (points), transport models (lines and bands) and constrained by experimental data: STAR uses models SUBATECH [999], TAMU [1000], Duke [711], LBT [709], PHSD [995], and ALICE uses TAMU, MC@sHQ+EPOS2 [999], LIDO [713], LGR [1001], Catania [1002] at  $T=155 \text{ MeV}$ .

Relativistic heavy-ion collisions are expected to produce magnetic fields up to  $eB \sim (m_\pi)^2 \approx 10^{14} \text{ T}$  at its first instants, probably the largest magnet fields in nature [1003]. This field can alter the direct flow measured by the direct flow  $v_1$ , of positive and negative charged particles around the reaction plane. The charm quarks are formed at the earliest stages of the collision, and therefore will have to overcome much larger magnetic fields than charged particles. The asymmetry measured by STAR shows no charge asymmetry within the uncertainties [1004] and ALICE shows two standard deviations linear dependence with  $\eta$  shown in Figure 51-a [987]. The linear slope is around three orders of magnitude larger than for charged particles. The extension to this measurement to large rapidities in forward detectors can provide a larger lever arm to measure a larger charge asymmetry  $v_1$  in the coming years.



explaining conventional charmonium, but their application to an exotic state has provided new challenges.

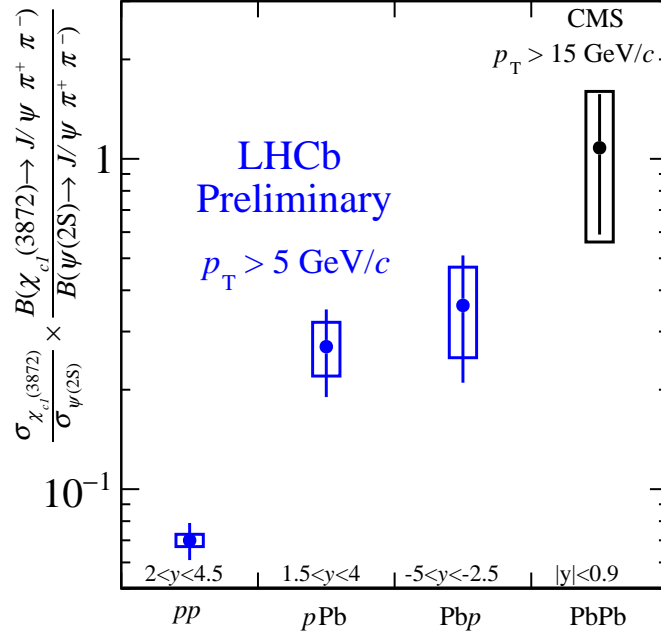


Figure 54: The ratio of X(3872) to  $\psi(2S)$  cross sections in various collision systems, as measured by LHCb [1013] and CMS [1010].

In smaller collision systems, the LHCb experiment has observed that the X(3872)/ $\psi(2S)$  ratio drops as a function of multiplicity in p+p collisions at 8 TeV, which was interpreted in terms of final-state interactions among co-moving particles disrupting the X(3872) hadrons. This data was interpreted to show support for both compact [1014] and molecular models [1015] of X(3872) structure. Preliminary LHCb results from pPb collisions at 8.16 TeV show an indication of enhancement of the X(3872)/ $\psi(2S)$  ratio, which falls between the values measured in p+p and Pb+Pb collisions [1013], which may indicate different effects on breakup and the hadronization process coming into play. The variation in the X(3872)/ $\psi(2S)$  ratio shows that the effect governing the production of the exotic X(3872) and the conventional  $\psi(2S)$  differ as system size changes.

### 3.4.5 Electroweak processes

Electroweak (EW) probes such as high- $p_T$  direct photons,  $W$  and  $Z$  bosons, top quarks, and high-mass di-leptons from Drell-Yan production are valuable probes of the initial state of the nuclear collision system before it forms a Quark-Gluon Plasma. Significant experimental and theoretical progress has been made since the previous Long-Range Plan, with first measurements of the top quark and high-mass Drell-Yan production in nuclear collision systems, substantially more detailed studies of high- $p_T$  direct photon,  $W$ , and  $Z$  production, and the incorporation of these data into global analyses.

Traditionally, these measurements have been valuable for understanding so-called “cold nuclear matter” effects on the rate of perturbative parton-parton scatterings, as commonly encoded in the modification of parton densities in the nuclei (nPDFs). Such measurements provide critical context needed to quantitatively interpret final state effects in nuclear collisions, such as parton energy loss or quarkonia dissociation in

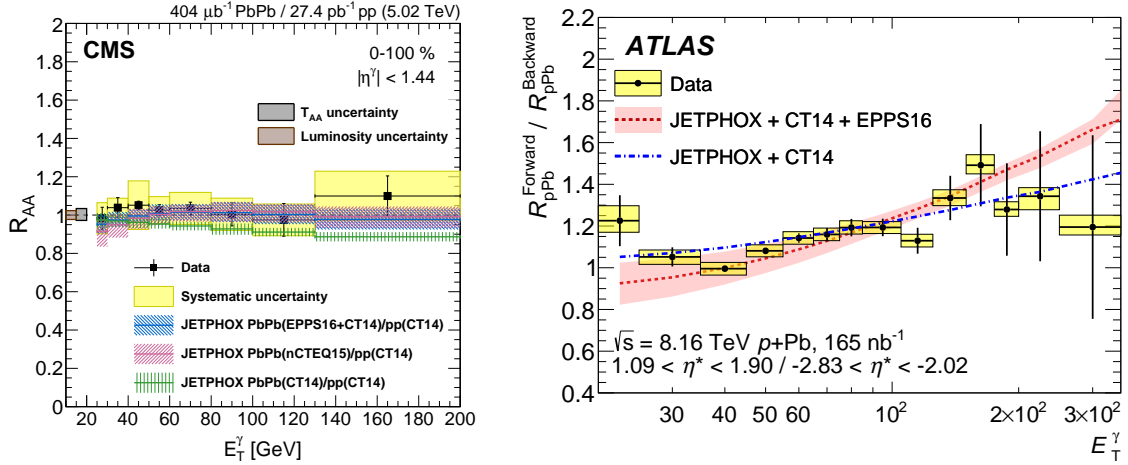


Figure 55: Measurements of isolated photon production in nuclear collisions: nuclear modification factor in Pb+Pb collisions by CMS [1022] (left), forward/backward ratio of nuclear modification factor in  $p$ +Pb collisions by ATLAS [1023] (right).

QGP. Because the precision of any extraction of QGP properties is automatically limited by the knowledge of initial state effects, data from electroweak probes are an integral part of the entire experimental “Hot QCD” physics program. Since the last Long Range Plan, electroweak boson data has gone from demonstrating the presence of nuclear PDF modifications to providing precision information for global nPDF analyses, with the experimental uncertainties currently smaller than the theoretical ones in some kinematic regions. Some recently released nPDF which rely on this data include nCTEQ15 [1016], EPPS21 [1017], and nNNPDF3.0 [1018] (with, e.g., specific discussions of the impact of LHC EW data in Refs. [1019, 1020]).

Additionally, since nPDF effects are not expected to be strongly centrality dependent, the centrality-dependent yields of these objects are seeing renewed use as a proxy to test the centrality selection framework, and in particular the estimation of geometric parameters such as  $T_{AA}$ , in  $p$ +A and A+A events. We summarize the recent progress and some future expectations here.

Note that measurements of boson-tagged jet energy loss are discussed above in Section 3.3.4, and measurements of thermal photons and lower-mass di-lepton probes are instead discussed earlier in Section 3.1.3.

*Direct photons.* Direct photons can probe the broadest kinematic. Because they are massless, they can be used to probe nPDFs at low  $Q^2 \sim (p_T^\gamma)^2$ , whereas the high-mass bosons are restricted to  $Q^2 \gtrsim m_{W/Z}^2$ . However, they come with significant experimental challenges (e.g. in the removal of backgrounds from neutral meson decays) and theoretical challenges (in the proper treatment of isolation criteria and fragmentation photon processes in calculations [1021]). Significant progress has been made as a result of the large luminosity of LHC Run 2 Pb+Pb and  $p$ +Pb data, and from continued improvements in the techniques to measure photons in a heavy-ion environment, including their identification and isolation at low  $p_T$ .

The large luminosity has enabled improved measurements in Pb+Pb collisions, demonstrated by the latest CMS measurement of the direct photon  $R_{AA}$  at mid-rapidity [1022] (left panel Figure 55). At the same time, technical improvements in older data have allowed us to extend the kinematic range where photon measurements can be made, bringing a sensitivity to a new kinematic region in nPDF modifications. The measurement by ATLAS in Run 1 data extends the coverage of direct photons to the forward rapidity region ( $|\eta| = 1.52\text{--}2.37$ ) [1024]. Finally, while the ATLAS and CMS measurements are typically restricted

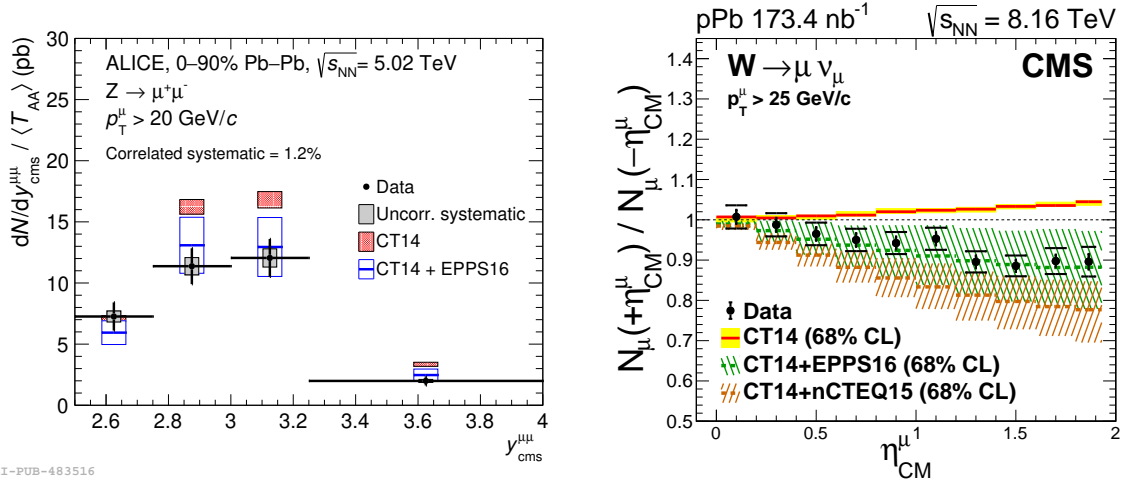


Figure 56: Measurements of heavy electroweak boson production in nuclear collisions: nuclear modification factor for  $Z$  production in Pb+Pb collisions at forward rapidity by ALICE [1028] (left), forward/backward ratio of  $W^{\pm}$  production as a function of muon pseudorapidity in  $p$ +Pb collisions by CMS [1029] (right).

to the range  $p_{\text{T}} \gtrsim 20$  GeV, the final Run 1 measurement by ALICE [282] can extend significantly lower, testing the comparison to pQCD-based expectations in the region  $p_{\text{T}} \gtrsim 5$  GeV. It should be noted, however, that the measurements in ATLAS and CMS are of isolated photons, whereas in ALICE the measurement is inclusive of all direct photons, potentially probing somewhat different physics.

In addition to the measurements above in Pb+Pb, ATLAS has produced the first isolated photon measurement in  $p$ +Pb collisions at the LHC [1023]. Here, the large acceptance is utilized for separate measurements in the forward-, mid-, and backward-rapidity regions, and to construct the ratios between them to cancel common uncertainties (right panel Figure 55). Coupled with the wide  $p_{\text{T}}^{\gamma}$  range, the double-differential measurement results in a broad probe of the shadowing, anti-shadowing, and EMC regions. The ATLAS  $p$ +Pb measurement is the first direct photon measurement to be included in global nPDF extractions [1018].

*Z bosons.*  $Z$  bosons are measured in their di-lepton decay modes to electrons or muons, which are unmodified by their resulting passage through the QGP. Although  $Z$  bosons are the rarest of the electroweak boson probes, these channels have the significant advantage that the  $Z$  yield can be measured with high purity (measurements have achieved QCD backgrounds levels of  $\approx 1\%$  in the  $Z$  mass window) and high precision (since excellent muon or  $e/\gamma$  capability is a key design principle for the EW HEP programs at the LHC).

Measurements of  $Z$  production have been made in the high-luminosity 8.16 TeV  $p$ +Pb data by ATLAS [1025], CMS [1026], and LHCb [1027], and these are key contributors to global nPDF fits. In fact, this channel has even been argued to be sensitive to the modification of the strange and charm content in bound nucleons [1019]. As a new development, the CMS measurement further reports on di-lepton production through the Drell-Yan process ( $q\bar{q} \rightarrow Z/\gamma^* \rightarrow l\bar{l}$ ) over the invariant mass range  $m_{ll} > 15$  GeV. This first measurement demonstrates that the heavy-flavor background for this process at the LHC can be overcome, and thus opens a new potential channel for future study.

In Pb+Pb data, measurements by CMS have demonstrated that the azimuthal anisotropy for  $Z$  bosons is compatible with zero [1030] and those by ATLAS are approaching the precision needed to give input to nPDF fits [1031]. Both experiments have also used the high-luminosity Pb+Pb data to explore the centrality dependence of  $Z$  production, discussed below. Finally, measurements in  $p$ +Pb and Pb+Pb are reported in

the far forward region ( $|\eta^\mu| > 2.5$ ) by ALICE [1028] (left panel of Figure 56). Although they feature significant uncertainties, they are complementary to the ones by ATLAS and CMS above and thus set the only constraints in an extreme kinematic region where nPDF modifications may be large.

*W bosons.*  $W^\pm$  bosons are significantly more abundant than  $Z$  bosons. They are produced dominantly via  $q\bar{q}$  annihilation and are thus particularly useful for setting constraints on the nPDF modification for light quarks. So far, they have been measured in their leptonic decay channel ( $W \rightarrow \nu l$ ), where one can have confidence that the decay products are not affected by the collision system (such as through jet quenching). Given the large resolution on the missing- $E_T$  from the unmeasured neutrino, the results are typically reported as a function of electron or muon kinematics only, resulting in a potentially weaker correlation to the hard-scattering kinematics.

CMS has recently reported a high-statistic measurement in 8.16 TeV  $p$ +Pb collisions [1029], where the data most sensitive to nPDF modification are the forward-backward ratios as a function of muon pseudorapidity (right panel of Figure 56). The data rejects the null hypothesis (i.e. of no nPDF modification) with large significance, and shows a preference for some global fits (such as EPPS16) over others (such as nCTEQ15). ATLAS has measured  $W^\pm$  production in 5.02 TeV [1032] Pb+Pb collisions, with fine selections on event centrality. These results are discussed in the sub-section below. Finally, as with the measurements of  $Z$  bosons above, ALICE has measured  $W^\pm$  boson production in both  $p$ +Pb and Pb+Pb in the forward region ( $|\eta^\mu| > 2.5$ ) [1033], which is kinematically complementary to those by ATLAS and CMS.

*Centrality dependence of EW boson production.* The  $1/T_{AA}$ -scaled yields of EW bosons, or their nuclear modification factor  $R_{AA}$ , in centrality-selected events serve as a good test of the overall centrality determination and geometric modeling of heavy-ion collisions, for which the experiments use the Monte Carlo Glauber model plus an accompanying model of particle production [1034]. Since EW boson yields are not expected to experience significant energy loss effects, deviations from  $T_{AA}$  scaling can therefore diagnose mis-modeling of the collision geometry or the presence of trivial or non-trivial correlations which affect the centrality classification of events with a hard sub-process.

These studies have been particularly motivated by the observation in ALICE that the charged particle  $R_{AA}$  strongly decreases in very peripheral ( $> 80\%$ ) Pb+Pb events [1035]. One potential explanation is a jet veto effect, wherein a low-multiplicity selection suppresses hard process rates, modeled by HG-Pythia [1036]. However, it remains to be seen whether the effect depends on the particular method of estimating  $T_{AA}$  or whether other effects, such as the presence of ultra-peripheral collisions in the peripheral event sample, may contribute.

The  $1/T_{AA}$ -scaled yields for  $Z$  bosons measured by CMS (left panel of Figure 57) systematically drop below unity in more peripheral events, compatible with the HG-Pythia prediction and thus supporting this interpretation. However, the  $R_{AA}$  values for  $Z$  and  $W^\pm$  bosons measured by ATLAS (right panel of Figure 57) systematically rise in more peripheral events. Some suggested explanations of the effect observed by ATLAS include a shadowing of the nucleon–nucleon cross section in heavy-ion collisions [1037] or a larger than expected neutron skin effect [1038]. Future work will be needed to resolve the picture. Nevertheless, if the uncertainties on  $Z$  or  $W$  yields become comparable to those on the traditional extraction of  $T_{AA}$ , one option for future measurements may be to use these yields as the *de facto* control on the event geometry.

Additionally, such centrality-dependent studies should be repeated in asymmetric systems such as  $p$ +Pb collisions. In these small systems, the association between experimentally-selected centrality and underlying geometry is more difficult [1039, 1040], and color fluctuation effects [1041, 1042] or additional QCD effects [1043, 1044] may contribute in novel ways to the correlation between hard process kinematics and the centrality signal. For example, a measurement of the centrality dependence of  $Z$  production in 5.02 TeV  $p$ +Pb collisions by ATLAS [1025] revealed a significant sensitivity to choices in the modeling

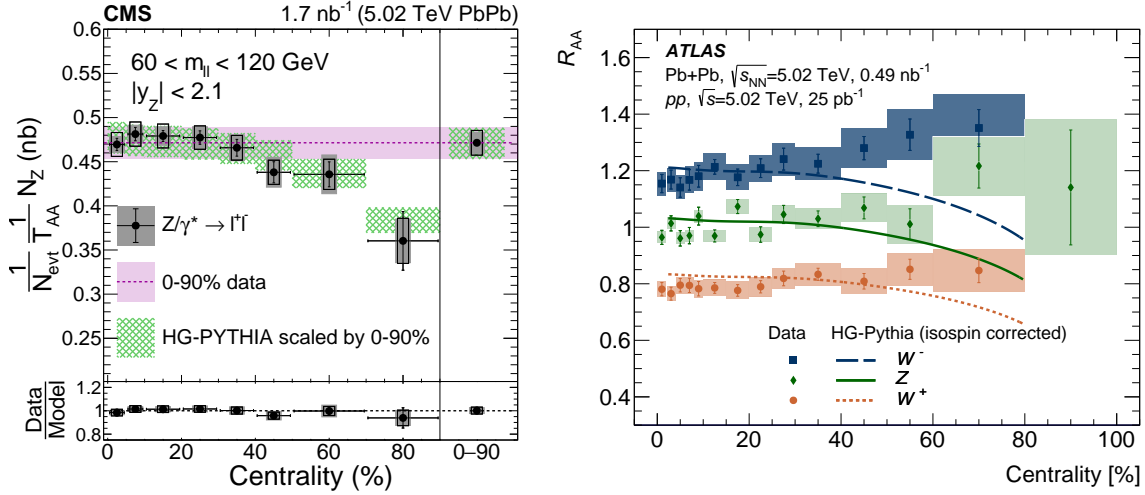


Figure 57: Centrality dependence of  $Z$  production from CMS (left) and  $Z$ ,  $W^+$ ,  $W^-$  production from ATLAS (right) in Pb+Pb collisions, both compared to the expectation from the HG-Pythia model [1036].

of the nucleon–nucleon interaction [1045, 1046], such as whether to allow “Glauber-Gribov” cross section fluctuations.

*Top quarks.* An intriguing development since the last Long Range Plan is the first measurements of  $t\bar{t}$  production in heavy-ion collisions at the LHC. In  $p$ +Pb collisions [1047],  $t\bar{t}$  production was observed by CMS by requiring an isolated lepton plus at least four jets, with a varying requirement on the number of observed  $b$ -jets to delineate background- and signal-dominated regions. While statistically limited,  $t\bar{t}$  production rates potentially offer an alternative way to probe the nuclear modifications on large- $x$  gluons, since they are dominantly formed through gluon–gluon fusion.

CMS has also found evidence of  $t\bar{t}$  production in Pb+Pb collisions [981]. In the Pb+Pb system,  $t\bar{t}$  detection is made more complicated by the quenching of the high-energy  $b$  and lighter quarks at the end of the top quark decay chain. This raises the possibility, therefore, of using  $t\bar{t}$  events to probe the parton-QGP interaction, rather than the initial state. Indeed, the delayed decays of top quarks have been proposed as a novel way to understand the time dependence of jet quenching [1048] with future data.

### 3.4.6 Ultra-peripheral Collisions

Disentangling initial-state and final-state effects in heavy-ion collisions is important for properly quantifying the properties of the QGP. One promising tool to reveal the intrinsic property of heavy nuclei at their initial state is through photon-induced interactions, commonly known as the *ultra-peripheral collision* (UPC). Typically, the UPC takes place when the impact parameter between the two colliding nuclei is greater than the sum of their radii. The interaction is initiated by one or multiple photons emitted from the fast-moving charged ions, and only photons interact with the other nucleus. For a review of UPC, see Refs. [1049–1053] and references therein. The physics prospects of UPC studies in Run 3&4 with the CERN LHC experiments have been recently reported in [1054–1056].

There are generally three types of UPC physics process: i) inclusive production; ii) semi-inclusive and/or jet production; iii) exclusive production. In the past decade, most of the UPC measurements focused on exclusive production, dominated by diffractive vector meson production. However, since the last Long Range Plan, there are increasing number of studies in both theory and experiment on jet photoproduction and inclusive particle photoproduction. As of now, it is widely realized that UPCs can be extremely illuminating

to understand the initial-state condition of heavy-ion collisions.

### 3.4.6.1 Vector meson photoproduction

**Vector meson in heavy nuclei** A general picture of vector meson (VM) photoproduction is the following. The quasi-real photon emitted by a nucleus fluctuates into a quark-antiquark pair, known as the color dipole, which forms a vector meson and scatters off the target nucleus. The interaction between the dipole and target is via a two-gluon exchange, leaving the event topology with a large rapidity gap between the VM and the target. In a leading order QCD calculation, the cross section of this interaction is expected to scale as the square of the gluon density,  $[xG(x, Q^2)]^2$ , which makes it an ideal probe to the nuclear Parton Distribution Function (nPDF). Note that in a recent study done at Next-to-Leading Order [1057], this expectation was found to be sensitive to quark distribution, which is one of the major theoretical achievements since the last long-range plan.

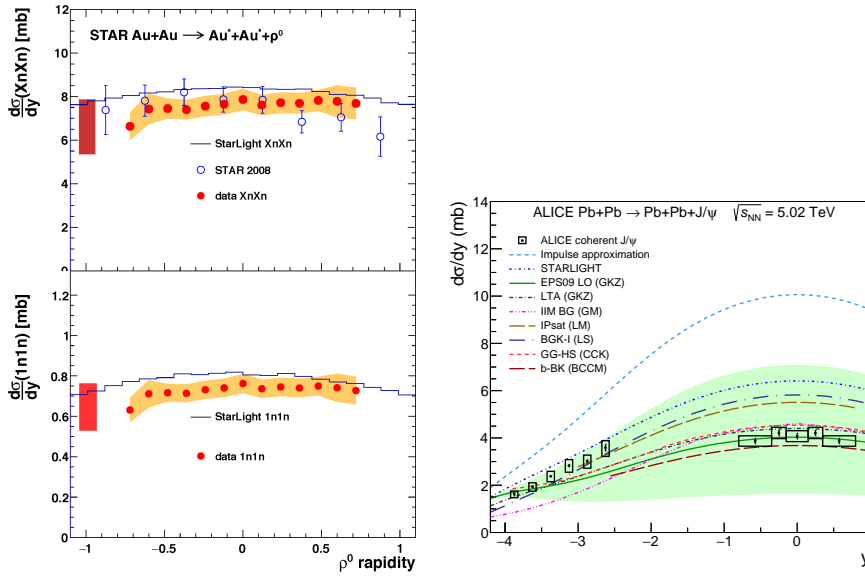


Figure 58: Left: coherent  $\rho^0$  photoproduction,  $d\sigma/dy$  as a function of  $y$ , in Au+Au UPC at  $\sqrt{s_{NN}} = 200$  GeV at RHIC using the STAR detector [1058]. The notation “1n” and “Xn” are neutron emission class measured by the ZDC, where “1n” denotes one neutron and “Xn” represents more than one neutron. Right: the same measurement based on  $J/\psi$  particle done by the LHC ALICE experiment at both central and forward rapidity in Pb+Pb UPCs at  $\sqrt{s_{NN}} = 5.02$  TeV [1059].

In the past decade, especially since the last NP long-range plan, one of the most important studies for initial-state condition of heavy-ion collisions is the coherent  $\rho^0$  and  $J/\psi$  photoproduction at RHIC and the LHC, respectively. In Figure 58, the differential cross section  $d\sigma/dy$  as a function of  $y$  for  $\rho^0$  (left) and  $J/\psi$  (right) photoproduction measured by STAR (RHIC) and ALICE (LHC) are shown, respectively. Similar measurements of coherent  $J/\psi$  photoproduction at the LHC have been made by LHCb [1060, 1061] and CMS [1062] as well. Theoretical and Monte Carlo models are compared with both data. It is unambiguously found by all LHC experiments that the coherent  $J/\psi$  photoproduction cross section in heavy nuclei is significantly suppressed compared to that of a free nucleon, shown by the difference with respect to the Impulse Approximation. Figure 58 right shows a large number of theoretical models compared with the data; these models can be categorized into two major physics models - i) nuclear shadowing model and ii) gluon saturation model.

For i), the shadowing model is based on nuclear PDFs which, by construction, capture some of the



nuclear modification present in lepton scattering data, as well as a dynamical modeling of shadowing through Leading Twist Approximation, which is based on Gribov-Glauber theory, QCD factorization, and HERA diffractive PDFs. One key feature of this model is that it does not have any suppression in a free nucleon. On the other hand for ii), gluon saturation models handle this problem differently, such that by a first principle argument of unitarity, gluon density cannot be infinity [1063]. As the energy of the initial state nucleon and nucleus increases in heavy-ion collisions, the growth of gluon density would slow down and naturally, it is expected to be suppressed with respect to a free nucleon. This should be present in both nucleon and nuclei, except that it is easier to observe this non-linear dynamics in heavy nuclei at the same given  $x$ , quantitatively determined by the saturation scale  $Q_s$  [1063]. Understanding the commonalities and differences has become one of the most important and urgent questions in order to narrow down what is responsible for such a large nuclear suppression seen in the data. The answer to this question has a direct impact to our understanding of the initial-state conditions of heavy-ion collisions.

Furthermore, differential cross section measurements of  $p_T^2$  in UPC VM photoproduction have been another major milestone since the last long-range plan, due to the higher statistic sample became available at both RHIC and the LHC. For coherent VM photoproduction, since the virtuality of the photon is small, the momentum transfer  $-t$  can be approximated by the  $p_T^2$  of the VM, which is a Fourier transform of the source in the coordinate space, e.g., gluons. Therefore, with the momentum transfer  $-t$  measured in UPCs, we have gained more access to the initial-state condition of heavy-ion collisions in an impact parameter dependent way. The momentum transfer  $-t$  distribution of  $\rho^0$  and  $J/\psi$  particle in coherent photoproduction have been measured at RHIC [1058] and at the LHC [1064], respectively. At RHIC, despite issues related to  $\rho^0$ , e.g., its soft mass scale and the overwhelming incoherent background, the measurement has been a major step forward by showing a proof-of-principle study. The data has been Fourier transformed from momentum space to the impact parameter space of partons. The first indication of diffractive structures, e.g., those in Ref. [1063] predicted at the EIC, has been observed. Similar measurement has been done at the LHC [1064] but with much limited  $-t$  range, due to similar challenges as seen at RHIC.

For other VM photoproduction in heavy nuclei, there are measurements of  $\psi(2S)$ , where the ratio to  $J/\psi$  has been studied. No significant deviation from that of a free proton has been observed [1059]. There is no measurement yet using  $\phi$  or  $\Upsilon$  in nucleus-nucleus UPC. The experimental challenge for  $\phi$  is the soft kaon daughters from  $\phi$  decay, which is below  $\sim 100$  MeV. For  $\Upsilon$ , the cross section is much smaller and more data is needed. However, UPC  $\Upsilon$  in p+Pb collisions has been measured for the first time by the CMS experiment [1065].

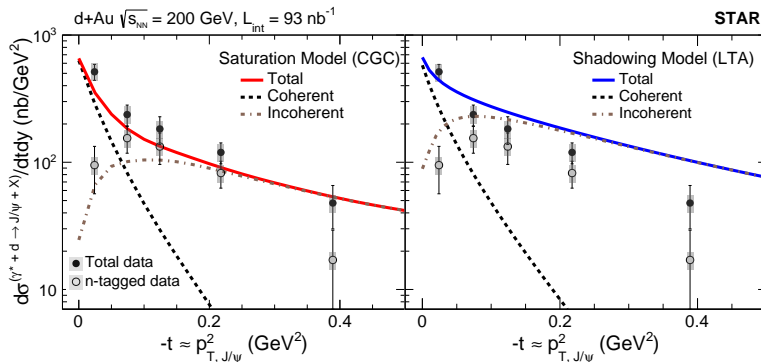


Figure 59: Differential cross section,  $d\sigma/dtdy$ , as a function of  $-t$  of  $J/\psi$  photoproduction in  $\gamma^*+d$  collisions. Color Glass Condensate and nuclear shadowing model Leading Twist Approximation are compared with data [1066].

**Vector meson in proton and light ions** UPC  $J/\psi$  in p+Pb collisions have been measured by the ALICE experiment at 5.02 TeV, where the lead nucleus is the photon emitter and the proton is the target [1067, 1068]. The measurements in UPC have been a complementary study to those at H1 and ZEUS experiments at e+p collider HERA, which covers a wider photon-proton center-of-mass energy  $W$  range. The quantitative energy dependence of the  $J/\psi$  photoproduction in proton, measured by these studies, have been an important input to study the gluon saturation phenomena.

Besides the energy dependence, another important lesson learned from  $J/\psi$  photoproduction in proton is the initial-state fluctuation of hot-spots [80], which has significantly impacted the understanding of small system collective dynamics in heavy-ion collisions. Although the initial study [80] was performed based on HERA data, recent measurement on d+Au UPC  $J/\psi$  photoproduction has further confirmed this phenomenon at RHIC energies. In Figure 59, differential cross sections  $d\sigma/dtdy$  of  $J/\psi$  photoproduction in d+Au UPC at center-of-mass energy  $\sqrt{s_{NN}} = 200$  GeV are shown. Two theoretical models, CGC and LTA discussed previously, are compared with data. The CGC calculation is found to describe the STAR data of incoherent production better, and sub-nucleonic fluctuation plays an important role in their model. In addition, authors of the nuclear shadowing model have found that the mismatch of this d+Au UPC data could be caused by the overestimation of proton dissociation at RHIC energy [1069]. Nevertheless, photoproduction of  $J/\psi$  in the simplest nuclear system, deuteron, has provided important insights to disentangle models and the first snapshot of gluon momentum (Fourier transform of the spatial coordinate) distributions inside the deuteron. This study has a close connection to those proposed at the EIC with spectator tagging technique [1070, 1071].

**Vector meson in hadronic medium** Conventionally, vector meson production from coherent photon induced processes is only visible and studied in UPCs, in which the two colliding nuclei stay intact to meet the coherent requirement. However, recent measurements of  $J/\psi$  photoproduction were observed in hadronic heavy-ion collisions at both RHIC [1072] and the LHC [1073]. To investigate the potential production mechanism behind the anomaly enhancements, STAR made differential measurements of the observed excesses compared to the p+p reference for  $J/\psi$  [1072]. The left panel of Figure 60 shows the excesses of  $J/\psi$  as a function of the number of participants ( $N_{\text{part}}$ ) for Au+Au collisions at  $\sqrt{s_{NN}} = 200$  GeV and U+U collisions at  $\sqrt{s_{NN}} = 193$  GeV. The observed excesses reveal no significant centrality dependence, which is beyond the expectation of hadronic production. The differential negative momentum transfer squared ( $-t$ ) distribution is shown in the right panel of Figure 60, which reveals the distribution of interaction positions for the production process. The slope of the  $-t$  distribution is similar to that observed in UPC  $J/\psi$  photoproduction [1058]. Furthermore, the first data point ( $-t < 0.001$  (GeV/c)<sup>2</sup>) is significantly lower than the extrapolation of the exponential fit, which is consistent with the destructive interference for coherent photoproduction in heavy-ion UPCs. These observations suggest that the anomaly excesses in peripheral heavy-ion collisions possess characteristics of diffractive production, and indicate the existence of the coherent photon-nucleus production mechanism in hadronic nuclear collisions.

Klusek-Gawenda and Szczurk first considered this question theoretically, and built up a phenomenological model of coherent photoproduction [1075] in heavy-ion collisions with nuclear overlap, which can reasonably describe the excesses observed at ALICE. In their model, the production processes are assumed to be exactly the same as those in UPC except for a modification to the photon flux to ignore the overlapping region. However, in this approach, the modification of photon flux is not unambiguous and it avoids the question of how the coherent requirement is satisfied in collisions with nuclear overlap. In Refs. [1074, 1076, 1077], they argue that although the whole nucleus cannot keep the coherent requirement, the spectator nucleons, free from hadronic interactions, could still act coherently for photoproduction, which should be attributed to the much longer lifetime of the spectator fragment compared to that of photoproduction processes. Therefore, the authors considered that the coherent processes occur either coupling to the

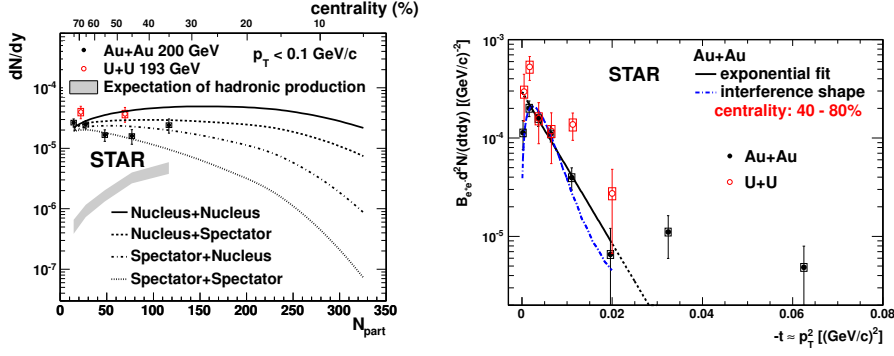


Figure 60: (left) STAR measurements of excess yields of  $J/\psi$  as a function of number of participants ( $N_{\text{part}}$ ) for Au+Au collisions at  $\sqrt{s_{\text{NN}}} = 200$  GeV and U+U collisions at  $\sqrt{s_{\text{NN}}} = 193$  GeV [1072]. (right) STAR measurements of excess yields of  $J/\psi$  as a function of the negative momentum transfer squared ( $-t$ ) for Au+Au collisions at  $\sqrt{s_{\text{NN}}} = 200$  GeV and U+U collisions at  $\sqrt{s_{\text{NN}}} = 193$  GeV [1072]. The data are shown together with theoretical predictions for coherent  $J/\psi$  photoproduction in a hadronic medium [1074].

whole nucleus or only the spectators, which results in four configurations. As revealed in Figure 60, the predictions from [1074] can describe the STAR measurements reasonably well, and the data seem to favor the spectator coupling scenario. The coherent produced  $J/\psi$ s are formed in the initial stage of the collisions, and therefore interact with the latter formed QGP from the nuclear overlapping region, which makes it a potentially powerful tool to probe QGP. The  $J/\psi$ s from coherent photoproduction are concentrated at very low transverse momentum, in which the regeneration contribution should be negligible. With sufficient statistics, this makes the coherent produced  $J/\psi$ s a clear probe for the study of color screening effect in QGP.

Currently, there are also limitations that prevent us from utilizing the additional produced  $J/\psi$ s to infer QGP properties. The first is that, due to the rare production rate, the experimental measurements lack precision at semi-central and central collisions. Recently, there have been new preliminary measurements from ALICE [1078] and STAR [1079] collaborations with improved precision; however, they are not sufficient. The second is that the baseline to determine the modification factor can only be obtained from theoretical predictions, which are model dependent and cannot be directly extracted from the  $\gamma+p$  measurements.

### 3.4.6.2 New directions in UPCs

**Electron and muon pair production** The production of lepton pairs in ultraperipheral collisions ( $\gamma\gamma \rightarrow l^+l^-$ , sometimes called the Breit-Wheeler process) serves to calibrate theoretical calculations of the nuclear photon fluxes, and also provide a clean environment to study their impact parameter dependence, which comes into play in a variety of processes. Measurements of exclusive lepton pair cross sections at the LHC in both muon [1080] and electron [1080] have shown good agreements with theory calculations and contribute to ongoing discussions of the role of higher-order Coulomb processes. In 2018, measurements of electromagnetic production of lepton pairs in hadronic heavy-ion collisions by the STAR [1081] and ATLAS [1082] collaborations showed transverse momentum broadening inconsistent with traditional “equivalent photon approximation” (EPA) predictions, although consistent in terms of total cross section. Both initial-state and final-state [1083, 1084] effects were investigated. Measurements by the STAR [1085] and CMS [1086] collaborations indicated significant broadening of the lepton pair momentum results from the initial photon flux, supporting the initial-state effect hypothesis, although not ruling out potential medium

interactions proposed previously by the STAR and ATLAS collaborations.

Theoretical progress from lowest order QED calculations indicates that the kinematic distribution of the initial photon flux contains strong impact parameter dependence [1087, 1088]. The transverse momentum distribution of these calculations matches well with measurements ultra-peripheral and peripheral collisions, while the traditional EPA calculations (STARLight) show tension in the form of a narrower distribution. Recent ATLAS results [1089] of transverse momentum and acoplanarity  $\alpha$  ( $\pi\alpha \simeq P_{\perp}/M_{ll}$ ) in central Pb+Pb collisions show that the full QED calculation can describe the depletion at  $\alpha \simeq 0$  better than the photon Wigner function [1084]. This difference may be caused by the breakdown of the real-photon approximation in the photon Wigner function at the extreme phase space, when both photon  $k_{\perp}$  ( $\lesssim 4$  MeV) approach zero and the conserved transition current could not be approximated as two real-photon vertex function [1088, 1090].

In addition, ultra-relativistic nuclei produce a highly Lorentz contracted radial electric field emanating from the nucleus, with a magnetic field circling the nucleus. Both the electric and magnetic field are almost entirely Lorentz-contracted into the plane perpendicular to the direction of motion. Therefore, at any given point, the fields appear as a nearly transverse linearly polarized electromagnetic wave. The significant azimuthal dependence of Breit-Wheeler process in ultra-peripheral and peripheral collisions [1085] are in good agreement with both SuperChic3 predictions, and with the lowest-order QED [1091], which predict a  $\cos 4\phi$  modulation of approximately  $-17\%$  (for the kinematic ranges applicable for  $e^+e^-$  measurements in ultra-peripheral collisions in STAR).

**Tau  $g - 2$**  The Breit-Wheeler process is able to produce pairs of tau leptons ( $\gamma\gamma \rightarrow \tau^+\tau^-$ ), providing a unique opportunity to measure the anomalous magnetic moment of the tau lepton:  $a_{\tau} = (g_{\tau} - 2)/2$  [1092]. Due to the larger mass of the tau, measurement of the anomalous magnetic moment provides stringent tests of fundamental predictions from QED and potentially probes physics beyond the standard model [1093, 1094]. In several channels, radiative corrections to  $a_{\tau}$  scale as  $m_{\tau}^2/m_{\mu}^2$  which is  $\sim 280$  times larger than for the muon, perhaps making these modifications observable in changes to the measured cross sections. This approach to  $a_{\tau}$  provides multiple benefits: the  $Z^2$  enhancement of the coherent photon field leads to large cross sections, the produced events are quite clean, and allow the distinct topology of tau decays to be identified, and the unique event characteristics allow efficient triggering and selection. In several recent papers [1095, 1096], ATLAS and CMS have measured  $\tau$  decays (in one channel in CMS, and in three in ATLAS), and the results for  $a_{\tau}$  have already reached the precision of previous constraints from  $e^+e^-$  experiments [1097].

**Light-by-Light (LbyL)** The elastic scattering of photons off of themselves is well known to be forbidden in classical electrodynamics, but it has long been predicted to occur via quantum processes – primarily box diagrams involving charged fermions and bosons, but also BSM particles that couple to photons. However, direct observation of this process was only made in LHC Run 2 (2016-2018) by the large LHC experiments [1098–1100]. Measurements benefit from the widest possible rapidity acceptance and the lowest  $p_T$  selection for the final state photons. The limited virtuality and transverse momentum of the initial state photons provides a strong handle against the primary backgrounds, misidentified electron-positron pairs, and central exclusive production of photons via gluon-initiated processes. This clean signal has been used for systematic searches for new physics. The most notable results have been for axion-like particles (ALPs) [1100]; the latest ATLAS data provide the most stringent limits to date [1101], far exceeding those set by electron-positron machines, and even the LHC p+p program, in the range  $5 < m_a < 100$  GeV.

**Quantum interference and the neutron skin** Vector meson photoproduction is of interest in quantum information systems. Photoproduction acts like a two-source interferometer, with production possible on

either of the nuclei. Near mid-rapidity and at low  $p_T$ , these two possibilities are indistinguishable, and so interfere with each other [1102]. The two processes are related by a parity transformation; vector mesons have negative parity, so the interference is destructive. Because the two production positions are well separated in space, with a typical median impact parameter of 20 to 40 fermi or more, depending on the beam energies and species and any requirements on the presence of neutrons from nuclear excitation [1103], the system is very close to a two-source interferometer. Since the typical lifetime of the  $\rho$  meson is less than the time required for particles to travel this distance, any interference must involve the products of the vector meson decay, so this is an example of the Einstein-Podolsky-Rosen paradox [1104]. The STAR Collaboration confirmed this interference in 2009 [1105]. Double vector meson production is also possible [1106, 1107]; this allows for even more complex quantum correlations [1108]. These studies require significantly improved luminosity and trigger efficiency than in current experiments, but are attractive possibilities for LHC Runs 3 and beyond.

**Dijets and open charm** Looking ahead, exploring new probes of gluons will be important to reduce the systematic uncertainties in transforming vector meson cross sections into parton distributions [1054, 1109]. This is especially important since recent NLO calculations of vector mesons have a surprisingly large contribution from quark PDFs, and also an unexpectedly large scale uncertainty [1110]. Photoproduction of dijets or open heavy quarks proceed via single gluon exchange, so should be less subject to these theoretical uncertainties. In addition, the  $Q^2$  is set by the pair or dijet invariant mass, so it is possible to probe parton distributions over a wide range of  $Q^2$  with a single process. Specifically, the system of jets reflects the initial scattering kinematics: the transverse momentum sum ( $H_T$ ) correlates with  $Q$ , the multijet mass and rapidity can be combined to determine the fractional photon energy  $z_\gamma$  and the nuclear Bjorken  $x_A$ , the fractions of the per-nucleon beam momentum carried by the photon and nuclear parton. Using these variables, ATLAS has measured (in a preliminary form [1111]) fully corrected cross sections which directly measure the nuclear parton structure (nPDFs) — providing access to some of the important early physics of the EIC. These events are triggered and selected using a one-sided topology of forward neutron production observed in the ATLAS ZDCs. They compared this with a Pythia + STARlight simulation. In the future, it should be possible to extend both the Bjorken- $x$  and  $Q^2$  range significantly by looking at softer jets (for lower  $x$  and  $Q^2$ ) and with more data (to get to higher  $Q^2$ ). Going further, it may be possible to use dijet events to directly measure the Wigner distribution [1112]. This takes advantage of the fact that there are two momentum scales in the problem - the  $p_T$  of the individual jets, and the  $p_T$  of the dijet system.

Dijet events have also been observed by ATLAS in events with no activity in either ZDC (0n0n), and the distributions have been found to resemble expectations from diffractive dijet (photon-pomeron) production [1113]. Diffractive dijet production is sensitive to the gluon distributions in the nuclei, as well as their polarization, which is expected to lead to distinctive angular decorrelation effects [1114, 1115]. CMS has studied this effect [1116] in events with two jets accompanied by rapidity gaps in both directions, defined by charged particles, as well as energy vetos in the forward calorimeters. By a measurement of the angle separating the dijet vector momentum sum ( $Q_T$ ) and different ( $P_T$ ), they calculate the mean  $\langle \cos(2\phi) \rangle$  which is sensitive to dijet decorrelation effects for jet  $p_T > 30$  GeV,  $Q_T < 25$  GeV, and dijet  $P_T > Q_T$ . The data are found to be drastically lower than expectations from RAPGAP [1117], which describes HERA data without gluon polarization. Its magnitude at lower  $Q_T$  is reproduced by models [1118] which assume the decorrelation induced by soft radiation, but the same model does not rise with  $Q_T$  as rapidly as the CMS data. This measurement is complementary to the STAR dilepton studies in probing polarization effects of gluons, as well as photons [1085, 1119].

During LHC Run 4 and beyond, photoproduction of dijets may also be studied in the ALICE FoCal [1120], allowing for measurements of parton distributions of protons and nuclei down to very low  $x$  values.

Using a similar approach as jets, it is possible to get to still lower  $x$  and  $Q^2 \gtrsim 2$  GeV<sup>2</sup> by studying

open charm, and maybe heavier quark hadrons. The cross sections for charm are large [1121], so statistics should be ample for reconstructing a number of different mesons and even meson pairs (the meson from both the  $c$  and the  $\bar{c}$ ). Bottom hadrons are also accessible, and even top production may be within reach [1122–1124]. The latter do not hadronize before they decay, so would require different methods to study. There is also information to be had in pairs with large rapidity gaps between them [1125].

**Collectivity in inclusive photonuclear events** High-energy photoproduction processes can be studied using UPCs in nuclear collisions and at the EIC. The specific interest is on the inclusive  $\gamma+A$  processes, but unlike at the EIC, the photons involved in UPCs are quasi-real. The first measurements in this direction was initiated by measuring harmonic anisotropy  $v_n(p+Pb)$  and  $v_n(\gamma+Pb)$  at the LHC by the ATLAS collaboration [446]. Once the non-flow (correlations due to conservation effects) are removed, a signature of long-range correlations is observed in  $\gamma+Pb$  processes. The trend of the ATLAS data has been explained by CGC calculations [446, 482]. For UPCs at top RHIC energies one expects the maximum energy of the quasi-real photon to be approximately  $E_\gamma \approx 3$  GeV. The typical range of the center-of-mass energy of the photon-nucleon system will therefore be  $W_{\gamma N} \approx 40$  GeV. Therefore, Au+Au collisions at  $\sqrt{s_{NN}} = 200$  GeV will provide access to the  $\gamma+Au$  process at 40 GeV center-of-mass energy. The specific interest is high-activity inclusive  $\gamma+Au$  process to search for collectivity. If collectivity is observed in  $\gamma+Au$  processes, it can provide a way to explore the creation of a many-body system exhibiting fluid behavior in photon-induced processes [483]. A recent calculation in Ref [483] assume  $\gamma + A$  processes are equivalent to collisions of vector mesons with ions ( $\rho+A$  collisions) and describe first measurements of harmonic coefficients  $v_n$  in photonuclear processes measured by the ATLAS collaboration [446]. The hypothesis of the  $\gamma + A$  process as a  $\rho + A$  collision and the formation of a fluid-dynamic medium can be tested at RHIC in a data-driven way. This can be done by comparing measurements in  $\gamma+Au$  processes at  $W_{\gamma N} \approx 40$  GeV and in  $d+Au$  collisions at  $\sqrt{s_{NN}} = 39$  GeV.

**Search for baryon junctions in photonuclear events** Photonuclear processes can also be used to study the origin of baryon stopping and baryon structure in general. One proposed mechanism to explain baryon stopping is the baryon junction: a nonperturbative Y-shaped configuration gluons which is attached to all three valence quarks. The baryon stopping at RHIC energy range is ideal for such a study. Preliminary data with Au+Au collisions at  $\sqrt{s_{NN}} = 54.4$  GeV shows strong baryon stopping in enriched  $\gamma+Au$  events with a strong dependence on rapidity. This important observation provides the necessary impetus for further exploration using various available data sets. In particular, it would be most interesting to test if this strong rapidity dependence of the  $\bar{p}/p$  yield is consistent with the picture of baryon junction that predicts an exponential dependence of stopping with rapidity of form  $\exp(-\alpha(y - Y_{beam}))$  with  $\alpha \approx 0.5$ . Extending these measurements with high statistics  $\gamma+Au$ -rich event samples, using Run 2023 and 2025 data on Au+Au collisions at  $\sqrt{s_{NN}} = 200$  GeV, will enable differential measurements of di-hadron correlations with different combinations of triggers and associated transverse momenta. These measurements will help search for collectivity, in addition to test the baryon-junction conjecture. Similar measurements can be done at the LHC although the net-proton yield and  $(1 - \bar{p}/p)$  are significantly smaller than at lower energies.

### 3.5 Interdisciplinary

The complex nature of studying quark-gluon plasma in heavy-ion collisions naturally lends itself to connections to other fields, either through a common set of tools or a mutual interest in related physics.

Connections include applications of holography in a number of different contexts, the study of cosmic rays [1126], exploration of applications of quantum computing to hot QCD [1127–1130], as well as the study of antimatter [1131–1133].

Other prominent interdisciplinary topics related to studies of hot QCD are highlighted below.

#### *Nuclear structure*

Connections with low-energy nuclear structure have been highlighted in Section 3.1.4, in particular the ability to probe nuclear deformation parameters [18]. Other connections with nuclear structure include attempts to constrain the neutron skin of heavy nuclei through diffractive photoproduction in ultraperipheral collisions [1058, 1134], a result that would be of high interest for the nuclear astrophysics community.

#### *Quantum electrodynamics and physics beyond the standard model*

Ultraperipheral collisions have been used to study quantum electrodynamic processes, including light-by-light scattering and the anomalous magnetic moment ( $a = (g - 2)/2$ ) of the tau lepton, both of which have potential to search for physics beyond the standard model (see Section 3.4.6).

#### *Phase diagram and relativistic fluid dynamics in astrophysics*

Significant overlap exists with the astrophysics community. The nuclear equation of state at large baryon chemical potential and the presence of a critical point and a first-order phase transition plays a large role in the study of neutron stars [1135]. A wide range of astrophysical observables could provide insights in the equation of state at finite  $\mu_B$ , including supernova explosions showing a second burst of neutrinos [225–230], neutron-star mergers showing different ejecta [1136–1138], waveforms [231, 232] or peak frequencies [233] in postmerger gravitational wave signal, neutron-star cooling [1139–1142], glitches in their spin evolution [1143, 1144], gravitational wave emissions from individual stars [1145–1149], and twin stars, two stars which possess approximately the same masses but with one being much more compact than the other, signaling a strong phase transition in their interior [1150–1155]. The multimessenger study of neutron star mergers with electromagnetic and gravitational waves further provides a connection with both hot and dense nuclear matter and with relativistic hydrodynamics [9, 1156]. Applications of relativistic hydrodynamics in both astrophysical and collider experiments have led to a surge of interest in the mathematical and physical foundations of the theory.

#### *Machine learning*

The computationally demanding simulations of hot QCD physics, combined with the enormous experimental data sets involved, have provided a fertile ground for applications of machine learning techniques. An area of particular interest has been quantification of uncertainties [3] to help constrain systematically the properties of strongly-interacting quark-gluon plasma. Machine learning applications have also been used widely to accelerate model-to-date comparisons and in analysing experimental signatures from large data sets [1157], for example.

## 4 Hot QCD facilities

There are two facilities in the world capable of creating the quark-gluon plasma in ultra-relativistic heavy-ion collisions, the Relativistic Heavy Ion Collider (RHIC) at Brookhaven National Laboratory (BNL) in New York and the Large Hadron Collider (LHC) at CERN in Switzerland. The impressive versatility and advances in the performance of these accelerators have enabled a wealth of experimental measurements and insights to the QGP since the last Long Range Plan which are discussed in Section 3. This section will focus on the facilities and detector upgrades that have enabled these scientific accomplishments to be realized. In particular, RHIC successfully completed the Beam Energy Scan II and built sPHENIX as recommended in last Long Range Plan, while the LHC experiments collected data in Run 2 and were upgraded in preparation for Run 3. Improvements to data acquisition capabilities at the experiments are essential for utilizing the unprecedented luminosities achieved at RHIC and LHC to achieve the most precise measurements which are capable of constraining the theoretical models. Progress on experimental measurements continues into this next decade as the new sPHENIX experiment together with the upgraded STAR experiment usher in a new era of RHIC measurements and with the start of Run-3 at the LHC.

### 4.1 RHIC

Since the previous Long Range Plan, RHIC has exceeded expectations delivering the luminosity needed for the crucial BES-II, as well as enabled a detailed study of the CME from collisions of isobars. Several upgrades to STAR will maximize the measurements achieved from these collisions. Meanwhile PHENIX completed data taking in 2016 in preparation for construction of sPHENIX, which is now the cusp of taking data. This section highlights these accomplishments and plans for future RHIC running.

**Isobars at RHIC** The 2018 RHIC run included isobar collisions of  $^{96}_{44}\text{Ru} + ^{96}_{44}\text{Ru}$  and  $^{96}_{40}\text{Zr} + ^{96}_{40}\text{Zr}$  to search for the chiral magnetic effect. The run should provide enough data to measure a significantly observable difference in the two collision species. To reduce the systematic uncertainties that arise from variations in run conditions a special run strategy was implemented which required synergy between the STAR collaboration and the RHIC Collider Accelerator Department. This strategy included alternating the isobar species between each beam store and maintaining a constant luminosity during a store and across isobar species. This program was successfully executed at RHIC and the necessary level of precision was achieved [357]. STAR also developed and executed a rigorous blind analysis method [390] when extracting these important results.

#### **Beam Energy Scan II**

In order to reach the desired luminosity, RHIC implemented an electron cooling upgrade, Low Energy RHIC electron Cooling (LEReC). The LEReC was successfully commissioned and brought into operation during the BES-II RHIC Runs in 2019–2021. To achieve energies below 7.7 GeV, a fixed-target program was engineered where a Au target was inserted in the STAR beam pipe [1158]. To maximize the physics output, the STAR detector at RHIC added several key subsystem upgrades: the inner TPC (iTPC) [1159], the Event Plane Detector (EPD) [1160] and the endcap Time-of-Flight (eTOF) [1161] Detector. These additions significantly improved the STAR detector tracking and particle identification capabilities, especially at large pseudo-rapidity and low transverse momentum regions. All of these upgrades were completed efficiently, and positively impacted the BES-II data.

**STAR upgrades at forward rapidity** Following the BES-II, STAR was equipped with the forward tracking system (FTS) and forward calorimetry system (FCS) enable measurements of neutral pions, photons, electrons, jets, and hadrons in the detectors that extend tracking and calorimeter coverage to  $2.5 < \eta < 4.0$  [1162]. The FTS consists of silicon mini-strip sensors as well as small-strip thin gap chambers (sTGCs). The FCS includes an electromagnetic calorimeter, which uses refurbished PHENIX lead-scintillator with SiPM-based readout electronics, as well as a hadronic calorimeter. In 2022, RHIC



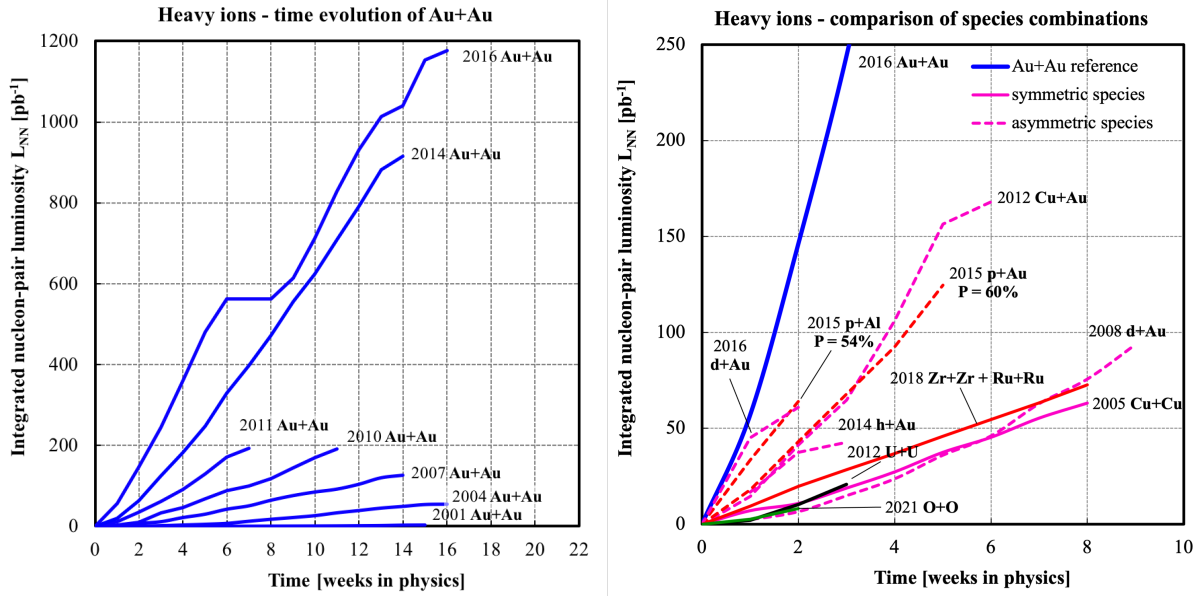


Figure 61: Left panel: The integrated luminosity for all RHIC Au+Au Collisions. Right panel: The integrated luminosity comparing all heavy-ion collision species at RHIC. Symmetric collisions are denoted with a solid line while asymmetric collision systems are denoted with a dashed line.

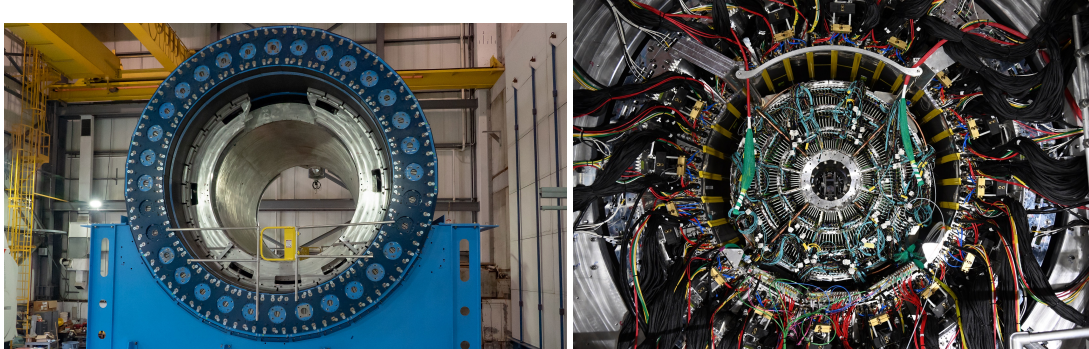


Figure 62: The sPHENIX outer hadronic calorimeter surrounding the solenoid magnet (left) and a close up image of the detectors inside of magnet prior to inserting the innermost detectors, INTT and MVTX (right).

collided polarized protons at 500 GeV. These upgrades and data are of particular interest to the cold QCD community and are useful in preparation of the future electron ion collider (EIC). However, starting with the 200 GeV Au+Au collisions in 2023, STAR will also utilize this extended rapidity range to address hot QCD topics such as measurements of long-range correlations to study early-time dynamics of heavy-ion collisions.

### sPHENIX

In the period since the last Long Range Plan, which recommended a "state-of-the-art jet detector at RHIC," the sPHENIX collaboration was formed and built the proposed experiment, which will start data taking in 2023. Photographs of the sPHENIX during assembly are shown in Fig. 62. sPHENIX, the first new heavy-ion experiment at RHIC since the start of RHIC collisions 23 years ago, is designed specifically to measure fully reconstructed jets and upsilons in the quark-gluon plasma [1163]. Such measurements required good hadronic and electromagnetic calorimeters as well as precise tracking. The tracking detectors,

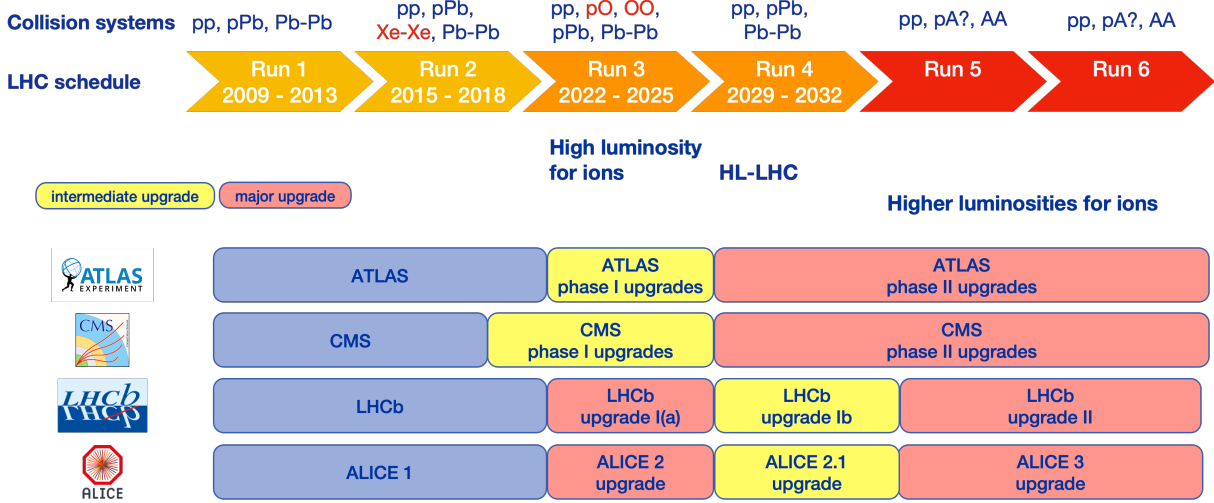


Figure 63: Overview of upgrades for LHC experiments from 2022 and onward.

a Time Projection Chamber (TPC), a silicon tracker (INTT), a silicon pixel vertex detector (MVTX), and a Micromegas-based tracker (TPOT) enable detailed jet substructure measurements, as well as heavy flavor tagging. These detectors and a high rate streaming DAQ will enable precise measurements of rare probes such as heavy-flavor tagged and direct-photon tagged jets, and potentially observe the highly suppressed and elusive  $\Upsilon(3S)$  state in Au+Au collisions at 200 GeV. The addition of the EPD will enable observables with respect to the reaction plane such as jet and open heavy flavor  $v_n$  measurements.

RHIC's run plans for the next three years include commissioning the sPHENIX detectors with Au+Au collisions in 2023, collecting high statistics datasets for Au+Au at 200 GeV in 2025 as well as p+p collisions and p+Au data in 2024. Precise p+p baseline measurements are essential as references for sPHENIX Au+Au measurements. Some of the projections for various observables, documented in [4] are highlighted in Sec. 5.3. It is clear there is interesting physics that RHIC, a unique facility, and its upgraded experiments could access beyond these three years. The beam use proposals for STAR and sPHENIX outline possibilities if the opportunity of additional RHIC running becomes available including exploring O+O collisions which would provide important insight into the transition from the smaller p+Au systems to larger Au+Au systems. The temperature dependence of any effect could also be compared to planned results from O+O collisions at a higher energy at the LHC. After operations cease, RHIC will begin transitioning into the EIC.

## 4.2 LHC

Figure 63 shows the timeline of upgrades for all four LHC experiments<sup>7</sup>, in the context of the expected collision systems. The performance of the LHC is expected to lead to continuous improvements in provided luminosities for both proton and ion collisions from Runs 3-6, with the High Luminosity era (HL-LHC) beginning by Run 4. The LHC itself will be upgraded for HL-LHC with new magnets, cavities, and collimators etc [1164]. By LHC Run 6, the provided integrated nucleon-nucleon luminosity for heavy-ion collisions is projected to be more than 100 times larger than what was provided for Run 2. Regarding the LHC experiments, prior to Run 3 (which started in 2022), ALICE underwent a major upgrade [1165]. An increase of ALICE's recorded luminosities by two orders of magnitude has been enabled via the introduction of a continuous readout system in the TPC, and for several other detectors. The new ITS2 system offers a greatly improved tracking performance using new inner trackers, which have a reduction of factor three in

<sup>7</sup>From the plenary presentation "The near- and mid-term future of the LHC" by Jochen Klein at Quark Matter 2022.

radiation lengths in the inner most layers, and factor three improvement in hit resolution compared to the ITS system used in Runs 1&2. ALICE has installed a new Forward Muon Tracker, with an ability (amongst others) to separate prompt and non-prompt  $J/\Psi$  production. The physics possibilities for ALICE in this scenario, and other LHC experiments, are discussed elsewhere [1054, 1166], and later in this paper. The major upgrade for the LHCb experiment also involved substantial gains in readout rates, comparable to those for ALICE. Tracking performance has been improved by the installation of a new vertex locator (VELO), a new upstream tracker (UT), and scintillating fibers (SciFi). Further details of LHCb upgrades for Run 3 can be found here [1167] (Upgrade I(a)). The ATLAS upgrades for Run 3 involved increased statistics and an improved ZDC (with new reaction plane capabilities) [1168], while for CMS these have led to increased bandwidth and improved tracking performance [1169] (Phase I).

The LHC Long Shutdown 3 (LS3) period will involve substantial upgrades for ATLAS [1170] and CMS [1171] (Phase II), in preparation for Run 4 (2029-2032), which marks the start of HL-LHC. Both ATLAS and CMS will achieve advances in their main tracking acceptance - roughly doubling  $\eta$  acceptance to  $|\eta| < 4$ . CMS will install a MIP Timing Detector (MTD), which will provide charged hadron identification (PID) over  $|\eta| < 3$  [1172]. A MIP timing detector will be installed in ATLAS over  $2.4 < |\eta| < 4$  [1173], which in addition to charged hadron identification, mitigates the effects of the pile-up in the forward region. ATLAS and CMS will also embark on a joint ZDC project [1174], with both experiments installing new ZDCs for Run 4, which are based on radiation-hard fused (Cherenkov light producing) silica rods. An additional factor of two improvements of the pointing resolution in ALICE will be achieved by the installation of ITS3, via the introduction of wafer-scale ultra-thin silicon pixel sensors closer to the interaction point. These are also being pursued by the ePIC detector at the EIC. ALICE will also install a Forward Calorimeter (FoCAL), positioned at forward rapidities of  $3.4 < \eta < 5.8$  with high granularity [1120]. It is designed to probe the structure of nucleons and nuclei in the unexplored regime of Bjorken- $x$  down to  $x \sim 10^{-6}$ .

For LHC Runs 5&6, a completely new detector has been proposed by the ALICE collaboration, named ALICE 3 [6]. It is a next-generation detector specifically designed for heavy-ion physics. Its main tracking system covers a large pseudorapidity range ( $|\eta| < 4$ ), and can reconstruct charged tracks down to  $p_T \sim 50$  MeV/c. The lightweight and small radiation length design will greatly reduce the background and improve tracking resolution for electromagnetic and heavy-flavor probes. Compared to the ALICE setup in Runs 3&4 (often referred to as ‘ALICE 2’), the pointing resolution at midrapidity is projected to be about three times better. This is in part achieved by placing a highly novel vertex detector 5mm from the beamline. The tracking system is placed in a superconducting solenoid with a field of up to  $B = 2$  T, to obtain a momentum resolution of 1–2% over a broad pseudorapidity and momentum range. This tracking is complemented by multiple sub-detector systems for particle identification; two TOF detectors and a RICH detector. These systems have the ability to identify leptons and photons in the thermal emission range of  $0.05 < p_T < 3$  GeV/c, which is inaccessible for other LHC experiments. Charged hadron identification on the  $3\sigma$  level is possible up to  $p_T \sim 14$  GeV/c, and decay hadrons can be reconstructed much more efficiently and cleanly at low- $p_T$  compared to ALICE 2. The fast readout systems will be able to record all of the expected heavy-ion luminosity provided by the LHC. The ALICE 3 program aims to collect an integrated luminosity of about  $35 \text{ nb}^{-1}$  with Pb+Pb collisions and  $18 \text{ fb}^{-1}$  with p+p collisions at top LHC energy. The potential to further increase the luminosity for ion running in the LHC by using smaller ions, e.g.  $^{84}\text{Kr}$  or  $^{128}\text{Xe}$ , as well as further runs with small collision systems, is being explored. The LHCb experiment will undergo a major upgrade for Runs 5&6 [1175] (Upgrade II). It will have no centrality limitation for A+A collisions - its Run 4 upgrade will provide measurement capacities for Pb+Pb 30-100% events. LHCb will also have enhanced PID capabilities.

## 5 Future Prospects

The previous sections describe the substantial progress in understanding hot QCD matter since the last long-range plan. However, there are many open questions that we are well equipped to tackle in the next decade. This section will highlight some of those prospective areas of research from macroscopic to the microscopic nature of the medium produced in heavy-ion collisions.

### 5.1 Macroscopic: collectivity, flow and thermal properties

#### 5.1.1 Open Questions and Future opportunities related to collectivity

With the advances made since the last long-range plan and the significant amount of data expected from the high luminosity era at the LHC (with additional upgraded detectors) as well as anticipated data from the Beam Energy Scan and sPHENIX, there are many open questions relevant to collectivity that are within our reach as well as new, exciting opportunities to explore:

- **Identified particles, diffusion, and charge fluctuations** It is now possible to incorporate  $g \rightarrow q\bar{q}$  interactions in the initial state such that baryon, strangeness, and electric charge fluctuations can be observed in the soft sector [71], opening the possibility of detailed charge correlation studies. Coupling this with hydrodynamic simulations that allow for fluctuations of baryons, strangeness, and electric conserved charges provides an exciting prospect for studying a wide variety of observables related to charge fluctuations at the LHC and top RHIC energies where the system is still nearly boost-invariant and high luminosity measurements are possible. On the theoretical side, challenges include incorporating baryons, strangeness, and electric charge diffusion, 4-dimensional equations of state, and conservation of baryons, strangeness, and electric charges at particlization (see [8] for details). However, this will have clear advantages because then one can constraint diffusion at low densities with high precision data such that it will provide an anchor for future work at large densities. Additionally, searches for the QCD critical point will require the incorporation of critical fluctuations within realistic relativistic viscous fluid dynamics simulations and the ability to account for these fluctuations at particlization as well.

On the experimental side, many measurements exist that are sensitive to this type of physics (beyond the standard charge fluctuations measures, see Section 3.1.2). Two-particle correlations with net baryons can be used to explore these additional transport properties of the hydrodynamic evolution. The baryon diffusion constant  $D_B$  is an example of such a parameter beyond  $\eta/s$  and  $\zeta/s$ . It characterizes the mobility of baryon number and is predicted to be finite at the LHC despite the fact that  $\mu_B \sim 0$ . A two-particle correlation function has been proposed to constrain  $D_B$  [1176]. It explores correlations of net-baryon fluctuations as a function of azimuthal and rapidity separations. Such an analysis has yet to be carried out from LHC Run 1 or 2 data since it is statistically challenging. It will be greatly aided by the increase of two orders of magnitude in the Pb+Pb integrated luminosity foreseen for Runs 3&4 for the ALICE detector, given its world-leading particle identification capabilities. The MIP detectors (enabling PID) installed in CMS and ATLAS from Run 4 will also provide an opportunity to refine and pursue such measurements.

Charge balance functions [1177–1180] are a useful method for constraint charge diffusion and will be possible to measure in a wider kinematic range with LHC upgrades. The recently published measurements of balance functions of identified charged hadrons ( $\pi$ , K, p) in Pb+Pb collisions from Runs 1&2 play an important role in constraining the charge diffusion coefficient  $D_e$  for quarks [138]. However, the central tracking acceptance of  $-1 < \eta < 1$  for Runs 1&2 leads to large uncertainties in  $D_e$  from ALICE balance functions data [1180], with values between  $0.5 < D_e(\text{Lattice QCD}) < 4$  being permissible. These uncertainties will be significantly reduced when the same measurements are performed the ATLAS/CMS setups in Run 4, and ALICE 3 in Run 5, as the acceptance where identified charged hadron measurements

can be made will increase to  $-4 < \eta < 4$ . The reduction in  $D_e$  uncertainties due to increases in the  $\Delta\eta$  coverage are expected to be at least a factor 4.

- **Hydrodynamics vs hadron transport at low beam energies** Due to the progress from the BES I, a number of relativistic viscous hydrodynamics codes with at least one conserved charged were able to compare to experimental data [43, 47, 352, 1181] (and one example of ideal hydrodynamics varying the equation of state [1182]). Generally, as the beam energy is lowered, hydrodynamics starts at lower temperatures and, therefore, the ratio of time spent in the QGP vs. hadron gas phase is tilted towards a longer hadron gas phase [1183]. It is unclear, however, at exactly what  $\sqrt{s_{NN}}$  that the effect of the QGP phase becomes negligible. Hadronic transport models, benefiting from their ability to describe non-equilibrium evolution (including evolution through unstable regions of the phase diagram) as well as a natural inclusion of baryon number, strangeness, and charge transport, play an important role at these lower  $\sqrt{s_{NN}}$  (see [1184] for a comprehensive review of used models and [9] for a deeper discussion on the theoretical developments needed in hadronic transport simulations). Recent hydrodynamic studies estimate that hydrodynamics is applicable down to  $\sqrt{s_{NN}} \sim 4 - 7.7$  GeV [47, 352], although work remains to ensure full consistency of most hydrodynamic models with a first-order phase transition. Recently linear stability constraints were derived for a multi-component relativistic viscous fluid [48], which may aid in the determination of the applicability of hydrodynamics in this regime. However, much of this discussion also hinges on a solid understanding of both the equation of state and corresponding transport coefficients, which may display unique features if critical points or first-order phase transitions are present. Thus, much work still remains.
- **Second-order transport coefficients** From the previously discussed theoretical calculations of transport coefficients, there is an understanding that  $\eta/s$  should have a minimum around the phase transition and a maximum in  $\zeta/s$  (although not necessarily at the same location because they undergo a cross-over phase transition); there is some evidence of this from Bayesian analyses [23, 152, 1185, 1186]. However, depending on the hydrodynamic theory and assumptions made when deriving the hydrodynamic equation of motion, different second-order transport coefficients may exist that can even couple shear and bulk together [49, 1187] or viscosity to diffusive currents [48, 1188, 1189]. These second-order transport coefficients have been calculated in kinetic theory [49, 1190] and non-conformal holography [141]. A number of studies have been performed on the influence and necessity of these second-order transport coefficients in simplistic models but significantly less work has been performed in 2+1 or 3+1 hydrodynamic simulations. The one exception is the Bayesian analysis in [1186] that confirmed the importance of these second-order transport coefficients in small systems. In addition, recent work has begun to explore the idea of third-order hydrodynamics [1191–1193] (although, it was shown that [1191] was acausal and unstable [1194]), but it is still too early to tell its influence yet. Thus, now that tighter constraints exist on the first-order transport coefficients thanks to theoretical calculations and Bayesian analyses, more systematic studies of these second-order transport coefficients are needed. In particular, studies that can identify experimental observables sensitive to their values. Most likely, their relevance is strongest in small systems, which emphasize the need for O+O collisions results from both the LHC and RHIC.
- **Hydrodynamic development to better understand small systems** Small systems have challenged the hydrodynamic paradigm in many ways and a number of open questions still exist. For instance, it is clear that a number of fluid cells have very large Knudsen and inverse Reynolds numbers in small systems (to the point where causality is violated). One approach to overcome this issue and also account for strangeness enhancement is the core-corona approach [83, 84]. However, this has only been explored in ideal hydrodynamics and, therefore, it would be an important test in viscous codes that have become standard in the field.

Jet-medium interactions may have a large impact in small systems but there may be numerical challenges when tackling such large gradients. To address this and other related challenges, it may be necessary to adopt practice from astrophysical fields, for example adaptive hydrodynamic schemes where the resolution varies depending on the local densities. Another approach may be anisotropic hydrodynamics [530, 1195–1197], which is designed to resolve potentially large momentum-space anisotropies in the local rest frame. For further discussion of experimental observables and the phenomenology related to small systems, see Sections 3.2 and 5.2.

- **Rapidity dependence** Many of the opportunities that exist, for example, in small systems, for low beam energies, and for jet-medium interactions, require relativistic viscous hydrodynamic codes that are fully three dimensional (i.e. that the assumption of boost invariance is relaxed). While a number of codes are now written in 3+1 (3 spatial, 1 time) dimensions, the third dimension significantly slows down computational time. Thus, computational advances with improved numerical algorithms are needed to overcome this computational cost. Additionally, there are added concerns on the correct description of the initial state (see Sec. 3.1.4 for further details). Groups have already begun to explore the effects of rapidity dependence, exploring a number of questions that are only possible with fully three-dimensional simulations. Is there a decorrelation or twisting of the event-plane angle as one varies rapidity [1198]? How do baryons, strangeness, and electric conserved charges propagate along the rapidity direction [46]? How sensitive are fluctuations of conserved charges to kinematic cuts [1199]? How are the initial conditions different for charm vs light quarks in a 3D picture [1200]? What can be learned about the equation of state from the slope of directed flow [1201, 1202]? Are there other levers offered by rapidity in the beam-energy scan [1203]?

### 5.1.2 *Narrowing the QCD critical point search*

The RHIC BES program has great potential for the discovery of the QCD critical point. Comprehensive and quantitative description of the dynamics of fluctuations, including non-Gaussian fluctuations, their freeze-out, and the effect of the critical point and the phase transition on the observable signatures need to be developed and implemented in simulations to realize that potential.

Thermodynamically, the smooth crossover at small  $\mu_B$ , the critical point, and the first-order phase boundary at finite  $\mu_B$ , are all intrinsically connected and could exist consistently. Therefore, it is natural to study heavy-ion collisions at high baryon density in order to search for the first-order phase boundary. In addition, the QCD phase structure as well as the nuclear matter equation of state at high  $\mu_B$  require detailed investigations. Baryonic interactions including nucleon-nucleon, hyperon-nucleon and hyperon-hyperon interactions are fundamental ingredients to understand QCD and the equation of state that governs the properties of nuclear matter and astrophysical objects such as neutron stars [1204, 1205]. High-statistics measurements including observables for rare probes in low-energy nuclear collisions need to be carried on in the next phase of high-rate experiments. Opportunities for high  $\mu_B$  measurements at FAIR are discussed in [10].

At higher densities, large collaborations such as MUSES [1206] and NP3M [1207] are working on providing an equation of state across the entire phase diagram and testing them in realistic merger simulations, where theory can be confronted against upcoming gravitational-wave data; these will be measured with unprecedented accuracy, starting already in May of 2023 [1208]. Better accuracy is also expected from upcoming nuclear and electromagnetic observational data. Together, these will allow us to determine what kind of phases dense matter presents and at what  $\mu_B$  phase transitions take place. In combination with heavy-ion collisions data analysis from the BES, this will allow us to understand the degrees of freedom at play (hyperons, heavier resonances, deconfined quarks, etc.) and interactions that give shape to the QCD phase diagram at large density.

### 5.1.3 Future opportunities to study thermal properties of the QGP

Photons and dileptons are the only soft and penetrating probes of relativistic nuclear collisions. They will play a crucial role in probing the QCD phase structure with heavy-ion collisions at  $\sqrt{s_{NN}} < 50$  GeV. The EM probes provide complementary information to hadronic measurements. To derive combined and robust experimental constraints on QGP properties, unified theoretical frameworks [2, 39] with the Bayesian Inference method play a central role in future phenomenological studies [23, 1209].

The precise measurements of photon and dilepton spectra will also provide experimental constraints on QGP EM current-current correlation function at different  $(T, \mu_B, \mu_S, \mu_Q)$  and the QGP electric conductivity [253, 1210]. They are valuable inputs for probing the inner workings of QGP, especially the effective degrees of freedom for electric charge carriers in the QGP. Systematic comparison with theory calculations from lattice QCD and other effective theories can elucidate how the strongly-coupled nature of QGP emerged from many-body interactions of quarks and gluons.

The STAR Beam Energy Scan (BES) program collected a vast amount of data in the  $\sqrt{s_{NN}} = 3$ -62 GeV region. With their upgraded inner TPC the STAR detector also improved the reconstruction of low- $p_T$  tracks. The improvement in the low- $p_T$  tracks would also enable better precision in the di-lepton and thermal photon reconstruction from the previous measurement [286]. As part of the Beam Energy Scan Phase II project, the STAR Collaboration collected over an order of magnitude more data than previously acquired in the energy range from 7.7 to 19.6 GeV, where the total baryon density changes substantially. These studies would allow us for a better understanding of the thermal radiation in the transition regions and also further clarify the connection between the chiral symmetry restoration and the  $\rho$  meson mass broadening in the  $M = 1 - 1.5$  GeV invariant mass region. In the future runs between 2023-2025, STAR will collect an order of magnitude or more statistics in comparison with the previous Au+Au datasets at 200 GeV. This will enable high precision measurements in both dilepton spectra and low- $p_T$  direct photons.

The ALICE detector also went under substantial upgrade in its tracking capabilities and data acquisition (ALICE-2). The ALICE-2 detector implemented a streaming readout with their tracking detector, allowing the collection of all the data at a much higher speed and without further bias from online triggers. At the same time, the conversion probability stays at a very similar level as in the previous runs, therefore, the total number of conversion photons in the upcoming proton-proton, proton-lead and lead-lead collisions will be in the order of magnitudes larger than in the previously published data. In Run 3 and 4, ALICE-2 will collect a sufficiently large data sample to perform a first measurement of thermal dilepton emission to determine the temperature of the early stage. With larger sampled luminosity, larger acceptance and excellent tracking of photon conversion products, ALICE-3 will further improve on these measurements of the temperature from the emission of photons and their elliptic flow. Future updates at ALICE should also improve measurements of yield fluctuations between neutral and charged mesons [1211], which can provide complementary evidence of chiral symmetry restoration [1212].

The precise double differential analysis of the dilepton production in both transverse momentum and mass is largely unexplored terrain. The most precise dilepton measurements are from SPS CERES [1213] and NA60 [1214], while at these energies the Drell-Yan processes significantly contribute to smaller invariant masses. The measurements from RHIC at 200 GeV suffer less from the Drell-Yan background, however, the large correlated background from heavy flavor requires a high-precision vertex detector. The new ALICE-2 tracking would provide great improvement in the separation of the prompt and non-prompt dilepton production to isolate the thermal contribution from the background. ALICE-3 tracking capability would further eliminate the heavy flavor background contribution from intermediate then high mass regions compared to the ALICE-2 Run 3 and Run 4 data sets.

The dilepton measurement at the high- $\mu_B$  region will be further explored with the new NA60+ upgrade at SPS in the 6-18 GeV collision energy range. The previously measured dilepton measurement [1214]

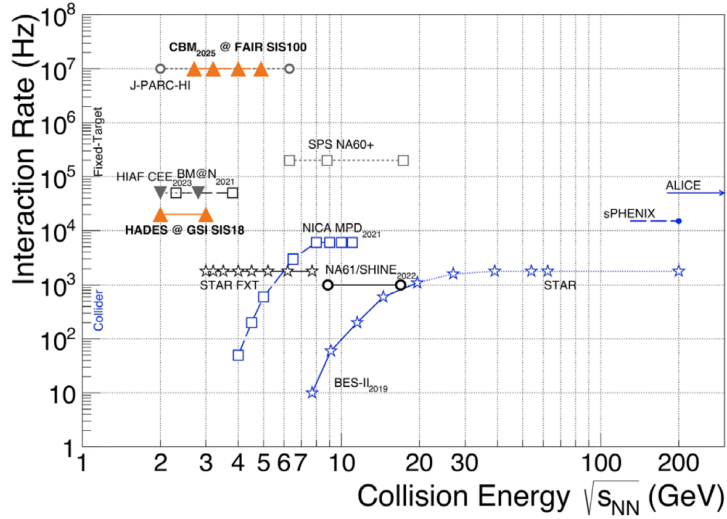


Figure 64: Comparison of the interaction rate and collision energy of current and future experiments in the high- $\mu_B$  region.

will be exceeded with the order of magnitude in statistics and the upgraded detector performance. The upcoming Facility for Antiproton and Ion Research (FAIR) will further explore the high- $\mu_B$  region, and the dedicated Compressed Baryonic Matter (CBM) experiment will be focused on the dilepton measurement in the 3-5 GeV collision region. Together with the STAR BES-II and STAR Fix target programs, the future detectors provide a high precision dilepton and thermal photon measurement lower energy regime around the expected critical point, see in Fig. 64.

#### 5.1.4 Future opportunities for studying the initial conditions

A window for collisions of new species will be opened at the LHC beyond 2028 and possibly before the shutdown of the RHIC upon successful completion of the sPHENIX program. More than 250 stable isotopes in the nuclide chart, 140 in isobar pairs or triplets, can be used [360]. Note that the nuclear structure and produced initial condition vary in a non-monotonic fashion with  $N$  and  $Z$ , whereas the hydrodynamic response connecting the initial and final state varies smoothly and slowly with the mass number,  $N + Z$ . Hence, we can choose isobar or isobar-like systems with nearly identical hydrodynamic response but large structure differences to probe the initial condition. Clearly, continued effort is needed to identify species that maximize the scientific impact. For the moment, we point out four possible directions (see also [18]):

- **Initial condition in large systems**, whose knowledge is crucial for the precision extraction of QGP transport properties. We need to first calibrate the coefficients e.g.  $c_{O,1}-c_{O,4}$  in Eq. (8) using systems that are close to those with well-known properties, such as doubly-magic  $^{208}\text{Pb}$  or  $^{132}\text{Sn}$ . These coefficients can then be used to make predictions for other species and check consistency with low-energy knowledge.
- **Initial condition from medium to small systems** to expose the role of sub-nucleon fluctuations, initial momentum anisotropy, and hydrodynamization process, by exploring isobar or isobar-like collisions in the region from  $^{12}\text{C}$  to  $^{48}\text{Ca}$  with different structures, e.g.  $^{16}\text{O}+^{16}\text{O}$  vs  $^{20}\text{Ne}+^{20}\text{Ne}$ , which are nowadays accessible to cutting-edge *ab initio* calculations, with the aim of improving our understanding of the emergence of collectivity.



- **Initial condition:  $\sqrt{s_{NN}}$  dependence and longitudinal structure.** At high energy, the initial condition is controlled by the distribution of low- $x$  partons, which depends on the beam energy and the rapidity. Exploiting isobar ratios for bulk observables as a function of rapidity and  $\sqrt{s_{NN}}$  may provide a new access route to the  $x$ -dependence of nPDF and gluon saturation, complementing thus the science goals of EIC.
- **Initial condition for hard probes** is typically modeled by convoluting information from the Glauber model with the nPDF, which contributes to a large uncertainty in the relevant transport properties, such as  $\hat{q}$  [691, 761, 827]. By constructing ratios of selected high- $p_T$  observables ( $R_{AA}$  for example) at a fixed centrality, jet quenching effects are expected to largely cancel. Deviation of ratios from unity then provide access to flavor-dependent nPDF, tailored for each underlying hard-scattering process [1038, 1215, 1216]. The determination of the impact parameter from bulk particles in combination with the observed hard processes will permit isobar ratios to access the differences in the transverse spatial distribution of partons, coming from structural differences in the collided nuclei.

### 5.1.5 Future opportunities to study chirality and vorticity in heavy-ion collisions

The current status of the CME search demonstrates a situation of both challenges and opportunities. The challenges are nontrivial and will require considerable future resources to enable integrated efforts between theorists and experimentalists to perform dedicated modelings and comprehensive analyses that will quantify any residue uncertainties such as non-flow corrections and conclusively extract any signal with high statistical significance. On the other hand, the opportunities of CME discovery, carrying magnificent implications for fundamental physics and substantial interests in other disciplines, are simply difficult to dismiss. Looking into the next decade, one anticipates a number of major thrusts for future developments.

With the rich isobar data set available, post-blind analysis efforts are important in order to fully capitalize on the contrast power only available with such an isobar pair. Alternative analysis approaches (e.g. based on identical multiplicity selection or event-shape measurements between event-plane/spectator-plane) may also provide fresh insights. In particular, a quantitative understanding of the bulk property difference between the isobar systems appears feasible with further theoretical studies. Once that is achieved, one can hope for an informed baseline with careful calibration of nonflow effect for the isobar comparison and thus a convincing answer for the CME signal level in the isobar collisions.

The Au+Au collision system is expected to have a higher CME signal fraction and holds strong future promise, given the aforementioned positive result from the event-plane and spectator-plane comparison analysis. The bottlenecks include the limited statistics and residue nonflow effect. The highly anticipated Au+Au collision runs at RHIC from 2023 to 2025 will provide events on the order of 20 billion that can help deliver a much-needed boost of statistics for the CME analysis. On the LHC side, the upcoming high-statistics measurements will soon provide an exciting opportunity for yet another scrutiny at extracting/constraining a potential CME signal at TeV energies. A close collaboration between theoretical and experimental efforts will further advance the simulation and analysis tools to substantially reduce various remaining uncertainties, thus paving the way for a decisive conclusion on the CME search.

Last but not least, it is highly desirable to map out the beam energy dependence of the CME phenomenon. Past CME measurements in the low-energy region were based on Beam Energy Scan I data, while now there is an abundance of high-statistics data from the Beam Energy Scan (BES) II program. Understanding their implications will require the development of a CME modeling framework for low-energy collisions. Furthermore, various new analysis methods and observables for the CME extraction have been mainly applied to top RHIC energy. Utilizing them for analyzing BES-II data will be very interesting. Ultimately, nailing down the beam energy dependence of CME will help reveal the QCD chiral symmetry restoration and contribute to determining the phase boundary via beam energy scan.

The global and local polarization measurements in heavy-ion collisions have opened a new direction in the study of the hottest and densest QCD matter, now under the fastest rotation [393, 395]. As the spin polarization at the lowest order depends linearly on the gradients of the hydrodynamic fields, it turns out to be a very sensitive probe of the hydrodynamic evolution and thus can help quantitatively constrain bulk matter properties. Despite the successful description of the average global polarization by various theoretical models, there still remain open questions. From the experimental point of view, more precise measurements are needed to constrain theoretical models and answer these questions. Analyses of high statistics BES-II data together with data from future experiments such as CBM [10] can reveal a complete picture of the energy dependence, especially at  $\sqrt{s_{NN}} < 10$  GeV, where there is little experimental data and theoretical models predict non-monotonic behavior. Quantifying the vorticity is important to better understand the QCD phase diagram as the vorticity also acts as the baryonic chemical potential [1217, 1218]. Also, the measurement of possible splitting in global polarization between  $\Lambda$  and  $\bar{\Lambda}$  is of great interest to constrain the lifetime of the magnetic field, which is also important for the study of chiral phenomena. In 2023 and 2025, high statistics data of Au+Au collisions at  $\sqrt{s_{NN}} = 200$  GeV will be collected by STAR with upgraded detectors in both mid and forward rapidities and by sPHENIX at RHIC. High statistics data at RHIC and the LHC will allow us to perform measurements sensitive to the electromagnetic field, such as charge-dependent directed flow including heavy-flavor hadrons. The new data will also allow us to measure the polarization of multistrangeness ( $\Xi$  and  $\Omega$ ) more precisely which helps to shed light on possible spin and particle species dependence and to measure rapidity dependence of global polarization which is predicted differently by models, especially in the forward region. For the local polarization, while considerable theoretical progress has been made with the newly found thermal shear contribution having potential for resolving the sign puzzle, more future studies are needed to understand the different implementation schemes as well as to achieve a quantitative explanation of data. A relevant direction is to extend the measurements to polarization induced by higher harmonic flow [417], which is being studied by STAR. Generally speaking, the global and local spin polarization phenomenon could develop into an important probe of the hydrodynamic fields (such as their initial conditions and gradients evolutions) in heavy ion collisions.

Regarding the spin alignment measurements, interesting results of  $\phi$  and  $K^{*0}$   $\rho_{00}$  were observed both at RHIC and the LHC. However, the interpretation of the results is currently under discussion. Recently, the ALICE Collaboration observed  $J/\psi$  transverse polarization relative to the event plane in the forward region ( $2.5 < y < 4$ ) as  $\lambda_\theta \sim 0.2$ , corresponding to  $\rho_{00} \sim 0.37$  [1219]. Heavy quarks are produced at a very early time by parton hard scattering, therefore there may be a large contribution from the initial magnetic field. It is of great interest to measure  $J/\psi$  polarization at RHIC energy, where less regeneration in  $J/\psi$  polarization, and helpful to understand how the different production mechanisms affect the spin polarization. The 2023+2025 runs at RHIC make measurements of  $J/\psi$  polarization possible at midrapidity, which can be directly compared to the results of light vector mesons and helps to understand the origin of polarization of vector mesons.

Furthermore, there are new directions to explore vortical structure in heavy-ion collisions. Event-by-event density fluctuations superimposed on the collective flow field should produce vorticity “hot spots” that may be probed by spin-spin correlations [415] while jet with medium interactions should produce vortical toroids centered on the jet [1220–1222]. Measurements of polarization induced by these phenomena would be experimentally difficult as the observable is sensitive to the experimental effects such as acceptance and efficiency. One possible direction will be a study in asymmetric collisions such as A+B or p+A collisions [1223], where a smaller projectile passes through the center of a larger target leading to a toroidal vortex [417, 1224]. Data of  $p$ +Au collisions at RHIC taken in 2024 and  $p$ +Pb data at the LHC will have the potential to discover this unique vortical structure arising as a fluid behavior, which may also bring new insight into the collectivity in small systems. Another interesting phenomenon that is possibly measurable is the generation of spin current called Spin Hall Effect [1225, 1226] whose signal is expected to be larger

at lower collision energy and BES-II data will provide a good opportunity to search for the effect.

## 5.2 Mesoscopic: emergence of the quark-gluon plasma and approach to equilibrium

### 5.2.1 Future Experimental Exploration of Collectivity in Small Systems

There are several directions that can be explored experimentally in the next decade to improve our understanding of the emergence of collectivity in small systems. Additional collision systems with different initial geometries and structures, as well as improved statistical precision for systems that have already been studied, may bring new insights. High-statistic data sets and improved detector capabilities can enable the exploration of new observables and new probes with different sensitivity to the underlying physical processes. Some examples of future measurements and directions are discussed below.

Measurements in the smallest collision systems, such as photon-proton interactions accessed through ultra-peripheral p+Pb collisions [447, 480] and  $e^+e^-$  collisions [448, 449] are presently statistics limited. Additional p+Pb data at the LHC will improve the multiplicity reach for  $\gamma$ -p collisions. A high statistics data sample on ultra-peripheral Au+Au collisions at  $\sqrt{s_{NN}} = 200$  will be collected during the upcoming RHIC Run 23 and 25. This along with the ultra-peripheral d+Au data from RHIC run 21 provide the opportunity to search for collectivity in  $\gamma$ -Au and  $\gamma$ -p collisions at  $W_{\gamma N} \approx 40$  with the extended pseudorapidity capability of the STAR detector [5]. There are also more archived data available from ALEPH at LEP2 for  $e^+e^-$  collisions at energies higher than those presently studied. The event multiplicity could reach more than 50 charged particles in these much simpler collisions that do not have complicated hadron structures or gluonic initial state radiation. Finding any evidence of collective flow in these events could improve our understanding of collectivity. Eventually, there will be new opportunities to study small systems at the Electron-Ion Collider [482].

In hadronic collisions, new measurements will be possible both at RHIC and at the LHC. Data from d+Au and O+O collisions at 200 GeV were already collected by the STAR experiment in 2021. These data sets include an upgraded STAR detector with extended coverage in rapidity (inner TPC), high-resolution event plane detector and forward-rapidity particle identification. A more direct comparison between the PHENIX and STAR measurements in d+Au collisions will improve the understanding of collective flow, nonflow correlations, and the three-dimensional system evolution in d+Au collisions. In addition, a high luminosity p+Au run is planned for 2024 with both sPHENIX and STAR taking data. The LHC planning also includes p+O and O+O runs in 2024. Correlation measurements in these collisions with different initial geometry and a smaller number of participating nucleons could provide new insights.

Another avenue of exploration is to investigate new observables. Different physics mechanisms have been proposed as possible sources for particle azimuthal correlations in small systems. The relative contribution from each mechanism could be different for different particle species due to differing particle production mechanisms and in-medium interactions. One such example is the comparison of  $v_2$  measured for light and heavy-flavor hadrons, including  $J/\Psi$ . Significant  $v_2$  for charm has been observed in high-multiplicity p+Pb collisions [467–471] and the mechanisms of these correlations, especially for  $J/\Psi$ , is not fully understood. Non-zero  $v_2$  has also been observed for open charm hadrons in high-multiplicity p+p collisions, but not yet found for  $J/\Psi$ . Future measurements of long-range correlations of  $J/\Psi$  in p+p collisions will give further handles to distinguish initial vs final state effects in the particle correlations. Correlations between  $v_2$  and mean  $p_T$  have also been proposed [478] for distinguishing different origins of azimuthal correlations and are already pursued [480]. Further studies with multi-particle observables [481] will be needed for detailed understanding of the interplay between collective effects and nonflow correlations. Ultimately, comparisons to theoretical models that properly include the correlations between the bulk system and the hard-scattered partons will be needed.

More broadly, the small-system evolution can be studied with event engineering, e.g. by selecting

events with large and small  $v_2$ . The selection criteria could include both hard and soft observables, such as number of jets, soft particle multiplicity, mean  $p_T$ , and others. The correlation between  $v_2$  and mean  $p_T$  is just one of many possible observables. Recently, there is a proposal to search for collectivity in a QCD system where a single-parton is propagating in vacuum [1227]. The measurement of  $v_2$  using the particles inside the jet cone in the jet coordinate system is proposed. Such measurements are accessible with the high-energy jets produced at the LHC. Another interesting proposal is to search for vortex rings in small collision systems [1224]. Existence of the vortex toroids may provide new evidence for hydrodynamic collective flow in the smallest QGP droplets.

### 5.2.2 *The next steps for understanding small systems*

Despite recent progress [426], many outstanding questions remain concerning the description of small systems. The answer to those questions requires a number of new experimental and theoretical developments, as briefly discussed below.

Many more theoretical developments are needed in order to fully determine the applicability of hydrodynamics in small systems. Most of what is understood about hydrodynamics comes from the gradient expansion. However, in rapidly expanding plasmas the gradient expansion can become divergent [506, 507, 1228, 1229], which motivated the idea of hydrodynamic attractors [526]. Though general properties of the hydrodynamic expansion have been worked out [1230–1234], these developments have not yet been put to use in realistic phenomenological investigations, especially in the case of small systems. Furthermore, through anisotropic hydrodynamics [509, 1195, 1235, 1236] it was understood that one may resum not only gradients but also the viscous stresses themselves, which significantly expands the regime of applicability of hydrodynamics. Further investigation is needed in this regard to determine the phenomenological impact of attractors and hydrodynamic resummation schemes. Additionally, even though hydrodynamic attractors are now starting to become part of the heavy-ion phenomenology toolbox [541], it remains unknown whether the QGP, realistically modeled as a rapidly expanding system in 3+1 dimensions, indeed approaches a hydrodynamic attractor at the relevant timescales needed in phenomenology. This question is even more pressing in small systems, due to their reduced size and lifetime. Despite some studies in this context [1237–1239], this question remains elusive due to the lack of a consistent framework capable of systematically investigating QCD in the far-from-equilibrium regime (at all values of coupling).

Additionally, in small systems where deviations from equilibrium can become very large, a systematic investigation of the nonlinear far-from-equilibrium properties of 2nd-order hydrodynamics, going beyond the initial results of [1240], is needed. Implementing causality constraints in simulations [33, 34] of small systems can be important to avoid numerical instabilities and also to better constrain the properties of the pre-hydrodynamic phase [78, 511] and the importance of conformal invariance violation [79, 1186, 1241].

The possibility of using different definitions of hydrodynamic variables (i.e., hydrodynamic frames) [1242–1247] opens up a number of questions in the formulation of hydrodynamics that can be particularly useful in the description of small systems. For example, new terms and coefficients appear at 2nd order [1247] that have never been explored before in phenomenological simulations. Furthermore, because of the fluctuation-dissipation theorem, the choice of hydrodynamic frame should also influence how thermal stochastic fluctuations take place in the fluid. The simplest version of this statement is widely understood in the field already, given the differences that appear when one considers fluctuations in the Eckart [1248] or the Landau frame [1249]. Further work is needed to systematically formulate 1st and 2nd order stochastic hydrodynamics in general hydrodynamic frames, going beyond existing work [88, 92, 1250, 1251]. Thermal fluctuations should become even more important with decreasing multiplicity, being especially relevant in small systems. Current phenomenological investigations [1252–1254] must be generalized to systematically determine the size of such effects, and their experimental consequences, in small systems.

### 5.2.3 Prospective studies of medium response to partonic excitation

In recent years, groups are beginning to explore jets fully coupled to hydrodynamic simulations wherein energy is dumped into the fluid by using a source term in hydrodynamics [573, 576, 1255] (see Section 3.3 for the influence this has on jet observables). Additionally, breakthroughs in the theoretical description of jet-medium interactions by the inclusion of flow in energy loss calculations allow for an even better, self-consistent picture [664, 1256]. An opportunity exists here to study the influence of this energy gain in the medium to study far-from-equilibrium phenomena. The presence of a jet was shown to alter the  $v_n(p_T)$  in the range of  $p_T \sim 2 - 10$  GeV in p+Pb collisions. Thus, collective flow observables in this  $p_T$  range in small systems provide an intriguing possibility to better understand jet-medium interactions. Another synergy has yet to be thoroughly exploited in that in initial studies [1257, 1258] multiparticle  $v_n$  calculations and experimental data were explored at high  $p_T > 10$  GeV. However, as we have discussed already in this section that there are an enormous number of collective flow observables such as symmetric cumulants, factorization breaking,  $\rho(v_n, p_T)$  observables, etc that have never been calculated nor measured experimentally at high  $p_T$ . Given the high luminosity era at the LHC and sPHENIX, this is a perfect opportunity to exploit these high statistics.

To reveal the jet broadening effect from multiple soft scatterings and medium response experimentally,  $Z/\gamma$ -tagged reduces “survival bias” narrowing observed in the inclusive jet shape. The increased data acquisition and acceptance of the sPHENIX will enable a dramatic increase in the number of photon-tagged jet observables previously studied at RHIC. At HL-LHC, the available statistics of  $Z/\gamma$ -tagged jet events will increase by a factor of 5-10. The large datasets will provide high-accuracy data on the  $Z/\gamma$  tagged jet spectra, transverse momentum profile, fragmentation function, hadron angular distributions, and jet substructures.

This large data set will also enable more differential measurements to separate the contribution from medium-induced momentum broadening via multiple soft scattering, medium-induced radiation, medium response, and medium recoil effects. Measurements such as  $Z/\gamma$ -hadron 2D angular correlation and  $Z/\gamma$ -tagged subjet multiplicity have been proposed. Moreover, the large acceptance tracking detectors in ATLAS and CMS will enable us to study the long-range correlation between electroweak bosons, jets, and hadrons up to a  $|\eta| < 4$ .

The new capability of the CMS MTD will enable us to study the particle composition in the QGP wake. Example measurements include proton-to-pion ratios in and out of the jet cones as shown in Figure 65. The ALICE collaboration, who has studied particle ratios in jets for p+p and p+Pb collisions [1259, 1260], also expects to produce complementary measurements to these results in Pb+Pb collisions from Run 3 and Run 4 data.

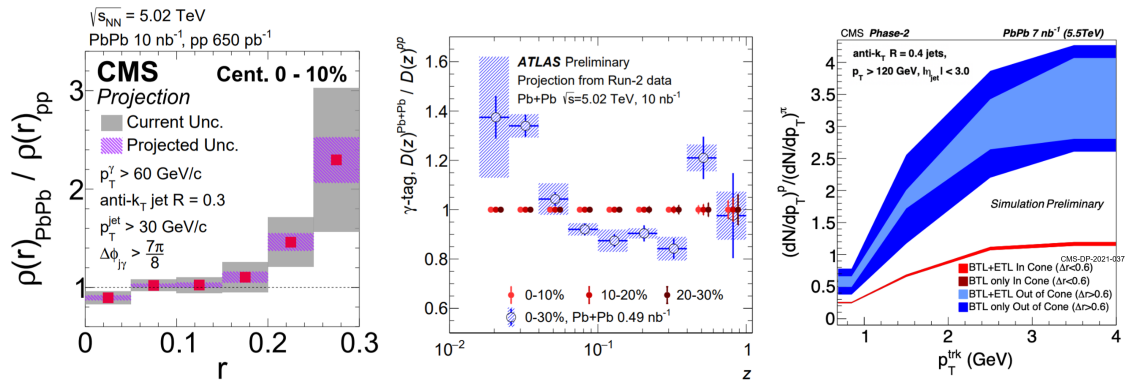


Figure 65: Projections for LHC measurements related to medium response [1261].

#### 5.2.4 Further investigations of jet quenching in small systems

As described in Sec. 3.2.2 the lack of energy loss signatures in experimental measurements of jets in small system may not be so surprising due to the limited pathlength of the produced medium. How large does the collision system need to be, to be able to measure energy loss effects? New calculations at NLO for jets and leading hadrons indicate that the baseline spectrum in p+p collisions can now be calculated with high accuracy. This will allow for even the smallest energy loss effects to become evident in intermediate systems such as those formed in light-ion collisions, e.g., O+O [1262, 1263].

To explore this question experimentally, it has been proposed to quantify the suppression in collisions of light ions which would fill the gap between the existing data from p+A and heavy-ion A+A collisions. The LHC plans to record data from O+O collisions during Run 3 which will provide information on the system size necessary to transition from partons escaping the medium to jet quenching. sPHENIX is well equipped to further our understanding of the future LHC results as indicated in their beam use proposal if the opportunity for running light ions arises. Specifically they demonstrate the kinematic reach to measure jets and heavy-flavor observables in O+O and Ar+Ar collisions. RHIC measurements would provide temperature dependence for the physics observed in these light-ion collisions as well as probe lower momentum partons that may experience stronger quenching.

### 5.3 Microscopic: Hard Probes

The successful operation of sPHENIX and the complementary heavy-ion program at LHC as well as the subsequent analysis of all collected data is crucial for realizing the goals of exploring the QGP at smaller length scales as set forth in the previous Long Range Plan. In particular, sPHENIX promises to deliver precision hard probes measurements to quantify properties of the QGP at the microscopic level, measurements that will be complementary to those planned at the LHC. This section will discuss planned measurements and opportunities for theoretical developments related to jets, open heavy flavor and quarkonia as well as electroweak and ultra-peripheral collision measurements related to nPDFs in the initial state of the collisions.

#### 5.3.1 Prospective jet measurements and theoretical advances

The anticipated statistical precision for the  $R_{AA}$  of jets expected from sPHENIX in 3 years of running is shown in the left panel of Figure 66 along with that of direct photons and hadrons which indicate a kinematic reach significantly beyond current RHIC measurements. The addition of the event plane detector (EPD) at STAR and sPHENIX will enable precise measurements of jet  $v_n$  in Au+Au collisions at 200 GeV. Figure 66 shows the precision of the expected sPHENIX jet  $v_2$  results. Jet  $v_2$  provides insight to the pathlength dependence of the energy loss mechanism in the QGP. These new results at the lower temperatures at RHIC would be complementary to existing LHC measurements. In addition to studying energy loss at the jet level, the tracking system in sPHENIX will enable studies of the jet constituents to explore modification to the fragmentation functions as well jet substructure observables.

#### Theoretical Advances

Theoretical developments in the period covered by the next long range plan include developments in the underlying theory of energy loss, improvements in event generators, both in their theoretical content and in their computational abilities, and a deeper understanding of transport coefficients leading to further elucidation of the degrees of freedom of the QGP. Separate from all of these is the rise of machine-learning techniques, Bayesian analysis and uncertainty quantification that have changed the day-to-day mechanics of how theoretical developments are judged in comparison with experimental data. Continued developments in the aforementioned arenas imply the possibility of deep advances in our understanding of jet medium interactions and the nature and interaction of the prevalent degrees of freedom of a strongly interacting plasma at  $T \sim (1 - 4)T_C$ .

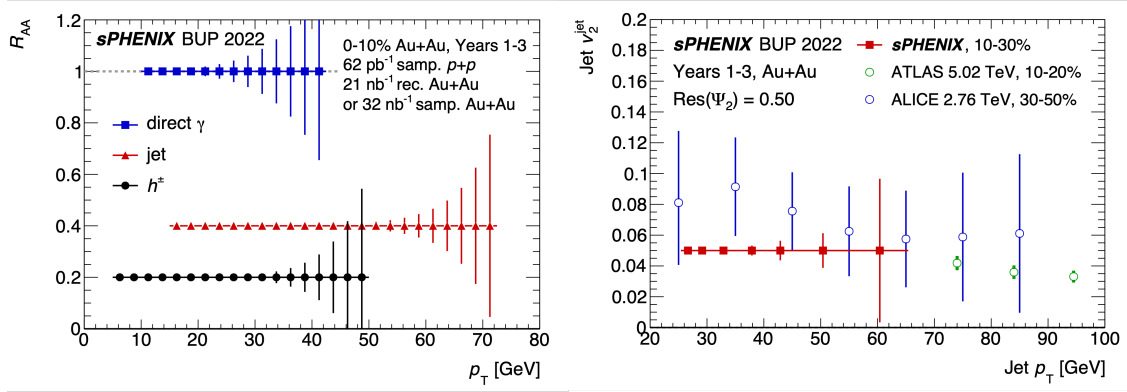


Figure 66: The anticipated statistical precision for sPHENIX to measure the  $R_{AA}$  of jets, direct photons and hadrons (left) as well as the jet  $v_2$  compared to existing measurements at the LHC [4]

In the period subsequent to the last Long Range Plan, major theoretical developments have included improvements in Glauber enhanced Soft Collinear Effective Theory (SCET<sub>G</sub>) [684, 1264], developments in the overarching formalism of energy loss [563, 618, 659, 679, 680, 694, 1265–1267], as well as the incorporation of coherence effects [619, 672]. The stage is now set for the appearance of higher order calculations of energy loss, which should lead to precision calculations with realistic estimates of the theoretical uncertainty.

On the event generator side, improvements in individual simulators such as the development of jet modification with hydrodynamic response [554, 555], is coupled with the development of frameworks where a variety of different energy loss simulators can be modularly incorporated within an extensive end-to-end generator [2]. In the upcoming interval of the current long range plan, we envision enhancements in the theoretical and phenomenological content of individual simulators, advancements in computational ability e.g., using machine learning routines to accelerate hydrodynamic simulations, and more elaborate Bayesian analysis combining hard and soft sectors in full 3+1D simulations.

With the advent of theoretical advances, and improvements in simulation, along with the ability to conduct rigorous Bayesian comparisons between theory and data, it will become possible to finally constrain the underlying structure of the quark-gluon plasma. Current calculations of jet transport coefficients at higher order [687], will soon be enhanced with lattice calculations using 3D EQCD calculations [688, 1268] and in full 4D lattice gauge theory [689, 690]. Comparing these calculations with extractions from Bayesian analysis [152, 1269], conducted using high statistics data from several colliding systems and energies, will allow us to reliably narrow down the quasi-particle structure of the plasma.

### Jet substructure

The next generation of substructure studies in heavy-ion collisions require higher theoretical accuracy and extending towards more differential measurements beyond inclusive ones. The emphasis here is on robust theoretical control in benchmarking a particular model of jet-medium interactions via calibrated Monte Carlo simulations. The novel experimental observables need to be sensitive to the physics of varying jet showers and topologies and simultaneously be robust to the heavy-ion background. While hard jet substructure is more immune to fluctuating heavy-ion background, its sensitivity to medium effects may be suppressed by the large-scale separation. On the other hand, soft jet substructure can be affected significantly by the medium. A systematic approach from hard to soft jet substructure is essential to decouple physical effects at various energy scales. Observables based on the most energetic jet particles which are recoil-free as discussed in Sec.3.3.5 might be the starting point of this program. Also, in order to meaningfully and unambiguously extract information from soft jet substructure, combination of knowledge about local under-

lying event fluctuation beyond practical background subtraction schemes will be increasingly necessary. An initiation of the unification of hard and soft probes should be attempted in the 2023 Long Range Plan.

With the upcoming measurements of several, different observables from the experiments at both RHIC and the LHC, one can eventually move towards a global analysis resulting in calibrated heavy-ion Monte Carlo models. In the coming years following the 2023 Long Range Plan, enabled by the new sPHENIX detector designed with both hadronic and electromagnetic calorimetry, high precision charged particle tracking and secondary vertex upgrades along with streaming readout will result in large statistics to push into the next era of jet substructure measurements at RHIC. For inclusive jets, the high statistics dataset will result in a direct comparison of jets at RHIC and the LHC. Upgrades to the STAR detector at RHIC will provide a complementary handle on the studies of jet substructure in vacuum and in heavy-ion collisions. With Runs 3 and 4 at the LHC, the extension of the dimensions of substructure studies such as the dependence on the heavy quark masses, regions of the emission phase-space sensitive to early time dynamics, has the potential to extract information related to the early pre-equilibrium state of the plasma.

#### **Coincidence measurements with jets**

One of the challenges in reconstructing jets at RHIC is the proximity to the size of the underlying event and upward fluctuations in the underlying event which give rise to so-called “fake” jets. The contribution of these fake jets is greatly reduced when the jet is tagged by an opposing hard particle such as a direct photon or heavy flavor quark. Photon tagged jets have long been referred to as the golden channel for studying energy loss in the QGP since the direct photon provides access to the kinematics of the initial hard scattering [1270]. In addition, these measurements can be used to further our understanding of the medium response as discussed in the mesoscopic section (Section 3.2.4). The b-tagging capabilities of sPHENIX and its high data acquisition rate will enable precise measurements of these rare probes.

#### **Heavy-flavor tagged jets**

The new sPHENIX MVTX will enable the first b-jet measurements at RHIC. The sPHENIX b-jets measurements will extend the kinematic range of the existing LHC measurements to lower jet  $p_T$  where a larger heavy-quark mass effect is expected and further constrain heavy quark diffusion transport parameter in addition to providing insight to its temperature dependence. Figure 67 show projections for the sPHENIX b-jet  $R_{AA}$  compared to theoretical models [1264], which it should be able to constrain.

The LHC has published heavy-flavor tagged jet measurements as discussed in Section 3.3.6 and will continue to utilize this capability for more differential measurements with the additional data collected in future LHC runs. Extensions of previous measurements of the distribution of D mesons in jets [818] to additional substructure measurements as well as comparisons to future RHIC studies probe the diffusion of charm quarks in the QGP and its dependence on temperature. Substructure measurements of b-jets compared to photon-jets (predominantly produced by light quarks) and inclusive jets (a significant fraction of which are produced from gluons) will further our understanding of the flavor dependent energy loss.

### **5.3.2 Prospective heavy-flavor and quarkonia measurements and theoretical advances**

#### **Quarkonia**

While tremendous progress has been made in the last decade in utilizing quarkonia to study the QGP in heavy-ion collisions, there is still a gap between a qualitative characterization of the QGP features as of now to a quantitative extraction of the QGP properties. To close the gap, advancements from both experimental and theoretical sides are urgently needed. The planned data-taking during 2023-2025 at RHIC [4, 5] and LHC Run 3 (2022-2025) and Run 4 (2029-2032) with unprecedented statistics and detector upgrades opens the door for significantly improving the precision of the current quarkonium measurements and accessing to new quarkonium states in heavy-ion collisions [1272].



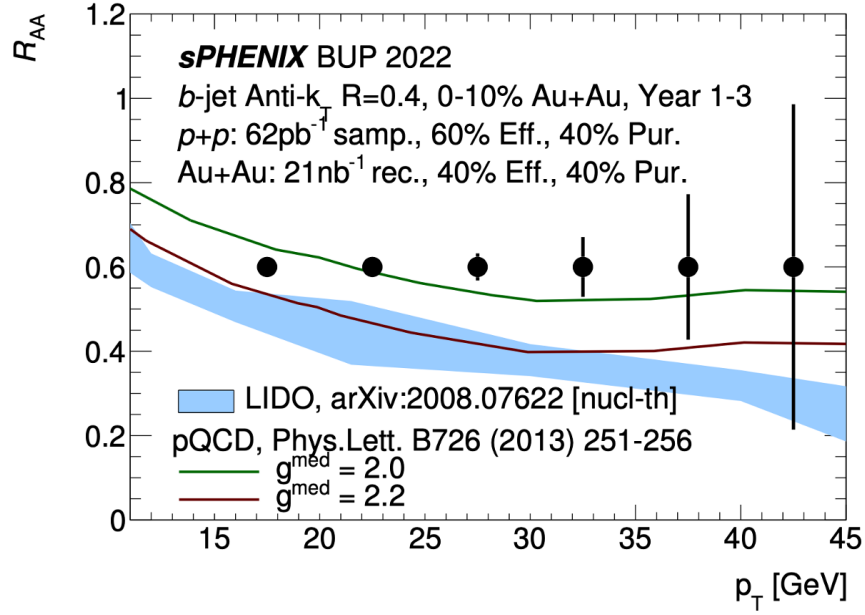


Figure 67: The anticipated statistical precision for measuring the  $R_{AA}$  of b-tagged jets compared to curves from a pQCD calculations with two coupling parameters to the QGP medium,  $g_{med}$  [1264], and a blue band representing a calculation based on the LIDO transport model [1271].

Quantification of the CNM effects is critically needed, especially at RHIC where no separate measurements of the three  $\Upsilon$  states in p+Au collision are currently available. Many model calculations rely on experimental measurements to constrain the CNM effects, and the uncertainties in the experimental data are often the dominate ones [886, 904]. Such a situation will be greatly improved with the 200 GeV p+Au dataset to be recorded in 2024 at RHIC. Another essential experimental input to model calculations is the total charm quark production cross section, which dictates the recombination contribution to the charmonia. The detector upgrades at both RHIC and the LHC will enable measurements of various charmed mesons and baryons down to zero  $p_T$ , from which the total charm quark yields can be extracted. See more details in Section 3.4.3.

At RHIC, the large sample of 200 GeV Au+Au collisions to be delivered in 2023 and 2025 and p+p collisions in 2024 will greatly improve the current measurements of the nuclear modification factors for  $\Upsilon(1S)$  and  $\Upsilon(2S)$  as a function of centrality and  $\Upsilon p_T$  [948]. Potentially, a real measurement of  $\Upsilon(3S)$   $R_{AA}$  could be achieved for the first time if a similar level of suppression as that observed at the LHC [952] is assumed as shown in the sPHENIX projections in Figure 68. A precise measurement of the  $J/\psi$  flow at midrapidity in Au+Au collisions will also become available thanks to the increased statistics and detector upgrades at forward rapidity. The latter introduces a rapidity gap between  $J/\psi$  measurement and event plane reconstruction to reduce the non-flow effect, a major source of uncertainties in the previous measurement [1273]. Such a measurement will be instrumental in understanding the recombination contribution to  $J/\psi$  production and provide complementary information on the extent to which deconfined charm quarks are thermalized in the medium at RHIC. Furthermore, we will be able to access  $\psi(2S)$  mesons, the most loosely bounded quarkonium shown in Figure 47, for the first time in 200 GeV Au+Au collisions, which will extend the lever arm with which quarkonia are used to probe the QGP.

At the LHC, Pb+Pb collisions at  $\sqrt{s_{NN}} = 5.02$  TeV with a total integrated luminosity of  $13 \text{ nb}^{-1}$  are expected to be delivered in Run 3 and 4. With such a large data sample and enhanced detector capabilities,

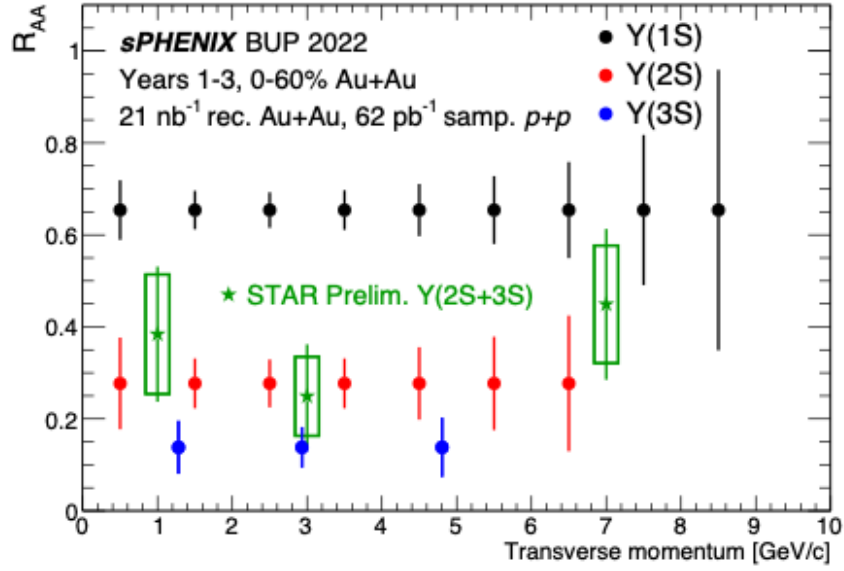


Figure 68: Projected statistical precision of the different upsilon states with 3 years of data collection with sPHENIX. The suppressed 3S state previously observed at LHC would be a new discovery at RHIC energies.

high-precision differential measurements in centrality, transverse momentum and rapidity for the three  $\Upsilon$  states will become a reality [1274]. Elliptic flow of  $\Upsilon(1S)$  can also be measured with good precision, even though its constraining power will be limited due to the small signal. Nevertheless, it will provide valuable insights into the  $\Upsilon$  recombination and the degree of bottom quark thermalization in the QGP. Precise measurements of  $\psi(2S)$  production in these collisions will become feasible, which is expected to be decisive in distinguishing different models of charmonium recombination [103]. These measurements of the suppression levels for the excited quarkonium states are essential for interpreting the results of the ground states because of the feeddown contribution. Furthermore, the  $p_T$  reach of the  $J/\psi$  ( $\Upsilon$ )  $R_{AA}$  will be extended to about 80 (50) GeV/ $c$ , compared to the 50 (30) GeV/ $c$  with the current data [1274]. Such an increase in statistics and kinematic reach, together with  $\psi(2S)$  measurements, will greatly enhance our ability to study possible contributions of parton energy loss to the suppression of high- $p_T$   $J/\psi$  [947]. In addition, the fixed-target program at the LHCb by injecting noble gases through the SMOG (System for Measuring Overlap with Gas) device has recently been upgraded and is now participating in the LHC Run 3 data-taking. It is anticipated to record about 15M  $J/\psi$ , 150k  $\psi(2S)$  and 7k  $\Upsilon(1S)$  in p+Ar collisions at  $\sqrt{s_{NN}} = 115$  GeV, and similar statistics in Pb+Ar collisions at  $\sqrt{s_{NN}} = 72$  GeV [1275], bridging the gap between SPS and top RHIC energies. These data will prove valuable in studying the interplay of various contributions to quarkonium production in heavy-ion collision at varying collision energies. The P-wave charmonium states,  $\chi_{c1}$  and  $\chi_{c2}$  [1276] whose binding energies are between those of  $J/\psi$  and  $\psi(2S)$ , will also become accessible in heavy-ion collisions by the LHCb experiment. Their measurements will provide additional tests of hot medium effect and constitute important inputs for understanding feeddown contributions to  $J/\psi$ .

A heavy-ion collision is a complex process that involves distinct phases with different dynamics. Its full understanding requires to piece together measurements of all the probes into a coherent picture, and there is no exception when it comes to quarkonia. With the wealth of high-precision quarkonium measurements to be carried out in the next decade, it is highly desirable to incorporate quarkonium physics into a common framework with other sub-fields in order to utilize the multi-messenger approach to study the properties of

the QGP. Such an integration could pave the way for extracting the novel chromoelectric field correlator for quarkonium from the anticipated high-precision results based on the Bayesian analysis.

### Heavy Flavor measurements

The current heavy flavor data sets are already responsible to rule out transport models and constrain medium parameters, examples are the nuclear PDFs shown in Figure 49 and the diffusion parameter in Figure 52. Detector upgrades and higher luminosity heavy-ion collisions will enable new channels and tools for the understanding of cold and hot medium. A better understanding of heavy quark hadronization and how it recombines in hot medium is needed. More precise measurements of  $\Lambda_c$  and  $D_s$  are expected at RHIC and LHC. Charm hadron spectroscopy, as explored by ALICE in p+p collisions [968], is going to be extended to p+A and A+A collisions at LHC. The ALICE/ITS upgrade [1277] is dedicated to heavy flavor measurements with the goal to access D-hadrons at rest. LHCb is already able to perform heavy flavor spectroscopy as part of its core flavor physics program. The current upgrade will enable LHCb to take more central Pb+Pb events and its new fixed target program will explore p+A and A+A collisions at  $\sqrt{s_{NN}} \sim 40 - 115$  GeV/c, expecting to measure 150M  $D^0$ s and 1.5M  $\Lambda_c$ s per year of operation [1275]. More exotic charm hadrons as expected to be seen for the first time in heavy-ion collisions.

The b-quark hadronization is nearly unexplored experimentally. More abundant and precise B-meson measurements will be seen with the upgraded luminosities at LHC. The CMS experiment expects integrated luminosity of 5-10 nb<sup>-1</sup> in Pb+Pb during LHC Run3, a factor 3-5 increase from the current integrated luminosity. B-meson flow and top production in Pb+Pb can be explored at different  $p_T$  and event centralities. The upcoming high luminosity RHIC operation will also enable the exploration of b hadrons by STAR and sPHENIX. A silicon detector similar to the one used in ALICE has been installed in sPHENIX which will enable its b-hadron physics as one of its pillars [1278].

The separation of initial and final state effects is still an experimental and theoretical challenge for the use of heavy flavor for QGP tomography. High statistics can also allow more measurements of heavy flavor correlation with hadrons, jets and direct photons in different event plane configurations. This kind of analysis are very sensitive to in-medium effects and pose a very good suppression of effects caused by nuclear medium before the hard scattering.

Finally, the coming years will also be a preparation for the next decade heavy-ion program. Technical Design Reports and Letter of Intent have been prepared for LHC Run4,5 with specific proposals for heavy-ion physics. CMS plans for a MIP time of flight detector which will bring particle identification for CMS [1279] reducing the large combinatorial backgrounds CMS faces when dealing with HF decays. LHCb will continue pushing for a detector able to measure very central Pb+Pb collisions with better segmentation and timing capabilities and explore HF states with a difficult access to zero  $p_T$ , such as  $D^*$ , in its Upgrade2 program [1167]. The new-generation heavy-ion experiment proposed by the ALICE collaboration, ALICE 3, will be based on fast silicon trackers to enable the full luminosity that LHC can provide, full range particle identification and extend the acceptance for HF decays to  $p_T \sim 0$  and rapidity coverage to  $\eta \sim 4$  [6].

### Heavy flavor and quarkonia theory developments

The theoretical progress in our understanding of heavy quark and quarkonium dynamics inside the QGP was discussed in Section 3.4.3. The key transport and thermodynamic properties of the QGP that can be probed by measuring heavy quark and quarkonium production in heavy-ion collisions are chromoelectric field correlators that are defined gauge-invariantly and nonperturbatively. The correlator for single heavy quark diffusion is different from that for quarkonium at low temperatures. Nonperturbative determination of the novel chromoelectric field correlator for quarkonium is an important theoretical question that should be addressed in the next Long Range Plan, which has never been done. Both the Euclidean lattice QCD and AdS/CFT methods can be utilized to learn some aspects of this correlator at both zero and finite frequencies. Beyond these nonperturbative methods, one may investigate calculating this correlator by using real-time

field theory simulation on a quantum computer in the next Long Range Plan. Besides direct theoretical calculations, we can also use Bayesian analysis to extract this correlator from experimental data. The data at the RHIC energy is of particular importance in our extraction of the finite frequency dependence of the chromoelectric field correlator, since at the RHIC energy the low temperature regime of the QGP is more important. A good Bayesian extraction requires experimental data in a wide kinetic range with high precision, as well as solid theoretical calculations that have as little model dependence as possible. Current application of nonrelativistic effective field theories of QCD and the open quantum system framework is only applicable to quarkonium production at low  $p_T$ . How to generalize the framework to study quarkonium production at intermediate  $p_T$  should be explored in the next Long Range Plan. Quantum computing [1128, 1130] and machine learning techniques should be investigated to speed up solving the Lindblad equation in the Brownian motion limit, which would be necessary if we want to study charmonium production in the open quantum system framework. The nPDF uncertainty is another big factor that can influence the Bayesian analysis, which we want to reduce as much as possible. Also, the nPDF uncertainty is small in observables like  $R_{AA}$  ratios of different quarkonium states. The nonperturbative determination of the novel correlator for quarkonium in the next Long Range Plan would be a joint effort between the theory, computation and experiment communities and it will involve not only the quarkonium community but also many other subfields of the heavy-ion and nuclear physics.

On the lattice side, the calculations of bottomonium properties and the complex potential have been performed on  $N_\tau = 12$  lattices. To better constrain the spectral functions one clearly needs calculations with larger  $N_\tau$ . As discussed above all calculations of the heavy quark diffusion coefficient have been performed in quenched approximation. The use of the recently developed gradient flow approach developed for this problem [848] will allow performing the calculations in QCD with physical quark masses. In addition to the heavy quark diffusion, which is encoded in the chromo-electric correlator with the Wilson lines in the fundamental representation it is important to study the chromo-electric correlation function with the adjoint Wilson line. As discussed above, this correlation function encodes the transport properties of quarkonia. The lattice calculation of this correlation function also needs lattices with a large temporal extent. The calculations with larger  $N_\tau$  and physical quark masses will require the use of exascale computing resources, which are allocated through ALCC and INCITE programs. To take advantage of the exascale resources existing lattice QCD codes have to be adapted to the ever-changing computational hardware. This will require funding from programs like SciDAC, which will support the workforce development of computational nuclear physicists and sustain this workforce needs in the long run. The lattice calculations with larger  $N_\tau$  will not be limited to the calculations of bottomonium properties at non-zero temperature, the complex  $Q\bar{Q}$  potential, and the heavy quark diffusion coefficient. With small additional computational investments and the use of extended meson operators, one would be able to access the in-medium properties of open heavy-flavor hadrons as well as of charmonia. The availability of lattices with larger  $N_\tau$  will also benefit the study of charm fluctuations and charm baryon number correlations, allowing to fully control the discretization effects and provide more first principle QCD information on the charm production in A+A collisions. Furthermore, these lattices will be also used in the study of spatial bottomonium correlation functions and refine the estimates of the bottomonium melting temperatures.

At high virtualities, the SCET formalism developed by [653] should be extended to obtain the heavy flavor pair production rate of  $g \rightarrow Q + \bar{Q}$ , while that SCET formalism should be combined with the  $\hat{q}(Q^2)$  calculation in Ref. [619] to provide a  $\hat{q}(M, Q^2)$ . At lower virtualities, an important extension to light flavor HTL-resummed AMY rates has been to consider finite-size effects. This has been achieved [1280] using Zakharov's light-cone path integral formalism [608, 651], thus bridging the gap between infinite-sized medium result assumed by AMY and a finite-sized medium in the opacity expansion by Gyulassy-Levai-Vitev (GLV) [706]. Finite-size effects of low-virtuality interactions between light flavor and the QGP are included within the Modular Algorithm for Relativistic Treatment of heavy IoN Interactions (MARTINI)

Monte Carlo event generator [1281]. A natural continuation is to formally combine finite-size effects [1280] within the heavy flavor calculation of Ref. [656]. Some progress in that direction, combining elements of formal treatment with phenomenological input, is explored in Ref. [705].

Drawing on the expertise of leading scientists in the U.S., the new nuclear theory topical collaboration, HEFTY will tackle challenges in describing heavy flavor quarks in QCD matter. More specifically, the HEFTY collaboration aims to develop a comprehensive theoretical framework encompassing the evolution of heavy flavor from the initial production of heavy quarks in the early stages of the collisions, to their diffusion through the QGP as well as the hadronization process resulting in final-state heavy-flavor particles.

### **Future Prospectives with Exotic Hadrons**

The only exotic hadron measured in heavy-ion collisions to date is the X(3872), which is generally considered to consist of a charm-anticharm pair and a quark-antiquark pair,  $c\bar{c}q\bar{q}$ . Statistical hadronization models expect the recently discovered  $T_{cc}^+$  hadron [1282], which is consistent with a tetraquark of the form  $cc\bar{q}\bar{q}$ , to be produced at nearly the same rate as X(3872), representing a huge enhancement due to recombination [1283]. Production of the "fully-charmed"  $c\bar{c}c\bar{c}$  tetraquarks is also expected to be dramatically enhanced in Pb+Pb collisions [1284], and measurements would provide significant new constraints on models of charm quark hadronization. There is also potential for measuring exotic states produced via interactions with photons in ultra-peripheral collisions [1285], which may be relevant for constraining projections of exotic hadron production at the forthcoming EIC.

The data on exotic hadron production in heavy-ion collisions remains limited by significant uncertainties. However, all experiments at the LHC are pursuing relevant upgrades that will enable future measurements. The recent upgrade to the ALICE TPC readout will enable significantly higher luminosity to be recorded, aiding measurements of relatively rare exotic states. The CMS collaboration is pursuing the addition of particle ID with precision time-of-flight measurements and a large acceptance tracking system up to  $|\eta| < 4$ . Those upgrades will help reduce combinatorial backgrounds and increase the acceptance when reconstructing exotic hadron decays. The LHCb experiment recently upgraded the entire tracking system, enabling measurements up to  $\sim 30\%$  centrality in Pb+Pb collisions. A major upgrade to the LHCb fixed-target system will enable high-statistics p+A measurements at center-of-mass energies near  $\sim 100$  GeV, where the charm cross-section is relatively small and potential effects of  $D$  meson recombination into hadronic molecules will be small. In the further future, the ALICE3 and LHCb Upgrade II detectors will have full particle ID, precision vertexing, and fast DAQ systems, and will be well-suited for measurements of X(3872) and other exotic hadrons in central Pb+Pb collisions. Future measurements of femtoscopic correlations between components of hadronic molecules may also yield new information on the size and masses of exotic molecular bound states. There is also no theoretical consensus on describing exotic production in heavy-ion collisions. However, as current research into exotic hadrons is largely driven by experiments, significant developments on the theoretical front can also be accomplished as more constraining data becomes available in the future.

### **5.3.3 Prospective measurements and theoretical advances related to initial state nPDFs**

#### **Electroweak probes**

All the processes described in Section 3.4.5 are rare probes and thus directly benefit from increases in luminosity. In addition, the dominant uncertainties in some channels are evaluated using data-driven methods (e.g. photon purities), and thus larger luminosities also confer reduced systematic uncertainties as well. At the LHC [1054], approximately  $13 \text{ nb}^{-1}$  of Pb+Pb and  $1200 \text{ nb}^{-1}$  of p+Pb data may be collected by ATLAS and CMS in Runs 3 and 4, representing increases by a factor of six to seven over that available in Runs 1 and 2. At the same time, measurements by ALICE and LHCb will provide measurements in a complementary kinematic range (such as at low photon- $p_T$  or forward rapidity for heavy bosons).

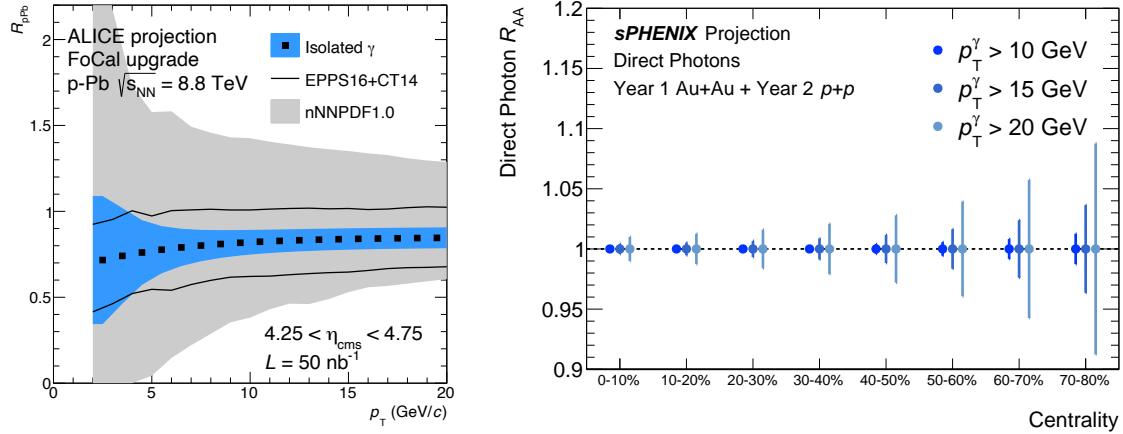


Figure 69: Left: Projected uncertainties for a measurement of the  $R_{pPb}$  for forward photons with the ALICE FoCal, compared to the existing theoretical uncertainties [1286, 1287]. Right: Projected statistical uncertainties for a measurement of the  $R_{AA}$  for direct photons in sPHENIX as a function of centrality, using only Year-1 (2023) and Year-2 (2024) data.

The larger luminosity and improved detector capabilities may also allow access to new channels entirely, such as measurements of isolated di-photons in  $p$ +Pb collisions (produced dominantly via a quark box diagram and thus sensitive to gluon densities), forward photons with the ALICE FoCal [1120] (probing very low nuclear- $x$ , shown in the left panel of Figure 69), hadronic  $W$  decays, and multi-differential measurements such as photons in coincidence with leading jets [1288] (to better constrain the initial-state kinematics).

In the LHC Run 5, collisions of light ions with high luminosity would result in an enormous yield of electroweak probes for study. The smaller underlying event will also result in significantly improved systematic uncertainties, giving extraordinarily precise constraints on nPDFs in these systems. In fact, such constraints are expected to be necessary as the kinematic reach for jet probes will push far into the large- $x$  region, where the EMC effect is appreciable.

Finally, measurements of high- $p_T$  direct photons are expected to be a flagship of the physics program of the sPHENIX experiment at RHIC, which will have its commissioning run in 2023. These are enabled by the large acceptance, high rate, effective triggering, and excellent energy resolution of the sPHENIX EMCal. sPHENIX will use direct photons for photon-tagged jet energy loss measurements, nPDF measurements, and as an early check of the centrality calibration (right panel of Figure 69).

### Future studies with ultra-peripheral collisions

*Resolving photon energy ambiguities based on ZDC neutrons* Due to the independent QED process of Coulomb excitation, different impact parameter of the two colliding nuclei would have a different probability of producing evaporated neutrons. By combining the ZDC neutron categories for a given rapidity of VM, the cross section of  $\gamma^* + A \rightarrow VM + A'$  can be obtained for both low- and high-energy photon configuration separately. This experimental technique can extend the kinematic reach down to  $x \sim 10^{-5}$  or up to  $x \sim 10^{-1}$ . Based on Ref. [1289], the photon-nucleus cross section corresponding to photon energy  $k_1$  and  $k_2$  can be related to the photon flux as follows,

$$d\sigma^{BnCn}/dy = \Phi_{T,\gamma}^{BnCn}(k_1)\sigma_{\gamma^*+A \rightarrow J/\psi+A}(k_1) + \Phi_{T,\gamma}^{BnCn}(k_2)\sigma_{\gamma^*+A \rightarrow J/\psi+A}(k_2) \quad (35)$$

where  $\Phi_{T,\gamma}^{BnCn}$  is the average transversely polarized photon flux emitted from the A nucleus at the average rapidity in the selected  $y$  interval; the superscript  $BnCn$  corresponds to the neutron emission class such

that  $B$  and  $C$  can be 0 or  $X$ . Therefore, with three independent equations of  $0n0n$ ,  $0nXn$ , and  $XnXn$ , the coherent cross section at photon energy  $k_1$  and  $k_2$  can be obtained (only two independent equations are needed to solve two unknowns, but three provides additional constraints on the result). Note that this method only applies to coherent  $J/\psi$  photoproduction. Without the photon energy ambiguities, the kinematic reach in Bjorken- $x$  can be extended to much lower and the energy  $W_{\gamma^*N}$  dependence can be directly obtained. This is an economic way to go to small- $x$  in UPCs.

*UPC  $\phi$  photoproduction* Measuring  $\phi$  photoproduction has been challenging in UPCs mostly due to its soft decay to two kaons: the daughter kaons have an average of  $\sim 100$  MeV/ $c$  in transverse momentum, where tracking at such low  $p_T$  is already difficult and triggering UPC  $\phi$  meson decay requires fast detector, e.g., calorimeter or Time-of-Flight system, that are sitting far away from the vertex. Therefore, the soft kaons do not have enough momentum to reach these fast detectors. This is the same for LHC experiments as well as for the RHIC STAR experiment. Recently, one possible solution has been proposed, given the larger cross section of  $\phi$  than  $J/\psi$  and the high luminosity of the accelerator machine, one can reconstruct  $\phi$  from zero-bias or ZDC-based triggers only, without the requirement of fast detectors in the barrel. This new development in the trigger may provide a unique opportunity in studying photoproduction of  $\phi$ . In addition, although the EIC is the ultimate machine and experiment for exclusive production, photoproduction of  $\phi$  can be equally if not more difficult than that in UPCs. This measurement in UPCs at RHIC and at the LHC are truly complementary to  $\phi$  measurements at the EIC in terms of the energy and virtuality coverage [1290].

*Jet/high- $p_T$  particle and VM photoproduction double ratio measurement* Inspired by the EIC White Paper [1063], one of the most important day-one measurements is to obtain the relative fraction of diffractive DIS over the inclusive DIS cross section in both  $eA$  and  $ep$  collisions. It was discovered at the  $ep$  collider HERA that about  $\sim 12 - 15\%$  of the inclusive DIS cross section is diffractive. At the EIC, the most direct observation of gluon saturation predicted by the color glass condensate model is that this ratio will be enhanced in  $eA$  than in  $ep$ ; in other words, diffractive DIS cross section would be larger than  $\sim 12 - 15\%$  of the inclusive DIS cross section in  $eA$  collisions. However, the other major paradigm, as discussed earlier in Section 3.4.6.1, is the nuclear shadowing model, which predicts qualitatively the opposite. In the Leading Twist Approximation, the diffractive DIS cross section is expected to be less in  $eA$  than in  $ep$ . Therefore, this measurement becomes one of the best experimental tools to test the two models.

This measurement requires high-energy  $ep$  and  $eA$  collisions with significant photon virtuality  $Q^2$  at the EIC, which makes this impossible in UPCs. However, a similar observable might be possible in UPCs. Although the scale set by the photon virtuality in UPCs at the event level is small, the scale could be set by the mass or transverse momentum of the particle instead, e.g., the  $J/\psi$  and/or a high- $p_T$  particle. Exclusive  $J/\psi$  photoproduction is a diffractive process, while photoproduction of single high- $p_T$  particle or jet is an inclusive process. The ratio between them captures the key element of diffractive process over inclusive process, where the two models differ qualitatively. Therefore, a double ratio observable,  $R_R$ , in UPCs measurements can be roughly written as follows,

$$R_R = \frac{\sigma_{J/\psi}^{\text{exclusive}} / \sigma_{\text{jet,high-}p_T}^{\text{inclusive}} |_A}{\sigma_{J/\psi}^{\text{exclusive}} / \sigma_{\text{jet,high-}p_T}^{\text{inclusive}} |_P}. \quad (36)$$

Here the  $\sigma_{J/\psi}^{\text{exclusive}}$  in heavy nuclei and proton have been measured by various experiments, while  $\sigma_{\text{jet,high-}p_T}^{\text{inclusive}}$  has not yet been done. Theoretical predictions behind this observable in UPC events are being developed. This measurement might be the first rigorous experimental test to the saturation and nuclear shadowing model in UPCs. In addition, utilizing the wide kinematic reach from RHIC to the LHC could significantly advance our understanding of nuclear modification of the gluon densities in nuclei.

*Vector meson photoproduction using the FoCal detector at ALICE* For Run 4 at the LHC (2029–2032), the ALICE experiment will have in operation the FoCal detector [1120]. FoCal is a high-granularity, com-

pact silicon-tungsten (Si+W) sampling electromagnetic calorimeter with longitudinal segmentation backed by a conventional high granularity metal and scintillating hadronic calorimeter. While FoCal has been designed for measuring direct photons at forward rapidity with high precision in p+p and p+Pb collisions [1120], the study of UPCs is also an integral part of the FoCal physics program, as reported in [1291]. In particular, the future measurements of the energy dependence of  $\sigma(\gamma p)$  and  $\sigma(\gamma Pb)$  for the photoproduction of vector mesons using the FoCal detector should provide a clear signature of gluon saturation, probing nuclear gluon shadowing, and confronting several theoretical approaches. Here, we highlight two measurements in  $\gamma p$  interactions discussed in Ref. [1291] (see this reference for other high-profile UPC measurements with FoCal). As mentioned above, results from HERA showed that the photoproduction cross section,  $\sigma(\gamma p \rightarrow J/\psi p)$ , increases with center-of-mass energy following a power law. The result from ALICE [1067, 1068], extending down to  $x \sim 10^{-5}$ , showed no deviation from this behavior, although the uncertainties are large. The FoCal detector will provide access to an unexplored kinematic regime at small- $x$  where a different trend in the growth of the cross section might occur. At high energies, there are three non-linear QCD model predictions, namely, the Hot Spot model (CCT) [1292], the NLO BFKL [1293] and the CGC-based calculations [1294]. To illustrate the prospects of observing saturation effects with FoCal, the projection of the energy dependence  $J/\psi$  photoproduction cross section in the FoCal acceptance was obtained using the NLO BFKL model [1293], as it is shown in Ref. [1291]. Similarly, if saturation occurs, the future FoCal UPC measurements would provide the first potential observation that the cross section of  $J/\psi$  deviates from a power-law energy dependence at high energies.

In addition, as discussed earlier, the dissociative process has received recent interest [80, 1292, 1295]. The FoCal data are uniquely positioned to probe the fluctuations of the proton target configurations for gluonic saturated matter. The observation of a significant reduction of the measured cross section as energy increases will provide a clear signature of gluon saturation at high energies. Specifically, it will be clear to measure the ratio of dissociative-to-exclusive  $J/\psi$  photoproduction as a function of  $W_{\gamma p}$ , including the H1 data [1296] and ALICE preliminary data, and comparisons to the BM and CCT predictions. See Ref. [1291] The FoCal projected points shown use the STARlight yield for the exclusive process, and the BM model prediction for the dissociative process.

*QED* ( $\gamma\gamma \rightarrow l^+l^-$ ) QED studies, e.g., with polarized photons, have been used and proposed as a tool to test and define the photon Wigner function [1084, 1086, 1087, 1297–1300], to probe the properties of the Quark-Gluon Plasma [1, 1081–1083, 1301–1303], to measure nuclear charge and mass radii [1090, 1119, 1301, 1304], to study gluon structure inside nuclei [1305–1307] and to investigate new quantum effects [1076, 1094, 1119, 1306, 1308, 1309]. Both RHIC and the LHC plan future data collection that will allow high precision multi-differential analysis of these  $\gamma\gamma$  processes [1310, 1311]. Future measurements at STAR are expected to provide significantly higher precision measurements of the  $e^+e^-$  transverse momentum spectra and the  $\cos 4\phi$  modulation. Additionally, multi-differential measurements, such as the  $\cos 4\phi$  modulation strength versus pair  $p_T$ , will be possible. The increased precision on the pair  $p_T$  will provide additional constraining power to investigate the proposed final-state broadening effects. In addition to their effect on the  $p_T$  spectra, final state interactions would wash out the  $\cos 4\phi$  modulation strength that results from the initial colliding photon polarization. The predicted future precision could be achieved for the  $p_T$  and  $\cos 4\phi$  modulation measurements in future STAR analyses. The added precision in the  $\cos 4\phi$  modulation measurement is expected to allow experimental verification of impact parameter dependence predicted by the lowest order QED calculations (and therefore further test the  $k_\perp$ -factorization plus TMD treatment of the photon polarization [1312, 1313]). The future data taking campaigns planned for the LHC experiments will also allow improved measurements from ALICE of the  $\gamma\gamma \rightarrow e^+e^-$  process in a similar region of phase space as measured at RHIC, but in collisions with a much larger Lorentz-boost factor. Such measurements will provide further constraints on the treatment of the photon kinematic distributions over a range of photon energies. Similarly, future data taking and analyses by CMS and ATLAS [1089, 1311]



will allow additional precision measurements of the  $\gamma\gamma \rightarrow \mu^+\mu^-$  process in events with hadronic overlap, possibly shedding light on the presence (or lack) of medium induced modifications via differential measurements of the produced dilepton kinematics.

*The role of the ALICE 3 detector* Looking further ahead, by the mid/late 2030s, the proposed ALICE 3 detector [6] will have acceptance for both charged and neutral particles, over a very wide solid angle, with coverage expected for pseudorapidity  $|\eta| < 4$ . This will offer a very large increase in acceptance for more complex UPC final states. Upgrades from other LHC experiments will also significantly benefit the UPC program.

## 6 Summary

This document highlights the tremendous progress made, since the 2015 Long Range Plan in Nuclear Science, in understanding the properties of the quark-gluon plasma and how it develops in heavy-ion collisions from the microscopic to macroscopic level. The previous section on future prospects also illustrates the potential for future scientific discoveries and developments related to hot QCD, much of which is within our grasp in the coming decade. However, realization of these relies on support for the following:

- Successful operation of RHIC for the sPHENIX detector to fully achieve the scientific goals described in the previous Long Range Plan.
- Continued leadership and upgrades for the LHC experiments to study high temperature QGP.
- A thriving theory community to advance our description of QCD.
- Theory and experimental collaborations to develop tools such as Bayesian inference, which utilize the full suite of experimental data in extracting key quantities such as viscosity and the transport coefficients as well as furthering the interpretations of the experimental results.
- The computing resources needed and novel approaches such as machine learning to overcome the difficulties in addressing the most challenging questions in the field.
- A vibrant workforce to carry out the analysis of the wealth of experimental data collected including from BES-II.
- Programs enhancing the participation of underrepresented minorities in nuclear physics, which will enhance our ability to recruit the workforce needed to accomplish these goals in the next decade.

With the start of sPHENIX operations concurrently with those of the upgraded STAR detector at RHIC and the increased luminosity at the LHC, there is much to explore experimentally in the next decade, while there are also many opportunities to advance our theoretical understanding of hot QCD. This document highlights the accomplishments as well as open questions in describing heavy-ion collisions from the initial state, to collectivity and thermalization to penetrating probes as well as the interplay between these. The next decade will further advance our understanding of hot QCD matter and propel us toward a more complete description of nuclear matter under extreme conditions as well as the evolution of heavy-ion collisions.

## Bibliography

- [1] X. An *et al.*, “The BEST framework for the search for the QCD critical point and the chiral magnetic effect,” *Nucl. Phys. A*, vol. 1017, p. 122343, 2022, arXiv:2108.13867.
- [2] J. H. Putschke *et al.*, “The JETSCAPE framework,” 3 2019, arXiv:1903.07706.
- [3] D. R. Phillips *et al.*, “Get on the BAND Wagon: A Bayesian Framework for Quantifying Model Uncertainties in Nuclear Dynamics,” *J. Phys. G*, vol. 48, no. 7, p. 072001, 2021, arXiv:2012.07704.
- [4] sPHENIX Collaboration, “sPHENIX Beam Use Proposal,” 2022.
- [5] S. Collaboration, “The STAR Beam Use Request for Run-23-25,” 2022.
- [6] ALICE Collaboration, “Letter of intent for ALICE 3: A next-generation heavy-ion experiment at the LHC,” 11 2022, arXiv:2211.02491.
- [7] “Computational Nuclear Physics and AI/ML Workshop.” <https://indico.jlab.org/event/581/timetable/>.
- [8] A. Lovato *et al.*, “Long Range Plan: Dense matter theory for heavy-ion collisions and neutron stars,” 11 2022, arXiv:2211.02224.
- [9] A. Sorensen *et al.*, “Dense Nuclear Matter Equation of State from Heavy-Ion Collisions,” 1 2023, arXiv:2301.13253.
- [10] D. Almaalol *et al.*, “QCD Phase Structure and Interactions at High Baryon Density: Completion of BES Physics Program with CBM at FAIR,” 9 2022, arXiv:2209.05009.
- [11] M. Luzum and H. Petersen, “Initial State Fluctuations and Final State Correlations in Relativistic Heavy-Ion Collisions,” *J. Phys. G*, vol. 41, p. 063102, 2014, arXiv:1312.5503.
- [12] U. Heinz and R. Snellings, “Collective flow and viscosity in relativistic heavy-ion collisions,” *Ann. Rev. Nucl. Part. Sci.*, vol. 63, pp. 123–151, 2013, arXiv:1301.2826.
- [13] R. Derradi de Souza, T. Koide, and T. Kodama, “Hydrodynamic Approaches in Relativistic Heavy Ion Reactions,” *Prog. Part. Nucl. Phys.*, vol. 86, pp. 35–85, 2016, arXiv:1506.03863.
- [14] S. H. Lim, J. Carlson, C. Loizides, D. Lonardonì, J. E. Lynn, J. L. Nagle, J. D. Orjuela Koop, and J. Ouellette, “Exploring New Small System Geometries in Heavy Ion Collisions,” *Phys. Rev. C*, vol. 99, no. 4, p. 044904, 2019, arXiv:1812.08096.
- [15] N. Summerfield, B.-N. Lu, C. Plumberg, D. Lee, J. Noronha-Hostler, and A. Timmins, “ $^{16}\text{O}$   $^{16}\text{O}$  collisions at energies available at the BNL Relativistic Heavy Ion Collider and at the CERN Large Hadron Collider comparing  $\alpha$  clustering versus substructure,” *Phys. Rev. C*, vol. 104, no. 4, p. L041901, 2021, arXiv:2103.03345.
- [16] B. Bally, M. Bender, G. Giacalone, and V. Somà, “Evidence of the triaxial structure of  $^{129}\text{Xe}$  at the Large Hadron Collider,” *Phys. Rev. Lett.*, vol. 128, no. 8, p. 082301, 2022, arXiv:2108.09578.
- [17] G. Giacalone, J. Jia, and C. Zhang, “Impact of Nuclear Deformation on Relativistic Heavy-Ion Collisions: Assessing Consistency in Nuclear Physics across Energy Scales,” *Phys. Rev. Lett.*, vol. 127, no. 24, p. 242301, 2021, arXiv:2105.01638.
- [18] B. Bally *et al.*, “Imaging the initial condition of heavy-ion collisions and nuclear structure across the nuclide chart,” 9 2022, arXiv:2209.11042.
- [19] E. R. Most, S. P. Harris, C. Plumberg, M. G. Alford, J. Noronha, J. Noronha-Hostler, F. Pretorius, H. Witek, and N. Yunes, “Projecting the likely importance of weak-interaction-driven bulk viscosity in neutron star mergers,” *Mon. Not. Roy. Astron. Soc.*, vol. 509, no. 1, pp. 1096–1108, 2021, arXiv:2107.05094.
- [20] E. R. Most, A. Haber, S. P. Harris, Z. Zhang, M. G. Alford, and J. Noronha, “Emergence of microphysical viscosity in binary neutron star post-merger dynamics,” 7 2022, arXiv:2207.00442.

- [21] M. Bluhm, J. Hou, and T. Schäfer, “Determination of the density and temperature dependence of the shear viscosity of a unitary Fermi gas based on hydrodynamic flow,” *Phys. Rev. Lett.*, vol. 119, no. 6, p. 065302, 2017, arXiv:1704.03720.
- [22] S. Floerchinger, G. Giacalone, L. H. Heyen, and L. Tharwat, “Qualifying collective behavior in expanding ultracold gases as a function of particle number,” *Phys. Rev. C*, vol. 105, no. 4, p. 044908, 2022.
- [23] J. E. Bernhard, J. S. Moreland, and S. A. Bass, “Bayesian estimation of the specific shear and bulk viscosity of quark–gluon plasma,” *Nature Phys.*, vol. 15, no. 11, pp. 1113–1117, 2019.
- [24] F. G. Gardim, J. Noronha-Hostler, M. Luzum, and F. Grassi, “Effects of viscosity on the mapping of initial to final state in heavy ion collisions,” *Phys. Rev. C*, vol. 91, no. 3, p. 034902, 2015, arXiv:1411.2574.
- [25] L. Yan and J.-Y. Ollitrault, “Universal fluctuation-driven eccentricities in proton-proton, proton-nucleus and nucleus-nucleus collisions,” *Phys. Rev. Lett.*, vol. 112, p. 082301, 2014, arXiv:1312.6555.
- [26] G. Giacalone, J. Noronha-Hostler, and J.-Y. Ollitrault, “Relative flow fluctuations as a probe of initial state fluctuations,” *Phys. Rev. C*, vol. 95, no. 5, p. 054910, 2017, arXiv:1702.01730.
- [27] J. Noronha-Hostler, L. Yan, F. G. Gardim, and J.-Y. Ollitrault, “Linear and cubic response to the initial eccentricity in heavy-ion collisions,” *Phys. Rev. C*, vol. 93, no. 1, p. 014909, 2016, arXiv:1511.03896.
- [28] S. Rao, M. Sievert, and J. Noronha-Hostler, “Baseline predictions of elliptic flow and fluctuations for the RHIC Beam Energy Scan using response coefficients,” *Phys. Rev. C*, vol. 103, no. 3, p. 034910, 2021, arXiv:1910.03677.
- [29] M. D. Sievert and J. Noronha-Hostler, “CERN Large Hadron Collider system size scan predictions for PbPb, XeXe, ArAr, and OO with relativistic hydrodynamics,” *Phys. Rev. C*, vol. 100, no. 2, p. 024904, 2019, arXiv:1901.01319.
- [30] B. Schenke, C. Shen, and P. Tribedy, “Hybrid Color Glass Condensate and hydrodynamic description of the Relativistic Heavy Ion Collider small system scan,” *Phys. Lett. B*, vol. 803, p. 135322, 2020, arXiv:1908.06212.
- [31] J. S. Moreland, J. E. Bernhard, and S. A. Bass, “Alternative ansatz to wounded nucleon and binary collision scaling in high-energy nuclear collisions,” *Phys. Rev. C*, vol. 92, no. 1, p. 011901, 2015, arXiv:1412.4708.
- [32] B. Schenke, P. Tribedy, and R. Venugopalan, “Fluctuating Glasma initial conditions and flow in heavy ion collisions,” *Phys. Rev. Lett.*, vol. 108, p. 252301, 2012, arXiv:1202.6646.
- [33] C. Chiu and C. Shen, “Exploring theoretical uncertainties in the hydrodynamic description of relativistic heavy-ion collisions,” *Phys. Rev. C*, vol. 103, no. 6, p. 064901, 2021, arXiv:2103.09848.
- [34] C. Plumberg, D. Almaalol, T. Dore, J. Noronha, and J. Noronha-Hostler, “Causality violations in realistic simulations of heavy-ion collisions,” *Phys. Rev. C*, vol. 105, no. 6, p. L061901, 2022, arXiv:2103.15889.
- [35] M. Strickland, “Thermalization and isotropization in heavy-ion collisions,” *Pramana*, vol. 84, no. 5, pp. 671–684, 2015, arXiv:1312.2285.
- [36] P. Bozek, “Bulk and shear viscosities of matter created in relativistic heavy-ion collisions,” *Phys. Rev. C*, vol. 81, p. 034909, 2010, arXiv:0911.2397.
- [37] I. Karpenko, P. Huovinen, and M. Bleicher, “A 3+1 dimensional viscous hydrodynamic code for relativistic heavy ion collisions,” *Comput. Phys. Commun.*, vol. 185, pp. 3016–3027, 2014, arXiv:1312.4160.

- [38] J. Noronha-Hostler, J. Noronha, and F. Grassi, “Bulk viscosity-driven suppression of shear viscosity effects on the flow harmonics at energies available at the BNL Relativistic Heavy Ion Collider,” *Phys. Rev. C*, vol. 90, no. 3, p. 034907, 2014, arXiv:1406.3333.
- [39] C. Shen, Z. Qiu, H. Song, J. Bernhard, S. Bass, and U. Heinz, “The iEBE-VISHNU code package for relativistic heavy-ion collisions,” *Comput. Phys. Commun.*, vol. 199, pp. 61–85, 2016, arXiv:1409.8164.
- [40] S. Ryu, J. F. Paquet, C. Shen, G. S. Denicol, B. Schenke, S. Jeon, and C. Gale, “Importance of the Bulk Viscosity of QCD in Ultrarelativistic Heavy-Ion Collisions,” *Phys. Rev. Lett.*, vol. 115, no. 13, p. 132301, 2015, arXiv:1502.01675.
- [41] R. D. Weller and P. Romatschke, “One fluid to rule them all: viscous hydrodynamic description of event-by-event central p+p, p+Pb and Pb+Pb collisions at  $\sqrt{s} = 5.02$  TeV,” *Phys. Lett. B*, vol. 774, pp. 351–356, 2017, arXiv:1701.07145.
- [42] K. Okamoto and C. Nonaka, “A new relativistic viscous hydrodynamics code and its application to the Kelvin–Helmholtz instability in high-energy heavy-ion collisions,” *Eur. Phys. J. C*, vol. 77, no. 6, p. 383, 2017, arXiv:1703.01473.
- [43] G. S. Denicol, C. Gale, S. Jeon, A. Monnai, B. Schenke, and C. Shen, “Net baryon diffusion in fluid dynamic simulations of relativistic heavy-ion collisions,” *Phys. Rev. C*, vol. 98, no. 3, p. 034916, 2018, arXiv:1804.10557.
- [44] L. Du and U. Heinz, “(3+1)-dimensional dissipative relativistic fluid dynamics at non-zero net baryon density,” *Comput. Phys. Commun.*, vol. 251, p. 107090, 2020, arXiv:1906.11181.
- [45] A. Monnai, “Dissipative Hydrodynamic Effects on Baryon Stopping,” *Phys. Rev. C*, vol. 86, p. 014908, 2012, arXiv:1204.4713.
- [46] J. A. Fotakis, M. Greif, C. Greiner, G. S. Denicol, and H. Niemi, “Diffusion processes involving multiple conserved charges: A study from kinetic theory and implications to the fluid-dynamical modeling of heavy ion collisions,” *Phys. Rev. D*, vol. 101, no. 7, p. 076007, 2020, arXiv:1912.09103.
- [47] A. Schäfer, I. Karpenko, X.-Y. Wu, J. Hammelmann, and H. Elfner, “Particle production in a hybrid approach for a beam energy scan of Au+Au/Pb+Pb collisions between  $\sqrt{s_{NN}} = 4.3$  GeV and  $\sqrt{s_{NN}} = 200.0$  GeV,” *Eur. Phys. J. A*, vol. 58, no. 11, p. 230, 2022, arXiv:2112.08724.
- [48] D. Almaalol, T. Dore, and J. Noronha-Hostler, “Stability of multi-component relativistic viscous hydrodynamics from Israel-Stewart and reproducing DNMR from maximizing the entropy,” 9 2022, arXiv:2209.11210.
- [49] G. S. Denicol, H. Niemi, E. Molnar, and D. H. Rischke, “Derivation of transient relativistic fluid dynamics from the Boltzmann equation,” *Phys. Rev. D*, vol. 85, p. 114047, 2012, arXiv:1202.4551. [Erratum: *Phys.Rev.D* 91, 039902 (2015)].
- [50] M. Troyer and U.-J. Wiese, “Computational complexity and fundamental limitations to fermionic quantum Monte Carlo simulations,” *Phys. Rev. Lett.*, vol. 94, p. 170201, 2005, arXiv:cond-mat/0408370.
- [51] J. Ghiglieri, G. D. Moore, and D. Teaney, “QCD Shear Viscosity at (almost) NLO,” *JHEP*, vol. 03, p. 179, 2018, arXiv:1802.09535.
- [52] I. Danhoni and G. D. Moore, “Hot and Dense QCD Shear Viscosity at Leading Log,” 12 2022, arXiv:2212.02325.
- [53] T. D. Cohen, H. Lamm, S. Lawrence, and Y. Yamauchi, “Quantum algorithms for transport coefficients in gauge theories,” *Phys. Rev. D*, vol. 104, no. 9, p. 094514, 2021, arXiv:2104.02024.
- [54] J. Grefa, M. Hippert, J. Noronha, J. Noronha-Hostler, I. Portillo, C. Ratti, and R. Rougemont, “Transport coefficients of the quark-gluon plasma at the critical point and across the first-order

- line,” *Phys. Rev. D*, vol. 106, no. 3, p. 034024, 2022, arXiv:2203.00139.
- [55] G. P. Kadam and H. Mishra, “Dissipative properties of hot and dense hadronic matter in an excluded-volume hadron resonance gas model,” *Phys. Rev. C*, vol. 92, no. 3, p. 035203, 2015, arXiv:1506.04613.
- [56] G. P. Kadam and H. Mishra, “Medium modification of hadron masses and the thermodynamics of the hadron resonance gas model,” *Phys. Rev. C*, vol. 93, no. 2, p. 025205, 2016, arXiv:1509.06998.
- [57] G. Kadam and S. Pawar, “Hadron resonance gas EoS and the fluidity of matter produced in HIC,” *Adv. High Energy Phys.*, vol. 2019, p. 6795041, 2019, arXiv:1802.01942.
- [58] R. K. Mohapatra, H. Mishra, S. Dash, and B. K. Nandi, “Transport coefficients of hadronic matter in a van der Waals hadron resonance gas model,” 1 2019, arXiv:1901.07238.
- [59] E. McLaughlin, J. Rose, T. Dore, P. Parotto, C. Ratti, and J. Noronha-Hostler, “Building a testable shear viscosity across the QCD phase diagram,” *Phys. Rev. C*, vol. 105, no. 2, p. 024903, 2022, arXiv:2103.02090.
- [60] J. B. Rose, J. M. Torres-Rincon, A. Schäfer, D. R. Oliinychenko, and H. Petersen, “Shear viscosity of a hadron gas and influence of resonance lifetimes on relaxation time,” *Phys. Rev. C*, vol. 97, no. 5, p. 055204, 2018, arXiv:1709.03826.
- [61] J. Rais, K. Gallmeister, and C. Greiner, “Shear viscosity to entropy density ratio of Hagedorn states,” *Phys. Rev. D*, vol. 102, no. 3, p. 036009, 2020, arXiv:1909.04522.
- [62] D. Sahu and R. Sahoo, “Thermodynamic and transport properties of matter formed in pp, p-Pb, Xe–Xe and Pb–Pb collisions at the Large Hadron Collider using color string percolation model,” *J. Phys. G*, vol. 48, no. 12, p. 125104, 2021, arXiv:2006.04185.
- [63] M. Heffernan, S. Jeon, and C. Gale, “Hadronic transport coefficients from the linear  $\sigma$  model at finite temperature,” *Phys. Rev. C*, vol. 102, no. 3, p. 034906, 2020, arXiv:2005.12793.
- [64] O. Soloveva, P. Moreau, and E. Bratkovskaya, “Transport coefficients for the hot quark-gluon plasma at finite chemical potential  $\mu_B$ ,” *Phys. Rev. C*, vol. 101, no. 4, p. 045203, 2020, arXiv:1911.08547.
- [65] V. Mykhaylova, M. Bluhm, K. Redlich, and C. Sasaki, “Quark-flavor dependence of the shear viscosity in a quasiparticle model,” *Phys. Rev. D*, vol. 100, no. 3, p. 034002, 2019, arXiv:1906.01697.
- [66] M. Haas, L. Fister, and J. M. Pawłowski, “Gluon spectral functions and transport coefficients in Yang–Mills theory,” *Phys. Rev. D*, vol. 90, p. 091501, 2014, arXiv:1308.4960.
- [67] N. Christiansen, M. Haas, J. M. Pawłowski, and N. Strodthoff, “Transport Coefficients in Yang–Mills Theory and QCD,” *Phys. Rev. Lett.*, vol. 115, no. 11, p. 112002, 2015, arXiv:1411.7986.
- [68] A. Dubla, S. Masciocchi, J. M. Pawłowski, B. Schenke, C. Shen, and J. Stachel, “Towards QCD-assisted hydrodynamics for heavy-ion collision phenomenology,” *Nucl. Phys. A*, vol. 979, pp. 251–264, 2018, arXiv:1805.02985.
- [69] J. Noronha-Hostler, J. Noronha, and C. Greiner, “Transport Coefficients of Hadronic Matter near  $T(c)$ ,” *Phys. Rev. Lett.*, vol. 103, p. 172302, 2009, arXiv:0811.1571.
- [70] F. Karsch, D. Kharzeev, and K. Tuchin, “Universal properties of bulk viscosity near the QCD phase transition,” *Phys. Lett. B*, vol. 663, pp. 217–221, 2008, arXiv:0711.0914.
- [71] P. Carzon, M. Martinez, M. D. Sievert, D. E. Wertepny, and J. Noronha-Hostler, “Monte Carlo event generator for initial conditions of conserved charges in nuclear geometry,” *Phys. Rev. C*, vol. 105, no. 3, p. 034908, 2022, arXiv:1911.12454.
- [72] F. Cooper and G. Frye, “Comment on the Single Particle Distribution in the Hydrodynamic and Statistical Thermodynamic Models of Multiparticle Production,” *Phys. Rev. D*, vol. 10, p. 186, 1974.
- [73] J. Weil *et al.*, “Particle production and equilibrium properties within a new hadron transport approach for heavy-ion collisions,” *Phys. Rev. C*, vol. 94, no. 5, p. 054905, 2016, arXiv:1606.06642.

- [74] M. Habich, J. L. Nagle, and P. Romatschke, “Particle spectra and HBT radii for simulated central nuclear collisions of C + C, Al + Al, Cu + Cu, Au + Au, and Pb + Pb from  $\sqrt{s} = 62.4 - 2760$  GeV,” *Eur. Phys. J. C*, vol. 75, no. 1, p. 15, 2015, arXiv:1409.0040.
- [75] C. Shen, J.-F. Paquet, G. S. Denicol, S. Jeon, and C. Gale, “Collectivity and electromagnetic radiation in small systems,” *Phys. Rev. C*, vol. 95, no. 1, p. 014906, 2017, arXiv:1609.02590.
- [76] C. Aidala *et al.*, “Creation of quark–gluon plasma droplets with three distinct geometries,” *Nature Phys.*, vol. 15, no. 3, pp. 214–220, 2019, arXiv:1805.02973.
- [77] J. Liu, C. Shen, and U. Heinz, “Pre-equilibrium evolution effects on heavy-ion collision observables,” *Phys. Rev. C*, vol. 91, no. 6, p. 064906, 2015, arXiv:1504.02160. [Erratum: *Phys.Rev.C* 92, 049904 (2015)].
- [78] A. Kurkela, A. Mazeliauskas, J.-F. Paquet, S. Schlichting, and D. Teaney, “Matching the Nonequilibrium Initial Stage of Heavy Ion Collisions to Hydrodynamics with QCD Kinetic Theory,” *Phys. Rev. Lett.*, vol. 122, no. 12, p. 122302, 2019, arXiv:1805.01604.
- [79] T. N. da Silva, D. D. Chinellato, A. V. Giannini, M. N. Ferreira, G. S. Denicol, M. Hippert, M. Luzum, J. Noronha, and J. Takahashi, “Pre-hydrodynamic evolution in large and small systems,” 11 2022, arXiv:2211.10561.
- [80] H. Mäntysaari and B. Schenke, “Evidence of strong proton shape fluctuations from incoherent diffraction,” *Phys. Rev. Lett.*, vol. 117, no. 5, p. 052301, 2016, arXiv:1603.04349.
- [81] J. S. Moreland, J. E. Bernhard, and S. A. Bass, “Bayesian calibration of a hybrid nuclear collision model using p-Pb and Pb-Pb data at energies available at the CERN Large Hadron Collider,” *Phys. Rev. C*, vol. 101, no. 2, p. 024911, 2020, arXiv:1808.02106.
- [82] G. Nijs and W. van der Schee, “Predictions and postdictions for relativistic lead and oxygen collisions with the computational simulation code Trajectum,” *Phys. Rev. C*, vol. 106, no. 4, p. 044903, 2022, arXiv:2110.13153.
- [83] Y. Kanakubo, Y. Tachibana, and T. Hirano, “Unified description of hadron yield ratios from dynamical core-corona initialization,” *Phys. Rev. C*, vol. 101, no. 2, p. 024912, 2020, arXiv:1910.10556.
- [84] Y. Kanakubo, Y. Tachibana, and T. Hirano, “Interplay between core and corona components in high-energy nuclear collisions,” *Phys. Rev. C*, vol. 105, no. 2, p. 024905, 2022, arXiv:2108.07943.
- [85] C. Shen and B. Schenke, “Dynamical initial state model for relativistic heavy-ion collisions,” *Phys. Rev. C*, vol. 97, no. 2, p. 024907, 2018, arXiv:1710.00881.
- [86] M. Nahrgang, M. Bluhm, T. Schaefer, and S. A. Bass, “Diffusive dynamics of critical fluctuations near the QCD critical point,” *Phys. Rev. D*, vol. 99, no. 11, p. 116015, 2019, arXiv:1804.05728.
- [87] K. Rajagopal, G. Ridgway, R. Weller, and Y. Yin, “Understanding the out-of-equilibrium dynamics near a critical point in the QCD phase diagram,” *Phys. Rev. D*, vol. 102, no. 9, p. 094025, 2020, arXiv:1908.08539.
- [88] X. An, G. Basar, M. Stephanov, and H.-U. Yee, “Relativistic Hydrodynamic Fluctuations,” *Phys. Rev. C*, vol. 100, no. 2, p. 024910, 2019, arXiv:1902.09517.
- [89] M. Nahrgang and M. Bluhm, “Modeling the diffusive dynamics of critical fluctuations near the QCD critical point,” *Phys. Rev. D*, vol. 102, no. 9, p. 094017, 2020, arXiv:2007.10371.
- [90] M. Bluhm *et al.*, “Dynamics of critical fluctuations: Theory – phenomenology – heavy-ion collisions,” *Nucl. Phys. A*, vol. 1003, p. 122016, 2020, arXiv:2001.08831.
- [91] X. An, G. Başar, M. Stephanov, and H.-U. Yee, “Evolution of Non-Gaussian Hydrodynamic Fluctuations,” *Phys. Rev. Lett.*, vol. 127, no. 7, p. 072301, 2021, arXiv:2009.10742.
- [92] M. Martinez, T. Schäfer, and V. Skokov, “Critical behavior of the bulk viscosity in QCD,” *Phys. Rev. D*, vol. 100, no. 7, p. 074017, 2019, arXiv:1906.11306.

- [93] L. Du, U. Heinz, K. Rajagopal, and Y. Yin, “Fluctuation dynamics near the QCD critical point,” *Phys. Rev. C*, vol. 102, no. 5, p. 054911, 2020, arXiv:2004.02719.
- [94] M. Pradeep, K. Rajagopal, M. Stephanov, and Y. Yin, “Freezing out fluctuations in Hydro+ near the QCD critical point,” *Phys. Rev. D*, vol. 106, no. 3, p. 036017, 2022, arXiv:2204.00639.
- [95] G. Pihan, M. Bluhm, M. Kitazawa, T. Sami, and M. Nahrgang, “Critical net-baryon fluctuations in an expanding system,” *Phys. Rev. C*, vol. 107, no. 1, p. 014908, 2023, arXiv:2205.12834.
- [96] T. Schaefer and V. Skokov, “Dynamics of non-Gaussian fluctuations in model A,” *Phys. Rev. D*, vol. 106, no. 1, p. 014006, 2022, arXiv:2204.02433.
- [97] X. An, G. Basar, M. Stephanov, and H.-U. Yee, “Non-Gaussian fluctuation dynamics in relativistic fluid,” 12 2022, arXiv:2212.14029.
- [98] M. Stephanov and Y. Yin, “Hydrodynamics with parametric slowing down and fluctuations near the critical point,” *Phys. Rev. D*, vol. 98, no. 3, p. 036006, 2018, arXiv:1712.10305.
- [99] L. Du, X. An, and U. Heinz, “Baryon transport and the QCD critical point,” *Phys. Rev. C*, vol. 104, no. 6, p. 064904, 2021, arXiv:2107.02302.
- [100] A. Monnai, S. Mukherjee, and Y. Yin, “Phenomenological Consequences of Enhanced Bulk Viscosity Near the QCD Critical Point,” *Phys. Rev. C*, vol. 95, no. 3, p. 034902, 2017, arXiv:1606.00771.
- [101] T. Dore, J. Noronha-Hostler, and E. McLaughlin, “Far-from-equilibrium search for the QCD critical point,” *Phys. Rev. D*, vol. 102, no. 7, p. 074017, 2020, arXiv:2007.15083.
- [102] T. Dore, J. M. Karthein, I. Long, D. Mroczek, J. Noronha-Hostler, P. Parotto, C. Ratti, and Y. Yamachi, “Critical lensing and kurtosis near a critical point in the QCD phase diagram in and out of equilibrium,” *Phys. Rev. D*, vol. 106, no. 9, p. 094024, 2022, arXiv:2207.04086.
- [103] A. Collaboration, “The ALICE experiment – A journey through QCD,” 11 2022, arXiv:2211.04384.
- [104] A. Adare *et al.*, “Measurements of directed, elliptic, and triangular flow in Cu+Au collisions at  $\sqrt{s_{NN}} = 200$  GeV,” *Phys. Rev. C*, vol. 94, no. 5, p. 054910, 2016, arXiv:1509.07784.
- [105] M. Abdallah *et al.*, “Azimuthal anisotropy measurements of strange and multistrange hadrons in  $U + U$  collisions at  $\sqrt{s_{NN}} = 193$  GeV at the BNL Relativistic Heavy Ion Collider,” *Phys. Rev. C*, vol. 103, no. 6, p. 064907, 2021, arXiv:2103.09451.
- [106] S. Acharya *et al.*, “Anisotropic flow of identified hadrons in Xe-Xe collisions at  $\sqrt{s_{NN}} = 5.44$  TeV,” *JHEP*, vol. 10, p. 152, 2021, arXiv:2107.10592.
- [107] A. Adare *et al.*, “Measurement of the higher-order anisotropic flow coefficients for identified hadrons in Au+Au collisions at  $\sqrt{s_{NN}} = 200$  GeV,” *Phys. Rev. C*, vol. 93, no. 5, p. 051902, 2016, arXiv:1412.1038.
- [108] S. Acharya *et al.*, “Anisotropic flow of identified particles in Pb-Pb collisions at  $\sqrt{s_{NN}} = 5.02$  TeV,” *JHEP*, vol. 09, p. 006, 2018, arXiv:1805.04390.
- [109] CMS Collaboration, “Strange hadron collectivity in pPb and PbPb collisions,” 4 2022, arXiv:2205.00080.
- [110] H. Niemi, G. S. Denicol, H. Holopainen, and P. Huovinen, “Event-by-event distributions of azimuthal asymmetries in ultrarelativistic heavy-ion collisions,” *Phys. Rev. C*, vol. 87, no. 5, p. 054901, 2013, arXiv:1212.1008.
- [111] A. Bilandzic, C. H. Christensen, K. Gulbrandsen, A. Hansen, and Y. Zhou, “Generic framework for anisotropic flow analyses with multiparticle azimuthal correlations,” *Phys. Rev. C*, vol. 89, no. 6, p. 064904, 2014, arXiv:1312.3572.
- [112] G. Aad *et al.*, “Measurement of the correlation between flow harmonics of different order in lead-lead collisions at  $\sqrt{s_{NN}} = 2.76$  TeV with the ATLAS detector,” *Phys. Rev. C*, vol. 92, no. 3, p. 034903, 2015, arXiv:1504.01289.



- [113] J. Qian and U. Heinz, “Hydrodynamic flow amplitude correlations in event-by-event fluctuating heavy-ion collisions,” *Phys. Rev. C*, vol. 94, no. 2, p. 024910, 2016, arXiv:1607.01732.
- [114] X. Zhu, Y. Zhou, H. Xu, and H. Song, “Correlations of flow harmonics in 2.76A TeV Pb–Pb collisions,” *Phys. Rev. C*, vol. 95, no. 4, p. 044902, 2017, arXiv:1608.05305.
- [115] G.-Y. Qin, H. Petersen, S. A. Bass, and B. Muller, “Translation of collision geometry fluctuations into momentum anisotropies in relativistic heavy-ion collisions,” *Phys. Rev. C*, vol. 82, p. 064903, 2010, arXiv:1009.1847.
- [116] Z. Qiu and U. W. Heinz, “Event-by-event shape and flow fluctuations of relativistic heavy-ion collision fireballs,” *Phys. Rev. C*, vol. 84, p. 024911, 2011, arXiv:1104.0650.
- [117] L. Yan and J.-Y. Ollitrault, “ $\nu_4, \nu_5, \nu_6, \nu_7$ : nonlinear hydrodynamic response versus LHC data,” *Phys. Lett. B*, vol. 744, pp. 82–87, 2015, arXiv:1502.02502.
- [118] P. F. Kolb, “ $v(4)$ : A Small, but sensitive observable for heavy ion collisions,” *Phys. Rev. C*, vol. 68, p. 031902, 2003, arXiv:nucl-th/0306081.
- [119] J. Adam *et al.*, “Correlated event-by-event fluctuations of flow harmonics in Pb-Pb collisions at  $\sqrt{s_{NN}} = 2.76$  TeV,” *Phys. Rev. Lett.*, vol. 117, p. 182301, 2016, arXiv:1604.07663.
- [120] S. Acharya *et al.*, “Systematic studies of correlations between different order flow harmonics in Pb-Pb collisions at  $\sqrt{s_{NN}} = 2.76$  TeV,” *Phys. Rev. C*, vol. 97, no. 2, p. 024906, 2018, arXiv:1709.01127.
- [121] H. Niemi, K. J. Eskola, and R. Paatelainen, “Event-by-event fluctuations in a perturbative QCD + saturation + hydrodynamics model: Determining QCD matter shear viscosity in ultrarelativistic heavy-ion collisions,” *Phys. Rev. C*, vol. 93, no. 2, p. 024907, 2016, arXiv:1505.02677.
- [122] G. Aad *et al.*, “Measurement of the correlation between flow harmonics of different order in lead-lead collisions at  $\sqrt{s_{NN}}=2.76$  TeV with the ATLAS detector,” *Phys. Rev. C*, vol. 92, no. 3, p. 034903, 2015, arXiv:1504.01289.
- [123] A. M. Sirunyan *et al.*, “Observation of Correlated Azimuthal Anisotropy Fourier Harmonics in  $pp$  and  $p + Pb$  Collisions at the LHC,” *Phys. Rev. Lett.*, vol. 120, no. 9, p. 092301, 2018, arXiv:1709.09189.
- [124] J. Adam *et al.*, “Correlation Measurements Between Flow Harmonics in Au+Au Collisions at RHIC,” *Phys. Lett. B*, vol. 783, pp. 459–465, 2018, arXiv:1803.03876.
- [125] L. Adamczyk *et al.*, “Global  $\Lambda$  hyperon polarization in nuclear collisions: evidence for the most vortical fluid,” *Nature*, vol. 548, pp. 62–65, 2017, arXiv:1701.06657.
- [126] J. Adam *et al.*, “Global polarization of  $\Lambda$  hyperons in Au+Au collisions at  $\sqrt{s_{NN}} = 200$  GeV,” *Phys. Rev. C*, vol. 98, p. 014910, 2018, arXiv:1805.04400.
- [127] S. Acharya *et al.*, “Global polarization of  $\Lambda$  and  $\bar{\Lambda}$  hyperons in Pb-Pb collisions at  $\sqrt{s_{NN}} = 2.76$  and 5.02 TeV,” *Phys. Rev. C*, vol. 101, no. 4, p. 044611, 2020, arXiv:1909.01281. [Erratum: Phys.Rev.C 105, 029902 (2022)].
- [128] J. Adam *et al.*, “Polarization of  $\Lambda$  ( $\bar{\Lambda}$ ) hyperons along the beam direction in Au+Au collisions at  $\sqrt{s_{NN}} = 200$  GeV,” *Phys. Rev. Lett.*, vol. 123, no. 13, p. 132301, 2019, arXiv:1905.11917.
- [129] S. Acharya *et al.*, “Polarization of  $\Lambda$  and  $\bar{\Lambda}$  Hyperons along the Beam Direction in Pb-Pb Collisions at  $\sqrt{s_{NN}}=5.02$  TeV,” *Phys. Rev. Lett.*, vol. 128, no. 17, p. 172005, 2022, arXiv:2107.11183.
- [130] M. Aaboud *et al.*, “Measurement of the azimuthal anisotropy of charged particles produced in  $\sqrt{s_{NN}} = 5.02$  TeV Pb+Pb collisions with the ATLAS detector,” *Eur. Phys. J. C*, vol. 78, no. 12, p. 997, 2018, arXiv:1808.03951.
- [131] S. Acharya *et al.*, “Higher harmonic non-linear flow modes of charged hadrons in Pb-Pb collisions at  $\sqrt{s_{NN}} = 5.02$  TeV,” *JHEP*, vol. 05, p. 085, 2020, arXiv:2002.00633.
- [132] S. Acharya *et al.*, “Linear and non-linear flow modes in Pb-Pb collisions at  $\sqrt{s_{NN}} = 2.76$  TeV,”

- Phys. Lett. B*, vol. 773, pp. 68–80, 2017, arXiv:1705.04377.
- [133] A. M. Sirunyan *et al.*, “Mixed higher-order anisotropic flow and nonlinear response coefficients of charged particles in PbPb collisions at  $\sqrt{s_{NN}} = 2.76$  and 5.02 TeV,” *Eur. Phys. J. C*, vol. 80, no. 6, p. 534, 2020, arXiv:1910.08789.
- [134] G. Aad *et al.*, “Measurement of event-plane correlations in  $\sqrt{s_{NN}} = 2.76$  TeV lead-lead collisions with the ATLAS detector,” *Phys. Rev. C*, vol. 90, no. 2, p. 024905, 2014, arXiv:1403.0489.
- [135] V. Khachatryan *et al.*, “Evidence for transverse momentum and pseudorapidity dependent event plane fluctuations in PbPb and pPb collisions,” *Phys. Rev. C*, vol. 92, no. 3, p. 034911, 2015, arXiv:1503.01692.
- [136] C. Shen, Z. Qiu, and U. Heinz, “Shape and flow fluctuations in ultracentral Pb + Pb collisions at the energies available at the CERN Large Hadron Collider,” *Phys. Rev. C*, vol. 92, no. 1, p. 014901, 2015, arXiv:1502.04636.
- [137] A. V. Giannini, M. N. Ferreira, M. Hippert, D. D. Chinellato, G. S. Denicol, M. Luzum, J. Noronha, T. N. da Silva, and J. Takahashi, “Assessing the ultra-central flow puzzle in the Bayesian era,” 3 2022, arXiv:2203.17011.
- [138] S. Acharya *et al.*, “General balance functions of identified charged hadron pairs of ( $\pi$ ,K,p) in Pb–Pb collisions at  $s_{NN}= 2.76$  TeV,” *Phys. Lett. B*, vol. 833, p. 137338, 2022, arXiv:2110.06566.
- [139] P. B. Arnold, C. Dogan, and G. D. Moore, “The Bulk Viscosity of High-Temperature QCD,” *Phys. Rev. D*, vol. 74, p. 085021, 2006, arXiv:hep-ph/0608012.
- [140] P. Kovtun, D. T. Son, and A. O. Starinets, “Viscosity in strongly interacting quantum field theories from black hole physics,” *Phys. Rev. Lett.*, vol. 94, p. 111601, 2005, arXiv:hep-th/0405231.
- [141] S. I. Finazzo, R. Rougemont, H. Marrochio, and J. Noronha, “Hydrodynamic transport coefficients for the non-conformal quark-gluon plasma from holography,” *JHEP*, vol. 02, p. 051, 2015, arXiv:1412.2968.
- [142] B. I. Abelev *et al.*, “Systematic Measurements of Identified Particle Spectra in  $pp$ ,  $d^+$  Au and Au+Au Collisions from STAR,” *Phys. Rev. C*, vol. 79, p. 034909, 2009, arXiv:0808.2041.
- [143] J. Adams *et al.*, “Azimuthal anisotropy in Au+Au collisions at  $s_{NN}^{1/2} = 200$ -GeV,” *Phys. Rev. C*, vol. 72, p. 014904, 2005, arXiv:nucl-ex/0409033.
- [144] L. Adamczyk *et al.*, “Third Harmonic Flow of Charged Particles in Au+Au Collisions at  $\sqrt{s_{NN}} = 200$  GeV,” *Phys. Rev. C*, vol. 88, no. 1, p. 014904, 2013, arXiv:1301.2187.
- [145] K. Aamodt *et al.*, “Centrality dependence of the charged-particle multiplicity density at mid-rapidity in Pb-Pb collisions at  $\sqrt{s_{NN}} = 2.76$  TeV,” *Phys. Rev. Lett.*, vol. 106, p. 032301, 2011, arXiv:1012.1657.
- [146] J. Adam *et al.*, “Measurement of transverse energy at midrapidity in Pb-Pb collisions at  $\sqrt{s_{NN}} = 2.76$  TeV,” *Phys. Rev. C*, vol. 94, no. 3, p. 034903, 2016, arXiv:1603.04775.
- [147] B. Abelev *et al.*, “Centrality dependence of  $\pi$ , K, p production in Pb-Pb collisions at  $\sqrt{s_{NN}} = 2.76$  TeV,” *Phys. Rev. C*, vol. 88, p. 044910, 2013, arXiv:1303.0737.
- [148] K. Aamodt *et al.*, “Higher harmonic anisotropic flow measurements of charged particles in Pb-Pb collisions at  $\sqrt{s_{NN}}=2.76$  TeV,” *Phys. Rev. Lett.*, vol. 107, p. 032301, 2011, arXiv:1105.3865.
- [149] B. B. Abelev *et al.*, “Event-by-event mean  $p_T$  fluctuations in  $pp$  and Pb-Pb collisions at the LHC,” *Eur. Phys. J. C*, vol. 74, no. 10, p. 3077, 2014, arXiv:1407.5530.
- [150] B. Schenke, C. Shen, and P. Tribedy, “Running the gamut of high energy nuclear collisions,” *Phys. Rev. C*, vol. 102, no. 4, p. 044905, 2020, arXiv:2005.14682.
- [151] E. W. Lemmon, “Thermophysical properties of fluid systems,” *NIST chemistry WebBook*, 2010.
- [152] D. Everett *et al.*, “Multisystem Bayesian constraints on the transport coefficients of QCD matter,”

- Phys. Rev. C*, vol. 103, no. 5, p. 054904, 2021, arXiv:2011.01430.
- [153] G. Nijs, W. van der Schee, U. Gürsoy, and R. Snellings, “Transverse Momentum Differential Global Analysis of Heavy-Ion Collisions,” *Phys. Rev. Lett.*, vol. 126, no. 20, p. 202301, 2021, arXiv:2010.15130.
- [154] J. E. Parkkila, A. Onnerstad, and D. J. Kim, “Bayesian estimation of the specific shear and bulk viscosity of the quark-gluon plasma with additional flow harmonic observables,” *Phys. Rev. C*, vol. 104, no. 5, p. 054904, 2021, arXiv:2106.05019.
- [155] J. Noronha-Hostler, G. S. Denicol, J. Noronha, R. P. G. Andrade, and F. Grassi, “Bulk Viscosity Effects in Event-by-Event Relativistic Hydrodynamics,” *Phys. Rev. C*, vol. 88, no. 4, p. 044916, 2013, arXiv:1305.1981.
- [156] G. Giacalone, J. Noronha-Hostler, M. Luzum, and J.-Y. Ollitrault, “Hydrodynamic predictions for 5.44 TeV Xe+Xe collisions,” *Phys. Rev. C*, vol. 97, no. 3, p. 034904, 2018, arXiv:1711.08499.
- [157] Y. Aoki, G. Endrodi, Z. Fodor, S. D. Katz, and K. K. Szabo, “The Order of the quantum chromodynamics transition predicted by the standard model of particle physics,” *Nature*, vol. 443, pp. 675–678, 2006, arXiv:hep-lat/0611014.
- [158] S. Borsanyi, Z. Fodor, J. N. Guenther, R. Kara, S. D. Katz, P. Parotto, A. Pasztor, C. Ratti, and K. K. Szabo, “QCD Crossover at Finite Chemical Potential from Lattice Simulations,” *Phys. Rev. Lett.*, vol. 125, no. 5, p. 052001, 2020, arXiv:2002.02821.
- [159] A. Bazavov *et al.*, “Chiral crossover in QCD at zero and non-zero chemical potentials,” *Phys. Lett. B*, vol. 795, pp. 15–21, 2019, arXiv:1812.08235.
- [160] K. Fukushima and C. Sasaki, “The phase diagram of nuclear and quark matter at high baryon density,” *Prog. Part. Nucl. Phys.*, vol. 72, pp. 99–154, 2013, arXiv:1301.6377.
- [161] A. Bzdak, S. Esumi, V. Koch, J. Liao, M. Stephanov, and N. Xu, “Mapping the Phases of Quantum Chromodynamics with Beam Energy Scan,” *Phys. Rept.*, vol. 853, pp. 1–87, 2020, arXiv:1906.00936.
- [162] A. Bazavov *et al.*, “Skewness, kurtosis, and the fifth and sixth order cumulants of net baryon-number distributions from lattice QCD confront high-statistics STAR data,” *Phys. Rev. D*, vol. 101, no. 7, p. 074502, 2020, arXiv:2001.08530.
- [163] D. Bollweg, D. A. Clarke, J. Goswami, O. Kaczmarek, F. Karsch, S. Mukherjee, P. Petreczky, C. Schmidt, and S. Sharma, “Equation of state and speed of sound of (2+1)-flavor QCD in strangeness-neutral matter at non-vanishing net baryon-number density,” 12 2022, arXiv:2212.09043.
- [164] S. Borsányi, Z. Fodor, J. N. Guenther, R. Kara, S. D. Katz, P. Parotto, A. Pásztor, C. Ratti, and K. K. Szabó, “Lattice QCD equation of state at finite chemical potential from an alternative expansion scheme,” *Phys. Rev. Lett.*, vol. 126, no. 23, p. 232001, 2021, arXiv:2102.06660.
- [165] J. Adam *et al.*, “Studying the phase diagram of qcd matter at rhic - a star whitepaper for bes-ii, 2014,” 2014, arXiv:https://drupal.star.bnl.gov/STAR/starnotes/public/sn0598.
- [166] A. Aprahamian *et al.*, “Reaching for the horizon: The 2015 long range plan for nuclear science,” 2015, arXiv:https://science.osti.gov/-/media/np/nsac/pdf/2015LRP/2015\_LRPNS\_091815.pdf.
- [167] L. Adamczyk *et al.*, “Beam Energy Dependence of Jet-Quenching Effects in Au+Au Collisions at  $\sqrt{s_{NN}} = 7.7, 11.5, 14.5, 19.6, 27, 39, \text{ and } 62.4 \text{ GeV}$ ,” *Phys. Rev. Lett.*, vol. 121, no. 3, p. 032301, 2018, arXiv:1707.01988.
- [168] L. Adamczyk *et al.*, “Observation of an Energy-Dependent Difference in Elliptic Flow between Particles and Antiparticles in Relativistic Heavy Ion Collisions,” *Phys. Rev. Lett.*, vol. 110, no. 14, p. 142301, 2013, arXiv:1301.2347.

- [169] M. A. Stephanov, “Non-Gaussian fluctuations near the QCD critical point,” *Phys. Rev. Lett.*, vol. 102, p. 032301, 2009, arXiv:0809.3450.
- [170] C. Athanasiou, K. Rajagopal, and M. Stephanov, “Using Higher Moments of Fluctuations and their Ratios in the Search for the QCD Critical Point,” *Phys. Rev. D*, vol. 82, p. 074008, 2010, arXiv:1006.4636.
- [171] Y. Hatta and M. A. Stephanov, “Proton number fluctuation as a signal of the QCD critical endpoint,” *Phys. Rev. Lett.*, vol. 91, p. 102003, 2003, arXiv:hep-ph/0302002. [Erratum: *Phys.Rev.Lett.* 91, 129901 (2003)].
- [172] J. Adam *et al.*, “Nonmonotonic Energy Dependence of Net-Proton Number Fluctuations,” *Phys. Rev. Lett.*, vol. 126, no. 9, p. 092301, 2021, arXiv:2001.02852.
- [173] M. Abdallah *et al.*, “Measurement of the Sixth-Order Cumulant of Net-Proton Multiplicity Distributions in Au+Au Collisions at  $\sqrt{s_{NN}} = 27, 54.4, \text{ and } 200 \text{ GeV}$  at RHIC,” *Phys. Rev. Lett.*, vol. 127, no. 26, p. 262301, 2021, arXiv:2105.14698.
- [174] S. Borsanyi, Z. Fodor, J. N. Guenther, S. K. Katz, K. K. Szabo, A. Pasztor, I. Portillo, and C. Ratti, “Higher order fluctuations and correlations of conserved charges from lattice QCD,” *JHEP*, vol. 10, p. 205, 2018, arXiv:1805.04445.
- [175] R. Bellwied, S. Borsanyi, Z. Fodor, J. N. Guenther, S. D. Katz, P. Parotto, A. Pasztor, D. Pesznyak, C. Ratti, and K. K. Szabo, “Corrections to the hadron resonance gas from lattice QCD and their effect on fluctuation-ratios at finite density,” *Phys. Rev. D*, vol. 104, no. 9, p. 094508, 2021, arXiv:2102.06625.
- [176] M. S. Abdallah *et al.*, “Measurements of Proton High Order Cumulants in  $\sqrt{s_{NN}} = 3 \text{ GeV}$  Au+Au Collisions and Implications for the QCD Critical Point,” *Phys. Rev. Lett.*, vol. 128, no. 20, p. 202303, 2022, arXiv:2112.00240.
- [177] M. S. Abdallah *et al.*, “Disappearance of partonic collectivity in sNN=3GeV Au+Au collisions at RHIC,” *Phys. Lett. B*, vol. 827, p. 137003, 2022, arXiv:2108.00908.
- [178] M. S. Abdallah *et al.*, “Probing strangeness canonical ensemble with  $K^-$ ,  $\phi(1020)$  and  $\Xi^-$  production in Au+Au collisions at sNN=3 GeV,” *Phys. Lett. B*, vol. 831, p. 137152, 2022, arXiv:2108.00924.
- [179] J. Adamczewski-Musch *et al.*, “Proton-number fluctuations in  $\sqrt{s_{NN}} = 2.4 \text{ GeV}$  Au + Au collisions studied with the High-Acceptance DiElectron Spectrometer (HADES),” *Phys. Rev. C*, vol. 102, no. 2, p. 024914, 2020, arXiv:2002.08701.
- [180] M. A. Stephanov, “On the sign of kurtosis near the QCD critical point,” *Phys. Rev. Lett.*, vol. 107, p. 052301, 2011, arXiv:1104.1627.
- [181] D. Mroczek, A. R. Nava Acuna, J. Noronha-Hostler, P. Parotto, C. Ratti, and M. A. Stephanov, “Quartic cumulant of baryon number in the presence of a QCD critical point,” *Phys. Rev. C*, vol. 103, no. 3, p. 034901, 2021, arXiv:2008.04022.
- [182] S. A. Bass *et al.*, “Microscopic models for ultrarelativistic heavy ion collisions,” *Prog. Part. Nucl. Phys.*, vol. 41, pp. 255–369, 1998, arXiv:nucl-th/9803035.
- [183] M. Bleicher *et al.*, “Relativistic hadron hadron collisions in the ultrarelativistic quantum molecular dynamics model,” *J. Phys. G*, vol. 25, pp. 1859–1896, 1999, arXiv:hep-ph/9909407.
- [184] P. Braun-Munzinger, B. Friman, K. Redlich, A. Rustamov, and J. Stachel, “Relativistic nuclear collisions: Establishing a non-critical baseline for fluctuation measurements,” *Nucl. Phys. A*, vol. 1008, p. 122141, 2021, arXiv:2007.02463.
- [185] M. Abdallah *et al.*, “Cumulants and correlation functions of net-proton, proton, and antiproton multiplicity distributions in Au+Au collisions at energies available at the BNL Relativistic Heavy Ion

- Collider,” *Phys. Rev. C*, vol. 104, no. 2, p. 024902, 2021, arXiv:2101.12413.
- [186] J. Adamczewski-Musch *et al.*, “Proton-number fluctuations in  $\sqrt{s_{NN}} = 2.4$  GeV Au + Au collisions studied with the High-Acceptance DiElectron Spectrometer (HADES),” *Phys. Rev. C*, vol. 102, no. 2, p. 024914, 2020, arXiv:2002.08701.
- [187] S. Borsanyi, J. N. Guenther, R. Kara, Z. Fodor, P. Parotto, A. Pasztor, C. Ratti, and K. K. Szabo, “Resummed lattice QCD equation of state at finite baryon density: Strangeness neutrality and beyond,” *Phys. Rev. D*, vol. 105, no. 11, p. 114504, 2022, arXiv:2202.05574.
- [188] J. Noronha-Hostler, P. Parotto, C. Ratti, and J. M. Stafford, “Lattice-based equation of state at finite baryon number, electric charge and strangeness chemical potentials,” *Phys. Rev. C*, vol. 100, no. 6, p. 064910, 2019, arXiv:1902.06723.
- [189] A. Monnai, B. Schenke, and C. Shen, “Equation of state at finite densities for QCD matter in nuclear collisions,” *Phys. Rev. C*, vol. 100, no. 2, p. 024907, 2019, arXiv:1902.05095.
- [190] P. Bedaque and A. W. Steiner, “Sound velocity bound and neutron stars,” *Phys. Rev. Lett.*, vol. 114, no. 3, p. 031103, 2015, arXiv:1408.5116.
- [191] I. Tews, J. Carlson, S. Gandolfi, and S. Reddy, “Constraining the speed of sound inside neutron stars with chiral effective field theory interactions and observations,” *Astrophys. J.*, vol. 860, no. 2, p. 149, 2018, arXiv:1801.01923.
- [192] G. Baym, S. Furusawa, T. Hatsuda, T. Kojo, and H. Togashi, “New Neutron Star Equation of State with Quark-Hadron Crossover,” *Astrophys. J.*, vol. 885, p. 42, 2019, arXiv:1903.08963.
- [193] T. Kojo, Y. Hidaka, L. McLerran, and R. D. Pisarski, “Quarkyonic Chiral Spirals,” *Nucl. Phys. A*, vol. 843, pp. 37–58, 2010, arXiv:0912.3800.
- [194] J. Estee *et al.*, “Probing the Symmetry Energy with the Spectral Pion Ratio,” *Phys. Rev. Lett.*, vol. 126, no. 16, p. 162701, 2021, arXiv:2103.06861.
- [195] X. Fan, J. Dong, and W. Zuo, “Density-dependent symmetry energy at subsaturation densities from nuclear mass differences,” *Phys. Rev. C*, vol. 89, no. 1, p. 017305, 2014, arXiv:1403.2055.
- [196] B.-A. Li, P. G. Krastev, D.-H. Wen, and N.-B. Zhang, “Towards Understanding Astrophysical Effects of Nuclear Symmetry Energy,” *Eur. Phys. J. A*, vol. 55, no. 7, p. 117, 2019, arXiv:1905.13175.
- [197] B. T. Reed, F. J. Fattoyev, C. J. Horowitz, and J. Piekarewicz, “Implications of PREX-2 on the Equation of State of Neutron-Rich Matter,” *Phys. Rev. Lett.*, vol. 126, no. 17, p. 172503, 2021, arXiv:2101.03193.
- [198] P.-G. Reinhard, X. Roca-Maza, and W. Nazarewicz, “Information Content of the Parity-Violating Asymmetry in Pb208,” *Phys. Rev. Lett.*, vol. 127, no. 23, p. 232501, 2021, arXiv:2105.15050.
- [199] T. Miyatsu, M.-K. Cheoun, K. Kim, and K. Saito, “Massive neutron stars with small radii in relativistic mean-field models optimized to nuclear ground states,” 9 2022, arXiv:2209.02861.
- [200] M. C. Miller *et al.*, “PSR J0030+0451 Mass and Radius from *NICER* Data and Implications for the Properties of Neutron Star Matter,” *Astrophys. J. Lett.*, vol. 887, no. 1, p. L24, 2019, arXiv:1912.05705.
- [201] T. E. Riley *et al.*, “A *NICER* View of PSR J0030+0451: Millisecond Pulsar Parameter Estimation,” *Astrophys. J. Lett.*, vol. 887, no. 1, p. L21, 2019, arXiv:1912.05702.
- [202] M. C. Miller *et al.*, “The Radius of PSR J0740+6620 from *NICER* and *XMM-Newton* Data,” *Astrophys. J. Lett.*, vol. 918, no. 2, p. L28, 2021, arXiv:2105.06979.
- [203] T. E. Riley *et al.*, “A *NICER* View of the Massive Pulsar PSR J0740+6620 Informed by Radio Timing and *XMM-Newton* Spectroscopy,” *Astrophys. J. Lett.*, vol. 918, no. 2, p. L27, 2021, arXiv:2105.06980.
- [204] B. P. Abbott *et al.*, “GW170817: Measurements of neutron star radii and equation of state,” *Phys.*

- Rev. Lett.*, vol. 121, no. 16, p. 161101, 2018, arXiv:1805.11581.
- [205] E. Fonseca *et al.*, “Refined Mass and Geometric Measurements of the High-mass PSR J0740+6620,” *Astrophys. J. Lett.*, vol. 915, no. 1, p. L12, 2021, arXiv:2104.00880.
- [206] R. W. Romani, D. Kandel, A. V. Filippenko, T. G. Brink, and W. Zheng, “PSR J0952–0607: The Fastest and Heaviest Known Galactic Neutron Star,” *Astrophys. J. Lett.*, vol. 934, no. 2, p. L18, 2022, arXiv:2207.05124.
- [207] R. Abbott *et al.*, “GW190814: Gravitational Waves from the Coalescence of a 23 Solar Mass Black Hole with a 2.6 Solar Mass Compact Object,” *Astrophys. J. Lett.*, vol. 896, no. 2, p. L44, 2020, arXiv:2006.12611.
- [208] E. Annala, T. Gorda, A. Kurkela, J. Nättilä, and A. Vuorinen, “Evidence for quark-matter cores in massive neutron stars,” *Nature Phys.*, vol. 16, no. 9, pp. 907–910, 2020, arXiv:1903.09121.
- [209] O. Komoltsev and A. Kurkela, “How Perturbative QCD Constrains the Equation of State at Neutron-Star Densities,” *Phys. Rev. Lett.*, vol. 128, no. 20, p. 202701, 2022, arXiv:2111.05350.
- [210] H. Tan, T. Dore, V. Dexheimer, J. Noronha-Hostler, and N. Yunes, “Extreme matter meets extreme gravity: Ultraheavy neutron stars with phase transitions,” *Phys. Rev. D*, vol. 105, no. 2, p. 023018, 2022, arXiv:2106.03890.
- [211] J. R. Stone, V. Dexheimer, P. A. M. Guichon, A. W. Thomas, and S. Typel, “Equation of state of hot dense hyperonic matter in the Quark–Meson–Coupling (QMC-A) model,” *Mon. Not. Roy. Astron. Soc.*, vol. 502, no. 3, pp. 3476–3490, 2021, arXiv:1906.11100.
- [212] A. Motornenko, J. Steinheimer, V. Vovchenko, S. Schramm, and H. Stoecker, “Equation of state for hot QCD and compact stars from a mean field approach,” *Phys. Rev. C*, vol. 101, no. 3, p. 034904, 2020, arXiv:1905.00866.
- [213] L. McLerran and S. Reddy, “Quarkyonic Matter and Neutron Stars,” *Phys. Rev. Lett.*, vol. 122, no. 12, p. 122701, 2019, arXiv:1811.12503.
- [214] M. A. Aloy, J. M. Ibáñez, N. Sanchis-Gual, M. Obergaulinger, J. A. Font, S. Serna, and A. Marquina, “Neutron star collapse and gravitational waves with a non-convex equation of state,” *Mon. Not. Roy. Astron. Soc.*, vol. 484, p. 4980, 2019, arXiv:1806.03314.
- [215] W.-J. Xie and B.-A. Li, “Bayesian inference of the dense-matter equation of state encapsulating a first-order hadron-quark phase transition from observables of canonical neutron stars,” *Phys. Rev. C*, vol. 103, no. 3, p. 035802, 2021, arXiv:2009.13653.
- [216] M.-Z. Han, Y.-J. Huang, S.-P. Tang, and Y.-Z. Fan, “Plausible presence of quark matter in neutron stars with masses above  $0.97M_{TOV}$ ,” *7* 2022, arXiv:2207.13613.
- [217] M. Hippert, E. S. Fraga, and J. Noronha, “Insights on the peak in the speed of sound of ultradense matter,” *Phys. Rev. D*, vol. 104, no. 3, p. 034011, 2021, arXiv:2105.04535.
- [218] Y. Fujimoto, K. Fukushima, L. D. McLerran, and M. Praszalowicz, “Trace Anomaly as Signature of Conformality in Neutron Stars,” *Phys. Rev. Lett.*, vol. 129, no. 25, p. 252702, 2022, arXiv:2207.06753.
- [219] V. Dexheimer, R. de Oliveira Gomes, S. Schramm, and H. Pais, “What do we learn about vector interactions from GW170817?,” *J. Phys. G*, vol. 46, no. 3, p. 034002, 2019, arXiv:1810.06109.
- [220] V. Dexheimer, R. O. Gomes, T. Klähn, S. Han, and M. Salinas, “GW190814 as a massive rapidly rotating neutron star with exotic degrees of freedom,” *Phys. Rev. C*, vol. 103, no. 2, p. 025808, 2021, arXiv:2007.08493.
- [221] L. L. Lopes, C. Biesdorf, K. D. Marquez, and D. P. Menezes, “Modified MIT Bag Models – part II: QCD phase diagram and hot quark stars,” *Phys. Scripta*, vol. 96, no. 6, p. 065302, 2021, arXiv:2009.13552.

- [222] R. D. Pisarski, “Remarks on nuclear matter: How an  $\omega_0$  condensate can spike the speed of sound, and a model of  $Z(3)$  baryons,” *Phys. Rev. D*, vol. 103, no. 7, p. L071504, 2021, arXiv:2101.05813.
- [223] E. R. Most and C. A. Raithel, “Impact of the nuclear symmetry energy on the post-merger phase of a binary neutron star coalescence,” *Phys. Rev. D*, vol. 104, no. 12, p. 124012, 2021, arXiv:2107.06804.
- [224] A. Pfaff, H. Hansen, and F. Gulminelli, “Bayesian analysis of the properties of hybrid stars with the Nambu–Jona-Lasinio model,” *Phys. Rev. C*, vol. 105, no. 3, p. 035802, 2022, arXiv:2112.09595.
- [225] I. Sagert, T. Fischer, M. Hempel, G. Pagliara, J. Schaffner-Bielich, A. Mezzacappa, F. K. Thielemann, and M. Liebendorfer, “Signals of the QCD phase transition in core-collapse supernovae,” *Phys. Rev. Lett.*, vol. 102, p. 081101, 2009, arXiv:0809.4225.
- [226] R. Ouyed, D. Leahy, and P. Jaikumar, “Predictions for signatures of the quark-nova in superluminous supernovae,” 11 2009, arXiv:0911.5424.
- [227] K. Nakazato, K. Sumiyoshi, and S. Yamada, “Stellar Core Collapse with Hadron-Quark Phase Transition,” *Astron. Astrophys.*, vol. 558, p. A50, 2013, arXiv:1309.3383.
- [228] T. Fischer, N.-U. F. Bastian, M.-R. Wu, P. Baklanov, E. Sorokina, S. Blinnikov, S. Typel, T. Klähn, and D. B. Blaschke, “Quark deconfinement as a supernova explosion engine for massive blue supergiant stars,” *Nature Astron.*, vol. 2, no. 12, pp. 980–986, 2018, arXiv:1712.08788.
- [229] T. Kuroda, T. Fischer, T. Takiwaki, and K. Kotake, “Core-collapse Supernova Simulations and the Formation of Neutron Stars, Hybrid Stars, and Black Holes,” *Astrophys. J.*, vol. 924, no. 1, p. 38, 2022, arXiv:2109.01508.
- [230] P. Jakobus, B. Mueller, A. Heger, A. Motornenko, J. Steinheimer, and H. Stoecker, “The role of the hadron-quark phase transition in core-collapse supernovae,” *Mon. Not. Roy. Astron. Soc.*, vol. 516, no. 2, pp. 2554–2574, 2022, arXiv:2204.10397.
- [231] E. R. Most, L. J. Papenfort, V. Dexheimer, M. Hanauske, S. Schramm, H. Stöcker, and L. Rezzolla, “Signatures of quark-hadron phase transitions in general-relativistic neutron-star mergers,” *Phys. Rev. Lett.*, vol. 122, no. 6, p. 061101, 2019, arXiv:1807.03684.
- [232] L. R. Weih, M. Hanauske, and L. Rezzolla, “Postmerger Gravitational-Wave Signatures of Phase Transitions in Binary Mergers,” *Phys. Rev. Lett.*, vol. 124, no. 17, p. 171103, 2020, arXiv:1912.09340.
- [233] S. Blacker, N.-U. F. Bastian, A. Bauswein, D. B. Blaschke, T. Fischer, M. Oertel, T. Sultani, and S. Typel, “Constraining the onset density of the hadron-quark phase transition with gravitational-wave observations,” *Phys. Rev. D*, vol. 102, no. 12, p. 123023, 2020, arXiv:2006.03789.
- [234] G. David, “Direct real photons in relativistic heavy ion collisions,” *Rept. Prog. Phys.*, vol. 83, no. 4, p. 046301, 2020, arXiv:1907.08893.
- [235] F. Geurts and R.-A. Tripolt, “Electromagnetic probes: Theory and experiment,” *Prog. Part. Nucl. Phys.*, vol. 128, p. 104004, 2023, arXiv:2210.01622.
- [236] M. Strickland, “Thermal photons and dileptons from nonequilibrium quark - gluon plasma,” *Phys. Lett. B*, vol. 331, pp. 245–250, 1994.
- [237] B. Schenke and M. Strickland, “Photon production from an anisotropic quark-gluon plasma,” *Phys. Rev. D*, vol. 76, p. 025023, 2007, arXiv:hep-ph/0611332.
- [238] M. Martinez and M. Strickland, “Pre-equilibrium dilepton production from an anisotropic quark-gluon plasma,” *Phys. Rev. C*, vol. 78, p. 034917, 2008, arXiv:0805.4552.
- [239] C. Shen, “Recent developments in the theory of electromagnetic probes in relativistic heavy-ion collisions,” in *7th International Conference on Hard and Electromagnetic Probes of High-Energy Nuclear Collisions*, 11 2015, arXiv:1511.07708.
- [240] C. Shen, “Electromagnetic Radiation from QCD Matter: Theory Overview,” *Nucl. Phys. A*, vol. 956,

- pp. 184–191, 2016, arXiv:1601.02563.
- [241] L. Bhattacharya, R. Ryblewski, and M. Strickland, “Photon production from a nonequilibrium quark-gluon plasma,” *Phys. Rev. D*, vol. 93, no. 6, p. 065005, 2016, arXiv:1507.06605.
  - [242] R. Ryblewski and M. Strickland, “Dilepton production from the quark-gluon plasma using (3+1)-dimensional anisotropic dissipative hydrodynamics,” *Phys. Rev. D*, vol. 92, no. 2, p. 025026, 2015, arXiv:1501.03418.
  - [243] J.-F. Paquet, “Probing the space-time evolution of heavy ion collisions with photons and dileptons,” *Nucl. Phys. A*, vol. 967, pp. 184–191, 2017, arXiv:1704.07842.
  - [244] B. S. Kasmaei and M. Strickland, “Dilepton production and elliptic flow from an anisotropic quark-gluon plasma,” *Phys. Rev. D*, vol. 99, no. 3, p. 034015, 2019, arXiv:1811.07486.
  - [245] B. S. Kasmaei and M. Strickland, “Photon production and elliptic flow from a momentum-anisotropic quark-gluon plasma,” *Phys. Rev. D*, vol. 102, no. 1, p. 014037, 2020, arXiv:1911.03370.
  - [246] M. Coquet, X. Du, J.-Y. Ollitrault, S. Schlichting, and M. Winn, “Intermediate mass dileptons as pre-equilibrium probes in heavy ion collisions,” *Phys. Lett. B*, vol. 821, p. 136626, 2021, arXiv:2104.07622.
  - [247] M. Coquet, X. Du, J.-Y. Ollitrault, S. Schlichting, and M. Winn, “Transverse mass scaling of dilepton radiation off a quark-gluon plasma,” *Nucl. Phys. A*, vol. 1030, p. 122579, 2023, arXiv:2112.13876.
  - [248] G. Vujanovic, “Electromagnetic probes of the Quark-Gluon Plasma,” in *29th International Conference on Ultra-relativistic Nucleus-Nucleus Collisions*, 8 2022, arXiv:2208.09526.
  - [249] A. Monnai, “Direct photons in hydrodynamic modeling of relativistic nuclear collisions,” *Int. J. Mod. Phys. A*, vol. 37, no. 11n12, p. 2230006, 2022, arXiv:2203.13208.
  - [250] R. Rapp, J. Wambach, and H. van Hees, “The Chiral Restoration Transition of QCD and Low Mass Dileptons,” *Landolt-Bornstein*, vol. 23, p. 134, 2010, arXiv:0901.3289.
  - [251] P. M. Hohler and R. Rapp, “Is  $\rho$ -Meson Melting Compatible with Chiral Restoration?,” *Phys. Lett. B*, vol. 731, pp. 103–109, 2014, arXiv:1311.2921.
  - [252] M. L. Bellac, *Thermal Field Theory*. Cambridge Monographs on Mathematical Physics, Cambridge University Press, 3 2011.
  - [253] J. I. Kapusta and C. Gale, *Finite-temperature field theory: Principles and applications*. Cambridge Monographs on Mathematical Physics, Cambridge University Press, 2006.
  - [254] J. Ghiglieri, J. Hong, A. Kurkela, E. Lu, G. D. Moore, and D. Teaney, “Next-to-leading order thermal photon production in a weakly coupled quark-gluon plasma,” *JHEP*, vol. 05, p. 010, 2013, arXiv:1302.5970.
  - [255] M. Laine, “NLO thermal dilepton rate at non-zero momentum,” *JHEP*, vol. 11, p. 120, 2013, arXiv:1310.0164.
  - [256] I. Ghisoiu and M. Laine, “Interpolation of hard and soft dilepton rates,” *JHEP*, vol. 10, p. 083, 2014, arXiv:1407.7955.
  - [257] J. Ghiglieri and G. D. Moore, “Low Mass Thermal Dilepton Production at NLO in a Weakly Coupled Quark-Gluon Plasma,” *JHEP*, vol. 12, p. 029, 2014, arXiv:1410.4203.
  - [258] J. Ghiglieri, O. Kaczmarek, M. Laine, and F. Meyer, “Lattice constraints on the thermal photon rate,” *Phys. Rev. D*, vol. 94, no. 1, p. 016005, 2016, arXiv:1604.07544.
  - [259] G. Jackson and M. Laine, “Testing thermal photon and dilepton rates,” *JHEP*, vol. 11, p. 144, 2019, arXiv:1910.09567.
  - [260] B. B. Brandt, M. Cè, A. Francis, T. Harris, H. B. Meyer, A. Steinberg, and A. Toniato, “Lattice QCD estimate of the quark-gluon plasma photon emission rate,” *PoS*, vol. LATTICE2019, p. 225, 2019, arXiv:1912.00292.



- [261] M. Cè, T. Harris, A. Krasniqi, H. B. Meyer, and C. Török, “Photon emissivity of the quark-gluon plasma: A lattice QCD analysis of the transverse channel,” *Phys. Rev. D*, vol. 106, no. 5, p. 054501, 2022, arXiv:2205.02821.
- [262] R. Rapp and J. Wambach, “Low mass dileptons at the CERN SPS: Evidence for chiral restoration?,” *Eur. Phys. J. A*, vol. 6, pp. 415–420, 1999, arXiv:hep-ph/9907502.
- [263] P. M. Hohler and R. Rapp, “Massive Yang–Mills for vector and axial-vector spectral functions at finite temperature,” *Annals Phys.*, vol. 368, pp. 70–109, 2016, arXiv:1510.00454.
- [264] C. Shen, J.-F. Paquet, U. Heinz, and C. Gale, “Photon Emission from a Momentum Anisotropic Quark-Gluon Plasma,” *Phys. Rev. C*, vol. 91, no. 1, p. 014908, 2015, arXiv:1410.3404.
- [265] S. Hauksson, C. Shen, S. Jeon, and C. Gale, “Bulk viscous corrections to photon production in the quark–gluon plasma,” *Nucl. Part. Phys. Proc.*, vol. 289-290, pp. 169–172, 2017, arXiv:1612.05517.
- [266] A. Czajka, S. Hauksson, C. Shen, S. Jeon, and C. Gale, “Bulk viscosity of strongly interacting matter in the relaxation time approximation,” *Phys. Rev. C*, vol. 97, no. 4, p. 044914, 2018, arXiv:1712.05905.
- [267] B. S. Kasmaei and M. Strickland, “Parton self-energies for general momentum-space anisotropy,” *Phys. Rev. D*, vol. 97, no. 5, p. 054022, 2018, arXiv:1801.00863.
- [268] S. Hauksson, S. Jeon, and C. Gale, “Photon emission from quark-gluon plasma out of equilibrium,” *Phys. Rev. C*, vol. 97, no. 1, p. 014901, 2018, arXiv:1709.03598.
- [269] S. Hauksson, S. Jeon, and C. Gale, “Probes of the quark-gluon plasma and plasma instabilities,” *Phys. Rev. C*, vol. 103, p. 064904, 2021, arXiv:2012.03640.
- [270] G. Vujanovic, C. Shen, G. S. Denicol, B. Schenke, S. Jeon, and C. Gale, “Probing the dissipative properties of a strongly interacting medium with dileptons,” *Prog. Part. Nucl. Phys.*, vol. 276-278, pp. 113–114, 2016, arXiv:1511.04625.
- [271] A. Bandyopadhyay, N. Haque, M. G. Mustafa, and M. Strickland, “Dilepton rate and quark number susceptibility with the Gribov action,” *Phys. Rev. D*, vol. 93, no. 6, p. 065004, 2016, arXiv:1508.06249.
- [272] G. Vujanovic, J.-F. Paquet, G. S. Denicol, M. Luzum, S. Jeon, and C. Gale, “Electromagnetic radiation as a probe of the initial state and of viscous dynamics in relativistic nuclear collisions,” *Phys. Rev. C*, vol. 94, no. 1, p. 014904, 2016, arXiv:1602.01455.
- [273] G. Vujanovic, G. S. Denicol, M. Luzum, S. Jeon, and C. Gale, “Investigating the temperature dependence of the specific shear viscosity of QCD matter with dilepton radiation,” *Phys. Rev. C*, vol. 98, no. 1, p. 014902, 2018, arXiv:1702.02941.
- [274] G. Vujanovic, J.-F. Paquet, C. Shen, G. S. Denicol, S. Jeon, C. Gale, and U. Heinz, “Exploring the influence of bulk viscosity of QCD on dilepton tomography,” *Phys. Rev. C*, vol. 101, p. 044904, 2020, arXiv:1903.05078.
- [275] E. V. Shuryak, “Quark-Gluon Plasma and Hadronic Production of Leptons, Photons and Psions,” *Phys. Lett. B*, vol. 78, p. 150, 1978.
- [276] R. C. Hwa and K. Kajantie, “Diagnosing Quark Matter by Measuring the Total Entropy and the Photon Or Dilepton Emission Rates,” *Phys. Rev. D*, vol. 32, p. 1109, 1985.
- [277] C. Shen, J.-F. Paquet, G. S. Denicol, S. Jeon, and C. Gale, “Electromagnetic radiation and collectivity in small quark–gluon droplets,” *Nucl. Part. Phys. Proc.*, vol. 289-290, pp. 161–164, 2017, arXiv:1612.05464.
- [278] C. Gale, S. Jeon, S. McDonald, J.-F. Paquet, and C. Shen, “Centrality dependence of the direct photon multiplicity in heavy ion collisions,” *PoS*, vol. HardProbes2018, p. 178, 2019, arXiv:1901.07019.

- [279] R. Rapp, “Theory of Soft Electromagnetic Emission in Heavy-Ion Collisions,” *Acta Phys. Polon. B*, vol. 42, pp. 2823–2852, 2011, arXiv:1110.4345.
- [280] R. Rapp and H. van Hees, “Thermal Dileptons as Fireball Thermometer and Chronometer,” *Phys. Lett. B*, vol. 753, pp. 586–590, 2016, arXiv:1411.4612.
- [281] A. Adare *et al.*, “Centrality dependence of low-momentum direct-photon production in Au+Au collisions at  $\sqrt{s_{NN}} = 200$  GeV,” *Phys. Rev. C*, vol. 91, no. 6, p. 064904, 2015, arXiv:1405.3940.
- [282] J. Adam *et al.*, “Direct photon production in Pb-Pb collisions at  $\sqrt{s_{NN}} = 2.76$  TeV,” *Phys. Lett. B*, vol. 754, pp. 235–248, 2016, arXiv:1509.07324.
- [283] L. Adamczyk *et al.*, “Direct virtual photon production in Au+Au collisions at  $\sqrt{s_{NN}} = 200$  GeV,” *Phys. Lett. B*, vol. 770, pp. 451–458, 2017, arXiv:1607.01447.
- [284] H. van Hees, C. Gale, and R. Rapp, “Thermal Photons and Collective Flow at the Relativistic Heavy-Ion Collider,” *Phys. Rev. C*, vol. 84, p. 054906, 2011, arXiv:1108.2131.
- [285] C. Shen, U. W. Heinz, J.-F. Paquet, and C. Gale, “Thermal photons as a quark-gluon plasma thermometer reexamined,” *Phys. Rev. C*, vol. 89, no. 4, p. 044910, 2014, arXiv:1308.2440.
- [286] J. Adam *et al.*, “Measurements of Dielectron Production in Au+Au Collisions at  $\sqrt{s_{NN}} = 27, 39,$  and 62.4 GeV from the STAR Experiment,” 10 2018, arXiv:1810.10159.
- [287] R. Rapp, “Dilepton Production in Heavy-Ion Collisions,” *PoS*, vol. CPOD2013, p. 008, 2013, arXiv:1306.6394.
- [288] E. L. Bratkovskaya, W. Cassing, V. P. Konchakovski, and O. Linnyk, “Parton-Hadron-String Dynamics at Relativistic Collider Energies,” *Nucl. Phys. A*, vol. 856, pp. 162–182, 2011, arXiv:1101.5793.
- [289] G. Vujanovic, G. S. Denicol, C. Shen, M. Luzum, B. Schenke, S. Jeon, and C. Gale, “Dilepton emission in high-energy heavy-ion collisions with dissipative hydrodynamics,” in *12th Conference on the Intersections of Particle and Nuclear Physics*, 10 2015, arXiv:1510.00441.
- [290] S. Endres, H. van Hees, J. Weil, and M. Bleicher, “Dilepton production and reaction dynamics in heavy-ion collisions at SIS energies from coarse-grained transport simulations,” *Phys. Rev. C*, vol. 92, no. 1, p. 014911, 2015, arXiv:1505.06131.
- [291] T. Galatyuk, P. M. Hohler, R. Rapp, F. Seck, and J. Stroth, “Thermal Dileptons from Coarse-Grained Transport as Fireball Probes at SIS Energies,” *Eur. Phys. J. A*, vol. 52, no. 5, p. 131, 2016, arXiv:1512.08688.
- [292] J. Staudenmaier, J. Weil, V. Steinberg, S. Endres, and H. Petersen, “Dilepton production and resonance properties within a new hadronic transport approach in the context of the GSI-HADES experimental data,” *Phys. Rev. C*, vol. 98, no. 5, p. 054908, 2018, arXiv:1711.10297.
- [293] J. Adamczewski-Musch *et al.*, “Probing dense baryon-rich matter with virtual photons,” *Nature Phys.*, vol. 15, no. 10, pp. 1040–1045, 2019.
- [294] K. Dusling, “Photons as a viscometer of heavy ion collisions,” *Nucl. Phys. A*, vol. 839, pp. 70–77, 2010, arXiv:0903.1764.
- [295] M. Dion, J.-F. Paquet, B. Schenke, C. Young, S. Jeon, and C. Gale, “Viscous photons in relativistic heavy ion collisions,” *Phys. Rev. C*, vol. 84, p. 064901, 2011, arXiv:1109.4405.
- [296] C. Shen, *The standard model for relativistic heavy-ion collisions and electromagnetic tomography*. PhD thesis, Ohio State U., 7 2014.
- [297] C. Shen, U. W. Heinz, J.-F. Paquet, I. Kozlov, and C. Gale, “Anisotropic flow of thermal photons as a quark-gluon plasma viscometer,” *Phys. Rev. C*, vol. 91, no. 2, p. 024908, 2015, arXiv:1308.2111.
- [298] C. Shen, U. Heinz, J.-F. Paquet, and C. Gale, “Thermal photon anisotropic flow serves as a quark-gluon plasma viscometer,” *Nucl. Phys. A*, vol. 932, p. 184, 2014, arXiv:1403.7558.

- [299] J.-F. Paquet, C. Shen, G. S. Denicol, M. Luzum, B. Schenke, S. Jeon, and C. Gale, “Production of photons in relativistic heavy-ion collisions,” *Phys. Rev. C*, vol. 93, no. 4, p. 044906, 2016, arXiv:1509.06738.
- [300] C. Gale, J.-F. Paquet, B. Schenke, and C. Shen, “Multimessenger heavy-ion collision physics,” *Phys. Rev. C*, vol. 105, no. 1, p. 014909, 2022, arXiv:2106.11216.
- [301] G. Vujanovic, J.-F. Paquet, G. S. Denicol, M. Luzum, B. Schenke, S. Jeon, and C. Gale, “Probing the non-equilibrium dynamics of hot and dense QCD with dileptons,” *Nucl. Phys. A*, vol. 931, pp. 701–705, 2014, arXiv:1408.1098.
- [302] A. Adare *et al.*, “Beam Energy and Centrality Dependence of Direct-Photon Emission from Ultrarelativistic Heavy-Ion Collisions,” *Phys. Rev. Lett.*, vol. 123, no. 2, p. 022301, 2019, arXiv:1805.04084.
- [303] U. A. Acharya *et al.*, “Nonprompt direct-photon production in Au+Au collisions at  $\sqrt{s_{NN}} = 200$  GeV,” 3 2022, arXiv:2203.17187.
- [304] C. Shen, J. F. Paquet, G. S. Denicol, S. Jeon, and C. Gale, “Thermal photon radiation in high multiplicity p+Pb collisions at the Large Hadron Collider,” *Phys. Rev. Lett.*, vol. 116, no. 7, p. 072301, 2016, arXiv:1504.07989.
- [305] C. Shen, C. Park, J.-F. Paquet, G. S. Denicol, S. Jeon, and C. Gale, “Direct photon production and jet energy-loss in small systems,” *Nucl. Phys. A*, vol. 956, pp. 741–744, 2016, arXiv:1601.03070.
- [306] I. Iatrakis, E. Kiritsis, C. Shen, and D.-L. Yang, “Holographic Photon Production in Heavy Ion Collisions,” *JHEP*, vol. 04, p. 035, 2017, arXiv:1609.07208.
- [307] O. Linnyk, V. Konchakovski, T. Steinert, W. Cassing, and E. L. Bratkovskaya, “Hadronic and partonic sources of direct photons in relativistic heavy-ion collisions,” *Phys. Rev. C*, vol. 92, no. 5, p. 054914, 2015, arXiv:1504.05699.
- [308] A. Schäfer, O. Garcia-Montero, J.-F. Paquet, H. Elfner, and C. Gale, “Out-of-equilibrium photon production in the late stages of relativistic heavy-ion collisions,” *Phys. Rev. C*, vol. 105, no. 4, p. 044910, 2022, arXiv:2111.13603.
- [309] N. P. M. Holt and R. Rapp, “Baryonic Sources of Thermal Photons,” *Eur. Phys. J. A*, vol. 56, no. 11, p. 292, 2020, arXiv:2008.00116.
- [310] F. Seck, T. Galatyuk, A. Mukherjee, R. Rapp, J. Steinheimer, J. Stroth, and M. Wiest, “Dilepton signature of a first-order phase transition,” *Phys. Rev. C*, vol. 106, no. 1, p. 014904, 2022, arXiv:2010.04614.
- [311] O. Savchuk, A. Motornenko, J. Steinheimer, V. Vovchenko, M. Bleicher, M. Gorenstein, and T. Galatyuk, “Enhanced dilepton emission from a phase transition in dense matter,” 9 2022, arXiv:2209.05267.
- [312] A. H. Rezaeian, M. Siddikov, M. Van de Klundert, and R. Venugopalan, “Analysis of combined HERA data in the Impact-Parameter dependent Saturation model,” *Phys. Rev. D*, vol. 87, no. 3, p. 034002, 2013, arXiv:1212.2974.
- [313] I. Balitsky, “Operator expansion for high-energy scattering,” *Nucl. Phys. B*, vol. 463, pp. 99–160, 1996, arXiv:hep-ph/9509348.
- [314] J. Jalilian-Marian, A. Kovner, L. D. McLerran, and H. Weigert, “The Intrinsic glue distribution at very small x,” *Phys. Rev. D*, vol. 55, pp. 5414–5428, 1997, arXiv:hep-ph/9606337.
- [315] E. Iancu, A. Leonidov, and L. D. McLerran, “Nonlinear gluon evolution in the color glass condensate. 1.,” *Nucl. Phys. A*, vol. 692, pp. 583–645, 2001, arXiv:hep-ph/0011241.
- [316] E. Ferreira, E. Iancu, A. Leonidov, and L. McLerran, “Nonlinear gluon evolution in the color glass condensate. 2.,” *Nucl. Phys. A*, vol. 703, pp. 489–538, 2002, arXiv:hep-ph/0109115.

- [317] Y. V. Kovchegov, “Unitarization of the BFKL pomeron on a nucleus,” *Phys. Rev. D*, vol. 61, p. 074018, 2000, arXiv:hep-ph/9905214.
- [318] H. Mäntysaari, B. Schenke, C. Shen, and P. Tribedy, “Imprints of fluctuating proton shapes on flow in proton-lead collisions at the LHC,” *Phys. Lett. B*, vol. 772, pp. 681–686, 2017, arXiv:1705.03177.
- [319] C. Gale, S. Jeon, B. Schenke, P. Tribedy, and R. Venugopalan, “Event-by-event anisotropic flow in heavy-ion collisions from combined Yang-Mills and viscous fluid dynamics,” *Phys. Rev. Lett.*, vol. 110, no. 1, p. 012302, 2013, arXiv:1209.6330.
- [320] P. Bozek, W. Broniowski, and J. Moreira, “Torqued fireballs in relativistic heavy-ion collisions,” *Phys. Rev. C*, vol. 83, p. 034911, 2011, arXiv:1011.3354.
- [321] J. Jia and P. Huo, “Forward-backward eccentricity and participant-plane angle fluctuations and their influences on longitudinal dynamics of collective flow,” *Phys. Rev. C*, vol. 90, no. 3, p. 034915, 2014, arXiv:1403.6077.
- [322] L.-G. Pang, H. Petersen, G.-Y. Qin, V. Roy, and X.-N. Wang, “Decorrelation of anisotropic flow along the longitudinal direction,” *Eur. Phys. J. A*, vol. 52, no. 4, p. 97, 2016, arXiv:1511.04131.
- [323] V. Khachatryan *et al.*, “Evidence for transverse momentum and pseudorapidity dependent event plane fluctuations in PbPb and pPb collisions,” *Phys. Rev. C*, vol. 92, no. 3, p. 034911, 2015, arXiv:1503.01692.
- [324] B. Schenke and S. Schlichting, “3D glasma initial state for relativistic heavy ion collisions,” *Phys. Rev. C*, vol. 94, no. 4, p. 044907, 2016, arXiv:1605.07158.
- [325] P. Bozek and W. Broniowski, “The torque effect and fluctuations of entropy deposition in rapidity in ultra-relativistic nuclear collisions,” *Phys. Lett. B*, vol. 752, pp. 206–211, 2016, arXiv:1506.02817.
- [326] S. Schlichting and P. Singh, “3-D structure of the Glasma initial state – Breaking boost-invariance by collisions of extended shock waves in classical Yang-Mills theory,” *Phys. Rev. D*, vol. 103, no. 1, p. 014003, 2021, arXiv:2010.11172.
- [327] M. Aaboud *et al.*, “Measurement of longitudinal flow decorrelations in Pb+Pb collisions at  $\sqrt{s_{NN}} = 2.76$  and 5.02 TeV with the ATLAS detector,” *Eur. Phys. J. C*, vol. 78, no. 2, p. 142, 2018, arXiv:1709.02301.
- [328] H. Petersen, J. Steinheimer, G. Burau, M. Bleicher, and H. Stöcker, “A Fully Integrated Transport Approach to Heavy Ion Reactions with an Intermediate Hydrodynamic Stage,” *Phys. Rev. C*, vol. 78, p. 044901, 2008, arXiv:0806.1695.
- [329] L.-G. Pang, G.-Y. Qin, V. Roy, X.-N. Wang, and G.-L. Ma, “Longitudinal decorrelation of anisotropic flows in heavy-ion collisions at the CERN Large Hadron Collider,” *Phys. Rev. C*, vol. 91, no. 4, p. 044904, 2015, arXiv:1410.8690.
- [330] K. Werner, I. Karpenko, T. Pierog, M. Bleicher, and K. Mikhailov, “Event-by-Event Simulation of the Three-Dimensional Hydrodynamic Evolution from Flux Tube Initial Conditions in Ultrarelativistic Heavy Ion Collisions,” *Phys. Rev. C*, vol. 82, p. 044904, 2010, arXiv:1004.0805.
- [331] W. van der Schee, P. Romatschke, and S. Pratt, “Fully Dynamical Simulation of Central Nuclear Collisions,” *Phys. Rev. Lett.*, vol. 111, no. 22, p. 222302, 2013, arXiv:1307.2539.
- [332] W. van der Schee and B. Schenke, “Rapidity dependence in holographic heavy ion collisions,” *Phys. Rev. C*, vol. 92, no. 6, p. 064907, 2015, arXiv:1507.08195.
- [333] W. Li, “Collective flow from AA, pA to pp collisions – Toward a unified paradigm,” *Nucl. Phys. A*, vol. 967, pp. 59–66, 2017, arXiv:1704.03576.
- [334] L. Adamczyk *et al.*, “Harmonic decomposition of three-particle azimuthal correlations at energies available at the BNL Relativistic Heavy Ion Collider,” *Phys. Rev. C*, vol. 98, no. 3, p. 034918, 2018, arXiv:1701.06496.

- [335] M. Aaboud *et al.*, “Measurement of forward-backward multiplicity correlations in lead-lead, proton-lead, and proton-proton collisions with the ATLAS detector,” *Phys. Rev. C*, vol. 95, no. 6, p. 064914, 2017, arXiv:1606.08170.
- [336] J. Jia, S. Radhakrishnan, and M. Zhou, “Forward-backward multiplicity fluctuation and longitudinal harmonics in high-energy nuclear collisions,” *Phys. Rev. C*, vol. 93, no. 4, p. 044905, 2016, arXiv:1506.03496.
- [337] A. Bzdak and D. Teaney, “Longitudinal fluctuations of the fireball density in heavy-ion collisions,” *Phys. Rev. C*, vol. 87, no. 2, p. 024906, 2013, arXiv:1210.1965.
- [338] A. Bzdak and K. Dusling, “Saturation scale fluctuations and multi-particle rapidity correlations,” *Phys. Rev. C*, vol. 94, p. 044918, 2016, arXiv:1607.03219.
- [339] S. A. Voloshin and T. Niida, “Ultrarelativistic nuclear collisions: Direction of spectator flow,” *Phys. Rev. C*, vol. 94, no. 2, p. 021901, 2016, arXiv:1604.04597.
- [340] M. Alvioli and M. Strikman, “Beam Fragmentation in Heavy Ion Collisions with Realistically Correlated Nuclear Configurations,” *Phys. Rev. C*, vol. 83, p. 044905, 2011, arXiv:1008.2328.
- [341] J. D. Brandenburg, N. Lewis, P. Tribedy, and Z. Xu, “Search for baryon junctions in photonuclear processes and isobar collisions at RHIC,” 5 2022, arXiv:2205.05685.
- [342] I. G. Bearden *et al.*, “Nuclear stopping in Au + Au collisions at  $\sqrt{s_{NN}} = 200$ -GeV,” *Phys. Rev. Lett.*, vol. 93, p. 102301, 2004, arXiv:nucl-ex/0312023.
- [343] L. Adamczyk *et al.*, “Bulk Properties of the Medium Produced in Relativistic Heavy-Ion Collisions from the Beam Energy Scan Program,” *Phys. Rev. C*, vol. 96, no. 4, p. 044904, 2017, arXiv:1701.07065.
- [344] K. Aamodt *et al.*, “Midrapidity antiproton-to-proton ratio in pp collisions at  $\sqrt{s} = 0.9$  and 7~TeV measured by the ALICE experiment,” *Phys. Rev. Lett.*, vol. 105, p. 072002, 2010, arXiv:1006.5432.
- [345] E. Abbas *et al.*, “Mid-rapidity anti-baryon to baryon ratios in pp collisions at  $\sqrt{s} = 0.9, 2.76$  and 7 TeV measured by ALICE,” *Eur. Phys. J. C*, vol. 73, p. 2496, 2013, arXiv:1305.1562.
- [346] D. Kharzeev, “Can gluons trace baryon number?,” *Phys. Lett. B*, vol. 378, pp. 238–246, 1996, arXiv:nucl-th/9602027.
- [347] B. Andersson, G. Gustafson, G. Ingelman, and T. Sjostrand, “Parton Fragmentation and String Dynamics,” *Phys. Rept.*, vol. 97, pp. 31–145, 1983.
- [348] L. Ahle *et al.*, “Anti-proton production in Au + Au collisions at 11.7-A-GeV/c,” *Phys. Rev. Lett.*, vol. 81, pp. 2650–2654, 1998.
- [349] H. Appelshauser *et al.*, “Baryon stopping and charged particle distributions in central Pb + Pb collisions at 158-GeV per nucleon,” *Phys. Rev. Lett.*, vol. 82, pp. 2471–2475, 1999, arXiv:nucl-ex/9810014.
- [350] I. C. Arsene *et al.*, “Nuclear stopping and rapidity loss in Au+Au collisions at  $\sqrt{s_{NN}} = 62.4$  GeV,” *Phys. Lett. B*, vol. 677, pp. 267–271, 2009, arXiv:0901.0872.
- [351] C. Adler *et al.*, “Midrapidity anti-proton to proton ratio from Au + Au collisions at  $\sqrt{s_{NN}} = 130$  GeV,” *Phys. Rev. Lett.*, vol. 86, p. 4778, 2001, arXiv:nucl-ex/0104022. [Erratum: *Phys.Rev.Lett.* 90, 119903 (2003)].
- [352] C. Shen and B. Schenke, “Longitudinal dynamics and particle production in relativistic nuclear collisions,” *Phys. Rev. C*, vol. 105, no. 6, p. 064905, 2022, arXiv:2203.04685.
- [353] S. E. Vance, M. Gyulassy, and X. N. Wang, “Baryon number transport via gluonic junctions,” *Phys. Lett. B*, vol. 443, pp. 45–50, 1998, arXiv:nucl-th/9806008.
- [354] V. Topor Pop, J. Barrette, C. Gale, S. Jeon, and M. Gyulassy, “Stopping power from SPS to LHC energies,” *J. Phys. G*, vol. 35, no. 5, p. 054001.15, 2008, arXiv:0705.2759.

- [355] H. Suganuma, T. T. Takahashi, F. Okiharu, and H. Ichie, “Lattice QCD study for the interquark force in three-quark and multi-quark systems,” *AIP Conf. Proc.*, vol. 756, no. 1, pp. 123–132, 2005, arXiv:hep-lat/0412026.
- [356] T. T. Takahashi, H. Matsufuru, Y. Nemoto, and H. Suganuma, “The Three quark potential in the SU(3) lattice QCD,” *Phys. Rev. Lett.*, vol. 86, pp. 18–21, 2001, arXiv:hep-lat/0006005.
- [357] M. Abdallah *et al.*, “Search for the chiral magnetic effect with isobar collisions at  $\sqrt{s_{NN}}=200$  GeV by the STAR Collaboration at the BNL Relativistic Heavy Ion Collider,” *Phys. Rev. C*, vol. 105, no. 1, p. 014901, 2022, arXiv:2109.00131.
- [358] G. Nijs and W. van der Schee, “Hadronic Nucleus-Nucleus Cross Section and the Nucleon Size,” *Phys. Rev. Lett.*, vol. 129, no. 23, p. 232301, 2022, arXiv:2206.13522.
- [359] G. Giacalone, “There and Sharp Again: The Circle Journey of Nucleons and Energy Deposition,” 8 2022, arXiv:2208.06839.
- [360] G. Giacalone, J. Jia, and V. Somà, “Accessing the shape of atomic nuclei with relativistic collisions of isobars,” *Phys. Rev. C*, vol. 104, no. 4, p. L041903, 2021, arXiv:2102.08158.
- [361] J. Jia, “Shape of atomic nuclei in heavy ion collisions,” *Phys. Rev. C*, vol. 105, no. 1, p. 014905, 2022, arXiv:2106.08768.
- [362] J. Jia and C.-J. Zhang, “Scaling approach to nuclear structure in high-energy heavy-ion collisions,” 11 2021, arXiv:2111.15559.
- [363] H.-j. Xu, W. Zhao, H. Li, Y. Zhou, L.-W. Chen, and F. Wang, “Probing nuclear structure with mean transverse momentum in relativistic isobar collisions,” 11 2021, arXiv:2111.14812.
- [364] C. Zhang, S. Bhatta, and J. Jia, “Ratios of collective flow observables in high-energy isobar collisions are insensitive to final-state interactions,” *Phys. Rev. C*, vol. 106, no. 3, p. L031901, 2022, arXiv:2206.01943.
- [365] J. Jia, “Probing triaxial deformation of atomic nuclei in high-energy heavy ion collisions,” *Phys. Rev. C*, vol. 105, no. 4, p. 044905, 2022, arXiv:2109.00604.
- [366] L. Adamczyk *et al.*, “Azimuthal anisotropy in U+U and Au+Au collisions at RHIC,” *Phys. Rev. Lett.*, vol. 115, no. 22, p. 222301, 2015, arXiv:1505.07812.
- [367] S. Acharya *et al.*, “Anisotropic flow in Xe-Xe collisions at  $\sqrt{s_{NN}} = 5.44$  TeV,” *Phys. Lett. B*, vol. 784, pp. 82–95, 2018, arXiv:1805.01832.
- [368] ATLAS Collaboration, “Correlations between flow and transverse momentum in Xe+Xe and Pb+Pb collisions at the LHC with the ATLAS detector: a probe of the heavy-ion initial state and nuclear deformation,” 4 2022, arXiv:2205.00039.
- [369] Haojie Xu talk, Chunjian Zhang poster, (STAR Collaboration), Constraints on neutron skin thickness and nuclear deformations using relativistic heavy-ion collisions from STAR, “<https://indico.cern.ch/event/895086/contributions/4724887/>, <https://indico.cern.ch/event/895086/contributions/4749420/>.”
- [370] J. Jia, G. Giacalone, and C. Zhang, “Separating the impact of nuclear skin and nuclear deformation on elliptic flow and its fluctuations in high-energy isobar collisions,” 6 2022, arXiv:2206.10449.
- [371] H.-j. Xu, H. Li, X. Wang, C. Shen, and F. Wang, “Determine the neutron skin type by relativistic isobaric collisions,” *Phys. Lett. B*, vol. 819, p. 136453, 2021, arXiv:2103.05595.
- [372] Y. Cao, S. E. Agbemava, A. V. Afanasjev, W. Nazarewicz, and E. Olsen, “Landscape of pear-shaped even-even nuclei,” *Phys. Rev. C*, vol. 102, no. 2, p. 024311, 2020, arXiv:2004.01319.
- [373] S. Shi, H. Zhang, D. Hou, and J. Liao, “Signatures of Chiral Magnetic Effect in the Collisions of Isobars,” *Phys. Rev. Lett.*, vol. 125, p. 242301, 2020, arXiv:1910.14010.
- [374] S. Shi, Y. Jiang, E. Lilleskov, and J. Liao, “Anomalous Chiral Transport in Heavy Ion Collisions from

- Anomalous-Viscous Fluid Dynamics,” *Annals Phys.*, vol. 394, pp. 50–72, 2018, arXiv:1711.02496.
- [375] S. Choudhury *et al.*, “Investigation of experimental observables in search of the chiral magnetic effect in heavy-ion collisions in the STAR experiment \*,” *Chin. Phys. C*, vol. 46, no. 1, p. 014101, 2022, arXiv:2105.06044.
- [376] R. Milton, G. Wang, M. Sergeeva, S. Shi, J. Liao, and H. Z. Huang, “Utilization of event shape in search of the chiral magnetic effect in heavy-ion collisions,” *Phys. Rev. C*, vol. 104, no. 6, p. 064906, 2021, arXiv:2110.01435.
- [377] N. Magdy, S. Shi, J. Liao, N. Ajitanand, and R. A. Lacey, “New correlator to detect and characterize the chiral magnetic effect,” *Phys. Rev. C*, vol. 97, no. 6, p. 061901, 2018, arXiv:1710.01717.
- [378] A. H. Tang, “Probe chiral magnetic effect with signed balance function,” *Chin. Phys. C*, vol. 44, no. 5, p. 054101, 2020, arXiv:1903.04622.
- [379] P. Christakoglou, S. Qiu, and J. Staa, “Systematic study of the chiral magnetic effect with the AVFD model at LHC energies,” *Eur. Phys. J. C*, vol. 81, no. 8, p. 717, 2021, arXiv:2106.03537.
- [380] M. S. Abdallah *et al.*, “Search for the Chiral Magnetic Effect via Charge-Dependent Azimuthal Correlations Relative to Spectator and Participant Planes in Au+Au Collisions at  $\sqrt{s_{NN}} = 200$  GeV,” *Phys. Rev. Lett.*, vol. 128, no. 9, p. 092301, 2022, arXiv:2106.09243.
- [381] V. Khachatryan *et al.*, “Observation of charge-dependent azimuthal correlations in  $p$ -Pb collisions and its implication for the search for the chiral magnetic effect,” *Phys. Rev. Lett.*, vol. 118, no. 12, p. 122301, 2017, arXiv:1610.00263.
- [382] A. M. Sirunyan *et al.*, “Constraints on the chiral magnetic effect using charge-dependent azimuthal correlations in  $p$ Pb and PbPb collisions at the CERN Large Hadron Collider,” *Phys. Rev. C*, vol. 97, no. 4, p. 044912, 2018, arXiv:1708.01602.
- [383] S. Acharya *et al.*, “Constraining the magnitude of the Chiral Magnetic Effect with Event Shape Engineering in Pb-Pb collisions at  $\sqrt{s_{NN}} = 2.76$  TeV,” *Phys. Lett. B*, vol. 777, pp. 151–162, 2018, arXiv:1709.04723.
- [384] S. Acharya *et al.*, “Constraining the Chiral Magnetic Effect with charge-dependent azimuthal correlations in Pb-Pb collisions at  $\sqrt{s_{NN}} = 2.76$  and 5.02 TeV,” *JHEP*, vol. 09, p. 160, 2020, arXiv:2005.14640.
- [385] M. S. Abdallah *et al.*, “Pair invariant mass to isolate background in the search for the chiral magnetic effect in Au + Au collisions at  $s_{NN}=200$  GeV,” *Phys. Rev. C*, vol. 106, no. 3, p. 034908, 2022, arXiv:2006.05035.
- [386] Y. Lin, “Measurement of the charge separation along the magnetic field with Signed Balance Function in 200 GeV Au + Au collisions at STAR,” *Nucl. Phys. A*, vol. 1005, p. 121828, 2021, arXiv:2002.11446.
- [387] J. Błoczynski, X.-G. Huang, X. Zhang, and J. Liao, “Azimuthally fluctuating magnetic field and its impacts on observables in heavy-ion collisions,” *Phys. Lett. B*, vol. 718, pp. 1529–1535, 2013, arXiv:1209.6594.
- [388] H.-j. Xu, J. Zhao, X. Wang, H. Li, Z.-W. Lin, C. Shen, and F. Wang, “Varying the chiral magnetic effect relative to flow in a single nucleus-nucleus collision,” *Chin. Phys. C*, vol. 42, no. 8, p. 084103, 2018, arXiv:1710.07265.
- [389] S. A. Voloshin, “Estimate of the signal from the chiral magnetic effect in heavy-ion collisions from measurements relative to the participant and spectator flow planes,” *Phys. Rev. C*, vol. 98, no. 5, p. 054911, 2018, arXiv:1805.05300.
- [390] J. Adam *et al.*, “Methods for a blind analysis of isobar data collected by the STAR collaboration,” *Nucl. Sci. Tech.*, vol. 32, no. 5, p. 48, 2021, arXiv:1911.00596.

- [391] D. E. Kharzeev, J. Liao, and S. Shi, “Implications of the isobar-run results for the chiral magnetic effect in heavy-ion collisions,” *Phys. Rev. C*, vol. 106, no. 5, p. L051903, 2022, arXiv:2205.00120.
- [392] Y. Feng, J. Zhao, H. Li, H.-j. Xu, and F. Wang, “Two- and three-particle nonflow contributions to the chiral magnetic effect measurement by spectator and participant planes in relativistic heavy ion collisions,” *Phys. Rev. C*, vol. 105, no. 2, p. 024913, 2022, arXiv:2106.15595.
- [393] F. Becattini and M. A. Lisa, “Polarization and Vorticity in the Quark–Gluon Plasma,” *Ann. Rev. Nucl. Part. Sci.*, vol. 70, pp. 395–423, 2020, arXiv:2003.03640.
- [394] F. Becattini, J. Liao, and M. Lisa, “Strongly Interacting Matter Under Rotation: An Introduction,” *Lect. Notes Phys.*, vol. 987, pp. 1–14, 2021, arXiv:2102.00933.
- [395] F. Becattini, “Spin and polarization: a new direction in relativistic heavy ion physics,” *Rept. Prog. Phys.*, vol. 85, no. 12, p. 122301, 2022, arXiv:2204.01144.
- [396] Z.-T. Liang and X.-N. Wang, “Globally polarized quark-gluon plasma in non-central A+A collisions,” *Phys. Rev. Lett.*, vol. 94, p. 102301, 2005, arXiv:nucl-th/0410079. [Erratum: *Phys.Rev.Lett.* 96, 039901 (2006)].
- [397] S. A. Voloshin, “Polarized secondary particles in unpolarized high energy hadron-hadron collisions?,” 10 2004, arXiv:nucl-th/0410089.
- [398] F. Becattini, F. Piccinini, and J. Rizzo, “Angular momentum conservation in heavy ion collisions at very high energy,” *Phys. Rev. C*, vol. 77, p. 024906, 2008, arXiv:0711.1253.
- [399] F. Becattini, I. Karpenko, M. Lisa, I. Upsal, and S. Voloshin, “Global hyperon polarization at local thermodynamic equilibrium with vorticity, magnetic field and feed-down,” *Phys. Rev. C*, vol. 95, no. 5, p. 054902, 2017, arXiv:1610.02506.
- [400] F. Becattini, V. Chandra, L. Del Zanna, and E. Grossi, “Relativistic distribution function for particles with spin at local thermodynamical equilibrium,” *Annals Phys.*, vol. 338, pp. 32–49, 2013, arXiv:1303.3431.
- [401] B. Fu, S. Y. F. Liu, L. Pang, H. Song, and Y. Yin, “Shear-Induced Spin Polarization in Heavy-Ion Collisions,” *Phys. Rev. Lett.*, vol. 127, no. 14, p. 142301, 2021, arXiv:2103.10403.
- [402] F. Becattini, M. Buzzegoli, G. Inghirami, I. Karpenko, and A. Palermo, “Local Polarization and Isothermal Local Equilibrium in Relativistic Heavy Ion Collisions,” *Phys. Rev. Lett.*, vol. 127, no. 27, p. 272302, 2021, arXiv:2103.14621.
- [403] Y. Jiang, Z.-W. Lin, and J. Liao, “Rotating quark-gluon plasma in relativistic heavy ion collisions,” *Phys. Rev. C*, vol. 94, no. 4, p. 044910, 2016, arXiv:1602.06580. [Erratum: *Phys.Rev.C* 95, 049904 (2017)].
- [404] M. S. Abdallah *et al.*, “Global  $\Lambda$ -hyperon polarization in Au+Au collisions at  $\sqrt{s_{NN}}=3$  GeV,” *Phys. Rev. C*, vol. 104, no. 6, p. L061901, 2021, arXiv:2108.00044.
- [405] R. Abou Yassine *et al.*, “Measurement of global polarization of  $\Lambda$  hyperons in few-GeV heavy-ion collisions,” *Phys. Lett. B*, vol. 835, p. 137506, 2022, arXiv:2207.05160.
- [406] B. Müller and A. Schäfer, “Chiral magnetic effect and an experimental bound on the late time magnetic field strength,” *Phys. Rev. D*, vol. 98, no. 7, p. 071902, 2018, arXiv:1806.10907.
- [407] Y. Guo, S. Shi, S. Feng, and J. Liao, “Magnetic Field Induced Polarization Difference between Hyperons and Anti-hyperons,” *Phys. Lett. B*, vol. 798, p. 134929, 2019, arXiv:1905.12613.
- [408] R.-h. Fang, L.-g. Pang, Q. Wang, and X.-n. Wang, “Polarization of massive fermions in a vortical fluid,” *Phys. Rev. C*, vol. 94, no. 2, p. 024904, 2016, arXiv:1604.04036.
- [409] L. P. Csernai, J. I. Kapusta, and T. Welle, “ $\Lambda$  and  $\bar{\Lambda}$  spin interaction with meson fields generated by the baryon current in high energy nuclear collisions,” *Phys. Rev. C*, vol. 99, no. 2, p. 021901, 2019, arXiv:1807.11521.



- [410] O. Vitiuk, L. V. Bravina, and E. E. Zabrodin, “Is different  $\Lambda$  and  $\bar{\Lambda}$  polarization caused by different spatio-temporal freeze-out picture?,” *Phys. Lett. B*, vol. 803, p. 135298, 2020, arXiv:1910.06292.
- [411] X. Guo, J. Liao, and E. Wang, “Spin Hydrodynamic Generation in the Charged Subatomic Swirl,” *Sci. Rep.*, vol. 10, no. 1, p. 2196, 2020, arXiv:1904.04704.
- [412] J. Adam *et al.*, “Global Polarization of  $\Xi$  and  $\Omega$  Hyperons in Au+Au Collisions at  $\sqrt{s_{NN}} = 200$  GeV,” *Phys. Rev. Lett.*, vol. 126, no. 16, p. 162301, 2021, arXiv:2012.13601.
- [413] D.-X. Wei, W.-T. Deng, and X.-G. Huang, “Thermal vorticity and spin polarization in heavy-ion collisions,” *Phys. Rev. C*, vol. 99, no. 1, p. 014905, 2019, arXiv:1810.00151.
- [414] R. L. Workman *et al.*, “Review of Particle Physics,” *PTEP*, vol. 2022, p. 083C01, 2022.
- [415] L.-G. Pang, H. Petersen, Q. Wang, and X.-N. Wang, “Vortical Fluid and  $\Lambda$  Spin Correlations in High-Energy Heavy-Ion Collisions,” *Phys. Rev. Lett.*, vol. 117, no. 19, p. 192301, 2016, arXiv:1605.04024.
- [416] F. Becattini and I. Karpenko, “Collective Longitudinal Polarization in Relativistic Heavy-Ion Collisions at Very High Energy,” *Phys. Rev. Lett.*, vol. 120, no. 1, p. 012302, 2018, arXiv:1707.07984.
- [417] S. A. Voloshin, “Vorticity and particle polarization in heavy ion collisions (experimental perspective),” *EPJ Web Conf.*, vol. 171, p. 07002, 2018, arXiv:1710.08934.
- [418] X.-L. Xia, H. Li, Z.-B. Tang, and Q. Wang, “Probing vorticity structure in heavy-ion collisions by local  $\Lambda$  polarization,” *Phys. Rev. C*, vol. 98, p. 024905, 2018, arXiv:1803.00867.
- [419] S. Alzhrani, S. Ryu, and C. Shen, “ $\Lambda$  spin polarization in event-by-event relativistic heavy-ion collisions,” *Phys. Rev. C*, vol. 106, no. 1, p. 014905, 2022, arXiv:2203.15718.
- [420] Z.-T. Liang and X.-N. Wang, “Spin alignment of vector mesons in non-central A+A collisions,” *Phys. Lett. B*, vol. 629, pp. 20–26, 2005, arXiv:nucl-th/0411101.
- [421] M. Abdallah *et al.*, “Observation of Global Spin Alignment of  $\phi$  and  $K^{*0}$  Vector Mesons in Nuclear Collisions,” 4 2022, arXiv:2204.02302.
- [422] S. Acharya *et al.*, “Evidence of Spin-Orbital Angular Momentum Interactions in Relativistic Heavy-Ion Collisions,” *Phys. Rev. Lett.*, vol. 125, no. 1, p. 012301, 2020, arXiv:1910.14408.
- [423] X.-L. Sheng, L. Oliva, and Q. Wang, “What can we learn from the global spin alignment of  $\phi$  mesons in heavy-ion collisions?,” *Phys. Rev. D*, vol. 101, no. 9, p. 096005, 2020, arXiv:1910.13684. [Erratum: Phys.Rev.D 105, 099903 (2022)].
- [424] X.-L. Sheng, L. Oliva, Z.-T. Liang, Q. Wang, and X.-N. Wang, “Spin alignment of vector mesons in heavy-ion collisions,” 5 2022, arXiv:2205.15689.
- [425] X.-L. Sheng, L. Oliva, Z.-T. Liang, Q. Wang, and X.-N. Wang, “Relativistic spin dynamics for vector mesons,” 6 2022, arXiv:2206.05868.
- [426] B. Schenke, “The smallest fluid on Earth,” *Rept. Prog. Phys.*, vol. 84, no. 8, p. 082301, 2021, arXiv:2102.11189.
- [427] S. S. Adler *et al.*, “Absence of suppression in particle production at large transverse momentum in  $\sqrt{s_{NN}} = 200$  GeV d + Au collisions,” *Phys. Rev. Lett.*, vol. 91, p. 072303, 2003, arXiv:nucl-ex/0306021.
- [428] J. Adams *et al.*, “Evidence from d + Au measurements for final state suppression of high  $p_T$  hadrons in Au+Au collisions at RHIC,” *Phys. Rev. Lett.*, vol. 91, p. 072304, 2003, arXiv:nucl-ex/0306024.
- [429] I. Arsene *et al.*, “Transverse momentum spectra in Au+Au and d+Au collisions at  $\sqrt{s_{NN}} = 200$  GeV and the pseudorapidity dependence of high  $p_T$  suppression,” *Phys. Rev. Lett.*, vol. 91, p. 072305, 2003, arXiv:nucl-ex/0307003.
- [430] B. B. Back *et al.*, “Centrality dependence of charged hadron transverse momentum spectra in d + Au collisions at  $\sqrt{s_{NN}} = 200$  GeV,” *Phys. Rev. Lett.*, vol. 91, p. 072302, 2003, arXiv:nucl-ex/0306025.

- [431] V. Khachatryan *et al.*, “Observation of Long-Range Near-Side Angular Correlations in Proton-Proton Collisions at the LHC,” *JHEP*, vol. 09, p. 091, 2010, arXiv:1009.4122.
- [432] S. Chatrchyan *et al.*, “Observation of Long-Range Near-Side Angular Correlations in Proton-Lead Collisions at the LHC,” *Phys. Lett. B*, vol. 718, pp. 795–814, 2013, arXiv:1210.5482.
- [433] B. Abelev *et al.*, “Long-range angular correlations on the near and away side in  $p$ -Pb collisions at  $\sqrt{s_{NN}} = 5.02$  TeV,” *Phys. Lett. B*, vol. 719, pp. 29–41, 2013, arXiv:1212.2001.
- [434] G. Aad *et al.*, “Observation of Associated Near-Side and Away-Side Long-Range Correlations in  $\sqrt{s_{NN}}=5.02$  TeV Proton-Lead Collisions with the ATLAS Detector,” *Phys. Rev. Lett.*, vol. 110, no. 18, p. 182302, 2013, arXiv:1212.5198.
- [435] R. Aaij *et al.*, “Measurements of long-range near-side angular correlations in  $\sqrt{s_{NN}} = 5$ TeV proton-lead collisions in the forward region,” *Phys. Lett. B*, vol. 762, pp. 473–483, 2016, arXiv:1512.00439.
- [436] A. Adare *et al.*, “Quadrupole Anisotropy in Dihadron Azimuthal Correlations in Central  $d$ +Au Collisions at  $\sqrt{s_{NN}}=200$  GeV,” *Phys. Rev. Lett.*, vol. 111, no. 21, p. 212301, 2013, arXiv:1303.1794.
- [437] A. Adare *et al.*, “Measurement of long-range angular correlation and quadrupole anisotropy of pions and (anti)protons in central  $d$ +Au collisions at  $\sqrt{s_{NN}}=200$  GeV,” *Phys. Rev. Lett.*, vol. 114, no. 19, p. 192301, 2015, arXiv:1404.7461.
- [438] L. Adamczyk *et al.*, “Long-range pseudorapidity dihadron correlations in  $d$ +Au collisions at  $\sqrt{s_{NN}} = 200$  GeV,” *Phys. Lett. B*, vol. 747, pp. 265–271, 2015, arXiv:1502.07652.
- [439] K. Dusling, W. Li, and B. Schenke, “Novel collective phenomena in high-energy proton–proton and proton–nucleus collisions,” *Int. J. Mod. Phys. E*, vol. 25, no. 01, p. 1630002, 2016, arXiv:1509.07939.
- [440] C. Loizides, “Experimental overview on small collision systems at the LHC,” *Nucl. Phys. A*, vol. 956, pp. 200–207, 2016, arXiv:1602.09138.
- [441] J. L. Nagle and W. A. Zajc, “Small System Collectivity in Relativistic Hadronic and Nuclear Collisions,” *Ann. Rev. Nucl. Part. Sci.*, vol. 68, pp. 211–235, 2018.
- [442] C. Aidala *et al.*, “Measurement of long-range angular correlations and azimuthal anisotropies in high-multiplicity  $p$ +Au collisions at  $\sqrt{s_{NN}} = 200$  GeV,” *Phys. Rev. C*, vol. 95, no. 3, p. 034910, 2017, arXiv:1609.02894.
- [443] C. Aidala *et al.*, “Measurements of azimuthal anisotropy and charged-particle multiplicity in  $d$ +Au collisions at  $\sqrt{s_{NN}} = 200, 62.4, 39,$  and  $19.6$  GeV,” *Phys. Rev. C*, vol. 96, no. 6, p. 064905, 2017, arXiv:1708.06983.
- [444] A. Adare *et al.*, “Measurements of elliptic and triangular flow in high-multiplicity  $^3\text{He}$ +Au collisions at  $\sqrt{s_{NN}} = 200$  GeV,” *Phys. Rev. Lett.*, vol. 115, no. 14, p. 142301, 2015, arXiv:1507.06273.
- [445] C. Aidala *et al.*, “Measurements of Multiparticle Correlations in  $d + \text{Au}$  Collisions at 200, 62.4, 39, and 19.6 GeV and  $p + \text{Au}$  Collisions at 200 GeV and Implications for Collective Behavior,” *Phys. Rev. Lett.*, vol. 120, no. 6, p. 062302, 2018, arXiv:1707.06108.
- [446] G. Aad *et al.*, “Two-particle azimuthal correlations in photonuclear ultraperipheral Pb+Pb collisions at 5.02 TeV with ATLAS,” *Phys. Rev. C*, vol. 104, no. 1, p. 014903, 2021, arXiv:2101.10771.
- [447] CMS Collaboration, “Two-particle azimuthal correlations in  $\gamma p$  interactions using pPb collisions at  $\sqrt{s_{NN}} = 8.16$  TeV,” 4 2022, arXiv:2204.13486.
- [448] A. Badea, A. Baty, P. Chang, G. M. Innocenti, M. Maggi, C. McGinn, M. Peters, T.-A. Sheng, J. Thaler, and Y.-J. Lee, “Measurements of two-particle correlations in  $e^+e^-$  collisions at 91 GeV with ALEPH archived data,” *Phys. Rev. Lett.*, vol. 123, no. 21, p. 212002, 2019, arXiv:1906.00489.
- [449] Y. C. Chen *et al.*, “Measurement of Two-Particle Correlations of Hadrons in  $e+e-$  Collisions at Belle,” *Phys. Rev. Lett.*, vol. 128, no. 14, p. 142005, 2022, arXiv:2201.01694.

- [450] I. Abt *et al.*, “Two-particle azimuthal correlations as a probe of collective behaviour in deep inelastic *ep* scattering at HERA,” *JHEP*, vol. 04, p. 070, 2020, arXiv:1912.07431.
- [451] S. Chatrchyan *et al.*, “Multiplicity and Transverse Momentum Dependence of Two- and Four-Particle Correlations in pPb and PbPb Collisions,” *Phys. Lett. B*, vol. 724, pp. 213–240, 2013, arXiv:1305.0609.
- [452] G. Aad *et al.*, “Measurement with the ATLAS detector of multi-particle azimuthal correlations in p+Pb collisions at  $\sqrt{s_{NN}}=5.02$  TeV,” *Phys. Lett. B*, vol. 725, pp. 60–78, 2013, arXiv:1303.2084.
- [453] V. Khachatryan *et al.*, “Evidence for Collective Multiparticle Correlations in p-Pb Collisions,” *Phys. Rev. Lett.*, vol. 115, no. 1, p. 012301, 2015, arXiv:1502.05382.
- [454] B. B. Abelev *et al.*, “Multiparticle azimuthal correlations in p -Pb and Pb-Pb collisions at the CERN Large Hadron Collider,” *Phys. Rev. C*, vol. 90, no. 5, p. 054901, 2014, arXiv:1406.2474.
- [455] V. Khachatryan *et al.*, “Evidence for collectivity in pp collisions at the LHC,” *Phys. Lett. B*, vol. 765, pp. 193–220, 2017, arXiv:1606.06198.
- [456] M. Aaboud *et al.*, “Measurement of long-range multiparticle azimuthal correlations with the subevent cumulant method in *pp* and *p + Pb* collisions with the ATLAS detector at the CERN Large Hadron Collider,” *Phys. Rev. C*, vol. 97, no. 2, p. 024904, 2018, arXiv:1708.03559.
- [457] S. Acharya *et al.*, “Investigations of Anisotropic Flow Using Multiparticle Azimuthal Correlations in pp, p-Pb, Xe-Xe, and Pb-Pb Collisions at the LHC,” *Phys. Rev. Lett.*, vol. 123, no. 14, p. 142301, 2019, arXiv:1903.01790.
- [458] M. Aaboud *et al.*, “Measurement of multi-particle azimuthal correlations in *pp*, *p+Pb* and low-multiplicity Pb+Pb collisions with the ATLAS detector,” *Eur. Phys. J. C*, vol. 77, no. 6, p. 428, 2017, arXiv:1705.04176.
- [459] S. Chatrchyan *et al.*, “Study of the Production of Charged Pions, Kaons, and Protons in pPb Collisions at  $\sqrt{s_{NN}} = 5.02$  TeV,” *Eur. Phys. J. C*, vol. 74, no. 6, p. 2847, 2014, arXiv:1307.3442.
- [460] B. B. Abelev *et al.*, “Long-range angular correlations of  $\pi$ , K and p in p-Pb collisions at  $\sqrt{s_{NN}} = 5.02$  TeV,” *Phys. Lett. B*, vol. 726, pp. 164–177, 2013, arXiv:1307.3237.
- [461] V. Khachatryan *et al.*, “Long-range two-particle correlations of strange hadrons with charged particles in pPb and PbPb collisions at LHC energies,” *Phys. Lett. B*, vol. 742, pp. 200–224, 2015, arXiv:1409.3392.
- [462] J. Adam *et al.*, “Multi-strange baryon production in p-Pb collisions at  $\sqrt{s_{NN}} = 5.02$  TeV,” *Phys. Lett. B*, vol. 758, pp. 389–401, 2016, arXiv:1512.07227.
- [463] J. Adam *et al.*, “Enhanced production of multi-strange hadrons in high-multiplicity proton-proton collisions,” *Nature Phys.*, vol. 13, pp. 535–539, 2017, arXiv:1606.07424.
- [464] V. Khachatryan *et al.*, “Multiplicity and rapidity dependence of strange hadron production in pp, pPb, and PbPb collisions at the LHC,” *Phys. Lett. B*, vol. 768, pp. 103–129, 2017, arXiv:1605.06699.
- [465] A. Adare *et al.*, “Measurements of mass-dependent azimuthal anisotropy in central *p+Au*, *d+Au*, and  $^3\text{He+Au}$  collisions at  $\sqrt{s_{NN}} = 200$  GeV,” *Phys. Rev. C*, vol. 97, p. 064904, 2018, arXiv:1710.09736.
- [466] A. M. Sirunyan *et al.*, “Strange hadron production in pp and pPb collisions at  $\sqrt{s_{NN}} = 5.02$  TeV,” *Phys. Rev. C*, vol. 101, no. 6, p. 064906, 2020, arXiv:1910.04812.
- [467] G. Aad *et al.*, “Measurement of azimuthal anisotropy of muons from charm and bottom hadrons in *pp* collisions at  $\sqrt{s} = 13$  TeV with the ATLAS detector,” *Phys. Rev. Lett.*, vol. 124, no. 8, p. 082301, 2020, arXiv:1909.01650.
- [468] S. Acharya *et al.*, “Search for collectivity with azimuthal  $J/\psi$ -hadron correlations in high multiplicity p-Pb collisions at  $\sqrt{s_{NN}} = 5.02$  and 8.16 TeV,” *Phys. Lett. B*, vol. 780, pp. 7–20, 2018,

arXiv:1709.06807.

- [469] A. M. Sirunyan *et al.*, “Elliptic flow of charm and strange hadrons in high-multiplicity pPb collisions at  $\sqrt{s_{NN}} = 8.16$  TeV,” *Phys. Rev. Lett.*, vol. 121, no. 8, p. 082301, 2018, arXiv:1804.09767.
- [470] A. M. Sirunyan *et al.*, “Studies of charm and beauty hadron long-range correlations in pp and pPb collisions at LHC energies,” *Phys. Lett. B*, vol. 813, p. 136036, 2021, arXiv:2009.07065.
- [471] CMS Collaboration, “Azimuthal anisotropy of  $\Upsilon(1S)$  mesons in pPb collisions at  $\sqrt{s_{NN}} = 8.16$  TeV,” tech. rep., CERN, Geneva, 2022.
- [472] J. L. Nagle, A. Adare, S. Beckman, T. Koblesky, J. Orjuela Koop, D. McGlinchey, P. Romatschke, J. Carlson, J. E. Lynn, and M. McCumber, “Exploiting Intrinsic Triangular Geometry in Relativistic He3+Au Collisions to Disentangle Medium Properties,” *Phys. Rev. Lett.*, vol. 113, no. 11, p. 112301, 2014.
- [473] P. Romatschke, “Light-Heavy Ion Collisions: A window into pre-equilibrium QCD dynamics?,” *Eur. Phys. J. C*, vol. 75, no. 7, p. 305, 2015.
- [474] STAR Collaboration, “Measurements of the elliptic and triangular azimuthal anisotropies in central 3He+Au, d+Au and p+Au collisions at  $\sqrt{s_{NN}} = 200$  GeV,” 10 2022, arXiv:2210.11352.
- [475] U. A. Acharya *et al.*, “Kinematic dependence of azimuthal anisotropies in  $p + Au$ ,  $d + Au$ , and  ${}^3\text{He} + Au$  at  $\sqrt{s_{NN}} = 200$  GeV,” *Phys. Rev. C*, vol. 105, no. 2, p. 024901, 2022, arXiv:2107.06634.
- [476] J. L. Nagle, R. Belmont, S. H. Lim, and B. Seidlitz, “Checking nonflow assumptions and results via PHENIX published correlations in  $p + p$ ,  $p+Au$ ,  $d+Au$ , and  ${}^3\text{He}+Au$  at  $\sqrt{s_{NN}}=200$  GeV,” *Phys. Rev. C*, vol. 105, no. 2, p. 024906, 2022, arXiv:2107.07287.
- [477] W. Zhao, S. Ryu, C. Shen, and B. Schenke, “3D structure of anisotropic flow in small collision systems at energies available at the BNL Relativistic Heavy Ion Collider,” *Phys. Rev. C*, vol. 107, no. 1, p. 014904, 2023, arXiv:2211.16376.
- [478] G. Giacalone, B. Schenke, and C. Shen, “Observable signatures of initial state momentum anisotropies in nuclear collisions,” *Phys. Rev. Lett.*, vol. 125, no. 19, p. 192301, 2020, arXiv:2006.15721.
- [479] P. Bozek, “Transverse-momentum–flow correlations in relativistic heavy-ion collisions,” *Phys. Rev. C*, vol. 93, no. 4, p. 044908, 2016, arXiv:1601.04513.
- [480] G. Aad *et al.*, “Measurement of flow harmonics correlations with mean transverse momentum in lead-lead and proton-lead collisions at  $\sqrt{s_{NN}} = 5.02$  TeV with the ATLAS detector,” *Eur. Phys. J. C*, vol. 79, no. 12, p. 985, 2019, arXiv:1907.05176.
- [481] S. Tuo, “Correlation Between Multiparticle Cumulants and Mean Transverse Momentum in Small Collision Systems with the CMS Detector,” *Acta Phys. Pol. B Proc. Suppl.*, vol. 16, pp. 1–A67, 2023.
- [482] Y. Shi, L. Wang, S.-Y. Wei, B.-W. Xiao, and L. Zheng, “Exploring collective phenomena at the electron-ion collider,” *Phys. Rev. D*, vol. 103, no. 5, p. 054017, 2021, arXiv:2008.03569.
- [483] W. Zhao, C. Shen, and B. Schenke, “Collectivity in Ultraperipheral Pb+Pb Collisions at the Large Hadron Collider,” *Phys. Rev. Lett.*, vol. 129, no. 25, p. 252302, 2022, arXiv:2203.06094.
- [484] J. R. Christiansen and P. Z. Skands, “String Formation Beyond Leading Colour,” *JHEP*, vol. 08, p. 003, 2015, arXiv:1505.01681.
- [485] C. Bierlich and J. R. Christiansen, “Effects of color reconnection on hadron flavor observables,” *Phys. Rev. D*, vol. 92, no. 9, p. 094010, 2015, arXiv:1507.02091.
- [486] C. Bierlich, S. Chakraborty, G. Gustafson, and L. Lönnblad, “Setting the string shoving picture in a new frame,” *JHEP*, vol. 03, p. 270, 2021, arXiv:2010.07595.
- [487] Z.-W. Lin, C. M. Ko, B.-A. Li, B. Zhang, and S. Pal, “A Multi-phase transport model for relativistic heavy ion collisions,” *Phys. Rev. C*, vol. 72, p. 064901, 2005, arXiv:nucl-th/0411110.

- [488] J. L. Nagle, R. Belmont, K. Hill, J. Orjuela Koop, D. V. Perepelitsa, P. Yin, Z.-W. Lin, and D. McGlinchey, “Minimal conditions for collectivity in  $e^+e^-$  and  $p + p$  collisions,” *Phys. Rev. C*, vol. 97, no. 2, p. 024909, 2018, arXiv:1707.02307.
- [489] W. Florkowski, M. P. Heller, and M. Spalinski, “New theories of relativistic hydrodynamics in the LHC era,” *Rept. Prog. Phys.*, vol. 81, no. 4, p. 046001, 2018, arXiv:1707.02282.
- [490] P. Romatschke and U. Romatschke, *Relativistic Fluid Dynamics In and Out of Equilibrium*. Cambridge Monographs on Mathematical Physics, Cambridge University Press, 5 2019, arXiv:1712.05815.
- [491] S. Schlichting and D. Teaney, “The First fm/c of Heavy-Ion Collisions,” *Ann. Rev. Nucl. Part. Sci.*, vol. 69, pp. 447–476, 2019, arXiv:1908.02113.
- [492] J. Berges, M. P. Heller, A. Mazeliauskas, and R. Venugopalan, “QCD thermalization: Ab initio approaches and interdisciplinary connections,” *Rev. Mod. Phys.*, vol. 93, no. 3, p. 035003, 2021, arXiv:2005.12299.
- [493] P. M. Chesler and L. G. Yaffe, “Holography and colliding gravitational shock waves in asymptotically  $AdS_5$  spacetime,” *Phys. Rev. Lett.*, vol. 106, p. 021601, 2011, arXiv:1011.3562.
- [494] M. P. Heller, R. A. Janik, and P. Witaszczyk, “The characteristics of thermalization of boost-invariant plasma from holography,” *Phys. Rev. Lett.*, vol. 108, p. 201602, 2012, arXiv:1103.3452.
- [495] M. P. Heller, D. Mateos, W. van der Schee, and D. Trancanelli, “Strong Coupling Isotropization of Non-Abelian Plasmas Simplified,” *Phys. Rev. Lett.*, vol. 108, p. 191601, 2012, arXiv:1202.0981.
- [496] M. P. Heller, D. Mateos, W. van der Schee, and M. Triana, “Holographic isotropization linearized,” *JHEP*, vol. 09, p. 026, 2013, arXiv:1304.5172.
- [497] J. Casalderrey-Solana, M. P. Heller, D. Mateos, and W. van der Schee, “From full stopping to transparency in a holographic model of heavy ion collisions,” *Phys. Rev. Lett.*, vol. 111, p. 181601, 2013, arXiv:1305.4919.
- [498] P. M. Chesler and L. G. Yaffe, “Numerical solution of gravitational dynamics in asymptotically anti-de Sitter spacetimes,” *JHEP*, vol. 07, p. 086, 2014, arXiv:1309.1439.
- [499] P. M. Chesler and L. G. Yaffe, “Holography and off-center collisions of localized shock waves,” *JHEP*, vol. 10, p. 070, 2015, arXiv:1501.04644.
- [500] L. Keegan, A. Kurkela, P. Romatschke, W. van der Schee, and Y. Zhu, “Weak and strong coupling equilibration in nonabelian gauge theories,” *JHEP*, vol. 04, p. 031, 2016, arXiv:1512.05347.
- [501] M. Spaliński, “On the hydrodynamic attractor of Yang–Mills plasma,” *Phys. Lett. B*, vol. 776, pp. 468–472, 2018, arXiv:1708.01921.
- [502] G. S. Denicol, U. W. Heinz, M. Martinez, J. Noronha, and M. Strickland, “New Exact Solution of the Relativistic Boltzmann Equation and its Hydrodynamic Limit,” *Phys. Rev. Lett.*, vol. 113, no. 20, p. 202301, 2014, arXiv:1408.5646.
- [503] G. S. Denicol, U. W. Heinz, M. Martinez, J. Noronha, and M. Strickland, “Studying the validity of relativistic hydrodynamics with a new exact solution of the Boltzmann equation,” *Phys. Rev. D*, vol. 90, no. 12, p. 125026, 2014, arXiv:1408.7048.
- [504] A. Kurkela and Y. Zhu, “Isotropization and hydrodynamization in weakly coupled heavy-ion collisions,” *Phys. Rev. Lett.*, vol. 115, no. 18, p. 182301, 2015, arXiv:1506.06647.
- [505] D. Bazow, G. S. Denicol, U. Heinz, M. Martinez, and J. Noronha, “Analytic solution of the Boltzmann equation in an expanding system,” *Phys. Rev. Lett.*, vol. 116, no. 2, p. 022301, 2016, arXiv:1507.07834.
- [506] G. S. Denicol and J. Noronha, “Divergence of the Chapman-Enskog expansion in relativistic kinetic theory,” 8 2016, arXiv:1608.07869.

- [507] M. P. Heller, A. Kurkela, M. Spaliński, and V. Svensson, “Hydrodynamization in kinetic theory: Transient modes and the gradient expansion,” *Phys. Rev. D*, vol. 97, no. 9, p. 091503, 2018, arXiv:1609.04803.
- [508] P. Romatschke, “Relativistic Fluid Dynamics Far From Local Equilibrium,” *Phys. Rev. Lett.*, vol. 120, no. 1, p. 012301, 2018, arXiv:1704.08699.
- [509] M. Strickland, J. Noronha, and G. Denicol, “Anisotropic nonequilibrium hydrodynamic attractor,” *Phys. Rev. D*, vol. 97, no. 3, p. 036020, 2018, arXiv:1709.06644.
- [510] M. Strickland, “The non-equilibrium attractor for kinetic theory in relaxation time approximation,” *JHEP*, vol. 12, p. 128, 2018, arXiv:1809.01200.
- [511] A. Kurkela, A. Mazeliauskas, J.-F. Paquet, S. Schlichting, and D. Teaney, “Effective kinetic description of event-by-event pre-equilibrium dynamics in high-energy heavy-ion collisions,” *Phys. Rev. C*, vol. 99, no. 3, p. 034910, 2019, arXiv:1805.00961.
- [512] A. Kurkela, W. van der Schee, U. A. Wiedemann, and B. Wu, “Early- and Late-Time Behavior of Attractors in Heavy-Ion Collisions,” *Phys. Rev. Lett.*, vol. 124, no. 10, p. 102301, 2020, arXiv:1907.08101.
- [513] M. Strickland and U. Tantary, “Exact solution for the non-equilibrium attractor in number-conserving relaxation time approximation,” *JHEP*, vol. 10, p. 069, 2019, arXiv:1903.03145.
- [514] G. S. Denicol and J. Noronha, “Exact hydrodynamic attractor of an ultrarelativistic gas of hard spheres,” *Phys. Rev. Lett.*, vol. 124, no. 15, p. 152301, 2020, arXiv:1908.09957.
- [515] D. Almaalol, A. Kurkela, and M. Strickland, “Nonequilibrium Attractor in High-Temperature QCD Plasmas,” *Phys. Rev. Lett.*, vol. 125, no. 12, p. 122302, 2020, arXiv:2004.05195.
- [516] X. Du and S. Schlichting, “Equilibration of weakly coupled QCD plasmas,” *Phys. Rev. D*, vol. 104, no. 5, p. 054011, 2021, arXiv:2012.09079.
- [517] X. Du and S. Schlichting, “Equilibration of the Quark-Gluon Plasma at Finite Net-Baryon Density in QCD Kinetic Theory,” *Phys. Rev. Lett.*, vol. 127, no. 12, p. 122301, 2021, arXiv:2012.09068.
- [518] V. E. Ambrus, S. Schlichting, and C. Werthmann, “Development of transverse flow at small and large opacities in conformal kinetic theory,” *Phys. Rev. D*, vol. 105, no. 1, p. 014031, 2022, arXiv:2109.03290.
- [519] S. Jaiswal, J.-P. Blaizot, R. S. Bhalerao, Z. Chen, A. Jaiswal, and L. Yan, “From moments of the distribution function to hydrodynamics: The nonconformal case,” *Phys. Rev. C*, vol. 106, no. 4, p. 044912, 2022, arXiv:2208.02750.
- [520] H. Alalawi and M. Strickland, “Far-from-equilibrium attractors for massive kinetic theory in the relaxation time approximation,” 10 2022, arXiv:2210.00658.
- [521] N. Mullins, G. S. Denicol, and J. Noronha, “Far-from-equilibrium kinetic dynamics of  $\lambda\phi^4$  theory in an expanding universe,” *Phys. Rev. D*, vol. 106, no. 5, p. 056024, 2022, arXiv:2207.07786.
- [522] V. E. Ambrus, S. Schlichting, and C. Werthmann, “Establishing the range of applicability of hydrodynamics in high-energy collisions,” 11 2022, arXiv:2211.14356.
- [523] V. E. Ambrus, S. Schlichting, and C. Werthmann, “Opacity dependence of transverse flow, pre-equilibrium and applicability of hydrodynamics in heavy-ion collisions,” 11 2022, arXiv:2211.14379.
- [524] G. S. Rocha, G. S. Denicol, and J. Noronha, “Perturbative approaches in relativistic kinetic theory and the emergence of first-order hydrodynamics,” *Phys. Rev. D*, vol. 106, no. 3, p. 036010, 2022, arXiv:2205.00078.
- [525] X. Du, M. P. Heller, S. Schlichting, and V. Svensson, “Exponential approach to the hydrodynamic attractor in Yang-Mills kinetic theory,” *Phys. Rev. D*, vol. 106, no. 1, p. 014016, 2022,

- arXiv:2203.16549.
- [526] M. P. Heller and M. Spalinski, “Hydrodynamics Beyond the Gradient Expansion: Resurgence and Resummation,” *Phys. Rev. Lett.*, vol. 115, no. 7, p. 072501, 2015, arXiv:1503.07514.
  - [527] R. Baier, P. Romatschke, D. T. Son, A. O. Starinets, and M. A. Stephanov, “Relativistic viscous hydrodynamics, conformal invariance, and holography,” *JHEP*, vol. 04, p. 100, 2008, arXiv:0712.2451.
  - [528] G. Baym, “Thermal equilibration in ultra-relativistic heavy-ion collisions,” *Phys. Lett. B*, vol. 138, pp. 18–22, 1984.
  - [529] W. Florkowski, R. Ryblewski, and M. Strickland, “Anisotropic Hydrodynamics for Rapidly Expanding Systems,” *Nucl. Phys. A*, vol. 916, pp. 249–259, 2013, arXiv:1304.0665.
  - [530] W. Florkowski, R. Ryblewski, and M. Strickland, “Testing viscous and anisotropic hydrodynamics in an exactly solvable case,” *Phys. Rev. C*, vol. 88, p. 024903, 2013, arXiv:1305.7234.
  - [531] W. Florkowski, E. Maksymiuk, R. Ryblewski, and M. Strickland, “Exact solution of the (0+1)-dimensional Boltzmann equation for a massive gas,” *Phys. Rev. C*, vol. 89, no. 5, p. 054908, 2014, arXiv:1402.7348.
  - [532] M. Strickland, M. Nopoush, and R. Ryblewski, “Anisotropic hydrodynamics for conformal Gubser flow,” *Nucl. Phys. A*, vol. 956, pp. 268–271, 2016, arXiv:1512.07334.
  - [533] J. Brewer, L. Yan, and Y. Yin, “Adiabatic hydrodynamization in rapidly-expanding quark–gluon plasma,” *Phys. Lett. B*, vol. 816, p. 136189, 2021, arXiv:1910.00021.
  - [534] R. Baier, A. H. Mueller, D. Schiff, and D. T. Son, “‘Bottom up’ thermalization in heavy ion collisions,” *Phys. Lett. B*, vol. 502, pp. 51–58, 2001, arXiv:hep-ph/0009237.
  - [535] C. Chattopadhyay, S. Jaiswal, L. Du, U. Heinz, and S. Pal, “Non-conformal attractor in boost-invariant plasmas,” *Phys. Lett. B*, vol. 824, p. 136820, 2022, arXiv:2107.05500.
  - [536] S. Jaiswal, C. Chattopadhyay, L. Du, U. Heinz, and S. Pal, “Nonconformal kinetic theory and hydrodynamics for Bjorken flow,” *Phys. Rev. C*, vol. 105, no. 2, p. 024911, 2022, arXiv:2107.10248.
  - [537] H. Alalawi, J. Boyd, C. Shen, and M. Strickland, “The impact of fluctuating initial conditions on bottomonium suppression in 5.02 TeV heavy-ion collisions,” 11 2022, arXiv:2211.06363.
  - [538] J. D. Bjorken, “Highly Relativistic Nucleus-Nucleus Collisions: The Central Rapidity Region,” *Phys. Rev. D*, vol. 27, pp. 140–151, 1983.
  - [539] S. Borsanyi, G. Endrodi, Z. Fodor, A. Jakovac, S. D. Katz, S. Krieg, C. Ratti, and K. K. Szabo, “The QCD equation of state with dynamical quarks,” *JHEP*, vol. 11, p. 077, 2010, arXiv:1007.2580.
  - [540] A. Bazavov *et al.*, “Equation of state in (2+1)-flavor QCD,” *Phys. Rev. D*, vol. 90, p. 094503, 2014, arXiv:1407.6387.
  - [541] G. Giacalone, A. Mazeliauskas, and S. Schlichting, “Hydrodynamic attractors, initial state energy and particle production in relativistic nuclear collisions,” *Phys. Rev. Lett.*, vol. 123, no. 26, p. 262301, 2019, arXiv:1908.02866.
  - [542] M. P. Heller and V. Svensson, “How does relativistic kinetic theory remember about initial conditions?,” *Phys. Rev. D*, vol. 98, no. 5, p. 054016, 2018, arXiv:1802.08225.
  - [543] F. Gelis, E. Iancu, J. Jalilian-Marian, and R. Venugopalan, “The Color Glass Condensate,” *Ann. Rev. Nucl. Part. Sci.*, vol. 60, pp. 463–489, 2010, arXiv:1002.0333.
  - [544] A. Kurkela, U. A. Wiedemann, and B. Wu, “Flow in AA and pA as an interplay of fluid-like and non-fluid like excitations,” *Eur. Phys. J. C*, vol. 79, no. 11, p. 965, 2019, arXiv:1905.05139.
  - [545] J. Adam *et al.*, “Centrality Dependence of the Charged-Particle Multiplicity Density at Midrapidity in Pb-Pb Collisions at  $\sqrt{s_{NN}} = 5.02$  TeV,” *Phys. Rev. Lett.*, vol. 116, no. 22, p. 222302, 2016, arXiv:1512.06104.

- [546] B. Alver *et al.*, “Phobos results on charged particle multiplicity and pseudorapidity distributions in Au+Au, Cu+Cu, d+Au, and p+p collisions at ultra-relativistic energies,” *Phys. Rev. C*, vol. 83, p. 024913, 2011, arXiv:1011.1940.
- [547] J. Brewer, A. Mazeliauskas, and W. van der Schee, “Opportunities of OO and pO collisions at the LHC,” in *Opportunities of OO and pO collisions at the LHC*, 3 2021, arXiv:2103.01939.
- [548] ALICE Collaboration, “Multiplicity dependence of charged-particle production in pp, p-Pb, Xe-Xe and Pb-Pb collisions at the LHC,” 11 2022, arXiv:2211.15326.
- [549] A. Adare *et al.*, “Pseudorapidity Dependence of Particle Production and Elliptic Flow in Asymmetric Nuclear Collisions of p+Al, p+Au, d+Au, and  $^3\text{He}+\text{Au}$  at  $\sqrt{s_{NN}} = 200$  GeV,” *Phys. Rev. Lett.*, vol. 121, no. 22, p. 222301, 2018, arXiv:1807.11928.
- [550] G. Başar and D. Teaney, “Scaling relation between pA and AA collisions,” *Phys. Rev. C*, vol. 90, no. 5, p. 054903, 2014, arXiv:1312.6770.
- [551] A. Kurkela, U. A. Wiedemann, and B. Wu, “Opacity dependence of elliptic flow in kinetic theory,” *Eur. Phys. J. C*, vol. 79, no. 9, p. 759, 2019, arXiv:1805.04081.
- [552] R. B. Neufeld, “Mach cones in the quark-gluon plasma: Viscosity, speed of sound, and effects of finite source structure,” *Phys. Rev. C*, vol. 79, p. 054909, 2009, arXiv:0807.2996.
- [553] Y. Tachibana and T. Hirano, “Interplay between Mach cone and radial expansion and its signal in  $\gamma$ -jet events,” *Phys. Rev. C*, vol. 93, no. 5, p. 054907, 2016, arXiv:1510.06966.
- [554] Z. Yang, W. Chen, Y. He, W. Ke, L. Pang, and X.-N. Wang, “Search for the Elusive Jet-Induced Diffusion Wake in Z/ $\gamma$ -Jets with 2D Jet Tomography in High-Energy Heavy-Ion Collisions,” *Phys. Rev. Lett.*, vol. 127, no. 8, p. 082301, 2021, arXiv:2101.05422.
- [555] Y. Tachibana, C. Shen, and A. Majumder, “Bulk medium evolution has considerable effects on jet observables,” *Phys. Rev. C*, vol. 106, no. 2, p. L021902, 2022, arXiv:2001.08321.
- [556] H. Li, F. Liu, G.-l. Ma, X.-N. Wang, and Y. Zhu, “Mach cone induced by  $\gamma$ -triggered jets in high-energy heavy-ion collisions,” *Phys. Rev. Lett.*, vol. 106, p. 012301, 2011, arXiv:1006.2893.
- [557] K. C. Zapp, F. Krauss, and U. A. Wiedemann, “A perturbative framework for jet quenching,” *JHEP*, vol. 03, p. 080, 2013, arXiv:1212.1599.
- [558] K. C. Zapp, “JEWEL 2.0.0: directions for use,” *Eur. Phys. J. C*, vol. 74, no. 2, p. 2762, 2014, arXiv:1311.0048.
- [559] S. Cao, T. Luo, G.-Y. Qin, and X.-N. Wang, “Heavy and light flavor jet quenching at RHIC and LHC energies,” *Phys. Lett. B*, vol. 777, pp. 255–259, 2018, arXiv:1703.00822.
- [560] T. Luo, S. Cao, Y. He, and X.-N. Wang, “Multiple jets and  $\gamma$ -jet correlation in high-energy heavy-ion collisions,” *Phys. Lett. B*, vol. 782, pp. 707–716, 2018, arXiv:1803.06785.
- [561] C. Park, S. Jeon, and C. Gale, “Jet modification with medium recoil in quark-gluon plasma,” *Nucl. Phys. A*, vol. 982, pp. 643–646, 2019, arXiv:1807.06550.
- [562] S. Schlichting and I. Soudi, “Medium-induced fragmentation and equilibration of highly energetic partons,” *JHEP*, vol. 07, p. 077, 2021, arXiv:2008.04928.
- [563] Y. Mehtar-Tani, S. Schlichting, and I. Soudi, “Jet thermalization in QCD kinetic theory,” 9 2022, arXiv:2209.10569.
- [564] A. K. Chaudhuri and U. Heinz, “Effect of jet quenching on the hydrodynamical evolution of QGP,” *Phys. Rev. Lett.*, vol. 97, p. 062301, 2006, arXiv:nucl-th/0503028.
- [565] T. Renk and J. Ruppert, “Mach cones in an evolving medium,” *Phys. Rev. C*, vol. 73, p. 011901, 2006, arXiv:hep-ph/0509036.
- [566] L. M. Satarov, H. Stoecker, and I. N. Mishustin, “Mach shocks induced by partonic jets in expanding quark-gluon plasma,” *Phys. Lett. B*, vol. 627, pp. 64–70, 2005, arXiv:hep-ph/0505245.



- [567] R. B. Neufeld, B. Muller, and J. Ruppert, “Sonic Mach Cones Induced by Fast Partons in a Perturbative Quark-Gluon Plasma,” *Phys. Rev. C*, vol. 78, p. 041901, 2008, arXiv:0802.2254.
- [568] J. Noronha, M. Gyulassy, and G. Torrieri, “Di-Jet Conical Correlations Associated with Heavy Quark Jets in anti-de Sitter Space/Conformal Field Theory Correspondence,” *Phys. Rev. Lett.*, vol. 102, p. 102301, 2009, arXiv:0807.1038.
- [569] G. Y. Qin, A. Majumder, H. Song, and U. Heinz, “Energy and momentum deposited into a QCD medium by a jet shower,” *Phys. Rev. Lett.*, vol. 103, p. 152303, 2009, arXiv:0903.2255.
- [570] B. Betz, J. Noronha, G. Torrieri, M. Gyulassy, and D. H. Rischke, “Universal Flow-Driven Conical Emission in Ultrarelativistic Heavy-Ion Collisions,” *Phys. Rev. Lett.*, vol. 105, p. 222301, 2010, arXiv:1005.5461.
- [571] R. B. Neufeld and I. Vitev, “Parton showers as sources of energy-momentum deposition in the QGP and their implication for shockwave formation at RHIC and at the LHC,” *Phys. Rev. C*, vol. 86, p. 024905, 2012, arXiv:1105.2067.
- [572] M. Schulc and B. Tomášik, “Anisotropic flow of the fireball fed by hard partons,” *Phys. Rev. C*, vol. 90, no. 6, p. 064910, 2014, arXiv:1409.6116.
- [573] Y. Tachibana and T. Hirano, “Momentum transport away from a jet in an expanding nuclear medium,” *Phys. Rev. C*, vol. 90, no. 2, p. 021902, 2014, arXiv:1402.6469.
- [574] Y. Tachibana *et al.*, “Hydrodynamic response to jets with a source based on causal diffusion,” *Nucl. Phys. A*, vol. 1005, p. 121920, 2021, arXiv:2002.12250.
- [575] Y. Tachibana, N.-B. Chang, and G.-Y. Qin, “Full jet in quark-gluon plasma with hydrodynamic medium response,” *Phys. Rev. C*, vol. 95, no. 4, p. 044909, 2017, arXiv:1701.07951.
- [576] M. Okai, K. Kawaguchi, Y. Tachibana, and T. Hirano, “New approach to initializing hydrodynamic fields and mini-jet propagation in quark-gluon fluids,” *Phys. Rev. C*, vol. 95, no. 5, p. 054914, 2017, arXiv:1702.07541.
- [577] W. Chen, S. Cao, T. Luo, L.-G. Pang, and X.-N. Wang, “Effects of jet-induced medium excitation in  $\gamma$ -hadron correlation in A+A collisions,” *Phys. Lett. B*, vol. 777, pp. 86–90, 2018, arXiv:1704.03648.
- [578] N.-B. Chang, Y. Tachibana, and G.-Y. Qin, “Nuclear modification of jet shape for inclusive jets and  $\gamma$ -jets at the LHC energies,” *Phys. Lett. B*, vol. 801, p. 135181, 2020, arXiv:1906.09562.
- [579] J. Casalderrey-Solana, J. G. Milhano, D. Pablos, K. Rajagopal, and X. Yao, “Jet Wake from Linearized Hydrodynamics,” *JHEP*, vol. 05, p. 230, 2021, arXiv:2010.01140.
- [580] Z. Yang, T. Luo, W. Chen, L.-G. Pang, and X.-N. Wang, “3D structure of jet-induced diffusion wake in an expanding quark-gluon plasma,” 3 2022, arXiv:2203.03683.
- [581] D. Pablos, M. Singh, S. Jeon, and C. Gale, “Minijet quenching in a concurrent jet+hydro evolution and the nonequilibrium quark-gluon plasma,” *Phys. Rev. C*, vol. 106, no. 3, p. 034901, 2022, arXiv:2202.03414.
- [582] Z. Yang, Y. He, W. Chen, W.-Y. Ke, L.-G. Pang, and X.-N. Wang, “Deep learning assisted jet tomography for the study of Mach cones in QGP,” 6 2022, arXiv:2206.02393.
- [583] W. Chen, S. Cao, T. Luo, L.-G. Pang, and X.-N. Wang, “Medium modification of  $\gamma$ -jet fragmentation functions in Pb+Pb collisions at LHC,” *Phys. Lett. B*, vol. 810, p. 135783, 2020, arXiv:2005.09678.
- [584] W. Zhao, W. Ke, W. Chen, T. Luo, and X.-N. Wang, “From Hydrodynamics to Jet Quenching, Coalescence, and Hadron Cascade: A Coupled Approach to Solving the RAA $\otimes$ v2 Puzzle,” *Phys. Rev. Lett.*, vol. 128, no. 2, p. 022302, 2022, arXiv:2103.14657.
- [585] A. M. Sirunyan *et al.*, “Jet properties in PbPb and pp collisions at  $\sqrt{s_{NN}} = 5.02$  TeV,” *JHEP*, vol. 05, p. 006, 2018, arXiv:1803.00042.
- [586] A. M. Sirunyan *et al.*, “First measurement of large area jet transverse momentum spectra in heavy-

- ion collisions,” *JHEP*, vol. 05, p. 284, 2021, arXiv:2102.13080.
- [587] M. Aaboud *et al.*, “Measurement of jet fragmentation in Pb+Pb and *pp* collisions at  $\sqrt{s_{NN}} = 5.02$  TeV with the ATLAS detector,” *Phys. Rev. C*, vol. 98, no. 2, p. 024908, 2018, arXiv:1805.05424.
- [588] G. Aad *et al.*, “Measurement of angular and momentum distributions of charged particles within and around jets in Pb+Pb and *pp* collisions at  $\sqrt{s_{NN}} = 5.02$  TeV with the ATLAS detector,” *Phys. Rev. C*, vol. 100, no. 6, p. 064901, 2019, arXiv:1908.05264. [Erratum: *Phys.Rev.C* 101, 059903 (2020)].
- [589] M. Aaboud *et al.*, “Comparison of Fragmentation Functions for Jets Dominated by Light Quarks and Gluons from *pp* and Pb+Pb Collisions in ATLAS,” *Phys. Rev. Lett.*, vol. 123, no. 4, p. 042001, 2019, arXiv:1902.10007.
- [590] A. M. Sirunyan *et al.*, “Jet Shapes of Isolated Photon-Tagged Jets in Pb-Pb and *pp* Collisions at  $\sqrt{s_{NN}} = 5.02$  TeV,” *Phys. Rev. Lett.*, vol. 122, no. 15, p. 152001, 2019, arXiv:1809.08602.
- [591] U. Acharya *et al.*, “Measurement of jet-medium interactions via direct photon-hadron correlations in Au+Au and *d* +Au collisions at  $\sqrt{s_{NN}} = 200$  GeV,” *Phys. Rev. C*, vol. 102, no. 5, p. 054910, 2020, arXiv:2005.14270.
- [592] G. Aad *et al.*, “Medium-Induced Modification of *Z*-Tagged Charged Particle Yields in *Pb + Pb* Collisions at 5.02 TeV with the ATLAS Detector,” *Phys. Rev. Lett.*, vol. 126, no. 7, p. 072301, 2021, arXiv:2008.09811.
- [593] A. M. Sirunyan *et al.*, “Using *Z* Boson Events to Study Parton-Medium Interactions in Pb-Pb Collisions,” *Phys. Rev. Lett.*, vol. 128, no. 12, p. 122301, 2022, arXiv:2103.04377.
- [594] R. Baier, Y. L. Dokshitzer, A. H. Mueller, S. Peigne, and D. Schiff, “Radiative energy loss and *p*(*T*) broadening of high-energy partons in nuclei,” *Nucl. Phys. B*, vol. 484, pp. 265–282, 1997, arXiv:hep-ph/9608322.
- [595] V. Khachatryan *et al.*, “Charged-particle nuclear modification factors in PbPb and pPb collisions at  $\sqrt{s_{NN}} = 5.02$  TeV,” *JHEP*, vol. 04, p. 039, 2017, arXiv:1611.01664.
- [596] G. Aad *et al.*, “Measurement of long-range pseudorapidity correlations and azimuthal harmonics in  $\sqrt{s_{NN}} = 5.02$  TeV proton-lead collisions with the ATLAS detector,” *Phys. Rev. C*, vol. 90, no. 4, p. 044906, 2014, arXiv:1409.1792.
- [597] G. Aad *et al.*, “Transverse momentum and process dependent azimuthal anisotropies in  $\sqrt{s_{NN}} = 8.16$  TeV *p*+Pb collisions with the ATLAS detector,” *Eur. Phys. J. C*, vol. 80, no. 1, p. 73, 2020, arXiv:1910.13978.
- [598] ATLAS Collaboration, “Strong constraints on jet quenching in centrality-dependent *p*+Pb collisions at 5.02 TeV from ATLAS,” 6 2022, arXiv:2206.01138.
- [599] C. Aidala *et al.*, “Nonperturbative transverse momentum broadening in dihadron angular correlations in  $\sqrt{s_{NN}} = 200$  GeV proton-nucleus collisions,” *Phys. Rev. C*, vol. 99, no. 4, p. 044912, 2019, arXiv:1809.09045.
- [600] J. Adam *et al.*, “Measurement of dijet  $k_T$  in *p*-Pb collisions at  $\sqrt{s_{NN}}=5.02$  TeV,” *Phys. Lett. B*, vol. 746, pp. 385–395, 2015, arXiv:1503.03050.
- [601] G. F. Sterman and S. Weinberg, “Jets from Quantum Chromodynamics,” *Phys. Rev. Lett.*, vol. 39, p. 1436, 1977.
- [602] R. K. Ellis, D. A. Ross, and A. E. Terrano, “The Perturbative Calculation of Jet Structure in *e+ e-* Annihilation,” *Nucl. Phys. B*, vol. 178, pp. 421–456, 1981.
- [603] A. Bassetto, M. Ciafaloni, and G. Marchesini, “Jet Structure and Infrared Sensitive Quantities in Perturbative QCD,” *Phys. Rept.*, vol. 100, pp. 201–272, 1983.
- [604] R. Brock *et al.*, “Handbook of perturbative QCD: Version 1.0,” *Rev. Mod. Phys.*, vol. 67, pp. 157–248, 1995.

- [605] J. D. Bjorken, “Energy Loss of Energetic Partons in Quark - Gluon Plasma: Possible Extinction of High  $p_T$  Jets in Hadron - Hadron Collisions,” 8 1982.
- [606] X.-N. Wang and M. Gyulassy, “Gluon shadowing and jet quenching in A + A collisions at  $s^{*}(1/2) = 200\text{-GeV}$ ,” *Phys. Rev. Lett.*, vol. 68, pp. 1480–1483, 1992.
- [607] R. Baier, Y. L. Dokshitzer, A. H. Mueller, S. Peigne, and D. Schiff, “Radiative energy loss of high-energy quarks and gluons in a finite volume quark - gluon plasma,” *Nucl. Phys. B*, vol. 483, pp. 291–320, 1997, arXiv:hep-ph/9607355.
- [608] B. G. Zakharov, “Radiative energy loss of high-energy quarks in finite size nuclear matter and quark - gluon plasma,” *JETP Lett.*, vol. 65, pp. 615–620, 1997, arXiv:hep-ph/9704255.
- [609] M. Gyulassy, P. Levai, and I. Vitev, “NonAbelian energy loss at finite opacity,” *Phys. Rev. Lett.*, vol. 85, pp. 5535–5538, 2000, arXiv:nucl-th/0005032.
- [610] X.-N. Wang and X.-f. Guo, “Multiple parton scattering in nuclei: Parton energy loss,” *Nucl. Phys. A*, vol. 696, pp. 788–832, 2001, arXiv:hep-ph/0102230.
- [611] P. B. Arnold, G. D. Moore, and L. G. Yaffe, “Photon and gluon emission in relativistic plasmas,” *JHEP*, vol. 06, p. 030, 2002, arXiv:hep-ph/0204343.
- [612] C. A. Salgado and U. A. Wiedemann, “A Dynamical scaling law for jet tomography,” *Phys. Rev. Lett.*, vol. 89, p. 092303, 2002, arXiv:hep-ph/0204221.
- [613] J. M. Maldacena, “The Large N limit of superconformal field theories and supergravity,” *Adv. Theor. Math. Phys.*, vol. 2, pp. 231–252, 1998, arXiv:hep-th/9711200.
- [614] P. M. Chesler, K. Jensen, A. Karch, and L. G. Yaffe, “Light quark energy loss in strongly-coupled  $N = 4$  supersymmetric Yang-Mills plasma,” *Phys. Rev. D*, vol. 79, p. 125015, 2009, arXiv:0810.1985.
- [615] H. Liu, K. Rajagopal, and U. A. Wiedemann, “Calculating the jet quenching parameter from AdS/CFT,” *Phys. Rev. Lett.*, vol. 97, p. 182301, 2006, arXiv:hep-ph/0605178.
- [616] J. Casalderrey-Solana and D. Teaney, “Transverse Momentum Broadening of a Fast Quark in a  $N=4$  Yang Mills Plasma,” *JHEP*, vol. 04, p. 039, 2007, arXiv:hep-th/0701123.
- [617] S. Cao *et al.*, “Multistage Monte-Carlo simulation of jet modification in a static medium,” *Phys. Rev. C*, vol. 96, no. 2, p. 024909, 2017, arXiv:1705.00050.
- [618] P. Caucal, E. Iancu, A. H. Mueller, and G. Soyez, “Vacuum-like jet fragmentation in a dense QCD medium,” *Phys. Rev. Lett.*, vol. 120, p. 232001, 2018, arXiv:1801.09703.
- [619] A. Kumar, A. Majumder, and C. Shen, “Energy and scale dependence of  $\hat{q}$  and the “JET puzzle”,” *Phys. Rev. C*, vol. 101, no. 3, p. 034908, 2020, arXiv:1909.03178.
- [620] Y. Mehtar-Tani, C. A. Salgado, and K. Tywoniuk, “Jets in QCD Media: From Color Coherence to Decoherence,” *Phys. Lett. B*, vol. 707, pp. 156–159, 2012, arXiv:1102.4317.
- [621] R. Baier, Y. L. Dokshitzer, S. Peigne, and D. Schiff, “Induced gluon radiation in a QCD medium,” *Phys. Lett. B*, vol. 345, pp. 277–286, 1995, arXiv:hep-ph/9411409.
- [622] Y. He, T. Luo, X.-N. Wang, and Y. Zhu, “Linear Boltzmann Transport for Jet Propagation in the Quark-Gluon Plasma: Elastic Processes and Medium Recoil,” *Phys. Rev. C*, vol. 91, p. 054908, 2015, arXiv:1503.03313. [Erratum: Phys.Rev.C 97, 019902 (2018)].
- [623] R. Kunnawalkam Elayavalli and K. C. Zapp, “Medium response in JEWEL and its impact on jet shape observables in heavy ion collisions,” *JHEP*, vol. 07, p. 141, 2017, arXiv:1707.01539.
- [624] A. Kumar *et al.*, “Inclusive Jet and Hadron Suppression in a Multi-Stage Approach,” 4 2022, arXiv:2204.01163.
- [625] Y. Tachibana *et al.*, “Hard Jet Substructure in a Multi-stage Approach,” 1 2023, arXiv:2301.02485.
- [626] G. Aad *et al.*, “Measurements of azimuthal anisotropies of jet production in Pb+Pb collisions at

- $\sqrt{s_{NN}} = 5.02$  TeV with the ATLAS detector,” *Phys. Rev. C*, vol. 105, no. 6, p. 064903, 2022, arXiv:2111.06606.
- [627] S. Acharya *et al.*, “Measurement of the groomed jet radius and momentum splitting fraction in pp and Pb–Pb collisions at  $\sqrt{s_{NN}} = 5.02$  TeV,” *Phys. Rev. Lett.*, vol. 128, no. 10, p. 102001, 2022, arXiv:2107.12984.
- [628] S. Acharya *et al.*, “Jet-hadron correlations measured relative to the second order event plane in Pb-Pb collisions at  $\sqrt{s_{NN}} = 2.76$  TeV,” *Phys. Rev. C*, vol. 101, no. 6, p. 064901, 2020, arXiv:1910.14398.
- [629] M. Aaboud *et al.*, “Measurement of the nuclear modification factor for inclusive jets in Pb+Pb collisions at  $\sqrt{s_{NN}} = 5.02$  TeV with the ATLAS detector,” *Phys. Lett. B*, vol. 790, pp. 108–128, 2019, arXiv:1805.05635.
- [630] A. Majumder, “Incorporating Space-Time Within Medium-Modified Jet Event Generators,” *Phys. Rev. C*, vol. 88, p. 014909, 2013, arXiv:1301.5323.
- [631] S. Cao and A. Majumder, “Nuclear modification of leading hadrons and jets within a virtuality ordered parton shower,” *Phys. Rev. C*, vol. 101, no. 2, p. 024903, 2020, arXiv:1712.10055.
- [632] P. B. Arnold and W. Xiao, “High-energy jet quenching in weakly-coupled quark-gluon plasmas,” *Phys. Rev. D*, vol. 78, p. 125008, 2008, arXiv:0810.1026.
- [633] K. M. Burke *et al.*, “Extracting the jet transport coefficient from jet quenching in high-energy heavy-ion collisions,” *Phys. Rev. C*, vol. 90, no. 1, p. 014909, 2014, arXiv:1312.5003.
- [634] A. J. Larkoski, S. Marzani, G. Soyez, and J. Thaler, “Soft Drop,” *JHEP*, vol. 05, p. 146, 2014, arXiv:1402.2657.
- [635] ATLAS Collaboration, “Measurement of substructure-dependent jet suppression in Pb+Pb collisions at 5.02 TeV with the ATLAS detector,” 11 2022, arXiv:2211.11470.
- [636] M. Gyulassy and M. Plumer, “Jet Quenching in Dense Matter,” *Phys. Lett. B*, vol. 243, pp. 432–438, 1990.
- [637] X.-N. Wang and M. Gyulassy, “HIJING: A Monte Carlo model for multiple jet production in p p, p A and A A collisions,” *Phys. Rev. D*, vol. 44, pp. 3501–3516, 1991.
- [638] X.-N. Wang, “Effect of jet quenching on high  $p_T$  hadron spectra in high-energy nuclear collisions,” *Phys. Rev. C*, vol. 58, p. 2321, 1998, arXiv:hep-ph/9804357.
- [639] X.-N. Wang, Z. Huang, and I. Sarcevic, “Jet quenching in the opposite direction of a tagged photon in high-energy heavy ion collisions,” *Phys. Rev. Lett.*, vol. 77, pp. 231–234, 1996, arXiv:hep-ph/9605213.
- [640] K. Adcox *et al.*, “Suppression of hadrons with large transverse momentum in central Au+Au collisions at  $\sqrt{s_{NN}} = 130$ -GeV,” *Phys. Rev. Lett.*, vol. 88, p. 022301, 2002, arXiv:nucl-ex/0109003.
- [641] C. Adler *et al.*, “Centrality dependence of high  $p_T$  hadron suppression in Au+Au collisions at  $\sqrt{s_{NN}} = 130$ -GeV,” *Phys. Rev. Lett.*, vol. 89, p. 202301, 2002, arXiv:nucl-ex/0206011.
- [642] C. Adler *et al.*, “Disappearance of back-to-back high  $p_T$  hadron correlations in central Au+Au collisions at  $\sqrt{s_{NN}} = 200$ -GeV,” *Phys. Rev. Lett.*, vol. 90, p. 082302, 2003, arXiv:nucl-ex/0210033.
- [643] B. I. Abelev *et al.*, “Studying Parton Energy Loss in Heavy-Ion Collisions via Direct-Photon and Charged-Particle Azimuthal Correlations,” *Phys. Rev. C*, vol. 82, p. 034909, 2010, arXiv:0912.1871.
- [644] A. Adare *et al.*, “Photon-Hadron Jet Correlations in  $p+p$  and Au+Au Collisions at  $\sqrt{s_{NN}} = 200$  GeV,” *Phys. Rev. C*, vol. 80, p. 024908, 2009.
- [645] G. Aad *et al.*, “Measurement of the jet radius and transverse momentum dependence of inclusive jet suppression in lead-lead collisions at  $\sqrt{s_{NN}} = 2.76$  TeV with the ATLAS detector,” *Phys. Lett. B*, vol. 719, pp. 220–241, 2013, arXiv:1208.1967.
- [646] Y. Mehtar-Tani, J. G. Milhano, and K. Tywoniuk, “Jet physics in heavy-ion collisions,” *Int. J. Mod.*

- Phys. A*, vol. 28, p. 1340013, 2013, arXiv:1302.2579.
- [647] J.-P. Blaizot and Y. Mehtar-Tani, “Jet Structure in Heavy Ion Collisions,” *Int. J. Mod. Phys. E*, vol. 24, no. 11, p. 1530012, 2015, arXiv:1503.05958.
- [648] G.-Y. Qin and X.-N. Wang, “Jet quenching in high-energy heavy-ion collisions,” *Int. J. Mod. Phys. E*, vol. 24, no. 11, p. 1530014, 2015, arXiv:1511.00790.
- [649] A. Majumder and M. Van Leeuwen, “The Theory and Phenomenology of Perturbative QCD Based Jet Quenching,” *Prog. Part. Nucl. Phys.*, vol. 66, pp. 41–92, 2011, arXiv:1002.2206.
- [650] M. Gyulassy and X.-n. Wang, “Multiple collisions and induced gluon Bremsstrahlung in QCD,” *Nucl. Phys. B*, vol. 420, pp. 583–614, 1994, arXiv:nucl-th/9306003.
- [651] B. G. Zakharov, “Fully quantum treatment of the Landau-Pomeranchuk-Migdal effect in QED and QCD,” *JETP Lett.*, vol. 63, pp. 952–957, 1996, arXiv:hep-ph/9607440.
- [652] U. A. Wiedemann, “Gluon radiation off hard quarks in a nuclear environment: Opacity expansion,” *Nucl. Phys. B*, vol. 588, pp. 303–344, 2000, arXiv:hep-ph/0005129.
- [653] R. Abir and A. Majumder, “Drag-induced radiative energy loss from semihard heavy quarks,” *Phys. Rev. C*, vol. 94, no. 5, p. 054902, 2016, arXiv:1506.08648.
- [654] P. B. Arnold, G. D. Moore, and L. G. Yaffe, “Photon emission from quark gluon plasma: Complete leading order results,” *JHEP*, vol. 12, p. 009, 2001, arXiv:hep-ph/0111107.
- [655] P. B. Arnold, G. D. Moore, and L. G. Yaffe, “Effective kinetic theory for high temperature gauge theories,” *JHEP*, vol. 01, p. 030, 2003, arXiv:hep-ph/0209353.
- [656] S. Caron-Huot and G. D. Moore, “Heavy quark diffusion in perturbative QCD at next-to-leading order,” *Phys. Rev. Lett.*, vol. 100, p. 052301, 2008, arXiv:0708.4232.
- [657] P. Caucal, *Jet evolution in a dense QCD medium*. PhD thesis, Saclay, 9 2020, arXiv:2010.02874.
- [658] Y. Mehtar-Tani and K. Tywoniuk, “Sudakov suppression of jets in QCD media,” *Phys. Rev. D*, vol. 98, no. 5, p. 051501, 2018, arXiv:1707.07361.
- [659] C. Sirimanna, S. Cao, and A. Majumder, “Final-state gluon emission in deep-inelastic scattering at next-to-leading twist,” *Phys. Rev. C*, vol. 105, no. 2, p. 024908, 2022, arXiv:2108.05329.
- [660] C. Sirimanna, I. Soudi, G. Vujanovic, W.-J. Xing, S. Cao, and A. Majumder, “Quenching jets increases their flavor,” 11 2022, arXiv:2211.15553.
- [661] J.-P. Blaizot, F. Dominguez, E. Iancu, and Y. Mehtar-Tani, “Probabilistic picture for medium-induced jet evolution,” *JHEP*, vol. 06, p. 075, 2014, arXiv:1311.5823.
- [662] J.-P. Blaizot, E. Iancu, and Y. Mehtar-Tani, “Medium-induced QCD cascade: democratic branching and wave turbulence,” *Phys. Rev. Lett.*, vol. 111, p. 052001, 2013, arXiv:1301.6102.
- [663] Y. Mehtar-Tani and S. Schlichting, “Universal quark to gluon ratio in medium-induced parton cascade,” *JHEP*, vol. 09, p. 144, 2018, arXiv:1807.06181.
- [664] A. V. Sadofyev, M. D. Sievert, and I. Vitev, “Ab initio coupling of jets to collective flow in the opacity expansion approach,” *Phys. Rev. D*, vol. 104, no. 9, p. 094044, 2021, arXiv:2104.09513.
- [665] C. Andres, F. Dominguez, A. V. Sadofyev, and C. A. Salgado, “Jet broadening in flowing matter: Resummation,” *Phys. Rev. D*, vol. 106, no. 7, p. 074023, 2022, arXiv:2207.07141.
- [666] L. Antiporda, J. Bahder, H. Rahman, and M. D. Sievert, “Jet drift and collective flow in heavy-ion collisions,” *Phys. Rev. D*, vol. 105, no. 5, p. 054025, 2022, arXiv:2110.03590.
- [667] Y. Fu, J. Casalderrey-Solana, and X.-N. Wang, “Asymmetric transverse momentum broadening in an inhomogeneous medium,” 4 2022, arXiv:2204.05323.
- [668] P. Arnold, T. Gorda, and S. Iqbal, “The LPM effect in sequential bremsstrahlung: analytic results for sub-leading (single) logarithms,” *JHEP*, vol. 04, p. 085, 2022, arXiv:2112.05161.

- [669] P. Arnold, T. Gorda, and S. Iqbal, “The LPM effect in sequential bremsstrahlung: nearly complete results for QCD,” *JHEP*, vol. 11, p. 053, 2020, arXiv:2007.15018. [Erratum: *JHEP* 05, 114 (2022)].
- [670] P. Arnold, O. Elgedawy, and S. Iqbal, “The LPM effect in sequential bremsstrahlung: gluon shower development,” 2 2023, arXiv:2302.10215.
- [671] Y. Mehtar-Tani, C. A. Salgado, and K. Tywoniuk, “Anti-angular ordering of gluon radiation in QCD media,” *Phys. Rev. Lett.*, vol. 106, p. 122002, 2011, arXiv:1009.2965.
- [672] J. Casalderrey-Solana, Y. Mehtar-Tani, C. A. Salgado, and K. Tywoniuk, “New picture of jet quenching dictated by color coherence,” *Phys. Lett. B*, vol. 725, pp. 357–360, 2013, arXiv:1210.7765.
- [673] Y. Mehtar-Tani and K. Tywoniuk, “Radiative energy loss of neighboring subjects,” *Nucl. Phys. A*, vol. 979, pp. 165–203, 2018, arXiv:1706.06047.
- [674] Y. Mehtar-Tani, D. Pablos, and K. Tywoniuk, “Cone-Size Dependence of Jet Suppression in Heavy-Ion Collisions,” *Phys. Rev. Lett.*, vol. 127, no. 25, p. 252301, 2021, arXiv:2101.01742.
- [675] Y. Mehtar-Tani and K. Tywoniuk, “Jet (de)coherence in Pb–Pb collisions at the LHC,” *Phys. Lett. B*, vol. 744, pp. 284–287, 2015, arXiv:1401.8293.
- [676] Y. Mehtar-Tani and K. Tywoniuk, “Groomed jets in heavy-ion collisions: sensitivity to medium-induced bremsstrahlung,” *JHEP*, vol. 04, p. 125, 2017, arXiv:1610.08930.
- [677] P. Caucal, A. Soto-Ontoso, and A. Takacs, “Dynamically groomed jet radius in heavy-ion collisions,” *Phys. Rev. D*, vol. 105, no. 11, p. 114046, 2022, arXiv:2111.14768.
- [678] P. Caucal, E. Iancu, and G. Soyez, “Deciphering the  $z_g$  distribution in ultrarelativistic heavy ion collisions,” *JHEP*, vol. 10, p. 273, 2019, arXiv:1907.04866.
- [679] Y. Mehtar-Tani, “Gluon bremsstrahlung in finite media beyond multiple soft scattering approximation,” *JHEP*, vol. 07, p. 057, 2019, arXiv:1903.00506.
- [680] J. a. Barata, Y. Mehtar-Tani, A. Soto-Ontoso, and K. Tywoniuk, “Medium-induced radiative kernel with the Improved Opacity Expansion,” *JHEP*, vol. 09, p. 153, 2021, arXiv:2106.07402.
- [681] X. Feal and R. Vazquez, “Intensity of gluon bremsstrahlung in a finite plasma,” *Phys. Rev. D*, vol. 98, no. 7, p. 074029, 2018, arXiv:1811.01591.
- [682] C. Andres, L. Apolinário, and F. Dominguez, “Medium-induced gluon radiation with full resummation of multiple scatterings for realistic parton-medium interactions,” *JHEP*, vol. 07, p. 114, 2020, arXiv:2002.01517.
- [683] C. Andres, F. Dominguez, and M. Gonzalez Martinez, “From soft to hard radiation: the role of multiple scatterings in medium-induced gluon emissions,” *JHEP*, vol. 03, p. 102, 2021, arXiv:2011.06522.
- [684] M. D. Sievert, I. Vitev, and B. Yoon, “A complete set of in-medium splitting functions to any order in opacity,” *Phys. Lett. B*, vol. 795, pp. 502–510, 2019, arXiv:1903.06170.
- [685] E. Braaten and R. D. Pisarski, “Soft Amplitudes in Hot Gauge Theories: A General Analysis,” *Nucl. Phys. B*, vol. 337, pp. 569–634, 1990.
- [686] J. Frenkel and J. C. Taylor, “High Temperature Limit of Thermal QCD,” *Nucl. Phys. B*, vol. 334, pp. 199–216, 1990.
- [687] S. Caron-Huot, “O(g) plasma effects in jet quenching,” *Phys. Rev. D*, vol. 79, p. 065039, 2009, arXiv:0811.1603.
- [688] M. Panero, K. Rummukainen, and A. Schäfer, “Lattice Study of the Jet Quenching Parameter,” *Phys. Rev. Lett.*, vol. 112, no. 16, p. 162001, 2014, arXiv:1307.5850.
- [689] A. Majumder, “Calculating the jet quenching parameter  $\hat{q}$  in lattice gauge theory,” *Phys. Rev. C*, vol. 87, p. 034905, 2013, arXiv:1202.5295.

- [690] A. Kumar, A. Majumder, and J. H. Weber, “Jet transport coefficient  $q^{\wedge}$  in lattice QCD,” *Phys. Rev. D*, vol. 106, no. 3, p. 034505, 2022, arXiv:2010.14463.
- [691] R. Ehlers, “Bayesian analysis of QGP jet transport using multi-scale modeling applied to inclusive hadron and reconstructed jet data,” in *29th International Conference on Ultra-relativistic Nucleus-Nucleus Collisions*, 8 2022, arXiv:2208.07950.
- [692] D. Antonov and H. J. Pirner, “Jet quenching parameter  $q$  in the stochastic QCD vacuum with Landau damping,” *Eur. Phys. J. C*, vol. 55, pp. 439–447, 2008, arXiv:0710.1540.
- [693] T. Liou, A. H. Mueller, and B. Wu, “Radiative  $p_{\perp}$ -broadening of high-energy quarks and gluons in QCD matter,” *Nucl. Phys. A*, vol. 916, pp. 102–125, 2013, arXiv:1304.7677.
- [694] J.-P. Blaizot and Y. Mehtar-Tani, “Renormalization of the jet-quenching parameter,” *Nucl. Phys. A*, vol. 929, pp. 202–229, 2014, arXiv:1403.2323.
- [695] E. Iancu, “The non-linear evolution of jet quenching,” *JHEP*, vol. 10, p. 095, 2014, arXiv:1403.1996.
- [696] E. Iancu and D. N. Triantafyllopoulos, “Running coupling effects in the evolution of jet quenching,” *Phys. Rev. D*, vol. 90, no. 7, p. 074002, 2014, arXiv:1405.3525.
- [697] P. Caucal and Y. Mehtar-Tani, “Universality aspects of quantum corrections to transverse momentum broadening in QCD media,” *JHEP*, vol. 09, p. 023, 2022, arXiv:2203.09407.
- [698] P. Caucal and Y. Mehtar-Tani, “Anomalous diffusion in QCD matter,” *Phys. Rev. D*, vol. 106, no. 5, p. L051501, 2022, arXiv:2109.12041.
- [699] J. Ghiglieri and E. Weitz, “Classical vs quantum corrections to jet broadening in a weakly-coupled Quark-Gluon Plasma,” *JHEP*, vol. 11, p. 068, 2022, arXiv:2207.08842.
- [700] J. Casalderrey-Solana and X.-N. Wang, “Energy dependence of jet transport parameter and parton saturation in quark-gluon plasma,” *Phys. Rev. C*, vol. 77, p. 024902, 2008, arXiv:0705.1352.
- [701] P. Caucal and Y. Mehtar-Tani, “Transverse momentum broadening from NLL BFKL to all orders in pQCD,” 9 2022, arXiv:2209.08900.
- [702] W. Fan *et al.*, “Multi-scale evolution of charmed particles in a nuclear medium,” 8 2022, arXiv:2208.00983.
- [703] Y. Xu *et al.*, “Resolving discrepancies in the estimation of heavy quark transport coefficients in relativistic heavy-ion collisions,” *Phys. Rev. C*, vol. 99, no. 1, p. 014902, 2019, arXiv:1809.10734.
- [704] S. Cao *et al.*, “Toward the determination of heavy-quark transport coefficients in quark-gluon plasma,” *Phys. Rev. C*, vol. 99, no. 5, p. 054907, 2019, arXiv:1809.07894.
- [705] W. Ke, *Partonic transport model application to heavy flavor*. PhD thesis, Duke U., 2020, arXiv:2001.02766.
- [706] M. Gyulassy, P. Levai, and I. Vitev, “Jet quenching in thin quark gluon plasmas. 1. Formalism,” *Nucl. Phys. B*, vol. 571, pp. 197–233, 2000, arXiv:hep-ph/9907461.
- [707] S. Cao and X.-N. Wang, “Jet quenching and medium response in high-energy heavy-ion collisions: a review,” *Rept. Prog. Phys.*, vol. 84, no. 2, p. 024301, 2021, arXiv:2002.04028.
- [708] M. Djordjevic and M. Gyulassy, “Heavy quark radiative energy loss in QCD matter,” *Nucl. Phys. A*, vol. 733, pp. 265–298, 2004, arXiv:nucl-th/0310076.
- [709] S. Cao, T. Luo, G.-Y. Qin, and X.-N. Wang, “Linearized Boltzmann transport model for jet propagation in the quark-gluon plasma: Heavy quark evolution,” *Phys. Rev. C*, vol. 94, no. 1, p. 014909, 2016, arXiv:1605.06447.
- [710] S. Cao, G.-Y. Qin, and S. A. Bass, “Heavy-quark dynamics and hadronization in ultrarelativistic heavy-ion collisions: Collisional versus radiative energy loss,” *Phys. Rev. C*, vol. 88, p. 044907, 2013, arXiv:1308.0617.

- [711] S. Cao, G.-Y. Qin, and S. A. Bass, “Energy loss, hadronization and hadronic interactions of heavy flavors in relativistic heavy-ion collisions,” *Phys. Rev. C*, vol. 92, no. 2, p. 024907, 2015, arXiv:1505.01413.
- [712] Y. Xu, S. Cao, G.-Y. Qin, W. Ke, M. Nahrgang, J. Auvinen, and S. A. Bass, “Heavy-flavor dynamics in relativistic p-Pb collisions at  $\sqrt{s_{NN}} = 5.02$  TeV,” *Nucl. Part. Phys. Proc.*, vol. 276-278, pp. 225–228, 2016, arXiv:1510.07520.
- [713] W. Ke, Y. Xu, and S. A. Bass, “Modified Boltzmann approach for modeling the splitting vertices induced by the hot QCD medium in the deep Landau-Pomeranchuk-Migdal region,” *Phys. Rev. C*, vol. 100, no. 6, p. 064911, 2019, arXiv:1810.08177.
- [714] E. Meggiolaro, “A Remark on the high-energy quark quark scattering and the eikonal approximation,” *Phys. Rev. D*, vol. 53, pp. 3835–3845, 1996, arXiv:hep-th/9506043.
- [715] J. Aichelin, P. B. Gossiaux, and T. Gousset, “Gluon radiation by heavy quarks at intermediate energies,” *Phys. Rev. D*, vol. 89, no. 7, p. 074018, 2014, arXiv:1307.5270.
- [716] M. Attems, J. Brewer, G. M. Innocenti, A. Mazeliauskas, S. Park, W. van der Schee, and U. Wiedemann, “Medium-enhanced  $c\bar{c}$  radiation,” 9 2022, arXiv:2209.13600.
- [717] M. Attems, J. Brewer, G. M. Innocenti, A. Mazeliauskas, S. Park, W. van der Schee, and U. A. Wiedemann, “The medium-modified  $g \rightarrow c\bar{c}$  splitting function in the BDMPS-Z formalism,” *JHEP*, vol. 01, p. 080, 2023, arXiv:2203.11241.
- [718] A. M. Sirunyan *et al.*, “Charged-particle nuclear modification factors in XeXe collisions at  $\sqrt{s_{NN}} = 5.44$  TeV,” *JHEP*, vol. 10, p. 138, 2018, arXiv:1809.00201.
- [719] S. Chatrchyan *et al.*, “Study of high-pT charged particle suppression in PbPb compared to pp collisions at  $\sqrt{s_{NN}} = 2.76$  TeV,” *Eur. Phys. J. C*, vol. 72, p. 1945, 2012, arXiv:1202.2554.
- [720] ATLAS Collaboration, “Charged-hadron production in pp, p+Pb, Pb+Pb, and Xe+Xe collisions at  $\sqrt{s_{NN}} = 5$  TeV with the ATLAS detector at the LHC,” 11 2022, arXiv:2211.15257.
- [721] G. Aad *et al.*, “Transverse momentum, rapidity, and centrality dependence of inclusive charged-particle production in  $\sqrt{s_{NN}} = 5.02$  TeV p + Pb collisions measured by the ATLAS experiment,” *Phys. Lett. B*, vol. 763, pp. 313–336, 2016, arXiv:1605.06436.
- [722] G. Aad *et al.*, “Measurement of charged-particle spectra in Pb+Pb collisions at  $\sqrt{s_{NN}} = 2.76$  TeV with the ATLAS detector at the LHC,” *JHEP*, vol. 09, p. 050, 2015, arXiv:1504.04337.
- [723] S. Acharya *et al.*, “Production of pions, kaons, (anti-)protons and  $\phi$  mesons in Xe–Xe collisions at  $\sqrt{s_{NN}} = 5.44$  TeV,” *Eur. Phys. J. C*, vol. 81, no. 7, p. 584, 2021, arXiv:2101.03100.
- [724] S. Acharya *et al.*, “Production of charged pions, kaons, and (anti-)protons in Pb-Pb and inelastic pp collisions at  $\sqrt{s_{NN}} = 5.02$  TeV,” *Phys. Rev. C*, vol. 101, no. 4, p. 044907, 2020, arXiv:1910.07678.
- [725] A. M. Sirunyan *et al.*, “Comparing transverse momentum balance of b jet pairs in pp and PbPb collisions at  $\sqrt{s_{NN}} = 5.02$  TeV,” *JHEP*, vol. 03, p. 181, 2018, arXiv:1802.00707.
- [726] V. Khachatryan *et al.*, “Measurement of inclusive jet cross sections in pp and PbPb collisions at  $\sqrt{s_{NN}} = 2.76$  TeV,” *Phys. Rev. C*, vol. 96, no. 1, p. 015202, 2017, arXiv:1609.05383.
- [727] G. Aad *et al.*, “Measurements of the Nuclear Modification Factor for Jets in Pb+Pb Collisions at  $\sqrt{s_{NN}} = 2.76$  TeV with the ATLAS Detector,” *Phys. Rev. Lett.*, vol. 114, no. 7, p. 072302, 2015, arXiv:1411.2357.
- [728] S. Acharya *et al.*, “Measurements of inclusive jet spectra in pp and central Pb-Pb collisions at  $\sqrt{s_{NN}} = 5.02$  TeV,” *Phys. Rev. C*, vol. 101, no. 3, p. 034911, 2020, arXiv:1909.09718.
- [729] J. Adam *et al.*, “Measurement of jet suppression in central Pb-Pb collisions at  $\sqrt{s_{NN}} = 2.76$  TeV,” *Phys. Lett. B*, vol. 746, pp. 1–14, 2015, arXiv:1502.01689.
- [730] B. Abelev *et al.*, “Measurement of charged jet suppression in Pb-Pb collisions at  $\sqrt{s_{NN}} = 2.76$



- TeV,” *JHEP*, vol. 03, p. 013, 2014, arXiv:1311.0633.
- [731] V. Khachatryan *et al.*, “Measurement of transverse momentum relative to dijet systems in PbPb and pp collisions at  $\sqrt{s_{NN}} = 2.76$  TeV,” *JHEP*, vol. 01, p. 006, 2016, arXiv:1509.09029.
- [732] S. Chatrchyan *et al.*, “Jet momentum dependence of jet quenching in PbPb collisions at  $\sqrt{s_{NN}} = 2.76$  TeV,” *Phys. Lett. B*, vol. 712, pp. 176–197, 2012, arXiv:1202.5022.
- [733] S. Chatrchyan *et al.*, “Observation and studies of jet quenching in PbPb collisions at nucleon-nucleon center-of-mass energy = 2.76 TeV,” *Phys. Rev. C*, vol. 84, p. 024906, 2011, arXiv:1102.1957.
- [734] ATLAS Collaboration, “Measurements of the suppression and correlations of dijets in Pb+Pb collisions at  $\sqrt{s_{NN}} = 5.02$  TeV,” 5 2022, arXiv:2205.00682.
- [735] M. Aaboud *et al.*, “Measurement of jet  $p_T$  correlations in Pb+Pb and pp collisions at  $\sqrt{s_{NN}} = 2.76$  TeV with the ATLAS detector,” *Phys. Lett. B*, vol. 774, pp. 379–402, 2017, arXiv:1706.09363.
- [736] G. Aad *et al.*, “Observation of a Centrality-Dependent Dijet Asymmetry in Lead-Lead Collisions at  $\sqrt{s_{NN}} = 2.77$  TeV with the ATLAS Detector at the LHC,” *Phys. Rev. Lett.*, vol. 105, p. 252303, 2010, arXiv:1011.6182.
- [737] LHCb Collaboration, “Measurement of the radius dependence of charged-particle jet suppression in Pb-Pb collisions at  $\sqrt{s_{NN}} = 5.02$  TeV,” 3 2023, arXiv:2303.00592.
- [738] A. M. Sirunyan *et al.*, “Study of jet quenching with isolated-photon+jet correlations in PbPb and pp collisions at  $\sqrt{s_{NN}} = 5.02$  TeV,” *Phys. Lett. B*, vol. 785, pp. 14–39, 2018, arXiv:1711.09738.
- [739] A. M. Sirunyan *et al.*, “Study of Jet Quenching with  $Z$  + jet Correlations in Pb-Pb and pp Collisions at  $\sqrt{s_{NN}} = 5.02$  TeV,” *Phys. Rev. Lett.*, vol. 119, no. 8, p. 082301, 2017, arXiv:1702.01060.
- [740] S. Chatrchyan *et al.*, “Studies of jet quenching using isolated-photon+jet correlations in PbPb and pp collisions at  $\sqrt{s_{NN}} = 2.76$  TeV,” *Phys. Lett. B*, vol. 718, pp. 773–794, 2013, arXiv:1205.0206.
- [741] M. Aaboud *et al.*, “Measurement of photon–jet transverse momentum correlations in 5.02 TeV Pb + Pb and pp collisions with ATLAS,” *Phys. Lett. B*, vol. 789, pp. 167–190, 2019, arXiv:1809.07280.
- [742] S. Chatrchyan *et al.*, “Measurement of Jet Fragmentation in PbPb and pp Collisions at  $\sqrt{s_{NN}} = 2.76$  TeV,” *Phys. Rev. C*, vol. 90, no. 2, p. 024908, 2014, arXiv:1406.0932.
- [743] S. Chatrchyan *et al.*, “Measurement of jet fragmentation into charged particles in pp and PbPb collisions at  $\sqrt{s_{NN}} = 2.76$  TeV,” *JHEP*, vol. 10, p. 087, 2012, arXiv:1205.5872.
- [744] M. Aaboud *et al.*, “Measurement of jet fragmentation in 5.02 TeV proton-lead and proton-proton collisions with the ATLAS detector,” *Nucl. Phys. A*, vol. 978, p. 65, 2018, arXiv:1706.02859.
- [745] M. Aaboud *et al.*, “Measurement of jet fragmentation in Pb+Pb and pp collisions at  $\sqrt{s_{NN}} = 2.76$  TeV with the ATLAS detector at the LHC,” *Eur. Phys. J. C*, vol. 77, no. 6, p. 379, 2017, arXiv:1702.00674.
- [746] G. Aad *et al.*, “Measurement of inclusive jet charged-particle fragmentation functions in Pb+Pb collisions at  $\sqrt{s_{NN}} = 2.76$  TeV with the ATLAS detector,” *Phys. Lett. B*, vol. 739, pp. 320–342, 2014, arXiv:1406.2979.
- [747] ALICE Collaboration, “Measurement of inclusive and leading subjet fragmentation in pp and Pb-Pb collisions at  $\sqrt{s_{NN}} = 5.02$  TeV,” 4 2022, arXiv:2204.10270.
- [748] S. Acharya *et al.*, “Jet fragmentation transverse momentum distributions in pp and p-Pb collisions at  $\sqrt{s}$ ,  $\sqrt{s_{NN}} = 5.02$  TeV,” *JHEP*, vol. 09, p. 211, 2021, arXiv:2011.05904.
- [749] S. Acharya *et al.*, “Charged jet cross section and fragmentation in proton-proton collisions at  $\sqrt{s} = 7$  TeV,” *Phys. Rev. D*, vol. 99, no. 1, p. 012016, 2019, arXiv:1809.03232.
- [750] A. M. Sirunyan *et al.*, “Observation of Medium-Induced Modifications of Jet Fragmentation in Pb-Pb Collisions at  $\sqrt{s_{NN}} = 5.02$  TeV Using Isolated Photon-Tagged Jets,” *Phys. Rev. Lett.*, vol. 121, no. 24, p. 242301, 2018, arXiv:1801.04895.

- [751] CMS Collaboration, “Search for medium effects using jets from bottom quarks in PbPb collisions at  $\sqrt{s_{NN}} = 5.02$  TeV,” 10 2022, arXiv:2210.08547.
- [752] A. M. Sirunyan *et al.*, “In-medium modification of dijets in PbPb collisions at  $\sqrt{s_{NN}} = 5.02$  TeV,” *JHEP*, vol. 05, p. 116, 2021, arXiv:2101.04720.
- [753] A. M. Sirunyan *et al.*, “Measurement of b jet shapes in proton-proton collisions at  $\sqrt{s} = 5.02$  TeV,” *JHEP*, vol. 05, p. 054, 2021, arXiv:2005.14219.
- [754] V. Khachatryan *et al.*, “Decomposing transverse momentum balance contributions for quenched jets in PbPb collisions at  $\sqrt{s_{NN}} = 2.76$  TeV,” *JHEP*, vol. 11, p. 055, 2016, arXiv:1609.02466.
- [755] V. Khachatryan *et al.*, “Correlations between jets and charged particles in PbPb and pp collisions at  $\sqrt{s_{NN}} = 2.76$  TeV,” *JHEP*, vol. 02, p. 156, 2016, arXiv:1601.00079.
- [756] S. Chatrchyan *et al.*, “Modification of Jet Shapes in PbPb Collisions at  $\sqrt{s_{NN}} = 2.76$  TeV,” *Phys. Lett. B*, vol. 730, pp. 243–263, 2014, arXiv:1310.0878.
- [757] S. Acharya *et al.*, “Measurement of jet radial profiles in Pb-Pb collisions at  $\sqrt{s_{NN}} = 2.76$  TeV,” *Phys. Lett. B*, vol. 796, pp. 204–219, 2019, arXiv:1904.13118.
- [758] CMS Collaboration, “Azimuthal anisotropy of dijet events in PbPb collisions at  $\sqrt{s_{NN}} = 5.02$  TeV,” 10 2022, arXiv:2210.08325.
- [759] G. Aad *et al.*, “Measurement of the Azimuthal Angle Dependence of Inclusive Jet Yields in Pb+Pb Collisions at  $\sqrt{s_{NN}} = 2.76$  TeV with the ATLAS detector,” *Phys. Rev. Lett.*, vol. 111, no. 15, p. 152301, 2013, arXiv:1306.6469.
- [760] L. Cunqueiro and A. M. Sickles, “Studying the QGP with Jets at the LHC and RHIC,” *Prog. Part. Nucl. Phys.*, vol. 124, p. 103940, 2022, arXiv:2110.14490.
- [761] L. Apolinário, Y.-J. Lee, and M. Winn, “Heavy quarks and jets as probes of the QGP,” *Prog. Part. Nucl. Phys.*, vol. 127, p. 103990, 2022, arXiv:2203.16352.
- [762] Y. Akiba *et al.*, “The Hot QCD White Paper: Exploring the Phases of QCD at RHIC and the LHC,” 2 2015, arXiv:1502.02730.
- [763] H. A. Andrews *et al.*, “Novel tools and observables for jet physics in heavy-ion collisions,” *J. Phys. G*, vol. 47, no. 6, p. 065102, 2020, arXiv:1808.03689.
- [764] A. Adare *et al.*, “Medium modification of jet fragmentation in Au + Au collisions at  $\sqrt{s_{NN}} = 200$  GeV measured in direct photon-hadron correlations,” *Phys. Rev. Lett.*, vol. 111, no. 3, p. 032301, 2013, arXiv:1212.3323.
- [765] A. Adare *et al.*, “Suppression of away-side jet fragments with respect to the reaction plane in Au+Au collisions at  $\sqrt{s_{NN}} = 200$  GeV,” *Phys. Rev. C*, vol. 84, p. 024904, 2011, arXiv:1010.1521.
- [766] A. Adare *et al.*, “Azimuthal anisotropy of neutral pion production in Au+Au collisions at  $\sqrt{s_{NN}} = 200$  GeV: Path-length dependence of jet quenching and the role of initial geometry,” *Phys. Rev. Lett.*, vol. 105, p. 142301, 2010, arXiv:1006.3740.
- [767] M. S. Abdallah *et al.*, “Differential measurements of jet substructure and partonic energy loss in Au+Au collisions at  $\sqrt{s_{NN}} = 200$  GeV,” *Phys. Rev. C*, vol. 105, no. 4, p. 044906, 2022, arXiv:2109.09793.
- [768] J. Adam *et al.*, “Measurement of inclusive charged-particle jet production in Au + Au collisions at  $\sqrt{s_{NN}} = 200$  GeV,” *Phys. Rev. C*, vol. 102, no. 5, p. 054913, 2020, arXiv:2006.00582.
- [769] L. Adamczyk *et al.*, “Measurements of jet quenching with semi-inclusive hadron+jet distributions in Au+Au collisions at  $\sqrt{s_{NN}} = 200$  GeV,” *Phys. Rev. C*, vol. 96, no. 2, p. 024905, 2017, arXiv:1702.01108.
- [770] L. Adamczyk *et al.*, “Dijet imbalance measurements in Au + Au and pp collisions at  $\sqrt{s_{NN}} = 200$  GeV at STAR,” *Phys. Rev. Lett.*, vol. 119, no. 6, p. 062301, 2017, arXiv:1609.03878.

- [771] B. I. Abelev *et al.*, “System size dependence of associated yields in hadron-triggered jets,” *Phys. Lett. B*, vol. 683, pp. 123–128, 2010, arXiv:0904.1722.
- [772] S. Acharya *et al.*, “Medium modification of the shape of small-radius jets in central Pb-Pb collisions at  $\sqrt{s_{\text{NN}}} = 2.76$  TeV,” *JHEP*, vol. 10, p. 139, 2018, arXiv:1807.06854.
- [773] ALICE Collaboration, “Measurements of the groomed and ungroomed jet angularities in pp collisions at  $\sqrt{s} = 5.02$  TeV,” *JHEP*, vol. 05, p. 061, 2022, arXiv:2107.11303.
- [774] ATLAS Collaboration, “Measurement of  $R = 0.4$  jet mass in Pb+Pb and pp collisions at  $\sqrt{s_{\text{NN}}} = 5.02$  TeV with the ATLAS detector,” 5 2018.
- [775] S. Acharya *et al.*, “First measurement of jet mass in Pb–Pb and p–Pb collisions at the LHC,” *Phys. Lett. B*, vol. 776, pp. 249–264, 2018, arXiv:1702.00804.
- [776] A. M. Sirunyan *et al.*, “Measurement of the groomed jet mass in PbPb and pp collisions at  $\sqrt{s_{\text{NN}}} = 5.02$  TeV,” *JHEP*, vol. 10, p. 161, 2018, arXiv:1805.05145.
- [777] A. J. Larkoski, G. P. Salam, and J. Thaler, “Energy Correlation Functions for Jet Substructure,” *JHEP*, vol. 06, p. 108, 2013, arXiv:1305.0007.
- [778] A. J. Larkoski, J. Thaler, and W. J. Waalewijn, “Gaining (Mutual) Information about Quark/Gluon Discrimination,” *JHEP*, vol. 11, p. 129, 2014, arXiv:1408.3122.
- [779] F. A. Dreyer, G. P. Salam, and G. Soyez, “The Lund Jet Plane,” *JHEP*, vol. 12, p. 064, 2018, arXiv:1807.04758.
- [780] D. Bertolini, P. Harris, M. Low, and N. Tran, “Pileup Per Particle Identification,” *JHEP*, vol. 10, p. 059, 2014, arXiv:1407.6013.
- [781] P. Berta, M. Spousta, D. W. Miller, and R. Leitner, “Particle-level pileup subtraction for jets and jet shapes,” *JHEP*, vol. 06, p. 092, 2014, arXiv:1403.3108.
- [782] F. A. Dreyer, L. Necib, G. Soyez, and J. Thaler, “Recursive Soft Drop,” *JHEP*, vol. 06, p. 093, 2018, arXiv:1804.03657.
- [783] Y.-T. Chien and I. W. Stewart, “Collinear Drop,” *JHEP*, vol. 06, p. 064, 2020, arXiv:1907.11107.
- [784] D. Guest, K. Cranmer, and D. Whiteson, “Deep Learning and its Application to LHC Physics,” *Ann. Rev. Nucl. Part. Sci.*, vol. 68, pp. 161–181, 2018, arXiv:1806.11484.
- [785] K. Albertsson *et al.*, “Machine Learning in High Energy Physics Community White Paper,” *J. Phys. Conf. Ser.*, vol. 1085, no. 2, p. 022008, 2018, arXiv:1807.02876.
- [786] A. J. Larkoski, I. Moulton, and B. Nachman, “Jet Substructure at the Large Hadron Collider: A Review of Recent Advances in Theory and Machine Learning,” *Phys. Rept.*, vol. 841, pp. 1–63, 2020, arXiv:1709.04464.
- [787] R. Haake and C. Loizides, “Machine Learning based jet momentum reconstruction in heavy-ion collisions,” *Phys. Rev. C*, vol. 99, no. 6, p. 064904, 2019, arXiv:1810.06324.
- [788] J. Thaler and K. Van Tilburg, “Identifying Boosted Objects with N-subjettiness,” *JHEP*, vol. 03, p. 015, 2011, arXiv:1011.2268.
- [789] K. Datta and A. Larkoski, “How Much Information is in a Jet?,” *JHEP*, vol. 06, p. 073, 2017, arXiv:1704.08249.
- [790] P. T. Komiske, E. M. Metodiev, and J. Thaler, “Energy Flow Networks: Deep Sets for Particle Jets,” *JHEP*, vol. 01, p. 121, 2019, arXiv:1810.05165.
- [791] P. T. Komiske, E. M. Metodiev, and J. Thaler, “Energy flow polynomials: A complete linear basis for jet substructure,” *JHEP*, vol. 04, p. 013, 2018, arXiv:1712.07124.
- [792] Y.-T. Chien and R. Kunnawalkam Elayavalli, “Probing heavy ion collisions using quark and gluon jet substructure,” 3 2018, arXiv:1803.03589.

- [793] Y. Verma and S. Jena, “Jet characterization in Heavy Ion Collisions by QCD-Aware Graph Neural Networks,” 3 2021, arXiv:2103.14906.
- [794] Y. S. Lai, J. Mulligan, M. Płoskoń, and F. Ringer, “The information content of jet quenching and machine learning assisted observable design,” *JHEP*, vol. 10, p. 011, 2022, arXiv:2111.14589.
- [795] Y.-L. Du, D. Pablos, and K. Tywoniuk, “Classification of quark and gluon jets in hot QCD medium with deep learning,” *PoS*, vol. PANIC2021, p. 224, 2022, arXiv:2112.00681.
- [796] Y.-L. Du, D. Pablos, and K. Tywoniuk, “Jet tomography in hot QCD medium with deep learning,” *PoS*, vol. EPS-HEP2021, p. 302, 2022, arXiv:2112.00679.
- [797] Y.-L. Du, D. Pablos, and K. Tywoniuk, “Deep learning jet modifications in heavy-ion collisions,” *JHEP*, vol. 21, p. 206, 2020, arXiv:2012.07797.
- [798] L. Apolinário, N. F. Castro, M. Crispim Romão, J. G. Milhano, R. Pedro, and F. C. R. Peres, “Deep Learning for the classification of quenched jets,” *JHEP*, vol. 11, p. 219, 2021, arXiv:2106.08869.
- [799] L. Liu, J. Velkovska, and M. Verweij, “Identifying quenched jets in heavy ion collisions with machine learning,” 6 2022, arXiv:2206.01628.
- [800] Y.-T. Chien, A. Deshpande, M. M. Mondal, and G. Sterman, “Probing hadronization with flavor correlations of leading particles in jets,” *Phys. Rev. D*, vol. 105, no. 5, p. L051502, 2022, arXiv:2109.15318.
- [801] L. Apolinário, R. Kunnawalkam Elayavalli, and N. Olavo, “Transitioning from perturbative to non-perturbative splittings within QCD jets,” 12 2022, arXiv:2212.11846.
- [802] A. Andreassen, P. T. Komiske, E. M. Metodiev, B. Nachman, and J. Thaler, “OmniFold: A Method to Simultaneously Unfold All Observables,” *Phys. Rev. Lett.*, vol. 124, no. 18, p. 182001, 2020, arXiv:1911.09107.
- [803] V. Andreev *et al.*, “Measurement of Lepton-Jet Correlation in Deep-Inelastic Scattering with the H1 Detector Using Machine Learning for Unfolding,” *Phys. Rev. Lett.*, vol. 128, no. 13, p. 132002, 2022, arXiv:2108.12376.
- [804] A. M. Sirunyan *et al.*, “Measurement of the Splitting Function in  $pp$  and Pb-Pb Collisions at  $\sqrt{s_{\text{NN}}} = 5.02$  TeV,” *Phys. Rev. Lett.*, vol. 120, no. 14, p. 142302, 2018, arXiv:1708.09429.
- [805] J. Adam *et al.*, “Measurement of groomed jet substructure observables in p+p collisions at  $\sqrt{s} = 200$  GeV with STAR,” *Phys. Lett. B*, vol. 811, p. 135846, 2020, arXiv:2003.02114.
- [806] G. Aad *et al.*, “Measurement of the Lund Jet Plane Using Charged Particles in 13 TeV Proton-Proton Collisions with the ATLAS Detector,” *Phys. Rev. Lett.*, vol. 124, no. 22, p. 222002, 2020, arXiv:2004.03540.
- [807] S. Acharya *et al.*, “Direct observation of the dead-cone effect in quantum chromodynamics,” *Nature*, vol. 605, no. 7910, pp. 440–446, 2022, arXiv:2106.05713. [Erratum: *Nature* 607, E22 (2022)].
- [808] H. Chen, I. Moulton, X. Zhang, and H. X. Zhu, “Rethinking jets with energy correlators: Tracks, resummation, and analytic continuation,” *Phys. Rev. D*, vol. 102, no. 5, p. 054012, 2020, arXiv:2004.11381.
- [809] C. Andres, F. Dominguez, R. Kunnawalkam Elayavalli, J. Holguin, C. Marquet, and I. Moulton, “Resolving the Scales of the Quark-Gluon Plasma with Energy Correlators,” 9 2022, arXiv:2209.11236.
- [810] ALICE Collaboration, “Measurements of the groomed jet radius and momentum splitting fraction with the soft drop and dynamical grooming algorithms in pp collisions at  $\sqrt{s} = 5.02$  TeV,” 4 2022, arXiv:2204.10246.
- [811] Y. L. Dokshitzer and D. E. Kharzeev, “Heavy quark colorimetry of QCD matter,” *Phys. Lett. B*, vol. 519, pp. 199–206, 2001, arXiv:hep-ph/0106202.

- [812] V. Khachatryan *et al.*, “Transverse momentum spectra of inclusive b jets in pPb collisions at  $\sqrt{s_{NN}} = 5.02$  TeV,” *Phys. Lett. B*, vol. 754, p. 59, 2016, arXiv:1510.03373.
- [813] S. Acharya *et al.*, “Measurement of inclusive charged-particle b-jet production in pp and p-Pb collisions at  $\sqrt{s_{NN}} = 5.02$  TeV,” *JHEP*, vol. 01, p. 178, 2022, arXiv:2110.06104.
- [814] A. M. Sirunyan *et al.*, “Measurements of the charm jet cross section and nuclear modification factor in pPb collisions at  $\sqrt{s_{NN}} = 5.02$  TeV,” *Phys. Lett. B*, vol. 772, pp. 306–329, 2017, arXiv:1612.08972.
- [815] S. Chatrchyan *et al.*, “Evidence of b-Jet Quenching in PbPb Collisions at  $\sqrt{s_{NN}} = 2.76$  TeV,” *Phys. Rev. Lett.*, vol. 113, no. 13, p. 132301, 2014, arXiv:1312.4198. [Erratum: *Phys.Rev.Lett.* 115, 029903 (2015)].
- [816] ATLAS Collaboration, “Measurement of the nuclear modification factor of b-jets in 5.02 TeV Pb+Pb collisions with the ATLAS detector,” 4 2022, arXiv:2204.13530.
- [817] D. Roy, “An Investigation of Charm Quark Jet Spectrum and Shape Modifications in Au+Au Collisions at  $\sqrt{s_{NN}} = 200$  GeV,” in *29th International Conference on Ultra-relativistic Nucleus-Nucleus Collisions*, 7 2022, arXiv:2207.14434.
- [818] A. M. Sirunyan *et al.*, “Studies of charm quark diffusion inside jets using PbPb and pp collisions at  $\sqrt{s_{NN}} = 5.02$  TeV,” *Phys. Rev. Lett.*, vol. 125, no. 10, p. 102001, 2020, arXiv:1911.01461.
- [819] J. Sacks, W. J. Welch, T. J. Mitchell, and H. P. Wynn, “Design and Analysis of Computer Experiments,” *Statistical Science*, vol. 4, no. 4, pp. 409 – 423, 1989.
- [820] C. Currin, T. Mitchell, M. Morris, and D. Ylvisaker, “Bayesian prediction of deterministic functions, with applications to the design and analysis of computer experiments,” *Journal of the American Statistical Association*, vol. 86, no. 416, pp. 953–963, 1991, arXiv:<https://www.tandfonline.com/doi/pdf/10.1080/01621459.1991.10475138>.
- [821] M. C. Kennedy and A. O’Hagan, “Bayesian calibration of computer models,” *Journal of the Royal Statistical Society: Series B (Statistical Methodology)*, vol. 63, no. 3, pp. 425–464, 2001, arXiv:<https://rss.onlinelibrary.wiley.com/doi/pdf/10.1111/1467-9868.00294>.
- [822] C. E. Rasmussen and C. K. I. Williams, *Gaussian Processes for Machine Learning*. The MIT Press, 2006.
- [823] J. Goodman and J. Weare, “Ensemble samplers with affine invariance,” *Communications in Applied Mathematics and Computational Science*, vol. 5, p. 65, 2010.
- [824] D. Foreman-Mackey, D. W. Hogg, D. Lang, and J. Goodman, “emcee: The mcmc hammer,” *Publications of the Astronomical Society of the Pacific*, vol. 125, p. 306, feb 2013.
- [825] S. Cao *et al.*, “Determining the jet transport coefficient  $\hat{q}$  from inclusive hadron suppression measurements using Bayesian parameter estimation,” *Phys. Rev. C*, vol. 104, no. 2, p. 024905, 2021, arXiv:2102.11337.
- [826] W. Fan, *Multi Stage Heavy Quark Transport in Ultra-relativistic Heavy-ion Collisions*. PhD thesis, Duke U. (main), Duke U., 2022, arXiv:2207.12452.
- [827] M. Xie, W. Ke, H. Zhang, and X.-N. Wang, “Information field based global Bayesian inference of the jet transport coefficient,” 6 2022, arXiv:2206.01340.
- [828] Y. Xu, J. E. Bernhard, S. A. Bass, M. Nahrgang, and S. Cao, “Data-driven analysis for the temperature and momentum dependence of the heavy-quark diffusion coefficient in relativistic heavy-ion collisions,” *Phys. Rev. C*, vol. 97, no. 1, p. 014907, 2018, arXiv:1710.00807.
- [829] M. Xie, W. Ke, H. Zhang, and X.-N. Wang, “Global constraint on the jet transport coefficient from single hadron, dihadron and  $\gamma$ -hadron spectra in high-energy heavy-ion collisions,” 8 2022, arXiv:2208.14419.

- [830] M. Kordell and A. Majumder, “Event-by-Event Simulations of Jet Modification Using the MATTER Event Generator,” in *8th International Conference on Hard and Electromagnetic Probes of High-energy Nuclear Collisions: Hard Probes 2016*, 2 2017, arXiv:1702.05862.
- [831] W. Bialek, C. G. Callan, Jr., and S. P. Strong, “Field theories for learning probability distributions,” *Phys. Rev. Lett.*, vol. 77, pp. 4693–4697, 1996, arXiv:cond-mat/9607180.
- [832] T. Ensslin, “Information field theory,” *AIP Conf. Proc.*, vol. 1553, p. 184, 2013, arXiv:1301.2556.
- [833] J. C. Lemm, “Bayesian field theory: Nonparametric approaches to density estimation, regression, classification, and inverse quantum problems,” 1999.
- [834] B. Settles, “Active learning literature survey. 2010,” *Computer Sciences Technical Report*, vol. 1648, 2009.
- [835] D. Liyanage, Y. Ji, D. Everett, M. Heffernan, U. Heinz, S. Mak, and J.-F. Paquet, “Efficient emulation of relativistic heavy ion collisions with transfer learning,” *Phys. Rev. C*, vol. 105, no. 3, p. 034910, 2022, arXiv:2201.07302.
- [836] Y. Ji, S. Mak, D. Soeder, J.-F. Paquet, and S. A. Bass, “A graphical multi-fidelity gaussian process model, with application to emulation of expensive computer simulations,” 2021.
- [837] M. Mannarelli and R. Rapp, “Hadronic modes and quark properties in the quark-gluon plasma,” *Phys. Rev. C*, vol. 72, p. 064905, 2005, arXiv:hep-ph/0505080.
- [838] L. Ravagli and R. Rapp, “Quark Coalescence based on a Transport Equation,” *Phys. Lett. B*, vol. 655, pp. 126–131, 2007, arXiv:0705.0021.
- [839] S. Mukherjee, P. Petreczky, and S. Sharma, “Charm degrees of freedom in the quark gluon plasma,” *Phys. Rev. D*, vol. 93, no. 1, p. 014502, 2016, arXiv:1509.08887.
- [840] C. P. Herzog, A. Karch, P. Kovtun, C. Kozcaz, and L. G. Yaffe, “Energy loss of a heavy quark moving through N=4 supersymmetric Yang-Mills plasma,” *JHEP*, vol. 07, p. 013, 2006, arXiv:hep-th/0605158.
- [841] S. S. Gubser, “Comparing the drag force on heavy quarks in N=4 super-Yang-Mills theory and QCD,” *Phys. Rev. D*, vol. 76, p. 126003, 2007, arXiv:hep-th/0611272.
- [842] J. Casalderrey-Solana and D. Teaney, “Heavy quark diffusion in strongly coupled N=4 Yang-Mills,” *Phys. Rev. D*, vol. 74, p. 085012, 2006, arXiv:hep-ph/0605199.
- [843] O. Andreev, “Drag Force on Heavy Quarks and Spatial String Tension,” *Mod. Phys. Lett. A*, vol. 33, no. 06, p. 1850041, 2018, arXiv:1707.05045.
- [844] D. Banerjee, S. Datta, R. Gavai, and P. Majumdar, “Heavy Quark Momentum Diffusion Coefficient from Lattice QCD,” *Phys. Rev. D*, vol. 85, p. 014510, 2012, arXiv:1109.5738.
- [845] H. T. Ding, A. Francis, O. Kaczmarek, F. Karsch, H. Satz, and W. Soeldner, “Charmonium properties in hot quenched lattice QCD,” *Phys. Rev. D*, vol. 86, p. 014509, 2012, arXiv:1204.4945.
- [846] A. Francis, O. Kaczmarek, M. Laine, T. Neuhaus, and H. Ohno, “Nonperturbative estimate of the heavy quark momentum diffusion coefficient,” *Phys. Rev. D*, vol. 92, no. 11, p. 116003, 2015, arXiv:1508.04543.
- [847] N. Brambilla, V. Leino, P. Petreczky, and A. Vairo, “Lattice QCD constraints on the heavy quark diffusion coefficient,” *Phys. Rev. D*, vol. 102, no. 7, p. 074503, 2020, arXiv:2007.10078.
- [848] L. Altenkort, A. M. Eller, O. Kaczmarek, L. Mazur, G. D. Moore, and H.-T. Shu, “Heavy quark momentum diffusion from the lattice using gradient flow,” *Phys. Rev. D*, vol. 103, no. 1, p. 014511, 2021, arXiv:2009.13553.
- [849] S. Y. F. Liu and R. Rapp, “Spectral and transport properties of quark–gluon plasma in a nonperturbative approach,” *Eur. Phys. J. A*, vol. 56, no. 2, p. 44, 2020, arXiv:1612.09138.
- [850] S. Y. F. Liu and R. Rapp, “*T*-matrix Approach to Quark-Gluon Plasma,” *Phys. Rev. C*, vol. 97, no. 3,

- p. 034918, 2018, arXiv:1711.03282.
- [851] S. Caron-Huot, M. Laine, and G. D. Moore, “A Way to estimate the heavy quark thermalization rate from the lattice,” *JHEP*, vol. 04, p. 053, 2009, arXiv:0901.1195.
  - [852] N. Brambilla, V. Leino, J. Mayer-Stuedte, and P. Petreczky, “Heavy quark diffusion coefficient with gradient flow,” 6 2022, arXiv:2206.02861.
  - [853] D. Banerjee, S. Datta, and M. Laine, “Lattice study of a magnetic contribution to heavy quark momentum diffusion,” *JHEP*, vol. 08, p. 128, 2022, arXiv:2204.14075.
  - [854] D. Banerjee, R. Gavai, S. Datta, and P. Majumdar, “Temperature dependence of the static quark diffusion coefficient,” 6 2022, arXiv:2206.15471.
  - [855] A. Bouteffoux and M. Laine, “Mass-suppressed effects in heavy quark diffusion,” *JHEP*, vol. 12, p. 150, 2020, arXiv:2010.07316.
  - [856] M. Laine, “1-loop matching of a thermal Lorentz force,” *JHEP*, vol. 06, p. 139, 2021, arXiv:2103.14270.
  - [857] L. Altenkort, O. Kaczmarek, R. Larsen, S. Mukherjee, P. Petreczky, H.-T. Shu, and S. Stenbach, “Heavy Quark Diffusion from 2+1 Flavor Lattice QCD,” 2 2023, arXiv:2302.08501.
  - [858] G. D. Moore and D. Teaney, “How much do heavy quarks thermalize in a heavy ion collision?,” *Phys. Rev. C*, vol. 71, p. 064904, 2005, arXiv:hep-ph/0412346.
  - [859] S. Y. F. Liu and R. Rapp, “Heavy-light susceptibilities in a strongly coupled quark-gluon plasma,” *Phys. Rev. C*, vol. 106, no. 5, p. 055201, 2022, arXiv:2111.13620.
  - [860] G. Aarts, C. Allton, R. Bignell, T. J. Burns, S. C. García-Maseraque, S. Hands, B. Jäger, S. Kim, S. M. Ryan, and J.-I. Skullerud, “Open charm mesons at nonzero temperature: results in the hadronic phase from lattice QCD,” 9 2022, arXiv:2209.14681.
  - [861] A. Rothkopf, “Heavy Quarkonium in Extreme Conditions,” *Phys. Rept.*, vol. 858, pp. 1–117, 2020, arXiv:1912.02253.
  - [862] Y. Akamatsu, “Quarkonium in quark–gluon plasma: Open quantum system approaches re-examined,” *Prog. Part. Nucl. Phys.*, vol. 123, p. 103932, 2022, arXiv:2009.10559.
  - [863] R. Sharma, “Quarkonium propagation in the quark–gluon plasma,” *Eur. Phys. J. ST*, vol. 230, no. 3, pp. 697–718, 2021, arXiv:2101.04268.
  - [864] X. Yao, “Open quantum systems for quarkonia,” *Int. J. Mod. Phys. A*, vol. 36, no. 20, p. 2130010, 2021, arXiv:2102.01736.
  - [865] Y. Akamatsu, “Real-time quantum dynamics of heavy quark systems at high temperature,” *Phys. Rev. D*, vol. 87, no. 4, p. 045016, 2013, arXiv:1209.5068.
  - [866] Y. Akamatsu, “Heavy quark master equations in the Lindblad form at high temperatures,” *Phys. Rev. D*, vol. 91, no. 5, p. 056002, 2015, arXiv:1403.5783.
  - [867] R. Katz and P. B. Gossiaux, “The Schrödinger–Langevin equation with and without thermal fluctuations,” *Annals Phys.*, vol. 368, pp. 267–295, 2016, arXiv:1504.08087.
  - [868] N. Brambilla, M. A. Escobedo, J. Soto, and A. Vairo, “Quarkonium suppression in heavy-ion collisions: an open quantum system approach,” *Phys. Rev. D*, vol. 96, no. 3, p. 034021, 2017, arXiv:1612.07248.
  - [869] J.-P. Blaizot and M. A. Escobedo, “Quantum and classical dynamics of heavy quarks in a quark-gluon plasma,” *JHEP*, vol. 06, p. 034, 2018, arXiv:1711.10812.
  - [870] S. Kajimoto, Y. Akamatsu, M. Asakawa, and A. Rothkopf, “Dynamical dissociation of quarkonia by wave function decoherence,” *Phys. Rev. D*, vol. 97, no. 1, p. 014003, 2018, arXiv:1705.03365.
  - [871] Y. Akamatsu, M. Asakawa, S. Kajimoto, and A. Rothkopf, “Quantum dissipation of a heavy quark

- from a nonlinear stochastic Schrödinger equation,” *JHEP*, vol. 07, p. 029, 2018, arXiv:1805.00167.
- [872] T. Miura, Y. Akamatsu, M. Asakawa, and A. Rothkopf, “Quantum Brownian motion of a heavy quark pair in the quark-gluon plasma,” *Phys. Rev. D*, vol. 101, no. 3, p. 034011, 2020, arXiv:1908.06293.
- [873] N. Brambilla, M. A. Escobedo, M. Strickland, A. Vairo, P. Vander Griend, and J. H. Weber, “Bottomonium suppression in an open quantum system using the quantum trajectories method,” *JHEP*, vol. 05, p. 136, 2021, arXiv:2012.01240.
- [874] N. Brambilla, M. A. Escobedo, M. Strickland, A. Vairo, P. Vander Griend, and J. H. Weber, “Bottomonium production in heavy-ion collisions using quantum trajectories: Differential observables and momentum anisotropy,” *Phys. Rev. D*, vol. 104, no. 9, p. 094049, 2021, arXiv:2107.06222.
- [875] Y. Akamatsu, M. Asakawa, and S. Kajimoto, “Dynamics of in-medium quarkonia in SU(3) and SU(2) gauge theories,” *Phys. Rev. D*, vol. 105, no. 5, p. 054036, 2022, arXiv:2108.06921.
- [876] N. Brambilla, M. A. Escobedo, A. Islam, M. Strickland, A. Tiwari, A. Vairo, and P. Vander Griend, “Heavy quarkonium dynamics at next-to-leading order in the binding energy over temperature,” *JHEP*, vol. 08, p. 303, 2022, arXiv:2205.10289.
- [877] T. Miura, Y. Akamatsu, M. Asakawa, and Y. Kaida, “Simulation of Lindblad equations for quarkonium in the quark-gluon plasma,” *Phys. Rev. D*, vol. 106, no. 7, p. 074001, 2022, arXiv:2205.15551.
- [878] X. Yao and T. Mehen, “Quarkonium in-medium transport equation derived from first principles,” *Phys. Rev. D*, vol. 99, no. 9, p. 096028, 2019, arXiv:1811.07027.
- [879] X. Yao and T. Mehen, “Quarkonium Semiclassical Transport in Quark-Gluon Plasma: Factorization and Quantum Correction,” *JHEP*, vol. 02, p. 062, 2021, arXiv:2009.02408.
- [880] R. Rapp and X. Du, “Theoretical Perspective on Quarkonia from SPS via RHIC to LHC,” *Nucl. Phys. A*, vol. 967, pp. 216–224, 2017, arXiv:1704.07923.
- [881] X. Du, S. Y. F. Liu, and R. Rapp, “Extraction of the Heavy-Quark Potential from Bottomonium Observables in Heavy-Ion Collisions,” *Phys. Lett. B*, vol. 796, pp. 20–25, 2019, arXiv:1904.00113.
- [882] X. Du and R. Rapp, “Non-equilibrium charmonium regeneration in strongly coupled quark-gluon plasma,” *Phys. Lett. B*, vol. 834, p. 137414, 2022, arXiv:2207.00065.
- [883] X. Yao and B. Müller, “Approach to equilibrium of quarkonium in quark-gluon plasma,” *Phys. Rev. C*, vol. 97, no. 1, p. 014908, 2018, arXiv:1709.03529. [Erratum: *Phys.Rev.C* 97, 049903 (2018)].
- [884] X. Yao, W. Ke, Y. Xu, S. Bass, and B. Müller, “Quarkonium production in heavy ion collisions: coupled Boltzmann transport equations,” *Nucl. Phys. A*, vol. 982, pp. 755–758, 2019, arXiv:1807.06199.
- [885] X. Yao and B. Müller, “Quarkonium inside the quark-gluon plasma: Diffusion, dissociation, recombination, and energy loss,” *Phys. Rev. D*, vol. 100, no. 1, p. 014008, 2019, arXiv:1811.09644.
- [886] X. Yao, W. Ke, Y. Xu, S. A. Bass, and B. Müller, “Coupled Boltzmann Transport Equations of Heavy Quarks and Quarkonia in Quark-Gluon Plasma,” *JHEP*, vol. 01, p. 046, 2021, arXiv:2004.06746.
- [887] B. Wu, Z. Tang, M. He, and R. Rapp, “Charmonium,  $B_c$  and X(3872) Transport at the LHC,” 9 2022, arXiv:2209.13795.
- [888] B. Wu, Z. Tang, M. He, and R. Rapp, “Recombination of  $B_c$  Mesons in Ultra-Relativistic Heavy-Ion Collisions,” 2 2023, arXiv:2302.11511.
- [889] X. Yao and B. Müller, “Doubly charmed baryon production in heavy ion collisions,” *Phys. Rev. D*, vol. 97, no. 7, p. 074003, 2018, arXiv:1801.02652.
- [890] Y. Akamatsu and A. Rothkopf, “Stochastic potential and quantum decoherence of heavy quarkonium in the quark-gluon plasma,” *Phys. Rev. D*, vol. 85, p. 105011, 2012, arXiv:1110.1203.



- [891] A. Rothkopf, “A first look at Bottomonium melting via a stochastic potential,” *JHEP*, vol. 04, p. 085, 2014, arXiv:1312.3246.
- [892] J.-P. Blaizot and M. A. Escobedo, “Approach to equilibrium of a quarkonium in a quark-gluon plasma,” *Phys. Rev. D*, vol. 98, no. 7, p. 074007, 2018, arXiv:1803.07996.
- [893] X. Yao, W. Ke, Y. Xu, S. A. Bass, T. Mehen, and B. Müller, “Quarkonium Production in Heavy Ion Collisions: From Open Quantum System to Transport Equation,” *Nucl. Phys. A*, vol. 1005, p. 121854, 2021, arXiv:2002.04079.
- [894] L. Yan, P. Zhuang, and N. Xu, “Competition between  $J/\psi$  suppression and regeneration in quark-gluon plasma,” *Phys. Rev. Lett.*, vol. 97, p. 232301, 2006, arXiv:nucl-th/0608010.
- [895] Y.-p. Liu, Z. Qu, N. Xu, and P.-f. Zhuang, “ $J/\psi$  Transverse Momentum Distribution in High Energy Nuclear Collisions at RHIC,” *Phys. Lett. B*, vol. 678, pp. 72–76, 2009, arXiv:0901.2757.
- [896] X. Zhao and R. Rapp, “Charmonium in Medium: From Correlators to Experiment,” *Phys. Rev. C*, vol. 82, p. 064905, 2010, arXiv:1008.5328.
- [897] Y. Liu, B. Chen, N. Xu, and P. Zhuang, “ $\Upsilon$  Production as a Probe for Early State Dynamics in High Energy Nuclear Collisions at RHIC,” *Phys. Lett. B*, vol. 697, pp. 32–36, 2011, arXiv:1009.2585.
- [898] X. Zhao and R. Rapp, “Medium Modifications and Production of Charmonia at LHC,” *Nucl. Phys. A*, vol. 859, pp. 114–125, 2011, arXiv:1102.2194.
- [899] T. Song, K. C. Han, and C. M. Ko, “Charmonium production in relativistic heavy-ion collisions,” *Phys. Rev. C*, vol. 84, p. 034907, 2011, arXiv:1103.6197.
- [900] X. Du and R. Rapp, “Sequential Regeneration of Charmonia in Heavy-Ion Collisions,” *Nucl. Phys. A*, vol. 943, pp. 147–158, 2015, arXiv:1504.00670.
- [901] K. Zhou, Z. Chen, C. Greiner, and P. Zhuang, “Thermal Charm and Charmonium Production in Quark Gluon Plasma,” *Phys. Lett. B*, vol. 758, pp. 434–439, 2016, arXiv:1602.01667.
- [902] B. Chen and J. Zhao, “Bottomonium Continuous Production from Unequilibrium Bottom Quarks in Ultrarelativistic Heavy Ion Collisions,” *Phys. Lett. B*, vol. 772, pp. 819–824, 2017, arXiv:1704.05622.
- [903] J. Zhao and B. Chen, “Strong diffusion effect of charm quarks on  $J/\psi$  production in Pb–Pb collisions at the LHC,” *Phys. Lett. B*, vol. 776, pp. 17–21, 2018, arXiv:1705.04558.
- [904] X. Du, R. Rapp, and M. He, “Color Screening and Regeneration of Bottomonia in High-Energy Heavy-Ion Collisions,” *Phys. Rev. C*, vol. 96, no. 5, p. 054901, 2017, arXiv:1706.08670.
- [905] J. Zhao, B. Chen, and P. Zhuang, “Charmonium triangular flow in high energy nuclear collisions,” *Phys. Rev. C*, vol. 105, no. 3, p. 034902, 2022, arXiv:2112.00293.
- [906] C. Li and B. Chen, “Anisotropic Flows of Charmonium in the Relativistic Heavy-Ion Collisions,” *Mathematics*, vol. 10, no. 22, p. 4284, 2022, arXiv:2209.11996.
- [907] N. Brambilla, M. A. Escobedo, J. Soto, and A. Vairo, “Heavy quarkonium suppression in a fireball,” *Phys. Rev. D*, vol. 97, no. 7, p. 074009, 2018, arXiv:1711.04515.
- [908] A. M. Eller, J. Ghiglieri, and G. D. Moore, “Thermal Heavy Quark Self-Energy from Euclidean Correlators,” *Phys. Rev. D*, vol. 99, no. 9, p. 094042, 2019, arXiv:1903.08064. [Erratum: *Phys.Rev.D* 102, 039901 (2020)].
- [909] B. Scheihing-Hitschfeld and X. Yao, “Gauge Invariance of Non-Abelian Field Strength Correlators: the Axial Gauge Puzzle,” 5 2022, arXiv:2205.04477.
- [910] Y. Burnier, M. Laine, J. Langelage, and L. Mether, “Colour-electric spectral function at next-to-leading order,” *JHEP*, vol. 08, p. 094, 2010, arXiv:1006.0867.
- [911] T. Binder, K. Mukaida, B. Scheihing-Hitschfeld, and X. Yao, “Non-Abelian electric field correlator at NLO for dark matter relic abundance and quarkonium transport,” *JHEP*, vol. 01, p. 137, 2022,

- arXiv:2107.03945.
- [912] A. Bazavov, P. Petreczky, and A. Velytsky, *Quarkonium at Finite Temperature*, pp. 61–110. 2010, arXiv:0904.1748.
- [913] A. Mocsy, P. Petreczky, and M. Strickland, “Quarkonia in the Quark Gluon Plasma,” *Int. J. Mod. Phys. A*, vol. 28, p. 1340012, 2013, arXiv:1302.2180.
- [914] R. Larsen, S. Meinel, S. Mukherjee, and P. Petreczky, “Excited bottomonia in quark-gluon plasma from lattice QCD,” *Phys. Lett. B*, vol. 800, p. 135119, 2020, arXiv:1910.07374.
- [915] R. Larsen, S. Meinel, S. Mukherjee, and P. Petreczky, “Thermal broadening of bottomonia: Lattice nonrelativistic QCD with extended operators,” *Phys. Rev. D*, vol. 100, no. 7, p. 074506, 2019, arXiv:1908.08437.
- [916] A. Rothkopf, T. Hatsuda, and S. Sasaki, “Complex Heavy-Quark Potential at Finite Temperature from Lattice QCD,” *Phys. Rev. Lett.*, vol. 108, p. 162001, 2012, arXiv:1108.1579.
- [917] D. Bala, O. Kaczmarek, R. Larsen, S. Mukherjee, G. Parkar, P. Petreczky, A. Rothkopf, and J. H. Weber, “Static quark-antiquark interactions at nonzero temperature from lattice QCD,” *Phys. Rev. D*, vol. 105, no. 5, p. 054513, 2022, arXiv:2110.11659.
- [918] P. Petreczky, S. Sharma, and J. H. Weber, “Bottomonium melting from screening correlators at high temperature,” *Phys. Rev. D*, vol. 104, no. 5, p. 054511, 2021, arXiv:2107.11368.
- [919] X. Du and R. Rapp, “In-Medium Charmonium Production in Proton-Nucleus Collisions,” *JHEP*, vol. 03, p. 015, 2019, arXiv:1808.10014.
- [920] A. Adare *et al.*, “Nuclear Modification of  $\phi'$ ,  $\chi_c$ , and  $J/\psi$  Production in d+Au Collisions at  $\sqrt{s_{NN}}=200$  GeV,” *Phys. Rev. Lett.*, vol. 111, no. 20, p. 202301, 2013, arXiv:1305.5516.
- [921] U. Acharya *et al.*, “Measurement of  $J/\psi$  at forward and backward rapidity in  $p+p$ ,  $p+Al$ ,  $p+Au$ , and  $^3He+Au$  collisions at  $\sqrt{s_{NN}} = 200$  GeV,” *Phys. Rev. C*, vol. 102, no. 1, p. 014902, 2020, arXiv:1910.14487.
- [922] U. A. Acharya *et al.*, “Measurement of  $\psi(2S)$  nuclear modification at backward and forward rapidity in  $p+p$ ,  $p+Al$ , and  $p+Au$  collisions at  $\sqrt{s_{NN}} = 200$  GeV,” *Phys. Rev. C*, vol. 105, no. 6, p. 064912, 2022, arXiv:2202.03863.
- [923] M. Abdallah *et al.*, “Measurement of cold nuclear matter effects for inclusive  $J/\psi$  in p+Au collisions at sNN=200 GeV,” *Phys. Lett. B*, vol. 825, p. 136865, 2022, arXiv:2110.09666.
- [924] R. Aaij *et al.*, “Study of  $J/\psi$  production and cold nuclear matter effects in  $pPb$  collisions at  $\sqrt{s_{NN}} = 5$  TeV,” *JHEP*, vol. 02, p. 072, 2014, arXiv:1308.6729.
- [925] R. Aaij *et al.*, “Study of  $\psi(2S)$  production and cold nuclear matter effects in pPb collisions at  $\sqrt{s_{NN}} = 5$  TeV,” *JHEP*, vol. 03, p. 133, 2016, arXiv:1601.07878.
- [926] R. Aaij *et al.*, “Study of  $\Upsilon$  production in  $pPb$  collisions at  $\sqrt{s_{NN}} = 8.16$  TeV,” *JHEP*, vol. 11, p. 194, 2018, arXiv:1810.07655. [Erratum: JHEP 02, 093 (2020)].
- [927] M. Aaboud *et al.*, “Measurement of quarkonium production in proton–lead and proton–proton collisions at 5.02 TeV with the ATLAS detector,” *Eur. Phys. J. C*, vol. 78, no. 3, p. 171, 2018, arXiv:1709.03089.
- [928] A. M. Sirunyan *et al.*, “Measurement of prompt and nonprompt  $J/\psi$  production in pp and pPb collisions at  $\sqrt{s_{NN}} = 5.02$  TeV,” *Eur. Phys. J. C*, vol. 77, no. 4, p. 269, 2017, arXiv:1702.01462.
- [929] A. M. Sirunyan *et al.*, “Measurement of prompt  $\psi(2S)$  production cross sections in proton-lead and proton-proton collisions at  $\sqrt{s_{NN}} = 5.02$  TeV,” *Phys. Lett. B*, vol. 790, pp. 509–532, 2019, arXiv:1805.02248.
- [930] A. Tumasyan *et al.*, “Nuclear modification of  $\Upsilon$  states in pPb collisions at  $\sqrt{s_{NN}} = 5.02$  TeV,” *Phys. Lett. B*, vol. 835, p. 137397, 2022, arXiv:2202.11807.

- [931] B. B. Abelev *et al.*, “ $J/\psi$  production and nuclear effects in p-Pb collisions at  $\sqrt{s_{NN}} = 5.02$  TeV,” *JHEP*, vol. 02, p. 073, 2014, arXiv:1308.6726.
- [932] B. B. Abelev *et al.*, “Suppression of  $\psi(2S)$  production in p-Pb collisions at  $\sqrt{s_{NN}} = 5.02$  TeV,” *JHEP*, vol. 12, p. 073, 2014, arXiv:1405.3796.
- [933] J. Adam *et al.*, “Centrality dependence of  $\psi(2S)$  suppression in p-Pb collisions at  $\sqrt{s_{NN}} = 5.02$  TeV,” *JHEP*, vol. 06, p. 050, 2016, arXiv:1603.02816.
- [934] S. Acharya *et al.*, “ $\Upsilon$  production in p-Pb collisions at  $\sqrt{s_{NN}}=8.16$  TeV,” *Phys. Lett. B*, vol. 806, p. 135486, 2020, arXiv:1910.14405.
- [935] ALICE Collaboration, “Inclusive, prompt and non-prompt  $J/\psi$  production at midrapidity in p-Pb collisions at  $\sqrt{s_{NN}} = 5.02$  TeV,” *JHEP*, vol. 06, p. 011, 2022, arXiv:2105.04957.
- [936] J.-P. Lansberg and H.-S. Shao, “Towards an automated tool to evaluate the impact of the nuclear modification of the gluon density on quarkonium, D and B meson production in proton-nucleus collisions,” *Eur. Phys. J. C*, vol. 77, no. 1, p. 1, 2017, arXiv:1610.05382.
- [937] A. Kusina, J.-P. Lansberg, I. Schienbein, and H.-S. Shao, “Gluon Shadowing in Heavy-Flavor Production at the LHC,” *Phys. Rev. Lett.*, vol. 121, no. 5, p. 052004, 2018, arXiv:1712.07024.
- [938] F. Arleo, R. Kolevatov, S. Peigné, and M. Rustamova, “Centrality and  $p_T$  dependence of  $J/\psi$  suppression in proton-nucleus collisions from parton energy loss,” *JHEP*, vol. 05, p. 155, 2013, arXiv:1304.0901.
- [939] E. G. Ferreira, “Excited charmonium suppression in proton-nucleus collisions as a consequence of comovers,” *Phys. Lett. B*, vol. 749, pp. 98–103, 2015, arXiv:1411.0549.
- [940] B. Alessandro *et al.*, “A New measurement of  $J/\psi$  suppression in Pb-Pb collisions at 158-GeV per nucleon,” *Eur. Phys. J. C*, vol. 39, pp. 335–345, 2005, arXiv:hep-ex/0412036.
- [941] J. Adam *et al.*, “Measurement of inclusive  $J/\psi$  suppression in Au+Au collisions at  $\sqrt{s_{NN}} = 200$  GeV through the dimuon channel at STAR,” *Phys. Lett. B*, vol. 797, p. 134917, 2019, arXiv:1905.13669.
- [942] S. Acharya *et al.*, “ $J/\psi$  elliptic and triangular flow in Pb-Pb collisions at  $\sqrt{s_{NN}} = 5.02$  TeV,” *JHEP*, vol. 10, p. 141, 2020, arXiv:2005.14518.
- [943] M. He, B. Wu, and R. Rapp, “Collectivity of  $J/\psi$  Mesons in Heavy-Ion Collisions,” *Phys. Rev. Lett.*, vol. 128, no. 16, p. 162301, 2022, arXiv:2111.13528.
- [944] M. Aaboud *et al.*, “Prompt and non-prompt  $J/\psi$  and  $\psi(2S)$  suppression at high transverse momentum in 5.02 TeV Pb+Pb collisions with the ATLAS experiment,” *Eur. Phys. J. C*, vol. 78, no. 9, p. 762, 2018, arXiv:1805.04077.
- [945] A. Tumasyan *et al.*, “Fragmentation of jets containing a prompt  $J/\psi$  meson in PbPb and pp collisions at  $\sqrt{s_{NN}} = 5.02$  TeV,” *Phys. Lett. B*, vol. 825, p. 136842, 2022, arXiv:2106.13235.
- [946] A. M. Sirunyan *et al.*, “Study of  $J/\psi$  meson production inside jets in pp collisions at  $\sqrt{s} = 8$  TeV,” *Phys. Lett. B*, vol. 804, p. 135409, 2020, arXiv:1910.01686.
- [947] S.-L. Zhang, J. Liao, G.-Y. Qin, E. Wang, and H. Xing, “Unraveling Gluon Jet Quenching through  $J/\psi$  Production in Heavy-Ion Collisions,” 8 2022, arXiv:2208.08323.
- [948] STAR Collaboration, “Observation of sequential  $\Upsilon$  suppression in Au+Au collisions at  $\sqrt{s_{NN}} = 200$  GeV with the STAR experiment,” 7 2022, arXiv:2207.06568.
- [949] Z. Ye, “ $\Upsilon$  measurements in p+p, p+Au and Au+Au collisions at  $\sqrt{s_{NN}} = 200$  GeV with the STAR experiment,” *Nucl. Phys. A*, vol. 967, pp. 600–603, 2017.
- [950] Z. Zhang, “Cold Nuclear Matter Effects on  $J/\psi$  and  $\Upsilon$  Productions at RHIC with the STAR Experiment,” *PoS*, vol. HardProbes2020, p. 057, 2021.
- [951] A. M. Sirunyan *et al.*, “Measurement of nuclear modification factors of  $\Upsilon(1S)$ ,  $\Upsilon(2S)$ , and  $\Upsilon(3S)$

- mesons in PbPb collisions at  $\sqrt{s_{NN}} = 5.02$  TeV,” *Phys. Lett. B*, vol. 790, pp. 270–293, 2019, arXiv:1805.09215.
- [952] CMS Collaboration, “Observation of the  $\Upsilon(3S)$  meson and sequential suppression of  $\Upsilon$  states in PbPb collisions at  $\sqrt{s_{NN}} = 5.02$  TeV,” 2022.
- [953] A. M. Sirunyan *et al.*, “Measurement of prompt and nonprompt charmonium suppression in PbPb collisions at 5.02 TeV,” *Eur. Phys. J. C*, vol. 78, no. 6, p. 509, 2018, arXiv:1712.08959.
- [954] F.-M. Liu and S.-X. Liu, “Quark-gluon plasma formation time and direct photons from heavy ion collisions,” *Phys. Rev. C*, vol. 89, no. 3, p. 034906, 2014, arXiv:1212.6587.
- [955] C. Aidala *et al.*, “Measurements of  $\mu\mu$  pairs from open heavy flavor and Drell-Yan in  $p+p$  collisions at  $\sqrt{s} = 200$  GeV,” *Phys. Rev. D*, vol. 99, no. 7, p. 072003, 2019, arXiv:1805.02448.
- [956] P. Avery *et al.*, “Inclusive production of the charmed baryon  $\Lambda_c^+$  from  $e^+e^-$  annihilations at  $\sqrt{s} = 10.55$  GeV,” *Phys. Rev. D*, vol. 43, pp. 3599–3610, 1991.
- [957] H. Albrecht *et al.*, “Observation of the Charmed Baryon  $\Lambda_c$  in  $e^+e^-$  Annihilation at 10-GeV,” *Phys. Lett. B*, vol. 207, pp. 109–114, 1988.
- [958] L. Gladilin, “Fragmentation fractions of  $c$  and  $b$  quarks into charmed hadrons at LEP,” *Eur. Phys. J. C*, vol. 75, no. 1, p. 19, 2015, arXiv:1404.3888.
- [959] H. Abramowicz *et al.*, “Measurement of  $D^+$  and  $\Lambda_c^+$  production in deep inelastic scattering at HERA,” *JHEP*, vol. 11, p. 009, 2010, arXiv:1007.1945.
- [960] H. Abramowicz *et al.*, “Measurement of charm fragmentation fractions in photoproduction at HERA,” *JHEP*, vol. 09, p. 058, 2013, arXiv:1306.4862.
- [961] R. Aaij *et al.*, “Prompt charm production in pp collisions at  $\sqrt{s}=7$  TeV,” *Nucl. Phys. B*, vol. 871, pp. 1–20, 2013, arXiv:1302.2864.
- [962] R. Aaij *et al.*, “Prompt  $\Lambda_c^+$  production in  $pPb$  collisions at  $\sqrt{s_{NN}} = 5.02$  TeV,” *JHEP*, vol. 02, p. 102, 2019, arXiv:1809.01404.
- [963] S. Acharya *et al.*, “ $\Lambda_c^+$  Production and Baryon-to-Meson Ratios in pp and p-Pb Collisions at  $\sqrt{s_{NN}}=5.02$  TeV at the LHC,” *Phys. Rev. Lett.*, vol. 127, no. 20, p. 202301, 2021, arXiv:2011.06078.
- [964] J. Adam *et al.*, “First measurement of  $\Lambda_c$  baryon production in Au+Au collisions at  $\sqrt{s_{NN}} = 200$  GeV,” *Phys. Rev. Lett.*, vol. 124, no. 17, p. 172301, 2020, arXiv:1910.14628.
- [965] S. Acharya *et al.*, “Constraining hadronization mechanisms with  $\Lambda_c^+/D^0$  production ratios in Pb-Pb collisions at  $\sqrt{s_{NN}} = 5.02$  TeV,” 12 2021, arXiv:2112.08156.
- [966] LHCb Collaboration, “Measurement of the  $\Lambda_c^+$  to  $D^0$  production cross-section ratio in peripheral PbPb collisions,” 10 2022, arXiv:2210.06939.
- [967] A. M. Sirunyan *et al.*, “Production of  $\Lambda_c^+$  baryons in proton-proton and lead-lead collisions at  $\sqrt{s_{NN}} = 5.02$  TeV,” *Phys. Lett. B*, vol. 803, p. 135328, 2020, arXiv:1906.03322.
- [968] S. Acharya *et al.*, “Charm-quark fragmentation fractions and production cross section at midrapidity in pp collisions at the LHC,” *Phys. Rev. D*, vol. 105, no. 1, p. L011103, 2022, arXiv:2105.06335.
- [969] J. Adam *et al.*, “Centrality and transverse momentum dependence of  $D^0$ -meson production at mid-rapidity in Au+Au collisions at  $\sqrt{s_{NN}} = 200$  GeV,” *Phys. Rev. C*, vol. 99, no. 3, p. 034908, 2019, arXiv:1812.10224.
- [970] S. S. Adler *et al.*, “Centrality dependence of charm production from single electrons measurement in Au + Au collisions at  $\sqrt{s_{NN}} = 200$ -GeV,” *Phys. Rev. Lett.*, vol. 94, p. 082301, 2005, arXiv:nucl-ex/0409028.
- [971] V. Minissale, F. Scardina, and V. Greco, “Hadrons from coalescence plus fragmentation in AA collisions at energies available at the BNL Relativistic Heavy Ion Collider to the CERN Large Hadron

- Collider,” *Phys. Rev. C*, vol. 92, no. 5, p. 054904, 2015, arXiv:1502.06213.
- [972] R. Aaij *et al.*, “Measurement of  $B^+$ ,  $B^0$  and  $\Lambda_b^0$  production in  $p$ Pb collisions at  $\sqrt{s_{NN}} = 8.16$  TeV,” *Phys. Rev. D*, vol. 99, no. 5, p. 052011, 2019, arXiv:1902.05599.
- [973] R. Aaij *et al.*, “Study of prompt  $D^0$  meson production in  $p$ Pb collisions at  $\sqrt{s_{NN}} = 5$  TeV,” *JHEP*, vol. 10, p. 090, 2017, arXiv:1707.02750.
- [974] J. Adam *et al.*, “ $D$ -meson production in  $p$ -Pb collisions at  $\sqrt{s_{NN}} = 5.02$  TeV and in pp collisions at  $\sqrt{s} = 7$  TeV,” *Phys. Rev. C*, vol. 94, no. 5, p. 054908, 2016, arXiv:1605.07569.
- [975] J. L. Albacete *et al.*, “Predictions for Cold Nuclear Matter Effects in  $p$ +Pb Collisions at  $\sqrt{s_{NN}} = 8.16$  TeV,” *Nucl. Phys. A*, vol. 972, pp. 18–85, 2018, arXiv:1707.09973.
- [976] U. A. Acharya *et al.*, “Charm- and Bottom-Quark Production in Au+Au Collisions at  $\sqrt{s_{NN}} = 200$  GeV,” 3 2022, arXiv:2203.17058.
- [977] S. Collaboration *et al.*, “Evidence of Mass Ordering of Charm and Bottom Quark Energy Loss in Au+Au Collisions at RHIC,” 11 2021, arXiv:2111.14615.
- [978] S. Acharya *et al.*, “Measurement of beauty production via non-prompt  $D^0$  mesons in Pb-Pb collisions at  $\sqrt{s_{NN}} = 5.02$  TeV,” 2 2022, arXiv:2202.00815.
- [979] A. M. Sirunyan *et al.*, “Studies of Beauty Suppression via Nonprompt  $D^0$  Mesons in Pb-Pb Collisions at  $Q^2 = 4$  GeV<sup>2</sup>,” *Phys. Rev. Lett.*, vol. 123, no. 2, p. 022001, 2019, arXiv:1810.11102.
- [980] M. Aaboud *et al.*, “Measurement of the suppression and azimuthal anisotropy of muons from heavy-flavor decays in Pb+Pb collisions at  $\sqrt{s_{NN}} = 2.76$  TeV with the ATLAS detector,” *Phys. Rev. C*, vol. 98, no. 4, p. 044905, 2018, arXiv:1805.05220.
- [981] A. M. Sirunyan *et al.*, “Evidence for Top Quark Production in Nucleus-Nucleus Collisions,” *Phys. Rev. Lett.*, vol. 125, no. 22, p. 222001, 2020, arXiv:2006.11110.
- [982] S. Acharya *et al.*, “Prompt  $D^0$ ,  $D^+$ , and  $D^{*+}$  production in Pb–Pb collisions at  $\sqrt{s_{NN}} = 5.02$  TeV,” *JHEP*, vol. 01, p. 174, 2022, arXiv:2110.09420.
- [983] J. Adam *et al.*, “Observation of  $D_s^\pm/D^0$  enhancement in Au+Au collisions at  $\sqrt{s_{NN}} = 200$  GeV,” *Phys. Rev. Lett.*, vol. 127, p. 092301, 2021, arXiv:2101.11793.
- [984] S. Acharya *et al.*, “Measurement of  $D^0$ ,  $D^+$ ,  $D^{*+}$  and  $D_s^+$  production in Pb-Pb collisions at  $\sqrt{s_{NN}} = 5.02$  TeV,” *JHEP*, vol. 10, p. 174, 2018, arXiv:1804.09083.
- [985] A. M. Sirunyan *et al.*, “Measurement of  $B_s^0$  meson production in pp and PbPb collisions at  $\sqrt{s_{NN}} = 5.02$  TeV,” *Phys. Lett. B*, vol. 796, pp. 168–190, 2019, arXiv:1810.03022.
- [986] S. Acharya *et al.*, “Measurement of prompt  $D^0$ ,  $D^+$ ,  $D^{*+}$ , and  $D_s^+$  production in p–Pb collisions at  $\sqrt{s_{NN}} = 5.02$  TeV,” *JHEP*, vol. 12, p. 092, 2019, arXiv:1906.03425.
- [987] S. Acharya *et al.*, “Probing the effects of strong electromagnetic fields with charge-dependent directed flow in Pb-Pb collisions at the LHC,” *Phys. Rev. Lett.*, vol. 125, no. 2, p. 022301, 2020, arXiv:1910.14406.
- [988] L. Adamczyk *et al.*, “Measurement of  $D^0$  Azimuthal Anisotropy at Midrapidity in Au+Au Collisions at  $\sqrt{s_{NN}}=200$  GeV,” *Phys. Rev. Lett.*, vol. 118, no. 21, p. 212301, 2017, arXiv:1701.06060.
- [989] A. M. Sirunyan *et al.*, “Measurement of prompt  $D^0$  meson azimuthal anisotropy in Pb-Pb collisions at  $\sqrt{s_{NN}} = 5.02$  TeV,” *Phys. Rev. Lett.*, vol. 120, no. 20, p. 202301, 2018, arXiv:1708.03497.
- [990] T. Hachiya, “Nuclear modification factor and flow of charm and bottom quarks in Au+Au collisions at  $\sqrt{s_{NN}}=200$  GeV by the PHENIX Experiment,” *Nucl. Phys. A*, vol. 982, pp. 663–666, 2019.
- [991] M. Kelsey, “Nuclear modification factors, directed and elliptic flow of electrons from open heavy flavor decays in Au+Au collisions from STAR,” *Nucl. Phys. A*, vol. 1005, p. 121806, 2021, arXiv:2002.09057.

- [992] M. R. Lomnitz, “Measurement of  $D^0$  elliptic and triangular flow in Au+Au collisions at  $\sqrt{s_{NN}} = 200$  GeV at RHIC,” *J. Phys. Conf. Ser.*, vol. 779, no. 1, p. 012059, 2017.
- [993] N. Brambilla, M. A. Escobedo, A. Vairo, and P. Vander Griend, “Transport coefficients from in medium quarkonium dynamics,” *Phys. Rev. D*, vol. 100, no. 5, p. 054025, 2019, arXiv:1903.08063.
- [994] S. K. Das, F. Scardina, S. Plumari, and V. Greco, “Toward a solution to the  $R_{AA}$  and  $v_2$  puzzle for heavy quarks,” *Phys. Lett. B*, vol. 747, pp. 260–264, 2015, arXiv:1502.03757.
- [995] T. Song, H. Berrehrh, D. Cabrera, J. M. Torres-Rincon, L. Tolos, W. Cassing, and E. Bratkovskaya, “Tomography of the Quark-Gluon-Plasma by Charm Quarks,” *Phys. Rev. C*, vol. 92, no. 1, p. 014910, 2015, arXiv:1503.03039.
- [996] A. Andronic *et al.*, “Heavy-flavour and quarkonium production in the LHC era: from proton–proton to heavy-ion collisions,” *Eur. Phys. J. C*, vol. 76, no. 3, p. 107, 2016, arXiv:1506.03981.
- [997] W. A. Horowitz, “Fluctuating heavy quark energy loss in a strongly coupled quark-gluon plasma,” *Phys. Rev. D*, vol. 91, no. 8, p. 085019, 2015, arXiv:1501.04693.
- [998] F. Riek and R. Rapp, “Quarkonia and Heavy-Quark Relaxation Times in the Quark-Gluon Plasma,” *Phys. Rev. C*, vol. 82, p. 035201, 2010, arXiv:1005.0769.
- [999] M. Nahrgang, J. Aichelin, P. B. Gossiaux, and K. Werner, “Influence of hadronic bound states above  $T_c$  on heavy-quark observables in Pb + Pb collisions at the CERN Large Hadron Collider,” *Phys. Rev. C*, vol. 89, no. 1, p. 014905, 2014, arXiv:1305.6544.
- [1000] M. He and R. Rapp, “Hadronization and Charm-Hadron Ratios in Heavy-Ion Collisions,” *Phys. Rev. Lett.*, vol. 124, no. 4, p. 042301, 2020, arXiv:1905.09216.
- [1001] S. Li and J. Liao, “Data-driven extraction of heavy quark diffusion in quark-gluon plasma,” *Eur. Phys. J. C*, vol. 80, no. 7, p. 671, 2020, arXiv:1912.08965.
- [1002] S. Plumari, G. Coci, V. Minissale, S. K. Das, Y. Sun, and V. Greco, “Heavy - light flavor correlations of anisotropic flows at LHC energies within event-by-event transport approach,” *Phys. Lett. B*, vol. 805, p. 135460, 2020, arXiv:1912.09350.
- [1003] Y. Zhong, C.-B. Yang, X. Cai, and S.-Q. Feng, “A systematic study of magnetic field in Relativistic Heavy-ion Collisions in the RHIC and LHC energy regions,” *Adv. High Energy Phys.*, vol. 2014, p. 193039, 2014, arXiv:1408.5694.
- [1004] J. Adam *et al.*, “First Observation of the Directed Flow of  $D^0$  and  $\overline{D^0}$  in Au+Au Collisions at  $\sqrt{s_{NN}} = 200$  GeV,” *Phys. Rev. Lett.*, vol. 123, no. 16, p. 162301, 2019, arXiv:1905.02052.
- [1005] M. Gell-Mann, “A Schematic Model of Baryons and Mesons,” *Phys. Lett.*, vol. 8, pp. 214–215, 1964.
- [1006] G. Zweig, “An SU(3) model for strong interaction symmetry and its breaking. Version 1,” 1 1964.
- [1007] P. Koppenburg, “List of hadrons observed at the LHC.” LHCb-FIGURE-2021-001, Mar 2021. See 2022 update online.
- [1008] “New particles discovered at the LHC.” <https://www.nikhef.nl/~pkoppenb/particles.html>.
- [1009] S. Cho *et al.*, “Multi-quark hadrons from Heavy Ion Collisions,” *Phys. Rev. Lett.*, vol. 106, p. 212001, 2011, arXiv:1011.0852.
- [1010] A. M. Sirunyan *et al.*, “Evidence for X(3872) in Pb-Pb Collisions and Studies of its Prompt Production at  $\sqrt{s_{NN}}=5.02$  TeV,” *Phys. Rev. Lett.*, vol. 128, no. 3, p. 032001, 2022, arXiv:2102.13048.
- [1011] H. Zhang, J. Liao, E. Wang, Q. Wang, and H. Xing, “Deciphering the Nature of X(3872) in Heavy Ion Collisions,” *Phys. Rev. Lett.*, vol. 126, no. 1, p. 012301, 2021, arXiv:2004.00024.
- [1012] B. Wu, X. Du, M. Sibila, and R. Rapp, “X(3872)transport in heavy-ion collisions,” *Eur. Phys. J. A*, vol. 57, no. 4, p. 122, 2021, arXiv:2006.09945. [Erratum: *Eur.Phys.J.A* 57, 314 (2021)].

- [1013] LHCb Collaboration, “Modification of  $\chi_{c1}(3872)$  and  $\psi(2S)$  production in  $p$ Pb collisions at  $\sqrt{s_{NN}} = 8.16$  TeV, LHCb-CONF-2022-001,”
- [1014] A. Esposito, E. G. Ferreiro, A. Pilloni, A. D. Polosa, and C. A. Salgado, “The nature of  $X(3872)$  from high-multiplicity pp collisions,” *Eur. Phys. J. C*, vol. 81, no. 7, p. 669, 2021, arXiv:2006.15044.
- [1015] E. Braaten, L.-P. He, K. Ingles, and J. Jiang, “Production of  $X(3872)$  at High Multiplicity,” *Phys. Rev. D*, vol. 103, no. 7, p. L071901, 2021, arXiv:2012.13499.
- [1016] K. Kovarik *et al.*, “nCTEQ15 - Global analysis of nuclear parton distributions with uncertainties in the CTEQ framework,” *Phys. Rev. D*, vol. 93, no. 8, p. 085037, 2016, arXiv:1509.00792.
- [1017] K. J. Eskola, P. Paakkinen, H. Paukkuinen, and C. A. Salgado, “EPPS21: a global QCD analysis of nuclear PDFs,” *Eur. Phys. J. C*, vol. 82, no. 5, p. 413, 2022, arXiv:2112.12462.
- [1018] R. Abdul Khalek, R. Gauld, T. Giani, E. R. Nocera, T. R. Rabemananjara, and J. Rojo, “nNNPDF3.0: evidence for a modified partonic structure in heavy nuclei,” *Eur. Phys. J. C*, vol. 82, no. 6, p. 507, 2022, arXiv:2201.12363.
- [1019] A. Kusina, F. Lyonnet, D. B. Clark, E. Godat, T. Jezo, K. Kovarik, F. I. Oless, I. Schienbein, and J. Y. Yu, “Vector boson production in pPb and PbPb collisions at the LHC and its impact on nCTEQ15 PDFs,” *Eur. Phys. J. C*, vol. 77, no. 7, p. 488, 2017, arXiv:1610.02925.
- [1020] A. Kusina *et al.*, “Impact of LHC vector boson production in heavy ion collisions on strange PDFs,” *Eur. Phys. J. C*, vol. 80, no. 10, p. 968, 2020, arXiv:2007.09100.
- [1021] X. Chen, T. Gehrmann, E. W. N. Glover, M. Höfer, A. Huss, and R. Schürmann, “Single photon production at hadron colliders at NNLO QCD with realistic photon isolation,” *JHEP*, vol. 08, p. 094, 2022, arXiv:2205.01516.
- [1022] A. M. Sirunyan *et al.*, “The production of isolated photons in PbPb and pp collisions at  $\sqrt{s_{NN}} = 5.02$  TeV,” *JHEP*, vol. 07, p. 116, 2020, arXiv:2003.12797.
- [1023] M. Aaboud *et al.*, “Measurement of prompt photon production in  $\sqrt{s_{NN}} = 8.16$  TeV  $p$ +Pb collisions with ATLAS,” *Phys. Lett. B*, vol. 796, pp. 230–252, 2019, arXiv:1903.02209.
- [1024] G. Aad *et al.*, “Centrality, rapidity and transverse momentum dependence of isolated prompt photon production in lead-lead collisions at  $\sqrt{s_{NN}} = 2.76$  TeV measured with the ATLAS detector,” *Phys. Rev. C*, vol. 93, no. 3, p. 034914, 2016, arXiv:1506.08552.
- [1025] G. Aad *et al.*, “ $Z$  boson production in  $p$ +Pb collisions at  $\sqrt{s_{NN}} = 5.02$  TeV measured with the ATLAS detector,” *Phys. Rev. C*, vol. 92, no. 4, p. 044915, 2015, arXiv:1507.06232.
- [1026] A. M. Sirunyan *et al.*, “Study of Drell-Yan dimuon production in proton-lead collisions at  $\sqrt{s_{NN}} = 8.16$  TeV,” *JHEP*, vol. 05, p. 182, 2021, arXiv:2102.13648.
- [1027] L. Collaboration, “Measurement of the  $Z$  boson production cross-section in proton-lead collisions at  $\sqrt{s_{NN}} = 8.16$  TeV,” 5 2022, arXiv:2205.10213.
- [1028] S. Acharya *et al.*, “ $Z$ -boson production in p-Pb collisions at  $\sqrt{s_{NN}} = 8.16$  TeV and Pb-Pb collisions at  $\sqrt{s_{NN}} = 5.02$  TeV,” *JHEP*, vol. 09, p. 076, 2020, arXiv:2005.11126.
- [1029] A. M. Sirunyan *et al.*, “Observation of nuclear modifications in  $W^{\pm}$  boson production in pPb collisions at  $\sqrt{s_{NN}} = 8.16$  TeV,” *Phys. Lett. B*, vol. 800, p. 135048, 2020, arXiv:1905.01486.
- [1030] A. M. Sirunyan *et al.*, “Constraints on the Initial State of Pb-Pb Collisions via Measurements of  $Z$ -Boson Yields and Azimuthal Anisotropy at  $\sqrt{s_{NN}}=5.02$  TeV,” *Phys. Rev. Lett.*, vol. 127, no. 10, p. 102002, 2021, arXiv:2103.14089.
- [1031] G. Aad *et al.*, “ $Z$  boson production in Pb+Pb collisions at  $\sqrt{s_{NN}}=5.02$  TeV measured by the ATLAS experiment,” *Phys. Lett. B*, vol. 802, p. 135262, 2020, arXiv:1910.13396.
- [1032] G. Aad *et al.*, “Measurement of  $W^{\pm}$  boson production in Pb+Pb collisions at  $\sqrt{s_{NN}} = 5.02$  TeV with the ATLAS detector,” *Eur. Phys. J. C*, vol. 79, no. 11, p. 935, 2019, arXiv:1907.10414.

- [1033] ALICE Collaboration, “ $W^\pm$ -boson production in p–Pb collisions at  $\sqrt{s_{NN}} = 8.16$  TeV and PbPb collisions at  $\sqrt{s_{NN}} = 5.02$  TeV,” 4 2022, arXiv:2204.10640.
- [1034] D. d’Enterria and C. Loizides, “Progress in the Glauber Model at Collider Energies,” *Ann. Rev. Nucl. Part. Sci.*, vol. 71, pp. 315–344, 2021, arXiv:2011.14909.
- [1035] S. Acharya *et al.*, “Analysis of the apparent nuclear modification in peripheral Pb–Pb collisions at 5.02 TeV,” *Phys. Lett. B*, vol. 793, pp. 420–432, 2019, arXiv:1805.05212.
- [1036] C. Loizides and A. Morsch, “Absence of jet quenching in peripheral nucleus–nucleus collisions,” *Phys. Lett. B*, vol. 773, pp. 408–411, 2017, arXiv:1705.08856.
- [1037] K. J. Eskola, I. Helenius, M. Kuha, and H. Paukkunen, “Shadowing in inelastic nucleon-nucleon cross section?,” *Phys. Rev. Lett.*, vol. 125, no. 21, p. 212301, 2020, arXiv:2003.11856.
- [1038] F. Jonas and C. Loizides, “Centrality dependence of electroweak boson production in PbPb collisions at the CERN Large Hadron Collider,” *Phys. Rev. C*, vol. 104, no. 4, p. 044905, 2021, arXiv:2104.14903.
- [1039] J. Adam *et al.*, “Centrality dependence of particle production in p–Pb collisions at  $\sqrt{s_{NN}} = 5.02$  TeV,” *Phys. Rev. C*, vol. 91, no. 6, p. 064905, 2015, arXiv:1412.6828.
- [1040] D. V. Perepelitsa and P. A. Steinberg, “Calculation of centrality bias factors in  $p+A$  collisions based on a positive correlation of hard process yields with underlying event activity,” 12 2014, arXiv:1412.0976.
- [1041] M. Alvioli, B. A. Cole, L. Frankfurt, D. V. Perepelitsa, and M. Strikman, “Evidence for  $x$ -dependent proton color fluctuations in  $pA$  collisions at the CERN Large Hadron Collider,” *Phys. Rev. C*, vol. 93, no. 1, p. 011902, 2016, arXiv:1409.7381.
- [1042] M. Alvioli, L. Frankfurt, D. Perepelitsa, and M. Strikman, “Global analysis of color fluctuation effects in proton– and deuteron–nucleus collisions at RHIC and the LHC,” *Phys. Rev. D*, vol. 98, no. 7, p. 071502, 2018, arXiv:1709.04993.
- [1043] A. Bzdak, V. Skokov, and S. Bathe, “Centrality dependence of high energy jets in  $p+Pb$  collisions at energies available at the CERN Large Hadron Collider,” *Phys. Rev. C*, vol. 93, no. 4, p. 044901, 2016, arXiv:1408.3156.
- [1044] M. Kordell and A. Majumder, “Jets in  $d(p)$ -A Collisions: Color Transparency or Energy Conservation,” *Phys. Rev. C*, vol. 97, no. 5, p. 054904, 2018, arXiv:1601.02595.
- [1045] C. Loizides, “Glauber modeling of high-energy nuclear collisions at the subnucleon level,” *Phys. Rev. C*, vol. 94, no. 2, p. 024914, 2016, arXiv:1603.07375.
- [1046] G. Aad *et al.*, “Measurement of the centrality dependence of the charged-particle pseudorapidity distribution in proton–lead collisions at  $\sqrt{s_{NN}} = 5.02$  TeV with the ATLAS detector,” *Eur. Phys. J. C*, vol. 76, no. 4, p. 199, 2016, arXiv:1508.00848.
- [1047] A. M. Sirunyan *et al.*, “Observation of top quark production in proton-nucleus collisions,” *Phys. Rev. Lett.*, vol. 119, no. 24, p. 242001, 2017, arXiv:1709.07411.
- [1048] L. Apolinário, J. G. Milhano, G. P. Salam, and C. A. Salgado, “Probing the time structure of the quark-gluon plasma with top quarks,” *Phys. Rev. Lett.*, vol. 120, no. 23, p. 232301, 2018, arXiv:1711.03105.
- [1049] C. A. Bertulani, S. R. Klein, and J. Nystrand, “Physics of ultra-peripheral nuclear collisions,” *Ann. Rev. Nucl. Part. Sci.*, vol. 55, pp. 271–310, 2005, arXiv:nucl-ex/0502005.
- [1050] J. G. Contreras and J. D. Tapia Takaki, “Ultra-peripheral heavy-ion collisions at the LHC,” *Int. J. Mod. Phys. A*, vol. 30, p. 1542012, 2015.
- [1051] S. Klein and J. Nystrand, “Ultraperipheral nuclear collisions,” *Phys. Today*, vol. 70, no. 10, pp. 40–47, 2017.



- [1052] S. R. Klein and H. Mäntysaari, “Imaging the nucleus with high-energy photons,” *Nature Rev. Phys.*, vol. 1, no. 11, pp. 662–674, 2019, arXiv:1910.10858.
- [1053] S. Klein and P. Steinberg, “Photonuclear and Two-photon Interactions at High-Energy Nuclear Colliders,” *Ann. Rev. Nucl. Part. Sci.*, vol. 70, pp. 323–354, 2020, arXiv:2005.01872.
- [1054] Z. Citron *et al.*, “Report from Working Group 5: Future physics opportunities for high-density QCD at the LHC with heavy-ion and proton beams,” *CERN Yellow Rep. Monogr.*, vol. 7, pp. 1159–1410, 2019, arXiv:1812.06772.
- [1055] S. Klein *et al.*, “New opportunities at the photon energy frontier,” 9 2020, arXiv:2009.03838.
- [1056] M. Hentschinski *et al.*, “White Paper on Forward Physics, BFKL, Saturation Physics and Diffraction,” 3 2022, arXiv:2203.08129.
- [1057] K. J. Eskola, C. A. Flett, V. Guzey, T. Löytäinen, and H. Paukkunen, “Next-to-leading order perturbative QCD predictions for exclusive  $J/\psi$  photoproduction in oxygen-oxygen and lead-lead collisions at the LHC,” 10 2022, arXiv:2210.16048.
- [1058] L. Adamczyk *et al.*, “Coherent diffractive photoproduction of  $\rho^0$  mesons on gold nuclei at 200 GeV/nucleon-pair at the Relativistic Heavy Ion Collider,” *Phys. Rev. C*, vol. 96, no. 5, p. 054904, 2017, arXiv:1702.07705.
- [1059] S. Acharya *et al.*, “Coherent  $J/\psi$  and  $\psi'$  photoproduction at midrapidity in ultra-peripheral Pb-Pb collisions at  $\sqrt{s_{NN}} = 5.02$  TeV,” *Eur. Phys. J. C*, vol. 81, no. 8, p. 712, 2021, arXiv:2101.04577.
- [1060] R. Aaij *et al.*, “Study of coherent  $J/\psi$  production in lead-lead collisions at  $\sqrt{s_{NN}} = 5$  TeV,” *JHEP*, vol. 07, p. 117, 2022, arXiv:2107.03223.
- [1061] LHCb Collaboration, “Study of coherent charmonium production in ultra-peripheral lead-lead collisions,” 6 2022, arXiv:2206.08221.
- [1062] V. Khachatryan *et al.*, “Coherent  $J/\psi$  photoproduction in ultra-peripheral PbPb collisions at  $\sqrt{s_{NN}} = 2.76$  TeV with the CMS experiment,” *Phys. Lett. B*, vol. 772, pp. 489–511, 2017, arXiv:1605.06966.
- [1063] A. Accardi *et al.*, “Electron Ion Collider: The Next QCD Frontier: Understanding the glue that binds us all,” *Eur. Phys. J. A*, vol. 52, no. 9, p. 268, 2016, arXiv:1212.1701.
- [1064] S. Acharya *et al.*, “First measurement of the  $|\eta|$ -dependence of coherent  $J/\psi$  photonuclear production,” *Phys. Lett. B*, vol. 817, p. 136280, 2021, arXiv:2101.04623.
- [1065] A. M. Sirunyan *et al.*, “Measurement of exclusive  $\Upsilon$  photoproduction from protons in pPb collisions at  $\sqrt{s_{NN}} = 5.02$  TeV,” *Eur. Phys. J. C*, vol. 79, no. 3, p. 277, 2019, arXiv:1809.11080. [Erratum: *Eur.Phys.J.C* 82, 343 (2022)].
- [1066] M. Abdallah *et al.*, “Probing the Gluonic Structure of the Deuteron with  $J/\psi$  Photoproduction in d+Au Ultraperipheral Collisions,” *Phys. Rev. Lett.*, vol. 128, no. 12, p. 122303, 2022, arXiv:2109.07625.
- [1067] B. B. Abelev *et al.*, “Exclusive  $J/\psi$  photoproduction off protons in ultra-peripheral p-Pb collisions at  $\sqrt{s_{NN}} = 5.02$  TeV,” *Phys. Rev. Lett.*, vol. 113, no. 23, p. 232504, 2014, arXiv:1406.7819.
- [1068] S. Acharya *et al.*, “Energy dependence of exclusive  $J/\psi$  photoproduction off protons in ultra-peripheral p–Pb collisions at  $\sqrt{s_{NN}} = 5.02$  TeV,” *Eur. Phys. J. C*, vol. 79, no. 5, p. 402, 2019, arXiv:1809.03235.
- [1069] V. Guzey, E. Kryshen, M. Strikman, and M. Zhalov, “Comments on  $J/\psi$  photoproduction in d+Au UPCs at RHIC,” 6 2022, arXiv:2206.12120.
- [1070] Z. Tu, A. Jentsch, M. Baker, L. Zheng, J.-H. Lee, R. Venugopalan, O. Hen, D. Higinbotham, E.-C. Aschenauer, and T. Ullrich, “Probing short-range correlations in the deuteron via incoherent diffractive  $J/\psi$  production with spectator tagging at the EIC,” *Phys. Lett. B*, vol. 811, p. 135877,

- 2020, arXiv:2005.14706.
- [1071] A. Jentsch, Z. Tu, and C. Weiss, “Deep-inelastic electron-deuteron scattering with spectator nucleon tagging at the future Electron Ion Collider: Extracting free nucleon structure,” *Phys. Rev. C*, vol. 104, no. 6, p. 065205, 2021, arXiv:2108.08314.
  - [1072] J. Adam *et al.*, “Observation of excess  $J/\psi$  yield at very low transverse momenta in Au+Au collisions at  $\sqrt{s_{NN}} = 200$  GeV and U+U collisions at  $\sqrt{s_{NN}} = 193$  GeV,” *Phys. Rev. Lett.*, vol. 123, no. 13, p. 132302, 2019, arXiv:1904.11658.
  - [1073] J. Adam *et al.*, “Measurement of an excess in the yield of  $J/\psi$  at very low  $p_T$  in Pb-Pb collisions at  $\sqrt{s_{NN}} = 2.76$  TeV,” *Phys. Rev. Lett.*, vol. 116, no. 22, p. 222301, 2016, arXiv:1509.08802.
  - [1074] W. Zha, S. R. Klein, R. Ma, L. Ruan, T. Todoroki, Z. Tang, Z. Xu, C. Yang, Q. Yang, and S. Yang, “Coherent  $J/\psi$  photoproduction in hadronic heavy-ion collisions,” *Phys. Rev. C*, vol. 97, no. 4, p. 044910, 2018, arXiv:1705.01460.
  - [1075] M. Klusek-Gawenda and A. Szczurek, “Photoproduction of  $J/\psi$  mesons in peripheral and semi-central heavy ion collisions,” *Phys. Rev. C*, vol. 93, no. 4, p. 044912, 2016, arXiv:1509.03173.
  - [1076] W. Zha, L. Ruan, Z. Tang, Z. Xu, and S. Yang, “Double-slit experiment at fermi scale: coherent photoproduction in heavy-ion collisions,” *Phys. Rev. C*, vol. 99, no. 6, p. 061901, 2019, arXiv:1810.10694.
  - [1077] W. Zha, L. Ruan, Z. Tang, Z. Xu, and S. Yang, “Coherent photo-produced  $J/\psi$  and dielectron yields in isobaric collisions,” *Phys. Lett. B*, vol. 789, pp. 238–242, 2019, arXiv:1810.02064.
  - [1078] ALICE Collaboration, “Photoproduction of low- $p_T$   $J/\psi$  from peripheral to central Pb–Pb collisions at 5.02 TeV,” 4 2022, arXiv:2204.10684.
  - [1079] Z. Li, “Very low- $p_T$  di-muon production in peripheral Au+Au collision at  $\sqrt{s_{NN}} = 200$  GeV at STAR,” *PoS*, vol. ICHEP2022, p. 498, 11 2022.
  - [1080] ATLAS Collaboration, “Exclusive dielectron production in ultraperipheral Pb+Pb collisions at  $\sqrt{s_{NN}} = 5.02$  TeV with ATLAS,” 7 2022, arXiv:2207.12781.
  - [1081] J. Adam *et al.*, “Low- $p_T$   $e^+e^-$  pair production in Au+Au collisions at  $\sqrt{s_{NN}} = 200$  GeV and U+U collisions at  $\sqrt{s_{NN}} = 193$  GeV at STAR,” *Phys. Rev. Lett.*, vol. 121, no. 13, p. 132301, 2018, arXiv:1806.02295.
  - [1082] M. Aaboud *et al.*, “Observation of centrality-dependent acoplanarity for muon pairs produced via two-photon scattering in Pb+Pb collisions at  $\sqrt{s_{NN}} = 5.02$  TeV with the ATLAS detector,” *Phys. Rev. Lett.*, vol. 121, no. 21, p. 212301, 2018, arXiv:1806.08708.
  - [1083] S. Klein, A. H. Mueller, B.-W. Xiao, and F. Yuan, “Acoplanarity of a Lepton Pair to Probe the Electromagnetic Property of Quark Matter,” *Phys. Rev. Lett.*, vol. 122, no. 13, p. 132301, 2019, arXiv:1811.05519.
  - [1084] S. Klein, A. H. Mueller, B.-W. Xiao, and F. Yuan, “Lepton Pair Production Through Two Photon Process in Heavy Ion Collisions,” *Phys. Rev. D*, vol. 102, no. 9, p. 094013, 2020, arXiv:2003.02947.
  - [1085] J. Adam *et al.*, “Measurement of  $e^+e^-$  Momentum and Angular Distributions from Linearly Polarized Photon Collisions,” *Phys. Rev. Lett.*, vol. 127, no. 5, p. 052302, 2021, arXiv:1910.12400.
  - [1086] A. M. Sirunyan *et al.*, “Observation of Forward Neutron Multiplicity Dependence of Dimuon Acoplanarity in Ultraperipheral Pb-Pb Collisions at  $\sqrt{s_{NN}}=5.02$  TeV,” *Phys. Rev. Lett.*, vol. 127, no. 12, p. 122001, 2021, arXiv:2011.05239.
  - [1087] W. Zha, J. D. Brandenburg, Z. Tang, and Z. Xu, “Initial transverse-momentum broadening of Breit-Wheeler process in relativistic heavy-ion collisions,” *Phys. Lett. B*, vol. 800, p. 135089, 2020, arXiv:1812.02820.
  - [1088] M. Vidovic, M. Greiner, C. Best, and G. Soff, “Impact parameter dependence of the electromagnetic

- particle production in ultrarelativistic heavy ion collisions,” *Phys. Rev. C*, vol. 47, pp. 2308–2319, 1993.
- [1089] ATLAS Collaboration, “Measurement of muon pairs produced via  $\gamma\gamma$  scattering in non-ultraperipheral Pb+Pb collisions at  $\sqrt{s_{\text{NN}}} = 5.02$  TeV with the ATLAS detector,” 6 2022, arXiv:2206.12594.
- [1090] X. Wang, J. D. Brandenburg, L. Ruan, F. Shao, Z. Xu, C. Yang, and W. Zha, “Energy Dependence of the Breit-Wheeler process in Heavy-Ion Collisions and its Application to Nuclear Charge Radius Measurements,” 7 2022, arXiv:2207.05595.
- [1091] C. Li, J. Zhou, and Y.-J. Zhou, “Impact parameter dependence of the azimuthal asymmetry in lepton pair production in heavy ion collisions,” *Phys. Rev. D*, vol. 101, no. 3, p. 034015, 2020, arXiv:1911.00237.
- [1092] F. del Aguila, F. Cornet, and J. I. Illana, “The possibility of using a large heavy-ion collider for measuring the electromagnetic properties of the tau lepton,” *Phys. Lett. B*, vol. 271, pp. 256–260, 1991.
- [1093] L. Beresford and J. Liu, “New physics and tau  $g - 2$  using LHC heavy ion collisions,” *Phys. Rev. D*, vol. 102, no. 11, p. 113008, 2020, arXiv:1908.05180. [Erratum: *Phys.Rev.D* 106, 039902 (2022)].
- [1094] M. Dyndal, M. Klusek-Gawenda, M. Schott, and A. Szczurek, “Anomalous electromagnetic moments of  $\tau$  lepton in  $\gamma\gamma \rightarrow \tau^+\tau^-$  reaction in Pb+Pb collisions at the LHC,” *Phys. Lett. B*, vol. 809, p. 135682, 2020, arXiv:2002.05503.
- [1095] ATLAS Collaboration, “Observation of the  $\gamma\gamma \rightarrow \tau\tau$  process in Pb+Pb collisions and constraints on the  $\tau$ -lepton anomalous magnetic moment with the ATLAS detector,” 4 2022, arXiv:2204.13478.
- [1096] CMS Collaboration, “Observation of  $\tau$  lepton pair production in ultraperipheral lead-lead collisions at  $\sqrt{s_{\text{NN}}} = 5.02$  TeV,” 6 2022, arXiv:2206.05192.
- [1097] J. Abdallah *et al.*, “Study of tau-pair production in photon-photon collisions at LEP and limits on the anomalous electromagnetic moments of the tau lepton,” *Eur. Phys. J. C*, vol. 35, pp. 159–170, 2004, arXiv:hep-ex/0406010.
- [1098] M. Aaboud *et al.*, “Evidence for light-by-light scattering in heavy-ion collisions with the ATLAS detector at the LHC,” *Nature Phys.*, vol. 13, no. 9, pp. 852–858, 2017, arXiv:1702.01625.
- [1099] G. Aad *et al.*, “Observation of light-by-light scattering in ultraperipheral Pb+Pb collisions with the ATLAS detector,” *Phys. Rev. Lett.*, vol. 123, no. 5, p. 052001, 2019, arXiv:1904.03536.
- [1100] A. M. Sirunyan *et al.*, “Evidence for light-by-light scattering and searches for axion-like particles in ultraperipheral PbPb collisions at  $\sqrt{s_{\text{NN}}} = 5.02$  TeV,” *Phys. Lett. B*, vol. 797, p. 134826, 2019, arXiv:1810.04602.
- [1101] G. Aad *et al.*, “Measurement of light-by-light scattering and search for axion-like particles with 2.2  $\text{nb}^{-1}$  of Pb+Pb data with the ATLAS detector,” *JHEP*, vol. 03, p. 243, 2021, arXiv:2008.05355. [Erratum: *JHEP* 11, 050 (2021)].
- [1102] S. R. Klein and J. Nystrand, “Interference in exclusive vector meson production in heavy ion collisions,” *Phys. Rev. Lett.*, vol. 84, pp. 2330–2333, 2000, arXiv:hep-ph/9909237.
- [1103] A. J. Baltz, Y. Gorbunov, S. R. Klein, and J. Nystrand, “Two-Photon Interactions with Nuclear Breakup in Relativistic Heavy Ion Collisions,” *Phys. Rev. C*, vol. 80, p. 044902, 2009, arXiv:0907.1214.
- [1104] A. Einstein, B. Podolsky, and N. Rosen, “Can quantum mechanical description of physical reality be considered complete?,” *Phys. Rev.*, vol. 47, pp. 777–780, 1935.
- [1105] B. I. Abelev *et al.*, “Observation of Two-source Interference in the Photoproduction Reaction  $\text{Au Au} \rightarrow \text{Au Au rho}^0$ ,” *Phys. Rev. Lett.*, vol. 102, p. 112301, 2009, arXiv:0812.1063.

- [1106] S. Klein and J. Nystrand, “Exclusive vector meson production in relativistic heavy ion collisions,” *Phys. Rev. C*, vol. 60, p. 014903, 1999, arXiv:hep-ph/9902259.
- [1107] M. Klusek-Gawenda and A. Szczurek, “Double-scattering mechanism in the exclusive  $AA \rightarrow AA\rho^0\rho^0$  reaction in ultrarelativistic collisions,” *Phys. Rev. C*, vol. 89, no. 2, p. 024912, 2014, arXiv:1309.2463.
- [1108] G. Baur, K. Hencken, A. Aste, D. Trautmann, and S. R. Klein, “Multiphoton exchange processes in ultraperipheral relativistic heavy ion collisions,” *Nucl. Phys. A*, vol. 729, pp. 787–808, 2003, arXiv:nucl-th/0307031.
- [1109] A. Adeluyi and C. Bertulani, “Gluon distributions in nuclei probed at the CERN Large Hadron Collider,” *Phys. Rev. C*, vol. 84, p. 024916, 2011, arXiv:1104.4287.
- [1110] K. J. Eskola, C. A. Flett, V. Guzey, T. Löytäinen, and H. Paukkunen, “Exclusive  $J/\psi$  photoproduction in ultraperipheral Pb+Pb collisions at the CERN Large Hadron Collider calculated at next-to-leading order perturbative QCD,” *Phys. Rev. C*, vol. 106, no. 3, p. 035202, 2022, arXiv:2203.11613.
- [1111] ATLAS Collaboration, “Photo-nuclear jet production in ultra-peripheral Pb+Pb collisions at  $\sqrt{s_{NN}} = 5.02$  TeV with the ATLAS detector,” 2022.
- [1112] Y. Hatta, B.-W. Xiao, and F. Yuan, “Probing the Small- $x$  Gluon Tomography in Correlated Hard Diffractive Dijet Production in Deep Inelastic Scattering,” *Phys. Rev. Lett.*, vol. 116, no. 20, p. 202301, 2016, arXiv:1601.01585.
- [1113] V. Guzey and M. Klasen, “Diffractive dijet photoproduction in ultraperipheral collisions at the LHC in next-to-leading order QCD,” *JHEP*, vol. 04, p. 158, 2016, arXiv:1603.06055.
- [1114] A. Dumitru, V. Skokov, and T. Ullrich, “Measuring the Weizsäcker-Williams distribution of linearly polarized gluons at an electron-ion collider through dijet azimuthal asymmetries,” *Phys. Rev. C*, vol. 99, no. 1, p. 015204, 2019, arXiv:1809.02615.
- [1115] H. Mäntysaari, N. Mueller, and B. Schenke, “Diffractive Dijet Production and Wigner Distributions from the Color Glass Condensate,” *Phys. Rev. D*, vol. 99, no. 7, p. 074004, 2019, arXiv:1902.05087.
- [1116] CMS Collaboration, “Azimuthal correlations within exclusive dijets with large momentum transfer in photon-lead collisions,” 4 2022, arXiv:2205.00045.
- [1117] H. Jung, “Hard diffractive scattering in high-energy  $e p$  collisions and the Monte Carlo generator RAPGAP,” *Comput. Phys. Commun.*, vol. 86, pp. 147–161, 1995.
- [1118] Y. Hatta, B.-W. Xiao, F. Yuan, and J. Zhou, “Anisotropy in Dijet Production in Exclusive and Inclusive Processes,” *Phys. Rev. Lett.*, vol. 126, no. 14, p. 142001, 2021, arXiv:2010.10774.
- [1119] M. Abdallah *et al.*, “Tomography of ultrarelativistic nuclei with polarized photon-gluon collisions,” *Sci. Adv.*, vol. 9, no. 1, p. eabq3903, 2023, arXiv:2204.01625.
- [1120] ALICE Collaboration, “Letter of Intent: A Forward Calorimeter (FoCal) in the ALICE experiment,” 6 2020.
- [1121] S. R. Klein, J. Nystrand, and R. Vogt, “Heavy quark photoproduction in ultraperipheral heavy ion collisions,” *Phys. Rev. C*, vol. 66, p. 044906, 2002, arXiv:hep-ph/0206220.
- [1122] S. R. Klein, J. Nystrand, and R. Vogt, “Photoproduction of top in peripheral heavy ion collisions,” *Eur. Phys. J. C*, vol. 21, pp. 563–566, 2001, arXiv:hep-ph/0005157.
- [1123] V. P. Goncalves and M. V. T. Machado, “Diffractive photoproduction of heavy quarks in hadronic collisions,” *Phys. Rev. D*, vol. 75, p. 031502, 2007, arXiv:hep-ph/0612265.
- [1124] V. P. Gonçalves, G. Sampaio dos Santos, and C. R. Sena, “Inclusive heavy quark photoproduction in  $pp$ ,  $pPb$  and  $PbPb$  collisions at Run 2 LHC energies,” *Nucl. Phys. A*, vol. 976, pp. 33–45, 2018, arXiv:1711.04497.
- [1125] E. Huayra, E. G. De Oliveira, and R. Pasechnik, “Probing double parton scattering via associated

- open charm and bottom production in ultraperipheral  $pA$  collisions,” *Eur. Phys. J. C*, vol. 79, no. 10, p. 880, 2019, arXiv:1905.03294.
- [1126] J. Albrecht *et al.*, “The Muon Puzzle in cosmic-ray induced air showers and its connection to the Large Hadron Collider,” *Astrophys. Space Sci.*, vol. 367, no. 3, p. 27, 2022, arXiv:2105.06148.
- [1127] J. a. Barata and C. A. Salgado, “A quantum strategy to compute the jet quenching parameter  $\hat{q}$ ,” *Eur. Phys. J. C*, vol. 81, no. 10, p. 862, 2021, arXiv:2104.04661.
- [1128] W. A. de Jong, K. Lee, J. Mulligan, M. Płoskoń, F. Ringer, and X. Yao, “Quantum simulation of nonequilibrium dynamics and thermalization in the Schwinger model,” *Phys. Rev. D*, vol. 106, no. 5, p. 054508, 2022, arXiv:2106.08394.
- [1129] J. a. Barata, X. Du, M. Li, W. Qian, and C. A. Salgado, “Medium induced jet broadening in a quantum computer,” *Phys. Rev. D*, vol. 106, no. 7, p. 074013, 2022, arXiv:2208.06750.
- [1130] W. A. De Jong, M. Metcalf, J. Mulligan, M. Płoskoń, F. Ringer, and X. Yao, “Quantum simulation of open quantum systems in heavy-ion collisions,” *Phys. Rev. D*, vol. 104, no. 5, p. 051501, 2021, arXiv:2010.03571.
- [1131] L. Adamczyk *et al.*, “Measurement of Interaction between Antiprotons,” *Nature*, vol. 527, pp. 345–348, 2015, arXiv:1507.07158.
- [1132] J. Adam *et al.*, “Measurement of the mass difference and the binding energy of the hypertriton and antihypertriton,” *Nature Phys.*, vol. 16, no. 4, pp. 409–412, 2020, arXiv:1904.10520.
- [1133] J. Chen, D. Keane, Y.-G. Ma, A. Tang, and Z. Xu, “Antinuclei in Heavy-Ion Collisions,” *Phys. Rept.*, vol. 760, pp. 1–39, 2018, arXiv:1808.09619.
- [1134] J. Adam *et al.*, “Coherent  $\rho^0$  photoproduction in ultra-peripheral Pb-Pb collisions at  $\sqrt{s_{NN}} = 2.76$  TeV,” *JHEP*, vol. 09, p. 095, 2015, arXiv:1503.09177.
- [1135] J.-B. Wei, G. F. Burgio, A. R. Raduta, and H. J. Schulze, “Hot neutron stars and their equation of state,” *Phys. Rev. C*, vol. 104, no. 6, p. 065806, 2021, arXiv:2112.05323.
- [1136] A. Prakash, D. Radice, D. Logoteta, A. Perego, V. Nedora, I. Bombaci, R. Kashyap, S. Bernuzzi, and A. Endrizzi, “Signatures of deconfined quark phases in binary neutron star mergers,” *Phys. Rev. D*, vol. 104, no. 8, p. 083029, 2021, arXiv:2106.07885.
- [1137] Y. Fujimoto, K. Fukushima, K. Hotokezaka, and K. Kyutoku, “Gravitational Wave Signal for Quark Matter with Realistic Phase Transition,” 5 2022, arXiv:2205.03882.
- [1138] F. Di Clemente, A. Drago, and G. Pagliara, “Merger of a Neutron Star with a Black Hole: One-family versus Two-families Scenario,” *Astrophys. J.*, vol. 929, no. 1, p. 44, 2022, arXiv:2106.16151.
- [1139] K. W. Wong and M. C. Chu, “Cooling of a new born compact star with QCD phase transition,” *Phys. Rev. D*, vol. 70, p. 063004, 2004, arXiv:astro-ph/0405601.
- [1140] R. Negreiros, V. A. Dexheimer, and S. Schramm, “Quark core impact on hybrid star cooling,” *Phys. Rev. C*, vol. 85, p. 035805, 2012, arXiv:1011.2233.
- [1141] A. Sedrakian, “Cooling compact stars and phase transitions in dense QCD,” *Eur. Phys. J. A*, vol. 52, p. 44, 2016, arXiv:1509.06986.
- [1142] J. B. Wei, G. F. Burgio, H. J. Schulze, and D. Zappalà, “Cooling of hybrid neutron stars with microscopic equations of state,” *Mon. Not. Roy. Astron. Soc.*, vol. 498, no. 1, pp. 344–354, 2020, arXiv:2003.08079.
- [1143] F. Xiao, C.-M. Pi, S.-H. Yang, A.-Z. Zhou, and X.-P. Zheng, “First-order phase transitions in rotating hybrid stars and pulsar glitches,” *Research in Astronomy and Astrophysics*, vol. 11, pp. 679–686, June 2011.
- [1144] J. Singha, S. M. Vaneshwar, and A. Kumar, “Constraining the Parameterized Neutron Star Equation of State with Astronomical Observations,” *Res. Astron. Astrophys.*, vol. 22, no. 5, p. 055001, 2022,

- arXiv:2203.14722.
- [1145] M. Pitkin, “Prospects of observing continuous gravitational waves from known pulsars,” *Mon. Not. Roy. Astron. Soc.*, vol. 415, pp. 1849–1863, 2011, arXiv:1103.5867.
  - [1146] R. Mallick, S. Singh, and R. Prasad, “Gravitational wave signature from phase transition of a combusting neutron star to quark star,” *Mon. Not. Roy. Astron. Soc.*, vol. 507, no. 1, pp. 1318–1328, 2021, arXiv:2003.00693.
  - [1147] C. Constantinou, S. Han, P. Jaikumar, and M. Prakash, “g modes of neutron stars with hadron-to-quark crossover transitions,” *Phys. Rev. D*, vol. 104, no. 12, p. 123032, 2021, arXiv:2109.14091.
  - [1148] Z. Bai, W.-j. Fu, and Y.-x. Liu, “Identifying QCD Phase Transitions via the Gravitational Wave Frequency from a Supernova Explosion,” *Astrophys. J.*, vol. 922, no. 2, p. 266, 2021, arXiv:2109.12614.
  - [1149] E. L. Bratton, Z. Lin, F. Weber, M. G. Orsaria, I. F. Ranea-Sandoval, and N. Saavedra, “Gravitational-Wave Instabilities in Rotating Compact Stars,” *Galaxies*, vol. 10, no. 5, p. 94, 2022.
  - [1150] M. G. Alford, S. Han, and M. Prakash, “Generic conditions for stable hybrid stars,” *Phys. Rev. D*, vol. 88, no. 8, p. 083013, 2013, arXiv:1302.4732.
  - [1151] V. Dexheimer, R. Negreiros, and S. Schramm, “Role of strangeness in hybrid stars and possible observables,” *Phys. Rev. C*, vol. 91, no. 5, p. 055808, 2015, arXiv:1411.4623.
  - [1152] S. Benic, D. Blaschke, D. E. Alvarez-Castillo, T. Fischer, and S. Typel, “A new quark-hadron hybrid equation of state for astrophysics - I. High-mass twin compact stars,” *Astron. Astrophys.*, vol. 577, p. A40, 2015, arXiv:1411.2856.
  - [1153] J.-E. Christian and J. Schaffner-Bielich, “Twin Stars and the Stiffness of the Nuclear Equation of State: Ruling Out Strong Phase Transitions below  $1.7n_0$  with the New NICER Radius Measurements,” *Astrophys. J. Lett.*, vol. 894, no. 1, p. L8, 2020, arXiv:1912.09809.
  - [1154] R. Nandi and S. Pal, “Finding quark content of neutron stars in light of GW170817,” *Eur. Phys. J. ST*, vol. 230, no. 2, pp. 551–559, 2021, arXiv:2008.10943.
  - [1155] H. Tan, V. Dexheimer, J. Noronha-Hostler, and N. Yunes, “Finding Structure in the Speed of Sound of Supranuclear Matter from Binary Love Relations,” *Phys. Rev. Lett.*, vol. 128, no. 16, p. 161101, 2022, arXiv:2111.10260.
  - [1156] E. R. Most, A. Motornenko, J. Steinheimer, V. Dexheimer, M. Hanauske, L. Rezzolla, and H. Stoecker, “Probing neutron-star matter in the lab: connecting binary mergers to heavy-ion collisions,” 1 2022, arXiv:2201.13150.
  - [1157] L.-G. Pang, “Machine learning for high energy heavy ion collisions,” *Nucl. Phys. A*, vol. 1005, p. 121972, 2021.
  - [1158] J. Adam *et al.*, “Flow and interferometry results from Au+Au collisions at  $\sqrt{s_{NN}} = 4.5$  GeV,” *Phys. Rev. C*, vol. 103, no. 3, p. 034908, 2021, arXiv:2007.14005.
  - [1159] Q. Yang, “The STAR BES-II and Forward Rapidity Physics and Upgrades,” *Nucl. Phys. A*, vol. 982, pp. 951–954, 2019.
  - [1160] J. Adams *et al.*, “The STAR Event Plane Detector,” *Nucl. Instrum. Meth. A*, vol. 968, p. 163970, 2020, arXiv:1912.05243.
  - [1161] STAR Collaboration and CBM Collaboration eTOF Group, “Physics Program for the STAR/CBM eTOF Upgrade,” 9 2016, arXiv:1609.05102.
  - [1162] J. Brandenburg, “STAR Forward Rapidity Upgrade,” *PoS*, vol. HardProbes2020, p. 179, 2021.
  - [1163] A. Adare *et al.*, “An Upgrade Proposal from the PHENIX Collaboration,” 1 2015, arXiv:1501.06197.
  - [1164] Apollinari, G. and Béjar Alonso, I. and Brüning, O. and Fessia, P. and Lamont, M. and Rossi, L. and Tavian, L., “High-Luminosity Large Hadron Collider (HL-LHC): Technical Design Report V. 0.1,”

- vol. 4/2017, 2017.
- [1165] ALICE Collaboration, “ALICE upgrades during the LHC Long Shutdown 2,” 2 2023, arXiv:2302.01238.
  - [1166] N. Alizadehvandchali *et al.*, “Hot and Cold QCD White Paper from ALICE-USA: Input for 2023 U.S. Long Range Plan for Nuclear Science,” 12 2022, arXiv:2212.00512.
  - [1167] I. Bediaga *et al.*, “Framework TDR for the LHCb Upgrade: Technical Design Report,” 4 2012.
  - [1168] ATLAS Collaboration, “Letter of Intent for the Phase-I Upgrade of the ATLAS Experiment,” tech. rep., CERN, Geneva, 2011.
  - [1169] W. Adam *et al.*, “The CMS Phase-1 Pixel Detector Upgrade,” *JINST*, vol. 16, no. 02, p. P02027, 2021, arXiv:2012.14304.
  - [1170] CMS Collaboration, “Technical Proposal for the Phase-II Upgrade of the CMS Detector,” 6 2015.
  - [1171] ATLAS Collaboration, “Letter of Intent for the Phase-II Upgrade of the ATLAS Experiment,” 2012.
  - [1172] C. CMS, “A MIP Timing Detector for the CMS Phase-2 Upgrade,” tech. rep., CERN, Geneva, 2019.
  - [1173] M. P. Casado, “A High-Granularity Timing Detector for the ATLAS Phase-II upgrade,” *Nucl. Instrum. Methods Phys. Res., A*, vol. 1032, p. 166628, 2022.
  - [1174] R. Longo, “Joint ATLAS/CMS ZDC upgrade project for the High Luminosity LHC,” tech. rep., CERN, Geneva, 2022.
  - [1175] R. Aaij *et al.*, “Physics case for an LHCb Upgrade II - Opportunities in flavour physics, and beyond, in the HL-LHC era,” 8 2018, arXiv:1808.08865.
  - [1176] S. Floerchinger and M. Martinez, “Fluid dynamic propagation of initial baryon number perturbations on a Bjorken flow background,” *Phys. Rev. C*, vol. 92, no. 6, p. 064906, 2015, arXiv:1507.05569.
  - [1177] S. Pratt, J. Kim, and C. Plumberg, “Evolution of Charge Fluctuations and Correlations in the Hydrodynamic Stage of Heavy Ion Collisions,” *Phys. Rev. C*, vol. 98, no. 1, p. 014904, 2018, arXiv:1712.09298.
  - [1178] S. Pratt and C. Plumberg, “Determining the Diffusivity for Light Quarks from Experiment,” *Phys. Rev. C*, vol. 102, no. 4, p. 044909, 2020, arXiv:1904.11459.
  - [1179] S. Pratt, D. Oliinychenko, and C. Plumberg, “Using baryonic charge balance functions to resolve questions about the baryo-chemistry of the quark gluon plasma,” *Phys. Rev. C*, vol. 106, no. 6, p. 064911, 2022, arXiv:2210.03877.
  - [1180] S. Pratt and C. Plumberg, “Charge balance functions for heavy-ion collisions at energies available at the CERN Large Hadron Collider,” *Phys. Rev. C*, vol. 104, no. 1, p. 014906, 2021, arXiv:2104.00628.
  - [1181] J. Cimerman, I. Karpenko, B. Tomasik, and P. Huovinen, “Next-generation multi-fluid hydrodynamic model for RHIC BES,” 1 2023, arXiv:2301.11894.
  - [1182] C. Spieles and M. Bleicher, “Effects of the QCD phase transition on hadronic observables in relativistic hydrodynamic simulations of heavy-ion reactions in the FAIR/NICA energy regime,” *Eur. Phys. J. ST*, vol. 229, no. 22-23, pp. 3537–3550, 2020, arXiv:2006.01220.
  - [1183] J. Auvinen and H. Petersen, “Evolution of elliptic and triangular flow as a function of  $\sqrt{s_{NN}}$  in a hybrid model,” *Phys. Rev. C*, vol. 88, no. 6, p. 064908, 2013, arXiv:1310.1764.
  - [1184] H. Wolter *et al.*, “Transport model comparison studies of intermediate-energy heavy-ion collisions,” *Prog. Part. Nucl. Phys.*, vol. 125, p. 103962, 2022, arXiv:2202.06672.
  - [1185] J. E. Bernhard, J. S. Moreland, S. A. Bass, J. Liu, and U. Heinz, “Applying Bayesian parameter estimation to relativistic heavy-ion collisions: simultaneous characterization of the initial state and quark-gluon plasma medium,” *Phys. Rev. C*, vol. 94, no. 2, p. 024907, 2016, arXiv:1605.03954.

- [1186] G. Nijs, W. van der Schee, U. Gürsoy, and R. Snellings, “Bayesian analysis of heavy ion collisions with the heavy ion computational framework Trajectum,” *Phys. Rev. C*, vol. 103, no. 5, p. 054909, 2021, arXiv:2010.15134.
- [1187] G. S. Denicol, T. Koide, and D. H. Rischke, “Dissipative relativistic fluid dynamics: a new way to derive the equations of motion from kinetic theory,” *Phys. Rev. Lett.*, vol. 105, p. 162501, 2010, arXiv:1004.5013.
- [1188] J. A. Fotakis, E. Molnár, H. Niemi, C. Greiner, and D. H. Rischke, “Multicomponent relativistic dissipative fluid dynamics from the Boltzmann equation,” *Phys. Rev. D*, vol. 106, no. 3, p. 036009, 2022, arXiv:2203.11549.
- [1189] J. Sammet, M. Mayer, and D. H. Rischke, “Linear stability analysis of Israel-Stewart theory in the case of a nonzero background charge,” 2 2023, arXiv:2302.01070.
- [1190] G. S. Denicol, S. Jeon, and C. Gale, “Transport Coefficients of Bulk Viscous Pressure in the 14-moment approximation,” *Phys. Rev. C*, vol. 90, no. 2, p. 024912, 2014, arXiv:1403.0962.
- [1191] A. Jaiswal, “Relativistic third-order dissipative fluid dynamics from kinetic theory,” *Phys. Rev. C*, vol. 88, p. 021903, 2013, arXiv:1305.3480.
- [1192] M. Younus and A. Muronga, “Third order viscous hydrodynamics from the entropy four current,” *Phys. Rev. C*, vol. 102, no. 3, p. 034902, 2020, arXiv:1910.11735.
- [1193] C. V. P. de Brito and G. S. Denicol, “Third-order relativistic dissipative fluid dynamics from the method of moments,” 2 2023, arXiv:2302.09097.
- [1194] C. V. Brito and G. S. Denicol, “Linear causality and stability of third-order relativistic dissipative fluid dynamics,” *Phys. Rev. D*, vol. 105, no. 9, p. 096026, 2022, arXiv:2107.10319.
- [1195] M. Martinez and M. Strickland, “Dissipative Dynamics of Highly Anisotropic Systems,” *Nucl. Phys. A*, vol. 848, pp. 183–197, 2010, arXiv:1007.0889.
- [1196] M. Martinez, R. Ryblewski, and M. Strickland, “Boost-Invariant (2+1)-dimensional Anisotropic Hydrodynamics,” *Phys. Rev. C*, vol. 85, p. 064913, 2012, arXiv:1204.1473.
- [1197] D. Bazow, U. W. Heinz, and M. Strickland, “Second-order (2+1)-dimensional anisotropic hydrodynamics,” *Phys. Rev. C*, vol. 90, no. 5, p. 054910, 2014, arXiv:1311.6720.
- [1198] P. Bozek and W. Broniowski, “Longitudinal decorrelation measures of flow magnitude and event-plane angles in ultrarelativistic nuclear collisions,” *Phys. Rev. C*, vol. 97, no. 3, p. 034913, 2018, arXiv:1711.03325.
- [1199] V. Vovchenko, V. Koch, and C. Shen, “Proton number cumulants and correlation functions in Au-Au collisions at  $\sqrt{s_{NN}}=7.7\text{--}200$  GeV from hydrodynamics,” *Phys. Rev. C*, vol. 105, no. 1, p. 014904, 2022, arXiv:2107.00163.
- [1200] S. Chatterjee and P. Bozek, “Large directed flow of open charm mesons probes the three dimensional distribution of matter in heavy ion collisions,” *Phys. Rev. Lett.*, vol. 120, no. 19, p. 192301, 2018, arXiv:1712.01189.
- [1201] A. Andronic *et al.*, “Directed flow in Au + Au, Xe + CsI and Ni + Ni collisions and the nuclear equation of state,” *Phys. Rev. C*, vol. 67, p. 034907, 2003, arXiv:nucl-ex/0301009.
- [1202] Y. Nara, H. Niemi, J. Steinheimer, and H. Stöcker, “Equation of state dependence of directed flow in a microscopic transport model,” *Phys. Lett. B*, vol. 769, pp. 543–548, 2017, arXiv:1611.08023.
- [1203] L. Du, H. Gao, S. Jeon, and C. Gale, “Rapidity scan with multistage hydrodynamic and statistical thermal models,” 2 2023, arXiv:2302.13852.
- [1204] D. Lonardonì, A. Lovato, S. Gandolfi, and F. Pederiva, “Hyperon Puzzle: Hints from Quantum Monte Carlo Calculations,” *Phys. Rev. Lett.*, vol. 114, no. 9, p. 092301, 2015, arXiv:1407.4448.
- [1205] A. Collaboration *et al.*, “Unveiling the strong interaction among hadrons at the LHC,” *Nature*,



- vol. 588, pp. 232–238, 2020, arXiv:2005.11495. [Erratum: Nature 590, E13 (2021)].
- [1206] “MUSES.” <https://muses.physics.illinois.edu/>.
- [1207] “NP3M.” <https://np3m.org/>.
- [1208] B. P. Abbott *et al.*, “Prospects for observing and localizing gravitational-wave transients with Advanced LIGO, Advanced Virgo and KAGRA,” *Living Rev. Rel.*, vol. 21, no. 1, p. 3, 2018, arXiv:1304.0670.
- [1209] J.-F. Paquet and S. A. Bass, “Electromagnetic measurement of the temperature of quark-gluon plasma produced in central ultrarelativistic nuclear collisions,” 2022, arXiv:2205.12299.
- [1210] S. Floerchinger, C. Gebhardt, and K. Reygers, “Electrical conductivity of the quark-gluon plasma from the low energy limit of photon and dilepton spectra,” *Phys. Lett. B*, vol. 837, p. 137647, 2023, arXiv:2112.12497.
- [1211] S. Acharya *et al.*, “Neutral to charged kaon yield fluctuations in Pb – Pb collisions at  $\sqrt{s_{NN}}=2.76$  TeV,” *Phys. Lett. B*, vol. 832, p. 137242, 2022, arXiv:2112.09482.
- [1212] J. I. Kapusta, S. Pratt, and M. Singh, “Confronting anomalous kaon correlations measured in Pb-Pb collisions at  $\sqrt{s_{NN}}=2.76$  TeV,” *Phys. Rev. C*, vol. 107, no. 1, p. 014913, 2023, arXiv:2210.03257.
- [1213] G. Agakichiev *et al.*, “Low mass  $e^+e^-$  pair production in 158/A-GeV Pb - Au collisions at the CERN SPS, its dependence on multiplicity and transverse momentum,” *Phys. Lett. B*, vol. 422, pp. 405–412, 1998, arXiv:nucl-ex/9712008.
- [1214] R. Arnaldi *et al.*, “NA60 results on thermal dimuons,” *Eur. Phys. J. C*, vol. 61, pp. 711–720, 2009, arXiv:0812.3053.
- [1215] H. Paukkunen, “Neutron skin and centrality classification in high-energy heavy-ion collisions at the LHC,” *Phys. Lett. B*, vol. 745, pp. 73–78, 2015, arXiv:1503.02448.
- [1216] I. Helenius, H. Paukkunen, and K. J. Eskola, “Neutron-skin effect in direct-photon and charged hadron-production in Pb+Pb collisions at the LHC,” *Eur. Phys. J. C*, vol. 77, no. 3, p. 148, 2017, arXiv:1606.06910.
- [1217] Y. Jiang and J. Liao, “Pairing Phase Transitions of Matter under Rotation,” *Phys. Rev. Lett.*, vol. 117, no. 19, p. 192302, 2016, arXiv:1606.03808.
- [1218] Y. Fujimoto, K. Fukushima, and Y. Hidaka, “Deconfining Phase Boundary of Rapidly Rotating Hot and Dense Matter and Analysis of Moment of Inertia,” *Phys. Lett. B*, vol. 816, p. 136184, 2021, arXiv:2101.09173.
- [1219] ALICE Collaboration, “Measurement of the  $J/\psi$  polarization with respect to the event plane in Pb-Pb collisions at the LHC,” 4 2022, arXiv:2204.10171.
- [1220] B. Betz, M. Gyulassy, and G. Torrieri, “Polarization probes of vorticity in heavy ion collisions,” *Phys. Rev. C*, vol. 76, p. 044901, 2007, arXiv:0708.0035.
- [1221] Y. Tachibana and T. Hirano, “Emission of Low Momentum Particles at Large Angles from Jet,” *Nucl. Phys. A*, vol. 904-905, pp. 1023c–1026c, 2013, arXiv:1210.5567.
- [1222] W. M. Serenone, J. a. G. P. Barbon, D. D. Chinellato, M. A. Lisa, C. Shen, J. Takahashi, and G. Torrieri, “A polarization from thermalized jet energy,” *Phys. Lett. B*, vol. 820, p. 136500, 2021, arXiv:2102.11919.
- [1223] S. Shi, K. Li, and J. Liao, “Searching for the Subatomic Swirls in the CuCu and CuAu Collisions,” *Phys. Lett. B*, vol. 788, pp. 409–413, 2019, arXiv:1712.00878.
- [1224] M. A. Lisa, J. a. G. P. Barbon, D. D. Chinellato, W. M. Serenone, C. Shen, J. Takahashi, and G. Torrieri, “Vortex rings from high energy central p+A collisions,” *Phys. Rev. C*, vol. 104, no. 1, p. 011901, 2021, arXiv:2101.10872.
- [1225] S. Y. F. Liu and Y. Yin, “Spin Hall effect in heavy-ion collisions,” *Phys. Rev. D*, vol. 104, no. 5,

- p. 054043, 2021, arXiv:2006.12421.
- [1226] B. Fu, L. Pang, H. Song, and Y. Yin, “Signatures of the spin Hall effect in hot and dense QCD matter,” 1 2022, arXiv:2201.12970.
  - [1227] A. Baty, P. Gardner, and W. Li, “Collective evolution of a parton in the vacuum: the ultimate partonic ”droplet”, non-perturbative QCD and quantum entanglement,” 4 2021, arXiv:2104.11735.
  - [1228] M. P. Heller, R. A. Janik, and P. Witaszczyk, “Hydrodynamic Gradient Expansion in Gauge Theory Plasmas,” *Phys. Rev. Lett.*, vol. 110, no. 21, p. 211602, 2013, arXiv:1302.0697.
  - [1229] A. Buchel, M. P. Heller, and J. Noronha, “Entropy Production, Hydrodynamics, and Resurgence in the Primordial Quark-Gluon Plasma from Holography,” *Phys. Rev. D*, vol. 94, no. 10, p. 106011, 2016, arXiv:1603.05344.
  - [1230] S. Grozdanov, P. K. Kovtun, A. O. Starinets, and P. Tadić, “Convergence of the Gradient Expansion in Hydrodynamics,” *Phys. Rev. Lett.*, vol. 122, no. 25, p. 251601, 2019, arXiv:1904.01018.
  - [1231] S. Grozdanov, P. K. Kovtun, A. O. Starinets, and P. Tadić, “The complex life of hydrodynamic modes,” *JHEP*, vol. 11, p. 097, 2019, arXiv:1904.12862.
  - [1232] M. P. Heller, A. Serantes, M. Spaliński, V. Svensson, and B. Withers, “Hydrodynamic gradient expansion in linear response theory,” *Phys. Rev. D*, vol. 104, no. 6, p. 066002, 2021, arXiv:2007.05524.
  - [1233] M. P. Heller, A. Serantes, M. Spaliński, V. Svensson, and B. Withers, “Hydrodynamic Gradient Expansion Diverges beyond Bjorken Flow,” *Phys. Rev. Lett.*, vol. 128, no. 12, p. 122302, 2022, arXiv:2110.07621.
  - [1234] M. P. Heller, A. Serantes, M. Spaliński, V. Svensson, and B. Withers, “Relativistic Hydrodynamics: A Singulant Perspective,” *Phys. Rev. X*, vol. 12, no. 4, p. 041010, 2022, arXiv:2112.12794.
  - [1235] W. Florkowski and R. Ryblewski, “Highly-anisotropic and strongly-dissipative hydrodynamics for early stages of relativistic heavy-ion collisions,” *Phys. Rev. C*, vol. 83, p. 034907, 2011, arXiv:1007.0130.
  - [1236] M. Alqahtani, M. Nopoush, and M. Strickland, “Relativistic anisotropic hydrodynamics,” *Prog. Part. Nucl. Phys.*, vol. 101, pp. 204–248, 2018, arXiv:1712.03282.
  - [1237] P. Romatschke, “Relativistic Hydrodynamic Attractors with Broken Symmetries: Non-Conformal and Non-Homogeneous,” *JHEP*, vol. 12, p. 079, 2017, arXiv:1710.03234.
  - [1238] G. S. Denicol and J. Noronha, “Connecting far-from-equilibrium hydrodynamics to resummed transport coefficients and attractors,” *Nucl. Phys. A*, vol. 1005, p. 121748, 2021, arXiv:2003.00181.
  - [1239] M. P. Heller, R. Jefferson, M. Spaliński, and V. Svensson, “Hydrodynamic Attractors in Phase Space,” *Phys. Rev. Lett.*, vol. 125, no. 13, p. 132301, 2020, arXiv:2003.07368.
  - [1240] F. S. Bemfica, M. M. Disconzi, V. Hoang, J. Noronha, and M. Radosz, “Nonlinear Constraints on Relativistic Fluids Far from Equilibrium,” *Phys. Rev. Lett.*, vol. 126, no. 22, p. 222301, 2021, arXiv:2005.11632.
  - [1241] T. Nunes da Silva, D. Chinellato, M. Hippert, W. Serenone, J. Takahashi, G. S. Denicol, M. Luzum, and J. Noronha, “Pre-hydrodynamic evolution and its signatures in final-state heavy-ion observables,” *Phys. Rev. C*, vol. 103, p. 054906, 2021, arXiv:2006.02324.
  - [1242] F. S. Bemfica, M. M. Disconzi, and J. Noronha, “Causality and existence of solutions of relativistic viscous fluid dynamics with gravity,” *Phys. Rev. D*, vol. 98, no. 10, p. 104064, 2018, arXiv:1708.06255.
  - [1243] P. Kovtun, “First-order relativistic hydrodynamics is stable,” *JHEP*, vol. 10, p. 034, 2019, arXiv:1907.08191.
  - [1244] F. S. Bemfica, F. S. Bemfica, M. M. Disconzi, M. M. Disconzi, J. Noronha, and J. Noronha, “Nonlinear Causality of General First-Order Relativistic Viscous Hydrodynamics,” *Phys. Rev. D*, vol. 100,

- no. 10, p. 104020, 2019, arXiv:1907.12695. [Erratum: Phys.Rev.D 105, 069902 (2022)].
- [1245] R. E. Houtt and P. Kovtun, “Stable and causal relativistic Navier-Stokes equations,” *JHEP*, vol. 06, p. 067, 2020, arXiv:2004.04102.
- [1246] F. S. Bemfica, M. M. Disconzi, and J. Noronha, “First-Order General-Relativistic Viscous Fluid Dynamics,” *Phys. Rev. X*, vol. 12, no. 2, p. 021044, 2022, arXiv:2009.11388.
- [1247] J. Noronha, M. Spaliński, and E. Speranza, “Transient Relativistic Fluid Dynamics in a General Hydrodynamic Frame,” *Phys. Rev. Lett.*, vol. 128, no. 25, p. 252302, 2022, arXiv:2105.01034.
- [1248] C. Eckart, “The Thermodynamics of irreversible processes. 3.. Relativistic theory of the simple fluid,” *Phys. Rev.*, vol. 58, pp. 919–924, 1940.
- [1249] L. D. Landau and E. M. Lifshitz, *Fluid Mechanics*. Oxford, England: Butterworth-Heinemann, 2 ed., Aug. 1987.
- [1250] Y. Akamatsu, A. Mazeliauskas, and D. Teaney, “A kinetic regime of hydrodynamic fluctuations and long time tails for a Bjorken expansion,” *Nucl. Phys. A*, vol. 967, pp. 872–875, 2017, arXiv:1705.08199.
- [1251] Y. Akamatsu, A. Mazeliauskas, and D. Teaney, “Bulk viscosity from hydrodynamic fluctuations with relativistic hydrokinetic theory,” *Phys. Rev. C*, vol. 97, no. 2, p. 024902, 2018, arXiv:1708.05657.
- [1252] L. Yan and H. Grönqvist, “Hydrodynamical noise and Gubser flow,” *JHEP*, vol. 03, p. 121, 2016, arXiv:1511.07198.
- [1253] M. Singh, C. Shen, S. McDonald, S. Jeon, and C. Gale, “Hydrodynamic Fluctuations in Relativistic Heavy-Ion Collisions,” *Nucl. Phys. A*, vol. 982, pp. 319–322, 2019, arXiv:1807.05451.
- [1254] A. S. Aasen, S. Floerchinger, G. Giacalone, and D. Guenduez, “Thermal fluctuations on the freeze-out surface of heavy-ion collisions and their impact on particle correlations,” 8 2022, arXiv:2208.04806.
- [1255] R. P. G. Andrade, J. Noronha, and G. S. Denicol, “Jet quenching effects on the direct, elliptic, and triangular flow at energies available at the BNL Relativistic Heavy Ion Collider,” *Phys. Rev. C*, vol. 90, no. 2, p. 024914, 2014, arXiv:1403.1789.
- [1256] K. Rajagopal and A. V. Sadofyev, “Chiral drag force,” *JHEP*, vol. 10, p. 018, 2015, arXiv:1505.07379.
- [1257] A. M. Sirunyan *et al.*, “Azimuthal anisotropy of charged particles with transverse momentum up to 100 GeV/c in PbPb collisions at  $\sqrt{s_{NN}}=5.02$  TeV,” *Phys. Lett. B*, vol. 776, pp. 195–216, 2018, arXiv:1702.00630.
- [1258] B. Betz, M. Gyulassy, M. Luzum, J. Noronha, J. Noronha-Hostler, I. Portillo, and C. Ratti, “Cumulants and nonlinear response of high  $p_T$  harmonic flow at  $\sqrt{s_{NN}} = 5.02$  TeV,” *Phys. Rev. C*, vol. 95, no. 4, p. 044901, 2017, arXiv:1609.05171.
- [1259] S. Acharya *et al.*, “Production of  $\Lambda$  and  $K_s^0$  in jets in p–Pb collisions at  $\sqrt{s_{NN}}=5.02$  TeV and pp collisions at  $\sqrt{s}=7$  TeV,” *Phys. Lett. B*, vol. 827, p. 136984, 2022, arXiv:2105.04890.
- [1260] ALICE Collaboration, “Production of  $K_S^0$ ,  $\Lambda$  ( $\bar{\Lambda}$ ),  $\Xi^\pm$  and  $\Omega^\pm$  in jets and in the underlying event in pp and p–Pb collisions,” 11 2022, arXiv:2211.08936.
- [1261] G. K. Krintiras and A. G. S. Leiton, “The CMS Heavy Ion Group contribution to 2022 NSAC Long-Range Plan Town Hall Meeting (Hot and Cold QCD) – Letter of Interest,” 9 2022, arXiv:2209.11564.
- [1262] A. Huss, A. Kurkela, A. Mazeliauskas, R. Paatelainen, W. van der Schee, and U. A. Wiedemann, “Discovering Partonic Rescattering in Light Nucleus Collisions,” *Phys. Rev. Lett.*, vol. 126, no. 19, p. 192301, 2021, arXiv:2007.13754.
- [1263] A. Huss, A. Kurkela, A. Mazeliauskas, R. Paatelainen, W. van der Schee, and U. A. Wiedemann,

- “Predicting parton energy loss in small collision systems,” *Phys. Rev. C*, vol. 103, no. 5, p. 054903, 2021, arXiv:2007.13758.
- [1264] J. Huang, Z.-B. Kang, and I. Vitev, “Inclusive b-jet production in heavy ion collisions at the LHC,” *Phys. Lett. B*, vol. 726, pp. 251–256, 2013, arXiv:1306.0909.
- [1265] J. Casalderrey-Solana, D. C. Gulhan, J. G. Milhano, D. Pablos, and K. Rajagopal, “A Hybrid Strong/Weak Coupling Approach to Jet Quenching,” *JHEP*, vol. 10, p. 019, 2014, arXiv:1405.3864. [Erratum: *JHEP* 09, 175 (2015)].
- [1266] P. Arnold, “Universality (beyond leading log) of soft radiative corrections to  $\hat{q}$  in  $p_{\perp}$  broadening and energy loss,” *JHEP*, vol. 03, p. 134, 2022, arXiv:2111.05348.
- [1267] P. Arnold, T. Gorda, and S. Iqbal, “The LPM effect in sequential bremsstrahlung: incorporation of “instantaneous” interactions for QCD,” *JHEP*, vol. 11, p. 130, 2022, arXiv:2209.03971.
- [1268] G. D. Moore, S. Schlichting, N. Schlusser, and I. Soudi, “Non-perturbative determination of collisional broadening and medium induced radiation in QCD plasmas,” *JHEP*, vol. 10, p. 059, 2021, arXiv:2105.01679.
- [1269] W. Ke and X.-N. Wang, “QGP modification to single inclusive jets in a calibrated transport model,” *JHEP*, vol. 05, p. 041, 2021, arXiv:2010.13680.
- [1270] W. Dai, I. Vitev, and B.-W. Zhang, “Momentum imbalance of isolated photon-tagged jet production at rhic and lhc,” *Phys. Rev. Lett.*, vol. 110, p. 142001, Apr 2013.
- [1271] W. Ke, X.-N. Wang, W. Fan, and S. A. Bass, “Study of heavy-flavor jets in a transport approach,” *PoS*, vol. HardProbes2020, p. 060, 2021, arXiv:2008.07622.
- [1272] E. Chapon *et al.*, “Prospects for quarkonium studies at the high-luminosity LHC,” *Prog. Part. Nucl. Phys.*, vol. 122, p. 103906, 2022, arXiv:2012.14161.
- [1273] L. Adamczyk *et al.*, “Measurement of  $J/\psi$  Azimuthal Anisotropy in Au+Au Collisions at  $\sqrt{s_{NN}} = 200$  GeV,” *Phys. Rev. Lett.*, vol. 111, no. 5, p. 052301, 2013, arXiv:1212.3304.
- [1274] CMS Collaboration, “Open heavy flavor and quarkonia in heavy ion collisions at HL-LHC,” 2018.
- [1275] A. Bursche *et al.*, “Physics opportunities with the fixed-target program of the LHCb experiment using an unpolarized gas target,” 2018.
- [1276] R. Aaij *et al.*, “Measurement of the ratio of prompt  $\chi_c$  to  $J/\psi$  production in  $pp$  collisions at  $\sqrt{s} = 7$  TeV,” *Phys. Lett. B*, vol. 718, pp. 431–440, 2012, arXiv:1204.1462.
- [1277] B. Abelev *et al.*, “Technical Design Report for the Upgrade of the ALICE Inner Tracking System,” *J. Phys. G*, vol. 41, p. 087002, 2014.
- [1278] T. Marshall, “Heavy Flavor and Quarkonia Physics at sPHENIX,” *Rev. Mex. Fis. Suppl.*, vol. 3, no. 4, p. 040919, 2022.
- [1279] CMS Collaboration, “A MIP Timing Detector for the CMS Phase-2 Upgrade,” 2019.
- [1280] S. Caron-Huot and C. Gale, “Finite-size effects on the radiative energy loss of a fast parton in hot and dense strongly interacting matter,” *Phys. Rev. C*, vol. 82, p. 064902, 2010, arXiv:1006.2379.
- [1281] B. Schenke, C. Gale, and S. Jeon, “MARTINI: An Event generator for relativistic heavy-ion collisions,” *Phys. Rev. C*, vol. 80, p. 054913, 2009, arXiv:0909.2037.
- [1282] R. Aaij *et al.*, “Observation of an exotic narrow doubly charmed tetraquark,” *Nature Phys.*, vol. 18, no. 7, pp. 751–754, 2022, arXiv:2109.01038.
- [1283] Y. Hu, J. Liao, E. Wang, Q. Wang, H. Xing, and H. Zhang, “Production of doubly charmed exotic hadrons in heavy ion collisions,” *Phys. Rev. D*, vol. 104, no. 11, p. L111502, 2021, arXiv:2109.07733.
- [1284] J. Zhao, S. Shi, and P. Zhuang, “Fully-heavy tetraquarks in a strongly interacting medium,” *Phys.*

- Rev. D*, vol. 102, no. 11, p. 114001, 2020, arXiv:2009.10319.
- [1285] A. Esposito, C. A. Manzari, A. Pilloni, and A. D. Polosa, “Hunting for tetraquarks in ultraperipheral heavy ion collisions,” *Phys. Rev. D*, vol. 104, no. 11, p. 114029, 2021, arXiv:2109.10359.
- [1286] K. J. Eskola, P. Paakkinen, H. Paukkunen, and C. A. Salgado, “EPPS16: Nuclear parton distributions with LHC data,” *Eur. Phys. J. C*, vol. 77, no. 3, p. 163, 2017, arXiv:1612.05741.
- [1287] R. Abdul Khalek, J. J. Ethier, and J. Rojo, “Nuclear parton distributions from lepton-nucleus scattering and the impact of an electron-ion collider,” *Eur. Phys. J. C*, vol. 79, no. 6, p. 471, 2019, arXiv:1904.00018.
- [1288] ATLAS Collaboration, “Expected ATLAS Measurement Capabilities of Observables Sensitive to Nuclear Parton Distributions,” 2018.
- [1289] V. Guzey, M. Strikman, and M. Zhalov, “Disentangling coherent and incoherent quasielastic  $J/\psi$  photoproduction on nuclei by neutron tagging in ultraperipheral ion collisions at the LHC,” *Eur. Phys. J. C*, vol. 74, no. 7, p. 2942, 2014, arXiv:1312.6486.
- [1290] J. Arrington *et al.*, “EIC Physics from An All-Silicon Tracking Detector,” 2 2021, arXiv:2102.08337.
- [1291] A. Bylinkin, J. Nystrand, and D. Tapia Takaki, “Vector meson photoproduction in UPCs with FoCal,” 11 2022, arXiv:2211.16107.
- [1292] J. Cepila, J. G. Contreras, and J. D. Tapia Takaki, “Energy dependence of dissociative  $J/\psi$  photoproduction as a signature of gluon saturation at the LHC,” *Phys. Lett. B*, vol. 766, pp. 186–191, 2017, arXiv:1608.07559.
- [1293] I. Bautista, A. Fernandez Tellez, and M. Hentschinski, “BFKL evolution and the growth with energy of exclusive  $J/\psi$  and  $\Upsilon$  photoproduction cross sections,” *Phys. Rev. D*, vol. 94, no. 5, p. 054002, 2016, arXiv:1607.05203.
- [1294] N. Armesto and A. H. Rezaeian, “Exclusive vector meson production at high energies and gluon saturation,” *Phys. Rev. D*, vol. 90, no. 5, p. 054003, 2014, arXiv:1402.4831.
- [1295] H. Mäntysaari and B. Schenke, “Revealing proton shape fluctuations with incoherent diffraction at high energy,” *Phys. Rev. D*, vol. 94, no. 3, p. 034042, 2016, arXiv:1607.01711.
- [1296] C. Alexa *et al.*, “Elastic and Proton-Dissociative Photoproduction of  $J/\psi$  Mesons at HERA,” *Eur. Phys. J. C*, vol. 73, no. 6, p. 2466, 2013, arXiv:1304.5162.
- [1297] R.-j. Wang, S. Pu, and Q. Wang, “Lepton pair production in ultraperipheral collisions,” *Phys. Rev. D*, vol. 104, no. 5, p. 056011, 2021, arXiv:2106.05462.
- [1298] M. Klusek-Gawenda, W. Schäfer, and A. Szczurek, “Centrality dependence of dilepton production via  $\gamma\gamma$  processes from Wigner distributions of photons in nuclei,” *Phys. Lett. B*, vol. 814, p. 136114, 2021, arXiv:2012.11973.
- [1299] Z.-h. Sun, D.-x. Zheng, J. Zhou, and Y.-j. Zhou, “Studying Coulomb correction at EIC and EicC,” *Phys. Lett. B*, vol. 808, p. 135679, 2020, arXiv:2002.07373.
- [1300] W. Zha and Z. Tang, “Discovery of higher-order quantum electrodynamics effect for the vacuum pair production,” *JHEP*, vol. 08, p. 083, 2021, arXiv:2103.04605.
- [1301] J. D. Brandenburg, W. Zha, and Z. Xu, “Mapping the electromagnetic fields of heavy-ion collisions with the Breit-Wheeler process,” *Eur. Phys. J. A*, vol. 57, no. 10, p. 299, 2021, arXiv:2103.16623.
- [1302] Z. Wang, J. Zhao, C. Greiner, Z. Xu, and P. Zhuang, “Incomplete electromagnetic response of hot QCD matter,” *Phys. Rev. C*, vol. 105, no. 4, p. L041901, 2022, arXiv:2110.14302.
- [1303] M. Klusek-Gawenda, R. Rapp, W. Schäfer, and A. Szczurek, “Dilepton Radiation in Heavy-Ion Collisions at Small Transverse Momentum,” *Phys. Lett. B*, vol. 790, pp. 339–344, 2019, arXiv:1809.07049.
- [1304] D. Budker *et al.*, “Expanding Nuclear Physics Horizons with the Gamma Factory,” 6 2021,

- arXiv:2106.06584.
- [1305] Y. Hatta, B.-W. Xiao, F. Yuan, and J. Zhou, “Azimuthal angular asymmetry of soft gluon radiation in jet production,” *Phys. Rev. D*, vol. 104, no. 5, p. 054037, 2021, arXiv:2106.05307.
  - [1306] H. Xing, C. Zhang, J. Zhou, and Y.-J. Zhou, “The  $\cos 2\phi$  azimuthal asymmetry in  $\rho^0$  meson production in ultraperipheral heavy ion collisions,” *JHEP*, vol. 10, p. 064, 2020, arXiv:2006.06206.
  - [1307] J. Bor and D. Boer, “TMD evolution study of the  $\cos 2\phi$  azimuthal asymmetry in unpolarized  $J/\psi$  production at EIC,” *Phys. Rev. D*, vol. 106, no. 1, p. 014030, 2022, arXiv:2204.01527.
  - [1308] W. Zha, J. D. Brandenburg, L. Ruan, Z. Tang, and Z. Xu, “Exploring the double-slit interference with linearly polarized photons,” *Phys. Rev. D*, vol. 103, no. 3, p. 033007, 2021, arXiv:2006.12099.
  - [1309] I. Xu, N. Lewis, X. Wang, J. D. Brandenburg, and L. Ruan, “Search for Dark Photons in  $\gamma\gamma \rightarrow e^+e^-$  at RHIC,” 11 2022, arXiv:2211.02132.
  - [1310] STAR Collaboration, “SN0755 : The STAR Beam Use Request for Run-21, Run-22 and data taking in 2023-25 | The STAR experiment.” <https://drupal.star.bnl.gov/STAR/starnotes/public/sn0755>, 2021.
  - [1311] ATLAS Collaboration, “Prospects for Measurements of Photon-Induced Processes in Ultra-Peripheral Collisions of Heavy Ions with the ATLAS Detector in the LHC Runs 3 and 4 - CERN Document Server.” <http://cds.cern.ch/record/2641655/files/>, 2018.
  - [1312] C. Li, J. Zhou, and Y.-J. Zhou, “Probing the linear polarization of photons in ultraperipheral heavy ion collisions,” *Phys. Lett. B*, vol. 795, pp. 576–580, 2019, arXiv:1903.10084.
  - [1313] L. A. Harland-Lang, V. A. Khoze, and M. G. Ryskin, “Exclusive LHC physics with heavy ions: SuperChic 3,” *Eur. Phys. J. C*, vol. 79, no. 1, p. 39, 2019, arXiv:1810.06567.